The geography of contemporary urbanization and its effects on landscape sustainability in Harare Metropolitan Province

A cumulative dissertation for the degree

***Doctor rerum naturalium* (Dr. rer. nat)**

submitted to the

Department of Earth Sciences

by

Andrew Kudzanayi Marondedze

Berlin 2022

Andrew Kudzanayi Marondedze: The geography of contemporary urbanization and its effects on landscape sustainability in Harare Metropolitan Province.

Date of disputation: 13 June 2022

First supervisor

Prof. Dr. Brigitta Schütt
Freie Universität Berlin
Department of Earth Sciences
Institute of Earth Sciences
Malteserstraße 74-100
12249 Berlin
Germany

Second supervisor

Prof. Dr. Wiebke Bebermeier
Freie Universität Berlin
Department of Earth Sciences
Institute of Earth Sciences
Malteserstraße 74-100
12249 Berlin
Germany

"Printed and/or published with the support of the German Academic Exchange Service"

Abstract

This doctoral thesis examines independent variables as explanatory drivers influencing urban growth, axis of urban expansion and the impact of current and future land use and land cover (LULC) and climate change on the landscape of the Harare Metropolitan Province. Monitoring urban growth trends and LULC changes utilised multispectral remote sensing data, geographic information system technologies and binomial logistic regression. The LULC maps used in the study were generated by implementing machine learning support vector machines (SVMs), a supervised classification technique on Landsat 5 Thematic Mapper and Landsat 8 Operational Land Imager satellite images. The moderate resolution satellite images were enhanced with soil adjusted vegetation index (SAVI), enhanced built-up bareness index (EBBI), and modified normalized water difference index (MNWDI) spectral indices to improve feature delineation during data training and other classification procedures. The transformation of croplands and green spaces was revealed to occur at alarming rates predominantly in the south, south east, south west and north west parts of the Harare Metropolitan Province. The predominant variables significant for urban expansion were distance to trunk and secondary roads. In addition, steep slopes were determined as a topographic characteristic limiting rapid construction developments in the north and north-eastern parts of the province. Further, the eruption and sprouting of informal settlements due to political connotations and demand for shelter resulting from increasing urban migration overwhelmed the city and government plans to provide decent shelter.

The study also provides insights on the declining spatial soil loss rates between 1984 and 2018 with localized high soil erosion risk within active build-up areas, croplands, areas along footpaths and paved road sides. The validation of the RUSLE model using field mapping and measurements of soil erosion phenomena in urban environment was successful. This provides confidence to apply the RUSLE model to predict future spatial soil loss and potential soil erosion risk in the Epworth district of the Harare Metropolitan Province. The application of Markov chain model coupled with cellular automata provided future LULC distribution patterns for 2034 and 2050 for Epworth district. This displayed accelerated LULC change through the conversion of croplands and green spaces to built-up area mainly for residential purposes. Further, similar trends of declining soil loss rates were predicted for future scenarios between 2034 and 2050; with high soil erosion risk predicted along drainage channels and downslope. Therefore, by virtue of rampant LULC changes in Epworth district, green spaces and croplands were modified to impervious surfaces due to the increasing population and predominant demand for shelter leading to setting up of informal settlements. This exacerbates concentrated runoff and overland flow, increasing soil erosion risk along drainage channels and sloping areas as a result of minimized infiltration capacity.

In addition, trampling induced compaction on unpaved roads due to high traffic volumes and movements further contributes to accelerated overland flow. This facilitates the development of rills and ephemeral gullies on road sides and weak parts of the roads reducing mobility and access to properties. The encroachment of wetlands and river banks through the expansion of built-up areas and sand poaching activities does not only affect ecosystem functions but also impact negatively on livelihoods, nutrition and endangering lives due to the abandonment of disused pits. The study results show that spatiotemporal urban growth monitoring is fundamental in understanding urban growth patterns and revealing the more likely drivers influencing growth. Furthermore, mapping of soil erosion risk and estimating soil loss rates allow the application of the RUSLE method at a larger scale and to direct resources on areas potentially vulnerable to high soil erosion risk. The study results are highly valuable and highlight the need to promote reproducible documentation of data. Overall, this study provides insights that are imperative for authorities, land managers and policy makers to embrace for the advancement and attainment of sustainable smart cities as set by the UN agenda on Sustainable

Development Goals. As such the findings contribute to enhance our understanding of the implications of LULC and climate changes on the environment and human wellbeing.

Zusammenfassung

Im Rahmen dieser Doktorarbeit werden unabhängige Variablen als erklärende Faktoren für das städtische Wachstum und die Achse der Stadterweiterung sowie die Auswirkungen der künftig zu erwartenden Landnutzung und -bedeckung ebenso wie des Klimawandels auf die Harare Metropolitan Province untersucht. Diese Untersuchungen basieren auf der Verwendung multispektraler Fernerkundungsdaten und dem Einsatz geographischer Informationssysteme und binomialer logistischer Regressionen. Die durchgeführten Analysen der Landnutzungs- und -bedeckungsveränderungen basiert auf einer überwachten Klassifizierung von Satellitenbildern des Landsat 5 Thematic Mapper und des Landsat 8 Operational Land Imager. Dazu wurden Methoden des maschinellen Lernens mit Hilfe von Support Vector Machines (SVMs) eingesetzt. Die Satellitenbilder mit mittlerer Auflösung wurden mit dem bodenangepassten Vegetationsindex (SAVI), dem verbesserten Index für die bebaute Fläche (EBBI) und dem modifizierten normalisierten Wasserdifferenzindex (MNWDI) transformiert, um die Klassifizierungsverfahren zu verbessern.

Die Ergebnisse zeigen, dass die Umwandlung von Ackerland- und Grünlandflächen vor allem im Süden, Südosten, Südwesten und Nordwesten der Metropolregion Harare in Folge von Urbanisierungsprozessen stattfindet. Die in ihrem Einfluß auf die Stadterweiterung dominierenden Variablen sind die Entfernung zu Haupt- und Nebenstraßen. Steile Hänge schränken hingeben die bauliche städtische Entwicklung in den nördlichen und nordöstlichen Teilen der Metropolregion Harare ein. Die politisch bedingte Entstehung von informellen Siedlungen und der Bedarf an Behausungen infolge der zunehmenden Landflucht stellen die Pläne der Stadt und der Regierung zur Bereitstellung angemessener Unterkünfte vor große Herausforderungen.

Die Studie zeigt außerdem, dass die Bodenverlustraten durch Bodenerosion zwischen 1984 und 2018 in der Tendenz abgenommen haben. Nichtsdestotrotz gibt es lokal ein hohes Bodenerosionsrisiko vor allem in Baugebieten, auf Ackerflächen und entlang von Fußwegen und befestigen Straßen.

Die Modellierung des Bodenerosionsrisikos erfolgte unter Einsatz der Bodenabtragsgleichung RUSLE. Zur Validierung der Ergebnisse wurden Feldkartierungen und Messungen von Bodenerosionsphänomenen im städtischen Umfeld durchgeführt. Hier zeigt sich eine deutliche Übereinstimmung der Modellierungs- und Kartierungsergebnisse. Die Anwendung des RUSLE-Modells zur Vorhersage zu erwartender räumlicher Bodenverluste und des potenziellen Bodenerosionsrisikos im Epworth-Bezirk in der Harare Metropolitan Province ist damit zuverlässig möglich.

Unter Anwendung von Markov-Ketten in Verbindung mit zellulären Automaten wurde das Muster der zukünftigen Verteilung von Landbedeckungs- und -nutzungklassen im Bezirk Epworth für die Jahre 2034 und 2050 simuliert. Es zeigt sich, dass der Wandel der Landbedeckung und -nutzung durch die Umwandlung von Ackerland und Grünflächen in bebautes Gebiet vornehmlich durch eine Zunahme der Wohnbebauung geprägt sein wird. Dies ist vornehmlich auf die wachsende Bevölkerung und den vorherrschenden Bedarf an Unterkünften zurückzuführen, die bereits zur Errichtung informeller Siedlungen geführt hat. Entsprechend dieser Landbedeckungs- und Landnutzungsszenarien wurden für die Jahre abnehmende Bodenverlustraten vorhergesagt, wobei auch weiterhin von einem hohen Bodenerosionsrisiko vor allem entlang von Entwässerungskanälen und am Hangfuß auszugehen ist.

Darüber hinaus trägt die durch Trittschäden hervorgerufene Verdichtung auf unbefestigten Straßen als Folge des hohen Verkehrsaufkommens zu einer Zunahme des konzentrierten Oberflächenabfluss bei. Dies begünstigt die Entstehung von ephemeren Abflussrinnen entlang von Straßenrändern, was den Verkehr und den Zugang zu Grundstücken einschränkt. Die Ausdehnung bebauter Gebiete und illegaler Sandabbau beeinträchtigt darüber hinaus nicht nur Feuchtgebiete und Flussufer und damit deren Ökosystemfunktionen, sondern wirkt sich auch negativ auf die Lebensgrundlagen und die Ernährungssicherung aus; aufgegebene Sandgruben stellen zudem ein Sicherheitsrisiko dar.

Die Ergebnisse der Studie verdeutlichen, dass die raum-zeitliche Beobachtung des städtischen Wachstums von grundlegender Bedeutung für ein Verständnis der auf dieses städtische Wachstum Einfluß nehmenden Faktoren ist und damit für eine zuverlässige Prognose der zukünftigen Entwicklung. Die verwendeten Modellierungen des Bodenerosionsrisikos und die Schätzung der Bodenverlustraten mit der können im größeren Maßstab auch in anderen Gebieten eingesetzt werden. Zudem verdeutlicht die Studie die Notwendigkeit, eine reproduzierbare Dokumentation der Daten zu durchzuführen. Insgesamt liefert die Studie damit Erkenntnisse, die von Behörden, Landverwaltern und politischen Entscheidungsträgern für die Förderung und Verwirklichung nachhaltiger Stadtentwicklung im Sinne der UN-Agenda für nachhaltige Entwicklung berücksichtigt werden sollten. Somit tragen die Ergebnisse dazu bei, das Verständnis für die Auswirkungen von Landbedeckungs- und Landnutzungswandel und Klimaveränderungen auf die Umwelt und das menschliche Wohlergehen zu verbessern.

Table of contents

List of figures

List of tables

Dedication

This thesis is dedicated to my parents Mr Emilio and Mrs Simbisayi Marondedze, and to my love Rachel.

Acknowledgements

This thesis was supported by the Deutscher Akademischer Austauschdienst (DAAD) German Academic Exchange Service and the Government of Germany.

I give sincere gratitude to my supervisor Prof. Dr. Brigitta Schütt for the wise guidance, support and commitment that made me sail through in shaping my research work. I also thank Prof. Dr. Wiebke Bebermeier for the support during the course of my work. I am also indebted to the support I got from the FU Berlin Physical Geography and Earth Sciences Department staff members and colleagues. I am grateful for the support and every service from the departmental secretary, Frau Christiane Reuter at the time of study. Special thanks is expressed to Dr. Claudius Marondedze, Dr. Abel Chemura, Dr. Terrence. D Mushore, Dr. Shingai Nangombe, Dr. Fabian Becker, Fr. Gift V. Mubayiwa Prof. P. Borrelli, Herr Tobias Pohlmann, Noah M. Cheruiyot and Dr. Moritz Nykamp for the input and constant support they rendered throughout my studies. My sincere gratitude goes to my family, Limbani Pound, my officemate Juliet Katusiime Zizinga and all friends which I cannot mention by names. A special mention goes to my wife Rachel beginning from leaving her behind few weeks into our marriage, she has immensely inspired and supported me during the period of study, fieldwork and also by proof-reading all my writings. A lot of inspiration and courage for this work has been drawn from Dr Claudius Marondedze, a big brother and academic. But above all, glory be to God for his mercy which enabled me to overcome lows and turbulent times until the successful completion of this PhD journey.

CHAPTER 1: INTRODUCTION

1.1 Background

Urban growth and expansion threaten environmental sustainability when occurring at alarming rates combined with improper planning and policy implementation. This is due to the notion that urban areas are unequivocally dominated by built-up areas resulting in Land Use and Land Cover (LULC) changes, which modify the landscape. Urban landscape conversions and transformations markedly are as a consequence of human induced activities resulting in high density of impervious surfaces (Xu *et al*., 2000). Understanding the dynamics of LULC changes through the analysis of spatial patterns of built-up areas, and their interactions with the ecosystem becomes significant for investigating independent drivers influencing urban expansion.

The unprecedented population growth and imminent immigration have been primarily witnessed to impact on the increasing urbanization rates at global, regional and local levels (Mohan *et al.*, 2011; UN HABITAT 2007; Yu *et al*., 2019; ZimStats 2012). In that respect, the World Urbanization Prospects indicated that in 2014, 54% of the worlds' population lived in cities and it is projected to increase to 66% by 2050 with Asia and Africa having the fastest growing urbanization rates (UN 2014). This prompts the need for mapping and assessing trends of LULC changes in urban environments such as the Harare Metropolitan Province of Zimbabwe in order to develop policies and sustainable measures to curb environmental damage. To achieve such developments, remote sensing and GIS techniques are applied to unravel the spatiotemporal dynamics of LULC changes. In addition, the implementing of change detection analysis would promote better understanding and monitoring in change transitions in urban LULC. This is a post classification process of determining changes in the state of an object or phenomena between two or more dates using remote sensing data (Mukherjee 1987; Shalaby and Tateishi 2007; Singh 1989). Change detection of LULC is also an essential tool for decision-making and sustainable future urban planning.

According to Hegazy and Kaloop (2015) urban development can either happen in radical direction following growth around built cities or in linear patterns along the highways. This provides the pattern and axis of urban growth particularly by showing growth influencing characters including road network for easy transportation of goods and population mobility. Growth near cities could be linked to reduced time and cost effectiveness when accessing work places within the city and efficient connectivity. However, in cases of unrestrained and uncoordinated urban built-up area growth especially informal settlements, built-up area pattern

becomes difficult to describe due to their mushrooming characteristics (Chirisa and Muhomba 2013; Kamusoko *et al*., 2013). Retrospectively, the growth is neither supported with proper urban planning nor adequate infrastructure (Chirisa and Muhomba 2013; Kabantu et al. 2018). Henceforth, acquiring timely remote sensing data and the application of GIS techniques becomes significant to observe and analyse LULC changes.

The rapid LULC changes in the Harare Metropolitan Province have adversely affected its ecosystem resulting in the alteration of the local microclimate conditions for example increasing land surface temperatures (LST) causing outdoor thermal discomfort *(*Mushore *et al.*, 2017). Urban development is also linked with increases in human activities which in turn modify and transform natural lands (Mushore *et al*., 2017; Patley *et al*., 2018; Wania *et al*., 2014). Such perturbations including construction, movements from both humans and vehicles; and the clearing of green spaces for urban agriculture potentially escalate soil erosion risk due to reduced vegetation cover, litter and leaf coverage which protect soil from direct rainfall impact and surface runoff (Asiedu 2018; Kabantu *et al*., 2018). Climate change is also widely expected to impact negatively through increases in extreme precipitation and temperature magnitudes which however varies with location (Pruski and Nearing 2002). This will lead to an increase in soil erosion risks affecting crop productivity and economies (Ferreira *et al*., 2016; Nearing *et al*., *2005)*. Rainfall induced erosion vary and the impact depends on the rainfall characteristics (duration, volume and intensity) (IPCC 2007; Nearing 2001), and other contributing factors including topography, vegetation cover and soil susceptibility (Borrelli *et al.*, 2020; Hill and Schütt 2000; Renard *et al*., 1997).

In this regard, spatial and quantitative soil erosion risk on exposure information is fundamental for developing and planning sustainable measures to reduce the impact of soil erosion on the landscape and to humankind (Prasannakumar *et al.*, 2012; Alewell *et al.*, 2019). Therefore, this study aims at assessing spatial soil erosion risk, estimate soil loss for Epworth district of the Harare Metropolitan Province, and further predicts future soil erosion risk and their likely impacts in response to climate and land use changes. The investigations potentially require exploring urbanization and hydrological impacts on the landscape, regardless of the developmental needs for economic growth, investments and betterment of livelihoods. This becomes imminent due to the negative impacts resulting from human activities burdening the environment through over exploitation of natural resources (Hegazy and Kaloop 2015).

Sediments eroded from land surfaces during construction activities primarily in urban environments cause downstream significant problems including blocking water canals, compromising water quality (turbidity, deposition of pollutants) and siltation (Hogarth *et al*.,

2004; Shikangalah *et al*., 2017). Overall, the investigation sought to shed light on independent variables as urban growth explanatory drivers, quantify built-up area growth rate and the associated impacts of LULC and climate change on the landscape which is significant in addressing issues of sustainable urban development as targeted by Sustainable Development Goals (SDGs). The United Nations SDG 11 brings to attention the mandate to make cities safe, resilient and sustainable whilst, SDG 6 aims on the provision of proper water supply and sanitation as a basic right by 2030; which however, could be exasperating to attain considering the sprouting rate of urban settlements that are significantly unplanned and unrestricted due to political and socioeconomic influence.

1.2 Objectives

The specific objectives were to:

1. Determine and quantify independent variables as explanatory drivers influencing LULC change for the Harare Metropolitan province using multispectral remotely sensed data between 1984 and 2018.
2. Assess and estimate soil erosion risk for Epworth district of the Harare Metropolitan province between 2000 and 2018 time slices applying the Revised Universal Soil Loss Equation (RUSLE) model.
3. Predict future LULC distribution patterns for 2034 and 2050, and to assess climate change impacts on soil erosion risk for Epworth district of the Harare Metropolitan province for the same periods applying the RUSLE model based on representative concentration pathways (RCPs 4.5 & 8.5).

Thus, by quantitative and qualitative assessment of the above-mentioned specific objectives the research wants to answer the following questions:

1. Using multispectral remote sensing data, which independent drivers influence urban expansion and at what rate has LULC change occurred between: 1984-1990, 1990-2000, 2000-2008 and 2008-2018?
2. To what extent has estimated soil erosion risk and soil loss rate in 2000 and 2018 occurred as impacted by LULC change due to urbanization processes?
3. How does climate change affect the landscapes of an urbanizing district?

1.3 Thesis outline

The thesis consists of seven chapters. Three of the chapters are peer-reviewed research articles published in international journals. It is worth noting that the content of the peer-reviewed journals has been retained, duplicated and with some overlaps in the content of this thesis. Chapters from publications contain an abstract, introduction, materials and methods, results, discussion and conclusion sections. The thesis has been structured as follows: (1) Introduction (2) State of the art (3) Study site description (4) Mapping built-up area and axis of urban expansion using multispectral remote sensing and statistical modelling using binary logistic regression (5) Modelling spatial soil erosion risk and potential erosion using the empirical RUSLE model (6) Predicting impacts of future land use land cover and climate change on urban landscape (7) Synthesis and conclusion.

The introductory part of the thesis includes chapters' one up-to three. Chapter one serves as an introduction outlining the background, objectives for the study and the thesis structure**.** Chapter 2 highlights pertinent works that relate to the issues under study and investigation. This is done to address the objectives indicated in chapter one of the thesis through reviewing empirical works by other scholars. In that regard, the state of the art will identify knowledge gaps and challenges of methods applied, and consequently the need to develop other approaches as panacea to improved urban growth monitoring for sustainable development in cities. Chapter 3 serves to describe the research area by providing detailed information on the location, historical background and environmental characteristics. Descriptions beyond the borders of the Harare Metropolitan Province are also provided to enable better understanding of the entire country's relatedness and or variations of the physiography, climate and other characteristics. The introductory chapters of this thesis do not include detailed explanations of the methods applied. This is due to the avoidance of duplication as the methods are explained exclusively in the frame of the respective papers.

The analytical chapters, four to six are based on peer-reviewed papers and brief chapter synopsis has been provided. The main thrust for the chapters were to investigate trends of LULC, axis of urban expansion and further, to assess the influence of LULC and climate change on landscape sustainability through soil erosion risk assessments.

Analytical chapters' synopsis:

Chapter 4: Dynamics of land use and land cover changes in Harare, Zimbabwe: A case study on the linkage between drivers and the axis of urban expansion, *Marondedze A. K and Schütt B., 2019. Land*, vol. 8 (10). Own contribution: 80%.

In order to assess trends of LULC changes and their driving forces in urban environments, the study employs supervised classification of Landsat 5 Thematic Mapper (TM) and Landsat 8 Operational Land Imager (OLI) satellite images using support vector machines (SVMs). The research further established the influence of independent variables as urban growth explanatory drivers using the binary logistic regression modelling. The supervised classification generated using machine learning SVMs algorithms was enhanced through the use of spectral indices to improve the delineation of major land-use classes in a heterogeneous urban built-up area namely enhanced built-up and bareness index (EBBI), modified normalized difference water index (MNDWI) and soil adjusted vegetation index (SAVI). The analysis of urban growth explanatory variables using the logistic regression considered slope and the proximity characters (distance to main roads, secondary roads, open water bodies, streams and the city centre). The multispectral remotely sensed data from 1984, 1990, 2000, 2008 and 2018 were analysed and alarming rates of built-up area expansion were observed at the expense of croplands and disturbed green spaces within Harare Metropolitan Province. For the years 1984, 1990 and 2000 it was deducted that distance to the city centre, distance to roads (major and secondary) significantly influenced the expansion of urban built-up area. However, with the increasing extent of built-up area the influence of the distance to city centre as a driver decreased as the metropolitan expanded towards the peripheries encroaching peri-urban land area.

Chapter 5: Assessment of soil erosion using the RUSLE model for the Epworth District of the Harare Metropolitan Province, Zimbabwe, *Marondedze A. K and Schütt B., 2020. Sustainability, 12*, 853. Own contribution: 90%.

In this chapter, the study examines the impact of land use conversions through urbanization processes in Epworth district of the Harare Metropolitan as drivers of urban landscape fragmentation. To understand such trends LULC maps of 2000 and 2018 time slices were integrated to assess the impacts of LULC changes on potential erosion and soil erosion risk. In so doing, the RUSLE model was used to estimate potential erosion between 1984 and 2018 making use of long-term average annual precipitation (1984-2018) and further, the estimation of soil erosion risk for 2000 and 2018. For the estimation of potential erosion, the crop cover

management (C) and support practice (P) factors were used as identity elements (C and P = 1) and for the mapping of spatial soil erosion risk all RUSLE factors were incorporated as independent elements: soil erodibility (k), slope length and steepness (LS), rainfall erosivity (R), crop cover management (C) and support practice (P) factors. The general study findings reveal that there was positive correlation between areas of high soil erosion risk with high slope length and steepness factor, regardless of the declining estimated soil erosion risk between 2000 and 2018. The study analysis displayed that increasing impervious surfaces due to built-up area expansion and compaction as a result of traffic movement contributes to concentrated surface runoff and overland flow as observed primarily with deep incisions on the sides of paved roads and footpaths. The study introduced snap shot field measurements for the generation of spatial area damage map to facilitate the understanding and validation of the RUSLE model with *in-situ* field data.

Chapter 6: Predicting the Impact of Future Land Use and Climate Change on Potential Soil Erosion Risk in an Urban District of the Harare Metropolitan Province, Zimbabwe, *Marondedze A. K and Schütt B., 2021. Remote Sensing, 13,* 4360. Own Contribution: 90%.

This chapter aims at predicting future urban landscape responses to changes in LULC and climate. An integrated approach of CA-Markov model for the prediction of future LULC changes and the estimation of future soil erosion risk were investigated for the years 2034 and 2050 using the RUSLE model. The computation of rainfall erosivity factor employs model ensemble averages of 15 statistically downscaled global circulation models (GCMs) outcomes. The GCMs outcomes were retrieved from the NASA Exchange Global Daily Downscaled Projections (NEX-GDDP) at 0.25° by 0.25° spatial resolution under the representative concentration pathways (RCPs) 4.5 and 8.5 climate scenarios. For the assessment of climate variability, periods between 2019-2034 and 2035-2050 were applied to determine the rainfall erosivity factor for the prediction of future soil erosion risk. The predicted results showed that future LULC will occur at the expense of croplands and green spaces, with soil erosion risk predicted to decline over time for both climate scenarios. It is also argued that the observed long-term annual rainfall averages mask highly intensive and frequent interannual rainfall events, which massively increase soil erosion risk from bare and sparse shrublands.

Chapter 7: Modelling spatial landscape responses to urbanization and climate change applying remote sensing data: A synthesis

The chapter provides a synthesis of the findings, conclusions drawn from the study and overall reviews that will be developed for publishing. In this chapter, recommendations for future studies are laid out considering study limitations of the present study and other research gaps identified in the state-of-the-art chapter. The thesis concludes by providing a list of references.

CHAPTER 2: STATE OF THE ART

Chapter 2 presents advancement in the field through detailed mathematical models incorporating field data for the quantification of urban growth and impact on LULC and climate change on the urban landscape. Notably, chapter 2 elucidated the effectiveness and robustness of using machine-learning algorithms in improving satellite image classification and the significance of confusion matrix a post-classification technique in change detection analysis. The state-of-the-art chapter further sheds light on the impact of high-intensity precipitation events on soil erosion risk based on the projected increase in consecutive dry days with an overall decline on annual rainfall averages with regards to climate change responses.

2.1 The complexity of urban LULC change, dependencies and interactions

Urbanization is referred as an uneven spatiotemporal process involving the expansion of physical structures to the already existing compounded by surges in population, economic activities and immigration (Samson 2009). Due to lack of consensus definition on urbanization as a process various definitions exists but with little differences for example, Ghani and Kanbur (2013) describe urbanization as the assiduous involvement of human population in residential and industrial areas combined with their associated effects on the environment which extends to the adjacent rural landscape. While, (Zhang and He 2006) indicate that urbanization is associated with the conversion of land use for other purposes to meet population and economic growth demands. Unequivocally, several scholars concur on the principle that urban growth occurring at unprecedented rate attract challenges, which affect human-environment interactions. These encompass loss of vegetation, encroachment of fragile ecosystems such as wetlands causing ecosystem fragmentation, biodiversity loss and development of urban heat islands (microclimate environment) causing outdoor thermal discomfort in cities (As-syakur *et al*., 2012; Belal and Moghanm 2011; Jat *et al*., 2017; Melesse *et al*., 2007; Mushore *et al*., 2017; Opeyemi *et al*., 2019; Shikangalah *et al*., 2017; Zhang and He 2006; Zhang *et al.*, 2014).

Globally, urbanization rates are uneven with faster growth rates observed in developing countries (Bhatta 2010; UN 2014). The projected 2030 annual average urban growth rate estimates the highest trend for Sub-Saharan Africa at 3.6%, with 2.3% in East and North Africa, 2.2% for East Asia and the Pacific, 2.7% in South Asia, 1.5% in USA and the least urbanization rates were predicted for Europe at 0.04% (UN 2014). Additionally, the projected urbanization rates from the beginning of the 21st century shown that almost 2.5 billion people will be added to urban cities by 2050 (UN 2014). Urban expansion could be a positive indicator of social,

economic and political growth contributing to the improvement of material conditions (Akhter and Noon 2016; Khosrokhani and Pradhan 2014; Meshesha *et al*., 2014). Studies have indicated that spatial areal extent of numerous urban metropolitan areas is expanding adjacent to rural landscapes and urban peripheries (Araya and Cabral 2010; Hugo 2016; Xu *et al*., 2000). Urban expansion inevitably drives environmental problems including climate change (Mushore *et al*., 2017), rampant LULC changes resulting in the loss of agricultural land, downstream pollution, siltation, damage to roads and other infrastructure due to soil erosion processes (Melesse *et al*., 2007; Shikangalah *et al*., 2017).

Further, unplanned and unrestricted urban settlements accelerate LULC changes on urban landscapes accentuating environmental problems such as outdoor thermal discomfort and poor air quality (Jat *et al*., 2017; Mushore *et al*., 2017; Weeks *et al*., 2007), overexploitation of natural resources and modification of the landscape primarily by increasing impervious surfaces which accelerate overland flow, surface runoff and subsequent flooding (Hegazy and Kaloop 2015; Owoeye and Popoola 2017; Sayemuzzaman and Jha 2014). Also, LULC changes have direct impacts including surafce sealing which accelerates surface runoff, as well alteration of the hydrological cycle resulting from the removal of vegetation altering evapotranspiration processes and the dislocation of soil particles and sediment discharge downstream compromising water quality due to raindrop impact on bare surfaces (Asiedu 2018; Jinren, and Yingkui 2003; McCool *et al*., 1987; Weng 2001).

LULC change distribution varies in time and space (Pax-Lenney and Woodcock, 1997; Sinha and Kumar, 2013; Karamage *et al*., 2017) therefore, investigations on the drivers influencing landscape change are essential to curb environmental destruction. Accelerated LULC changes particularly in developing countries are characterized by urban sprawling, mushrooming informal settlements, invasion of urban agricultural land and encroachment of district boundaries to peri-urban land at the expense of the ecosystem (Akhter and Noon 2016; Hegazy and Kaloop 2015; Xu 2007). Soil erosion is among other negative impacts induced by urbanization processes, which however is affected by other intertwined factors including soil erodibility, rainfall erosivity, topographic characteristics, vegetation cover and management practices (Fournier, 1972; Wischmeier and Smith, 1978; Hill and Schütt, 2000; Cammeraat, 2004; Morgan, 2005; Verheijen *et al.*, 2009; Liu *et al.*, 2015; Panagos *et al*., 2015; Borrelli *et al.*, 2020).

The LULC change dynamics have become major components of managing, evaluating and monitoring environmental changes. The transformation of LULC is driven by numerous factors which can be complex due to dependencies and interactions in space and time (Al-

Hameedi *et al*., 2021; Zhai *et al*., 2021). For instance, the driving factors can be categorized as natural and human induced. The later considers political, social, economic and cultural activities while natural drivers such as site conditions (topography and soil conditions), floods and droughts can also be indirectly influenced by human activities (Mondal *et al*., 2015; Owoeye and Popoola 2017). As such, it is necessary to monitor and evaluate urban growth trends using geospatial technologies and remote sensing data to reduce deterioration of environmental quality and enhance sustainable urban development. According to the Brundtland report, sustainable development "*...seeks to meet the needs and aspirations of the present without compromising the ability to meet those of the future*" (Brundtland *et al*., 1987). Therefore, understanding drivers of LULC change and their impacts on the landscape of an urban area plays a pivotal role in the crafting and implementation of policies for effective future urban planning and management (Sinha *et al*., 2016; Xu *et al*., 2007; Yang *et al*., 2003).

Several studies have highlighted the significance of using multi-temporal remote sensing data for urban growth monitoring processes through establishing LULC trends (Al-Bilbisi 2019; As-syakur *et al*., 2012; Hegazy and Kaloop 2015; Kamusoko *et al*., 2013; Mushore *et al*., 2017; Yang *et al*., 2003). The remote sensing data provides historical and up-to-date spatiotemporal data suitable for environmental management. Urban growth monitoring is enabled through the use of change detection analysis which identify changes between two or more dates in the same geographical area (Shalaby and Tateishi 2007; Sinha and Kumar 2013). Having numerous change detection methods that apply multi-date satellite remote sensing data, the commonly used methods include classification-based techniques (map to map comparison) involving the detection of detailed change trajectories and the spectrally based (image to image) which allows detection of binary change/no-change (Green *et al*., 1994; Lu *et al*., 2004).

A change detection analysis highlights the expansion of built-up area at the expense of croplands, horticultural farms and the encroachment of administrative boundaries (Weng 2001). For Amman city in Jordan, spatial monitoring of urban expansion applied the multispectral remote sensing data and change detection analysis observing that between 1987-1997 urban growth increased by approximately 3.33% with other subsequent decades to 2017 having almost 2.04% growth rate (Al-Bilbisi 2019). This study reveals that urban growth predominantly took place along road networks and infrastructural development occurred at the expense of green spaces and other disturbed areas. Another study in Ujjain city, India utilized change detection criterion in Erdas Imagine software using moderate resolution Landsat imagery reports urban growth between 2005 and 2015 (Patley *et al*., 2018). Further, a change detection analysis between 1993 and 2001 in western Georgia using sub-pixel imperviousness

approach, a pixel-based change detection technique displays the abundance of urban monitoring and change detection techniques in remote sensing (Yang *et al*., 2003).

Rainfall induced erosion in urban areas has been reported due to LULC changes which influence vegetation loss (Opeyemi *et al*., 2019; Shikangalah *et al*., 2017) and decreasing infiltration capacity resulting from construction activities, traffic and human movements causing compaction of the land area (Dams *et al*., 2013; USDA. NRCS 2000). The rainfall erosive power varies depending on its intensity, volume and duration; and soil physical properties (Asiedu 2018; Borrelli *et al*., 2020; Nearing 2001; Zhang *et al*., 2013). However, to understand the impact of rainfall as a function of its erosive power to overcome soil shear forces, displace and transport soil particles to the point of deposition soil erosion models integrate rainfall erosivity (Wischmeier and Smith, 1978; Asiedu, 2018; Wang *et al*., 2018).

2.2 Urban growth theories

The ultimate explanation and description of how cities were formed and evolved cannot be addressed by a single theory or factor. Multiple theories have been laid out to explore development and existence of cities. Von Thünen's theory is among the first to explain the form and evolution of a city with an economic approach and the concept of a medieval village design (McDonagh 1997; von Thünen 1910). According to Burgess in 1923 (Park and Burgess 1967) a concentric ring approach was developed highlighting that cities expand from their original centers in a series of concentric zones. With the central business district (CBD) primarily for high rental fee uses such as department stores, financial institutions, theatres, office buildings (Park and Burgess 1967). Following the inner zone of high rental fees is the zone of transition proposed to constitute residences of low-income earning class mainly employed in the CBD with others linked to the activities of similar nature as those that occur in CBD. The transition zone exists as a function of low travelling and housing costs as well as poor buildings and packed structures (Park and Burgess 1967). The concentric zones move from the centric point "CBD" further apart attracting rising cost of living following increasing distances from the CBD indicating higher travelling and living costs. Such scenarios show social class structures between the low, medium and high-income earning members of the society. According to Burgess (1923) cities grew outwards to the peripheries in zones.

An alternative to the concentric ring theory is the sector theory by Hoyt (1939), urban development is modelled like "pie slices" with its growth described as extending from the CBD to the outskirts as individual sectors/wedges. For such scenario representation, transportation routes connecting from the CBD influence the axis of growth and provide natural boundaries

to the individual sectors. The theory suggests that outward expansion follows site selection on vacant land considering topographical characteristics, connectivity and natural beauty by high income groups or social classes leaving previous residential areas for the lower classes to more scenic areas (Hoyt 1939).

Additionally, the multiple nuclei theory by Harris and Ullman (1945), on urban land use development suggests that with the expansion of cities more additional business centers emanate primarily along major routes. These growing business centers alone become the nuclei and as a result harbor activities and business opportunities. Therefore, there are no concentric zones applied on multiple nuclei theories rather their development could be associated with poor connectivity to the CBD or increasing distance. As such, the Chicago school theories highlighted the market approach on residential areas and factors influencing urban development which in turn have an impact on LULC changes as these are continuous processes (Harris and Ullman 1945; Hoyt 1939; Park and Burgess 1967).

Criticism against the "Classics of Urban Theory" and development of new theoretical ideologies brought about by other scholars revealed that classical models addressed society questions and respectively nothing coherent on urban development (Harvey 1973; Castels 1978; McDowell 1983; Massey 1991; Black and Henderson 1999). However, Scott and Storper (2014) embrace the classical and new theoretical models highlighting that the assumptions of these models recognized that urban areas cannot be explicitly defined by theoretical frameworks rather they fundamentally consider agglomeration processes, land and human interactions in their developments. Overall, the urban theories or the "Classics of Urban Theory" notably shared urban development theories aiming at gaining a classical view and better understanding of the sociospatial segregation within a city. This can be linked to physical geography considering the influence of demographic growth and their socioeconomic impacts on the environment. This implies that city size will evolve over time in respect to population and economic growth (Black and Henderson 1999). The "Urban Land Nexus" theory by Scott and Storper (2014) also describes that cities group themselves into spatially extensive lattices characterized by processes which differentiate. In addition, cities have dynamic attributes with regards to social, political and economic phenomena. The Chicago school theories by Park and Burgess (1967), Harris and Ullman (1945), Hoyt (1939) prove that social clustering by class existed and their existence to date still subsist nevertheless the present research work investigates independent variables influencing urban growth, axis of expansion and their impacts on the landscape.

2.3 Remote sensing application in monitoring urban growth and landscape management

2.3.1 Image classification and analysis

The geographic information of urban systems can be timeously and accurately acquired through the use of remotely sensed data and geographic information systems (GIS) technology which allow data analysis, manipulation and storage including image classification processes for spectral analysis and characterization (As-syakur *et al*., 2012; Huang *et al*., 2002; Long and Srihar 2004; Patino and Duque 2013; Xu *et al*., 2007). Image classification is the procedure involving labelling and categorizing pixels based on spectral information into land cover classes either by applying supervised or unsupervised criterion (Long and Srihar 2004; Nooni *et al*., 2014; Vapnik 1998). In summary, to generate thematic maps various applications can be integrated including machine learning algorithms for the classification of multi and hyperspectral satellite images (Melgani and Bruzzone 2004; Nemmour and Chibani 2006). In the current study, supervised image classification techniques were applied using Support Vector Machines (SVMs). A brief description of classification techniques is provided distinctly highlighting the differences between supervised and unsupervised classification. However, the research work integrated the machine learning algorithms due to their robustness as non-parametric classifiers (Huang *et al*., 2002; Kamusoko *et al*., 2013; Knorn *et al*., 2009; Pal and Mather 2005). For example, the SVMs are statistical supervised classifiers based on machine learning theory (Vapnik 1998). The SVMs can be applied with minimum training areas to optimize the selection criteria of LULC classes by constructing hyperplanes in multidimensional spaces (Foody and Mathur 2004; Melgani and Bruzzone 2004) without requiring assumptions of data distribution which is a major limitation in remote sensing applications (Adelabu *et al*., 2015; Chemura and Mutanga 2017; Nooni *et al*., 2014).

Supervised classification is a technique that uses different classifiers including the machine learning algorithms allowing the user to predetermine the output attributes by using small proportion of labelled input attributes during training *(*Awad and Khanna *2*015*;* Berry *et al*., 2020; Hegazy and Kaloop 2015; MathWorks 2016; Melgani and Bruzzone 2004). Data training is the most fundamental stage for supervised classification and primarily dictates the classification accuracy (Foody and Mathur 2006). This results from the descriptive statistics of the training attributes selected from the image to characterize classes using algorithms following the application of expertise and prior knowledge of the area (Hegazy and Kaloop 2015; Lary 2010; Vapnik 1998). Burges (1998) revealed that SVMs were effective in pattern recognition therefore showing their significance as statistical learning tools with improved classification accuracy (Vapnik 1999). Further, the performance of SVMs has been observed to

surpass other classifiers including Artificial Neural Network, Maximum Likelihood, Parallelepiped and the Minimum distance (Adelabu *et al*., 2015; Chemura and Mutanga 2017; Huang *et al*., 2002; Kamusoko *et al*., 2013; Mou *et al*., 2018; Mushore *et al*., 2017; Nooni *et al*., 2014), SVMs showed better classification accuracy over Random Forest (RF) machine learning algorithms in the differentiation of tree species in semi-arid areas of Botswana. Nevertheless, both machine-learning algorithms attained high classification accuracy of over 85% with minimum training attributes. As such Foody and Mathur (2006) reiterate that the nature of the classier should determine the training paradigm and learning processes to ensure independency among classifiers. Additionally, machine learning algorithms have been deemed attractive and highly performing classifiers with regards to the applications involving nonlinear data and accuracy in articulating remote sensing challenges in many fields including agriculture or the detection of urban growth (Anselm *et al*., 2018; Dubeau *et al*., 2017; Nooni *et al*., 2014; Schubert *et al*., 2018).

In contrast, **unsupervised classification** applies clustering processes by which algorithms identify and examine unknown pixels and further divide them into different classes according to their natural groupings to establish structure in datasets (Berry *et al*., 2020; Dougherty *et al*., 1995; Jain 2010). For unsupervised classification there is no predetermination of attributes rather the approach uses all variables as inputs in the analysis (Berry *et al*., 2020). Abbas *et al.* (2016) highlight that the complexity of applying prior knowledge on noisy images during supervised classification processes reduces attribute labelling accuracy. As such, Wang and Cheng (2010) support the notion of unsupervised classification involving automatic classification and cluster analysis. For example, the K-Means classifier develops clusters following the identification of arbitrary values representing the same properties based on spectral characterization and the assigning of pixels to clusters on proximal basis using the Euclidean distance (Abbas *et al*., 2016; Jain 2010; Kulkarni *et al*., 2020; Venkateswaran *et al.*, 2013). The K-Means algorithms were developed to allow minimum cluster size, merging and splitting clusters (Jain 2010). Examples of unsupervised classifiers include the Iterative Self-Organizing Data Analysis Technique Algorithm (ISODATA) (Ball and Hall 1965), Forgy (Forgy 1965) and Fuzzy c-means (Dunn 1973) which are modifications of the K-Means algorithms with enhanced selection processes though they continue to integrate the clustering of attributes as their core principle.

2.3.2 Urban LULC feature delineation

Urbanization will continue to be witnessed as a result of increasing population and economic development. Consequently, rapid changes to LULC make it essential and indispensable to understand urban growth trends. Urban areas mostly in developing countries are regarded as more heterogenous and hence more challenging for monitoring and assessing change dynamics (Sakieh *et al*., 2015). This is attributed to poor urban planning, construction using different roofing materials, size of built-up units and their distribution (Jat *et al*., 2017; Sakieh *et al*., 2015). However, with the use of moderate to coarse spatial resolution satellite images the urban area landscape appears homogenous because different attributes of the land within a single grid cell are combined into one (Kadhim *et al*., 2016) and also high levels of spectral confusion resulting in misleading information (As-syakur *et al*., 2012). Following such scenarios, researchers have adopted various techniques of improving classification for better change detection analysis. For example, fusing Landsat 8 Operational Land Imager (OLI) NDVI at 30 m resolution with MODIS NDVI at 250 m improved overall classification accuracy of urban environments by 4% in comparison to single temporal Landsat remote sensing data (Jin et al., 2006).

Urban landscape feature delineation can also be improved through the use of spectral indices and machine learning algorithms such as random forest (RF) and support vector machines (SVMs) (As-syakur *et al*., 2012; Nooni *et al*., 2014; Chemura and Mutanga, 2017). Spectral indices have been developed and are calculated for the extraction of features of interest during mapping either through strong absorption or reflection in different spectral bands of the multispectral imagery (Im and Jensen 2008; Xu 2008). As such, numerous remote sensing spectral indices assist urban built-up area mapping including the Normalized difference vegetation index (NDVI), Normalized difference build-up index (NDBI), Enhanced build-up and bareness index (EBBI), Modified normalized difference water Index (MNDWI), Soil adjusted vegetation index (SAVI) (Bannari *et al*., 1995; Huete 1988; Mwakapuja *et al*., 2013; Sinha *et al*., 2016; Xu 2007). Further, the use of high spatial resolution images such as IKONOS, Quickbird, GeoEye and Worldview satellite series with 5 m or better spatial resolution makes it ideal for delineating individual buildings and enabling enhanced change detection analysis (Hu and Weng 2013). However, the commercialization of these sensors is a major limiting factor for many studies due to high costs. Nevertheless, several studies have adopted moderate resolution (10–100 m) remote sensing data due to easy accessibility and its spatial coverage. This makes it suitable for regional and global studies; more so data requirements for urban monitoring and evaluation over long periods make use of historical

information which primarily is archived on the early established coarse to moderate satellite databases (Hegazy and Kaloop 2015; Mukherjee *et al*., 2018; Mushore *et al*., 2017; Weng 2012; Zhang *et al*., 2013).

2.3.3 Factors influencing soil erosion

The empirical, physical and conceptual models have been developed to qualitatively and quantitatively assess soil erosion processes and their methods vary depending on the objectives and availability of data (Wischmeier and Smith, 1978; Nearing, 1997; Smith, 1999; Merritt *et al*., 2003). Both empirical and physical models represent natural processes but empirical models provide a dynamic approach based on statistical relevance while physical models are based on describing each individual process of a system resulting into complex models that require input data with high spatial and temporal resolution (Jetten *et al*., 2003; Legesse *et al*., 2004; Merritt *et al*., 2003; Nearing 2001; de Vente and Poesen 2005). Conceptual models resoundingly are a combination of empirical and physical based models suitable for providing indications of qualitative and quantitative processes within a watershed (Beck 1987). Due to limited empirical work on the impacts of urbanization and climate change on the landscape primarily soil erosion risks in Sub-Saharan Africa, the current research integrated remote sensing and geo-informatics. This approach is robust and cost effective for the estimation of current and future soil erosion risk as this is a desideratum for sustainable urban planning in the Harare Metropolitan province and for further research (Kabantu *et al*., 2018; Makinde and Oyebanji 2018; Opeyemi *et al*., 2019; Renard *et al*., 1997; Shikangalah *et al*., 2017).

Influence of Slope

The topographic characteristics of a landscape are considered valuable for soil erosion assessment. In this regard, the slope length and slope angle factors (LS) are required for spatial mapping of soil erosion risk in the RUSLE model. The LS factor accounts for soil loss and sediment yield down slope resulting from the combined effects of length and steepness of a slope converging onto a given point (Prasannakumar *et al*., 2012). It has been determined that the sediment yield per unit area is proportional to the LS factor (Wischmeier and Smith, 1978). The S factor measures the effect of slope steepness and the L factor describes the impact of slope length (Wischmeier and Smith, 1978; Panagos *et al*., 2015). The slope length has been widely defined as the distance from the point of origin of overland flow to the point where either slope gradient decreases to allow deposition or where the flow reaches defined channels

(Wischmeier and Smith, 1978). The LS factor calculations were developed from the initial unit plot and field scale measurements proposed considering the effect of slope on sheet, rill and inter-rill erosion by water (Wischmeier and Smith, 1978) (Table 2.1). The RUSLE modelling approach introduced modifications to the LS factor generation extending it to one-dimensional hill slope scale implementing various equations based on slope gradients (Renard *et al.,* 1997) with further advances considering complex topographic units by introducing contributing area and flow accumulation (Desmet and Govers 1996; Moore and Burch 1986).

To obtain the LS factor, digital elevation model (DEM) is widely used for this approach (Kefi *et al.*, 2011; Prasannakumar *et al.*, 2012; Panagos *et al*., 2015; Phinzi and Ngetar, 2019). The DEMs in soil erosion modelling include the ASTER Global DEM on which its datasets are obtained by stereoscopic techniques (Toutin and Gray 2000) and the Shuttle Radar Topography Mission (SRTM) that is obtained by radar interferometry (Moura-Bueno *et al*., 2016) all available at 90 m and 30 m spatial resolutions (Phinzi and Ngetar 2019). The landscape morphology either in its natural or modified state enormously contributes to soil loss. According to Desmet and Govers (1996) plan-concaved areas are zones of high flow accumulation and potentially have high LS values compared to convex areas. As such there is high correlation between soil loss and concaved sloppy areas due to the cumulative concentration of overland flow and surface runoff (Haan *et al*., 1994; Kefi *et al.*, 2011; Prasannakumar *et al*., 2012). The increase in slope length (L) and slope steepness (S) contribute to increased overland flow and increased erosion rates in the absence of vegetation and other soil erosion control practices (Renard *et al*., 1997; Karamage *et al*., 2017). That is, the steeper the slope of a landscape the higher the velocity of surface runoff and the longer the slope length the greater the amount of cumulative runoff corresponding to increased soil erosion (Desmet and Govers 1996; Moore and Burch 1986). Nevertheless, McCool *et al.* (1987) reiterate that soil loss is heavily linked to changes in slope steepness compared to changes in slope length.

Table 2.1 Commonly used equations for generating slope length and steepness (LS) factors.

No.	Equation	Source
1	$LS = \left(\frac{\lambda}{22.13}\right)^{m} (65.41\ sin^2\ \beta + 4.56 \sin \beta + 0.065)$ **where**: λ is the the slope length (m), m is the constant dependent on the value of slope, and β is the downhill slope angle categorized as: - 0.5 for slope angle greater than 2.86°, - 0.4 for slopes between 1.72° and 2.86°, - 0.3 for slopes between 0.57° and 1.72°, - 0.2 for slopes less than 0.57°.	Wischmeier and Smith (1978)
2	$LS = \left(Flow\ accumulation\ x\ \frac{Cell\ size}{22.13}\right)^{0.4} x \left(\frac{\sin Slope}{0.0896}\right)^{1.3}$ **where**: Flow accumulation shows the contribution of an area accumulated upslope for a given cell, Cell size is the size of the grid cell, and the sin Slope is the slope degree value in the trigonometric function sin.	Moore and Burch (1986)
3	$L_{ij} = \frac{\left(A_{ij-in} + D^2\right)^{m+1} - A_{ij-in}^{m+1}}{D^{m+2} x\ X_{ij}^{m}\ x\ 22.13^{m}}$ **where**: A_{ij-in} is the contributing area at the inlet of each grid cell (i, j) measured in m², D is the grid cell size (m), X_{ij} = sin a_{ij} + cos a_{ij} is the aspect direction of the grid cell (i, j), m is related to the ratio β of the interill erosion given as:	Desmet and Govers (1996)
	$m = \frac{\beta}{\beta + 1} \beta = \frac{\frac{\sin \theta}{0.0896}}{[0.56 + 3\ x\ (\sin \theta)^{0.8}]}$ **where**: θ is the slope in degrees. m value varies from 0 and 1. If the rill to interill ratio is near 0, m value approaches 0.	
4	$L = \left(\frac{\lambda}{72.6}\right)^{m}$ $m = \frac{\beta}{1 + \beta}$ $\beta = \frac{\left(\frac{\sin \theta}{0.0896}\right)}{[3.0\ x\ (\sin \theta)^{0.8} + 0.56]}$	Renard *et al.* (1997)
	If slope < 9%: $S = 10.8\ x\ \sin \theta + 0.03$ If slope ≥ 9%: $S = 16.8\ x\ \sin \theta - 0.50$ But if slope < 15ft: $S = 3.0\ x\ (\sin \theta)^{0.8} + 0.56$ λ is the the slope length (m) θ is the angle of slope m is slope dependent and classified as: 0.5 for slope > 2.86°, 0.4 for slopes between 1.72° and 2.86°, 0.3 for slopes between 0.57° and 1.72°, 0.2 for slopes less than 0.57°	

5	$LS = \left(\frac{Flow\ accumulatiom\ x\ Grid\ size}{22.13}\right)^{0.4} x \left(\frac{\sin Slope\ x\ 0.1745}{0.09}\right)^{1.4}$ **where:** Flow accumulation represents the generated flow from each and every cell following the generation of flow direction of filled DEM, Grid size is the length of cell side, and sin (Slope) is the slope degree value in the function sin.	Mitasova *et al.* (1996)
6	$LS = \frac{X}{22.1}\ m\ (0.065 + 0.045S + 0.0065S^2)$ **where:** X represents the slope length (m), S is the slope gradient (%) and m is the slope contingent variable.	Bizuwerk *et al.* (2008)

Influence of Rainfall

Rainfall erosivity is the aggressiveness of rainfall to mobilise soil particles due to the effect of its kinetic energy resulting from drop size, duration and intensity (Lal 1990; Owusu 2012). The rainfall erosivity impact is purported to contribute almost 80% of soil loss (Renard and Freimund 1994). Stocking and Elwell (1976) state that high intensity rains are damaging when vegetation cover is poor. The widely applied rainfall erosivity index is the R factor formerly used in the empirical based Universal Soil Loss Equation (USLE) (Wischmeier and Smith, 1978) and the later Revised Universal Soil Loss Equation (RUSLE) (Renard *et al*., 1997). The R factor is given as the sum of individual storm E*I* values for long term averaged annual rainfall (> 20 years) in order to account for cyclical rainfall patterns and variations (Wischmeier and Smith, 1978; Renard and Freimund, 1994). The R factor for a given period is obtained by summing the product of total storm kinetic energy (E) (MJ ha^{-1}) and the maximum amount of rainfall received within 30 consecutive minutes (I_{30}) (Renard and Freimund 1994) computed using Equation (2.1):

$$R = \frac{1}{n}\sum_{j=1}^{n}[\sum_{k=1}^{m}(E)_K(I_{30})_k]_j \qquad (2.1)$$

where R is the average annual rainfall erosivity (MJ mm ha^{-1} h^{-1} yr^{-1}), E is the total storm kinetic energy (MJ ha^{-1}), I_{30} is the maximum 30 min rainfall intensity (mm h^{-1}), j is an index of the number of years used in obtaining the average rainfall, k is an index of the number of storms in each year, n is the number of years used to derive the average R, and m is number of storms in each year.

Wischmeier & Smith (1978) state that total storm energy is a function of the intensities at which rainfall took place and its amount recorded at each time interval. Further, the kinetic energy of each rainfall unit depends on the sizes and terminal velocity of its raindrops (Wischmeier and Smith, 1978). This detailed data is provided by the pluviograph or autographic

rain gauge. However, due to the scarcity and unavailability of homogenous rainstorm data at most meteorological stations studies are adopting the use of mean monthly and annual rainfall data for the derivation of rainfall erosivity factor using estimation relations (Ferro *et al*., 1999; Merritt *et al*., 2004; Renard and Freimund 1994). The R factor estimation relations have been proposed to be predominantly location specific to reduce errors on the predicted soil loss rates, data scarcity and resources unavailability in carrying out spatial soil erosion modelling (Arnoldus 1977, 1980; Lo *et al*., 1985; Smithen and Schulze 1982).

Influence of Soil type

Soil erodibility is the susceptibility of the soil to erosion (Renard *et al*., 1997) and this is a function of its physical, chemical and pedologic characteristics including soil texture, structure, permeability, parent material, organic matter, stone coverage, bulk density, shear strength and other constituents (Wischmeier and Smith, 1978; Renard *et al*., 1997; Song, 2005). According to Morgan (2005), soil erodibility factor (K) is the mean annual soil loss per unit of rainfall erosivity in reference to a standard barren plot of fine tilth without conservation practices (Flangan and Nearing 1995; Renard *et al*., 1997). The erodibility of a soil driven by rainfall-runoff processes will increase proportionally with increasing amount of fine silt and sand particles (Lal 1994; Woldemariam *et al*., 2018). Soils with high organic matter content are more resistive to erosional forces and facilitate percolation of rainfall compared to soils with low soil organic matter and unstable aggregates (Nyamangara *et al*., 2014; Stocking and Elwell 1976). Clay rich soils with heavy presence of organic materials and decomposing residues forming stable aggregrates have high resistive forces to soil detachment hence soil erodibility factor is near 0 while highly susceptible soils have values near 1 (Wischmeier and Smith, 1978; Karamage *et al*., 2017; Woldemariam *et al*., 2018). Mhangara *et al.* (2012) indicate that low percentage of silt content corresponds to low soil erodibility regardless of sand and clay proportions. Soils with low levels of organic matter containing very low percentages of clays are susceptible to severe soil erosion driven by rainfall-runoff (Lal 1985). Additionally, high organic matter contents facilitate soil particle aggregation and infiltration (Nyamangara *et al*., 2014; Zakerinejad and Maerker 2015). Using the widely applied RUSLE model to map spatial soil erosion a combination of soil physical properties including soil texture, permeability, organic matter and structure were investigated to estimate the soils susceptibility to erosion process (Renard *et al*., 1997) following the Equation (2.2):

$$K = 2.8 \times 10^{-7} \times (12 - OM) \times M^{1.14} + 4.3 \times 10^{-3} \times (s - 2) + 3.3 \times 10^{-3} \times (p - 3) \qquad (2.2)$$

where K is the soil erodibility factor; OM is the percentage of organic matter; *s* is the soil structure code ranging between 1 and 4 defined as: 1 is friable, 2 is polyhedral, 3 is medium to coarse polyhedral and 4 is solid; p is the soil permeability code categorized into 6-code values (1 for rapid movement, 2 from moderate to rapid, 3 for moderate, 4 from slow to moderate, 5 for slow and 6 for very slow movement); M is the particle size parameter which is expressed as:

$$M = (\%\ \text{silt} + \%\ \text{very fine sand}) \times (100 - \%\ \text{clay}) \quad (2.3)$$

However, due to field data scarcity several alternative methods were designed for the estimation of soil erodibility applying available data for example Equation (2.4) generates K factor in the absence of soil structure and soil permeability (Sharpley and Williams, 1990).

$$K = Fcsand * Fsi - cl * Forgc * Fhisand * 0.1317 \quad (2.4)$$

where,
$$Fcsand = \left[0.2 + 0.3\ exp\left(-0.0256SAN\left(1 - \frac{SIL}{100}\right)\right)\right] \quad (2.4a)$$

$$Fsi - cl = \left[\frac{SIL}{CLA + SIL}\right]^{0.3} \quad (2.4b)$$

$$Forgc = \left[1.0 - \frac{0.25\ C}{C + \exp(3.72 - 2.95C)}\right] \quad (2.4c)$$

$$Fhisand = \left[1.0 - \frac{0.70\left(1 - \frac{SAN}{100}\right)}{\left(1 - \frac{SAN}{100}\right) + \exp\left[22.9\left(1 - \frac{SAN}{100}\right) - 5.51\right]}\right] \quad (2.4d)$$

where, K is soil erodibility factor (t ha h ha^{-1} MJ^{-1} mm^{-1}), SAN is sand weight content (%), SIL is silt weight content (%) and CLA represents clay weight content (%), C is the organic carbon content.

Influence of crop cover management factor (C)

The influence of humankind on crop cover management practices illustrates the significance of anthropogenic activities on ecosystem management and sustainability. In general, the crop cover management practices can be related to the human-environment interactions highlighting that everything people do has direct effects on the environment, whilst everything that

continuously occurs in the environment reciprocate affects humankind (Salisbury *et al.*, 2013). The crop cover management practices give an indication of the ratio of soil loss from land with specific vegetation cover to the corresponding soil loss under bare or tilled continuous fallow land (Wischmeier and Smith, 1978; Renard *et al*., 1997). The C factor ranges from 0 for non-erodible areas with high percentage of plant cover to 1 which corresponds to high soil erosion risk due to minimum vegetation cover or bareness as a result of extensive tillage increasing exposure to soil erosion (Renard *et al*., 1997). The leaf cover protects the soil from direct raindrop impact by dissipating precipitation velocity minimizing its effects on bare soil surface (Koirala *et al*., 2019; Ranzi *et al*., 2012). Biomass assists percolation of water through the reduction of surface runoff and also it reduces soil displacement by direct rainfall on bare areas (Opeyemi *et al*., 2019; Simonneaux *et al*., 2015).

Several methods exist for the calculation of C factor primarily making use of remotely sensed data and ground surveys for instance the USLE method (Wischmeier and Smith, 1978) derived the C factor based on empirical equations with measurements considering weighting of attributes including plant growth, ground cover, aerial cover and minimum drop height (Alena *et al*., 2013; Panagos *et al*., 2014). The C factor is also generated by applying the normalized difference vegetation index (NDVI) a vegetation growth index obtained by remote sensing into an exponential formula (Van der Knijff *et al*., 1999). The vegetation indices such as Normalized Difference Vegetation Index (NDVI) are applied to measure the biomass or vegetative vigor indicating differences in plant cover (Alexakis *et al*., 2013). The vegetation spectral properties apply the red (R) reflectance of the visible red bands which are Band 3 of ETM+ or Band 4 of OLI and the near-infrared (NIR) bands which are Band 4 of ETM+ and Band 5 of OLI sensors as shown on Equation (2.5) with values ranging between - 1 (non-vegetated) and + 1 (healthy vegetation) (Ahmed *et al*., 2013; Chen *et al*., 2006).

$$NDVI = (NIR - R)/(NIR + R) \tag{2.5}$$

This reveals the applicability of remote sensing on assessing C factor with other studies highlighting successes in its application (Equation 2.6) on similar terrain and climate conditions (Van der Knijff *et al*., 1999; Kouli *et al*., 2009; Prasannakumar *et al.*, 2012).

$$C = exp\left[-\alpha \frac{NDVI}{(\beta - NDVI)}\right] \tag{2.6}$$

where α and β are unitless parameters that determine the shape of the curve relating to NDVI and C factor with values 2 and 1 substituted for α and β.

According to Durigon *et al.* (2014) for tropical regions C factor values can be generated following the Equation (2.7):

$$C_r = \left(\frac{-NDVI+1}{2}\right) \quad (2.7)$$

where C_r is the denominated rescaled C factor.

The rescaled C factor was generated to modify the C factor obtained by Van der Knijff *et al.* (1999) following the notion that the rescaled C factor was more suitable for tropical climate conditions. The variation resulted due to intense rainfall experienced under tropical climate conditions causing an overestimation of the C factor when applying Equation 2.6 by Van der Knijff *et al.* (1999) which has been calibrated using European conditions (Durigon *et al*., 2014).

Influence of the support practices

The support practice factor index P in soil erosion modelling approaches represent the soil conservation practices that are applied for water harvesting and to control soil erosion by water including among others terracing, contour ridges and strip cropping (Wischmeier and Smith, 1978). The mechanical soil conservation practices reduce the amount and rate of soil erosion intrinsically by controlling rainfall-runoff processes such as runoff concentration, velocity, flow pattern and the hydraulic forces directed by runoff on soil surface (Renard *et al*., 1997; Prasannakumar *et al*., 2012; Panagos *et al*., 2015). The P factor values range between 0 and 1, where lower values closer to 0 reflect good conservation practices and increasing values closer to 1 show little to no conservation practices (Wischmeier and Smith, 1978; Renard *et al*., 1997). Expert knowledge can be used to generate P factor through the evaluation of farming activities either by field observations or analyzing classified images from remote sensing (Karydas *et al*., 2009; Panagos *et al*., 2014; Strand *et al*., 2002). Literature based P factor of 1 is widely adopted if there are no support practices registered on the research area (Adornado *et al.,* 2009; Panagos *et al.,* 2014). A support practice factor of 0.25 under zoned tillage management practice has been observed to potentially reduce soil loss by 75% in comparison with conventional tillage which adopts a high P factor value of 1 (Benavidez *et al*., 2018). Panagos *et al.* (2015b) investigated the influence of contour farming, stone walls and grass margins as support management practices on reducing the impact of soil erosion risk at European scale. The study concludes that grass margins reduced soil erosion by 57%, stonewalls by 38% and about 3% reduction in soil erosion risk for contour farming practices. As such P factors are significant in

scenario and sensitivity analysis on assessing impacts of different support management practices (Benavidez *et al*., 2018).

2.3.4 Impact of urban growth on soil erosion

Urban built-up area growth and expansion is inevitable due to demographic growth necessitated by migration and increasing economic activities, and therefore, the need for shelter to the growing population (Kucsicsa and Grigorescu 2018; Sudhira *et al*., 2004; Xu *et al*., 2007). This drives environmental issues for example the conversion of LULC to settlements at the expense of vegetation, agricultural areas and encroachment of fragile ecosystems (e.g. water bodies and wetlands) (Ashiagbor *et al*., 2013; Dibaba *et al*., 2020; Hegazy and Kaloop 2015; Xu 2008). The modification of urban landscape through LULC changes results in increased impervious surfaces reducing soil infiltration capacity (Sinha *et al*., 2016; USDA. NRCS 2000; Xu *et al*., 2007). Consequently, this contributes to increased soil erosion risk on vulnerable areas due to peak discharges which accentuate volume, duration and intensity of surface runoff including more frequent incidences of urban flooding (Weng 2001; Zhou *et al*., 2008) and decreases ground water recharge (Pappas *et al*., 2008; Rahaman *et al*., 2019). Additionally, such scenarios are culminated by blockage of water canals and culverts due to sediment deposition downslope. LULC changes combined with extended dry periods predominantly expose bare soil surfaces to direct raindrop impacts at the onset of wet season contributing to massive soil loss (Ligonja and Shrestha 2015; Shikangalah *et al*., 2017). Stocking and Elwell (1976) propose that soil erosion is a function of energy, resistive and protective forces. With energy forces affecting soil detachment and transportation while resistive forces refer to the ability to overcome stresses. Therefore, the need for plant cover to dissipate high energy raindrops before they reach the surface and the availability of biomass for protecting bare soil surfaces and facilitate infiltration (Borrelli *et al*., 2017; Simonneaux *et al*., 2015; Stocking and Elwell 1976).

2.3.5 Assessment of climate change impacts on soil erosion

Globally, extreme hydrological and temperature effects have been frequently observed due to climate change and global warming (Borrelli *et al*., 2020; Chen *et al*., 2020; Gupta and Kumar 2017; Nearing *et al*., 2005). The increasing rainfall erosivity as a result of climate change follows an increase in the magnitude and frequency of extreme rainfall events which significantly exacerbate soil loss due to increased runoff and concentrated overland flow (Borrelli *et al*., 2020; Favis-Mortlock and Guerra 1999; Nearing 2001; Poesen *et al*., 2003; Simonneaux *et al*., 2015). The resulting effect can be displayed by the rainfall erosivity factor

(R) in the Revised Universal Soil Loss Equation (RUSLE) model (Renard *et al*., 1997). The R factor is highly ranked among influential parameters affecting soil erosion (Borrelli *et al*., 2020; Nearing 2001). Increasing impervious surface area as a result of built-up area expansion coupled with severe hydrological regime changes as influenced by climate change further facilitates severe surface runoff and concentrated overland flow *(*Li and Fang 2016; Segura *et al.*, 2014). This generates sediments through soil erosion processes from sparse vegetated areas, bare land and other compacted areas (Opeyemi *et al*., 2019; Poesen *et al*., 2003; USDA. NRCS 2000). Nearing *et al.* (2005) indicate that the response of disturbed soil or bare land to small increases in rainfall intensity shows a non-linear response. Additionally, soil erosion processes threaten water bodies through siltation, turbidity and contamination by various substances including pesticides, nutrients and other chemical substances (Kouli *et al*., 2009; Nyakatawa *et al*., 2001; Opeyemi *et al*., 2019). Other associated impacts of concentrated runoff in urban environments include inaccessibility to properties resulting from landscape fragmentation through formation of gullies, damage to infrastructure and utilities encompassing powerlines and railway lines (Chalise *et al*., 2019; Opeyemi *et al*., 2019; Posthumus *et al*., 2015; Shikangalah *et al*., 2017).

Climate change effects are not only projected as intense across the globe but differ regionally with varying hydrological impacts on soil erosion (Chen *et al*., 2020; Hudson and Jones 2002; Pruski and Nearing 2002; Shongwe *et al*., 2009). The severity of climate change and influence vary with regions (Nearing *et al.*, 2005), for example in the Mediterranean region the frequency of high-intensity rainfall events were projected to increase with however declining average annual precipitation until the end of 21st century (Chen *et al*., 2020; Stefanidis and Stathis 2018). Similarly, for Sub-Saharan Africa the integration of regional climate models (RCMs) project an increase in the consecutive dry days with intervals of high-intensity rainfall exacerbating soil loss on vulnerable surfaces especially during the onset of the wet season (Girmay *et al*., 2021; Hudson and Jones 2002; Ligonja and Shrestha 2015). Further, Shongwe *et al.* (2009) indicate that some parts of the Sub-Saharan Africa will experience early rainfall onset and cessation with oscillating hydrological regimes dictating a decline on the average annual precipitation over time. For instance, the global circulation models (GCMs) projections show declining average annual rainfall for central Mozambique, extended areas of Botswana, northern and southern parts of Zimbabwe until the end of 21st century (Shongwe *et al*., 2009). Henceforth, the effect of climate change on rates of soil erosion will vary due to hydrological changes (Girmay *et al*., 2021; Nearing 2001) and other factors including land use change (Borrelli *et al*., 2020) which are influenced by demographic changes, economic activities and

policy implementation. The continuous soil loss is attributed to runoff impacts emanating from the projected increase in frequency and intensity of extreme rainfall events, nevertheless these events are masked on the average annual precipitation (Zhang *et al*., 2012). Borrelli *et al*. (2020) indicate that soil loss is also a function of the reorganization of future land use influenced by humankind and/natural factors.

CHAPTER 3: STUDY SITE DESCRIPTION

Chapter 3 describes the location, topography, pedolody and climate variability for the Harare Metropolitan Province and Zimbabwe at large. This sheds light on the aspects and attributes applied for the study works in following chapters of this thesis. The broad description further furnishes and display other attributes of areas adjacent and surrounding the research area including transitions and shifts that have occurred which will influence and contribute to the investigation findings.

3.1 Settlement decription and history

Harare Metropolitan Province is the capital city of Zimbabwe occupying an estimated area of 940 km^2 in total of the 390,757 km^2 Zimbabwe's area wide coverage. It is located between 17˚49'39.79" south latitude and 31˚03'12.13" east longitude (Figure 3.1) comprising the Harare urban, Harare rural, Chitungwiza and Epworth districts. Harare urban district is the largest district constituting the city centre and characterized with a hive of economic, residential and industrial activities followed by Harare rural district as the second largest district located to the south of the Harare urban district. Harare rural district is comprised of farming plots, the international airport and the fast-developing residential areas. Bordering Harare rural and Chitungwiza districts is the Manyame River and along the channel network are manifestation hubs of illegal sand mining posing threats to water quality, aquatic biodiversity and the ecosystem as large pits are abandoned at sites without rehabilitation measures. Chitungwiza district is located south of the metropolitan province approximately 25 km from the Harare central business district (CBD). Further, Epworth district is located approximately 12 km east of the city centre and it is the fastest growing urban district of Zimbabwe with the highest informal settlements across the country characterized by overcrowdings, densification and mushrooming growth (Chirisa and Muhomba 2013).

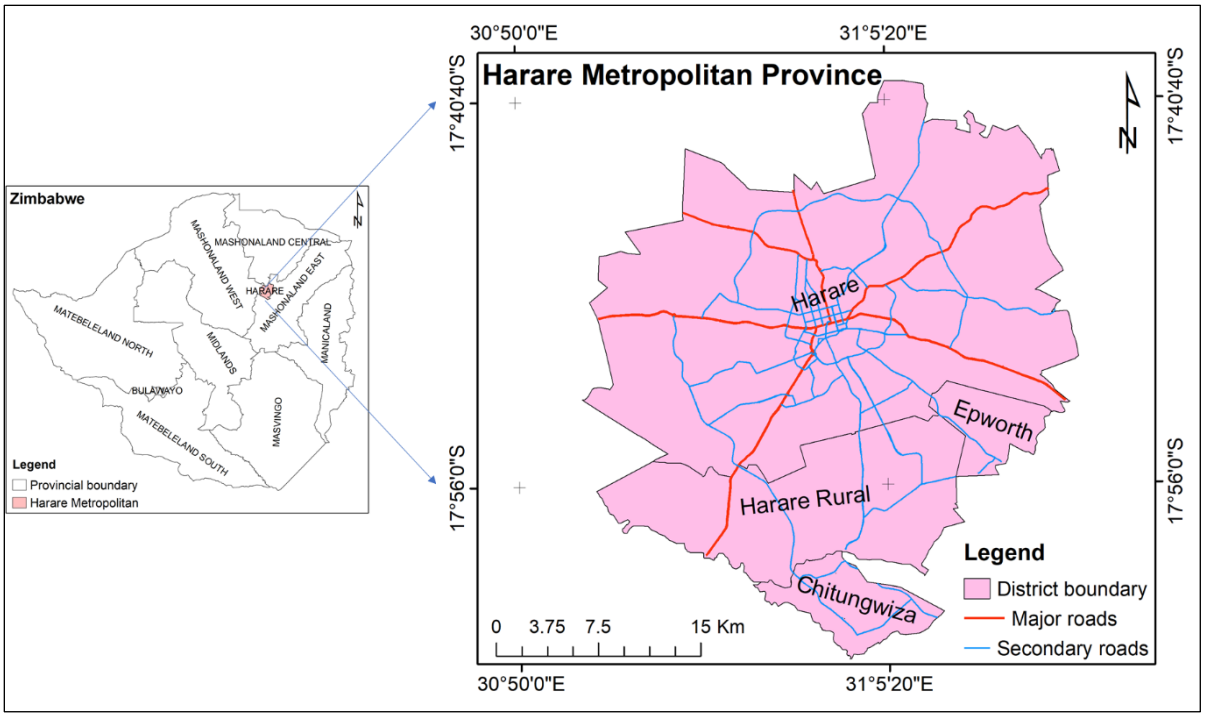

Figure 3. 1 Location of the Harare Metropolitan Province composed of Harare urban, Harare rural, Epworth and Chitungwiza districts. Plate (**a**) Provincial boundaries of Zimbabwe and plate (**b**) Harare Metropolitan Province indicating major and secondary road networks for connectivity.

The Harare Metropolitan Province experienced population increase from approximately 1.8 million in 2002 to an estimated population of 2.1 million in 2012 (CSO 2004; ZimStats 2012). With Harare urban district constituting about 70% of the population in the province in 2012 followed by 17% for Chitungwiza district, 8% for Epworth district and the least populated district being Harare rural hosting about 5% of the capital's population (ZimStats 2012).

The city of Harare, formerly Fort Salisbury was established around 1890 by the British settlers occupying the Kopje area of high relief for security purposes (Zinyama 1995). The growth of the newly founded city was aided by economic activities causing birth of dormitory high density suburbs such as Mbare established in 1907, Mabvuku 1952 and other residential areas developed in the southern and western parts of the city to accommodate the growing population particularly of the Africans (natives) as they provided labor to the British settlers (Zinyama 1995). The location and development of suburbs markedly gave a distinction on social class between the natives and British settlers. Suburbs located in the north and east parts of the city were characterized by spacious plot units, hilly and highly vegetated landscapes whilst small conjoined housing units occupied in the south-western African townships of Harare later became densely populated due to rural-urban migration (Cumming *et al*., 1993; Potts 2011; Zinyama 1995).

In 1986, the Epworth Local Board was developed following the handover of the Methodist mission church led settlement which was established in the late 1890s to the government of Zimbabwe (SDI 2009; Zinyama 1995). The Epworth settlement experienced soaring population during the late 1970s from rural to peri-urban migration during the epoch of the liberation struggle overwhelming the Methodist mission church administrative responsibilities (Zinyama 1995). Regardless of the formalization of this dormitory satellite Epworth district is regarded as the fastest growing informal settlement in Zimbabwe (Chirisa and Muhomba 2013). Epworth district was approximated to have host 500 families in 1950 (Butcher 1986) and the counted population of about 114,047 in 2002 that further increased to 167,462 in 2012 (CSO 2004; ZimStats 2012).

Chitungwiza district, a high-density residential suburb founded as a nuclei dormitory around 1970s to cater for the surge in urban population in the capital, is located south of the CBD and Manyame River (Zinyama 1995). The idea was to reduce population density in the city through outward expansion and allocation of residential units at the periphery where it would attract low housing costs regardless of the increasing distance and time to reach the CBD and industrial areas surrounding the city centre. The residential suburb sees large number of its population working and relying on services from the capital of Harare due to an imbalance between their industrial and commercial sector against population growth (Musemwa 2010).

3.2 Terrain and hydrological characteristics

The elevation of Zimbabwe ranges between 153 m and slightly above 2584 m a.s.l (Figure 3.2) with over 66% of the land area above 1000 m a.s.l lying on a plateau making Zimbabwe part of the Southern Africa Highveld (Lister 1987). Zimbabwe experiences very low altitude in the north along Zambezi river bordering Zimbabwe and Mozambique and in the south-eastern parts at the confluence of Runde and Save rivers. High-altitude areas between 1200-2000 m a.s.l extend from the northeast and the Eastern Highlands where the highest elevations occur at Inyangani mountains (> 2400 m a.s.l), also characterized by the plateau at such elevation and unique microclimate. Areas of high altitude spread from the north across the central to the south west parts of the country and the diagonally cross cutting high relief areas represent the Great Dyke mountains that extend to over 500 km across the country (Lister 1987).

For Harare Metropolitan Province, the elevation ranges between 1333 m and 1609 m a.s.l and the province is characterized by undulating to slightly rolling terrain in the upland areas and across the entire south and southwest parts. High elevations predominantly occur in

the northern and eastern parts of the province, with steep sloping relief more in the northern suburbs and high relief land area on a plateau to the east (Figure 3.2). The northern suburbs are markedly occupied by the elites and classified as low-density suburbs as a result of large plot sizes, low population density and steep terrain.

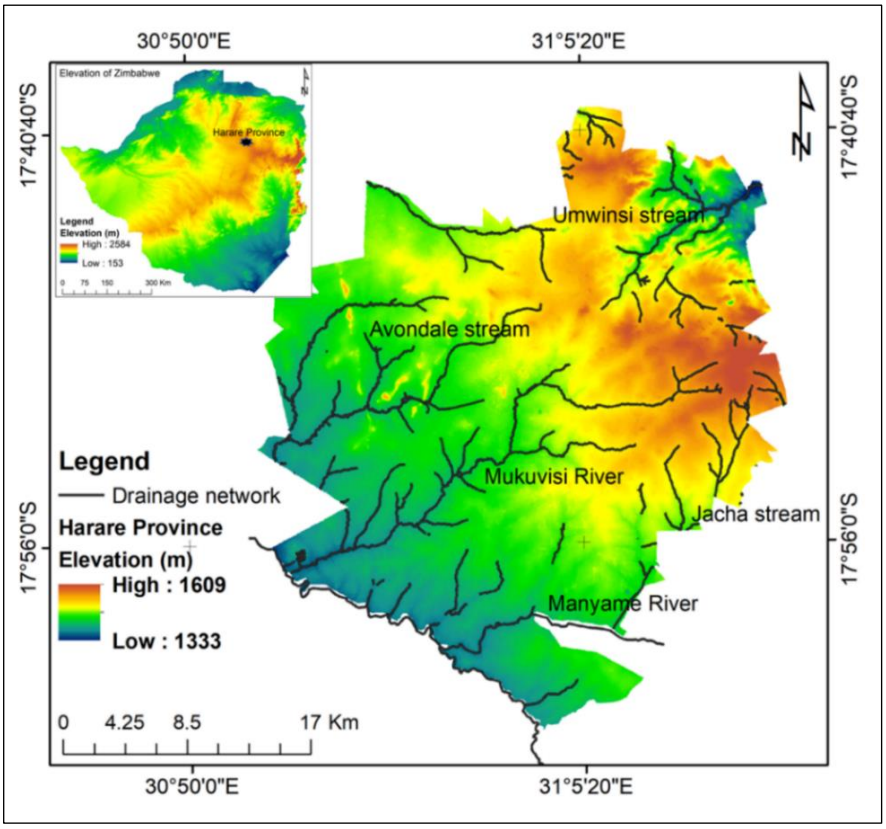

Figure 3. 2 General elevation variations of Zimbabwe. Small plate (**top left**) shows elevation of Zimbabwe; (b) the elevation and major drainage of the Harare Metropolitan Province in the main plate.

The Harare Metropolitan Province watershed embeds three micro-catchments of the Upper Manyame catchment in Zimbabwe (Figure 3.2). The micro-catchments include Manyame river, the mouth for Ruwa and Epworth drainage channels and downslope confluences with Nyatsime river, the Marimba which comprises of Anderson stream/Marimba river that drains from Marlborough suburb and from the University of Zimbabwe stream; and lastly, Mukuvisi river that headwaters from the east of the Harare province confluencing with several tributaries' downslope to the west. These micro-catchments of the Upper Manyame catchment experiences between 700 mm and 1000 mm of rainfall annually (Tibugari *et al.*, 2020) and are the headwaters of the Manyame river in Zimbabwe which drain into the Zambezi River basin (Rwasoka *et al.*, 2011). The micro-catchments consist of the CH4 and CH5 hydrological subzones estimated to have a mean annual runoff of 126 mm and 135 mm and evaporation rates for both subzones are estimated above 1600 mm yr^{-1} (Mazvimavi *et al.*, 2005). Gumindoga *et*

al. (2014) indicate that streamflow for Mukuvisi and Marimba sub-catchments increased regardless of land use changes between 1970 and 2006. The Marimba gauging station recorded increases in monthly average streamflow from 7.55 m^3 in 1970 to 35.01 m^3 in 2006 and the same increasing trend was recorded for Mukuvisi micro-catchment with a rise from 4.51 m^3 in 1970 to approximately 25.18 m^3 in 2006 (Gumindoga *et al*., 2014).

3.3 Soil and vegetation

The distribution of soil types varies spatially. It is dictated mainly by the parent material and factors including climate, biotic, topography and time (Nyamapfene 1991). These factors also contribute to soil's mineralogy, physical and chemical composition that influence its use and management. According to Nyamapfene (1991) soils of Zimbabwe are classified into four orders: Amorphic, Cacimorphic, Kaolinitic and Natric. Soil orders are divided into groups or families, the amorphic constitute lithosol and regosol; calcimorphic include vertisol and siallitic; kaolinitic has fersiallitic, paraferralitic and the orthoferrallitic and finally, the natric order constitutes only the sodic (Nyamapfene 1991; Thompson and Purves 1978). The fersiallistic and paraferrallitic soils of the kaolinitic order occur in Harare Metropolitan Province (Figure 3.3) (Nyamapfene 1991).

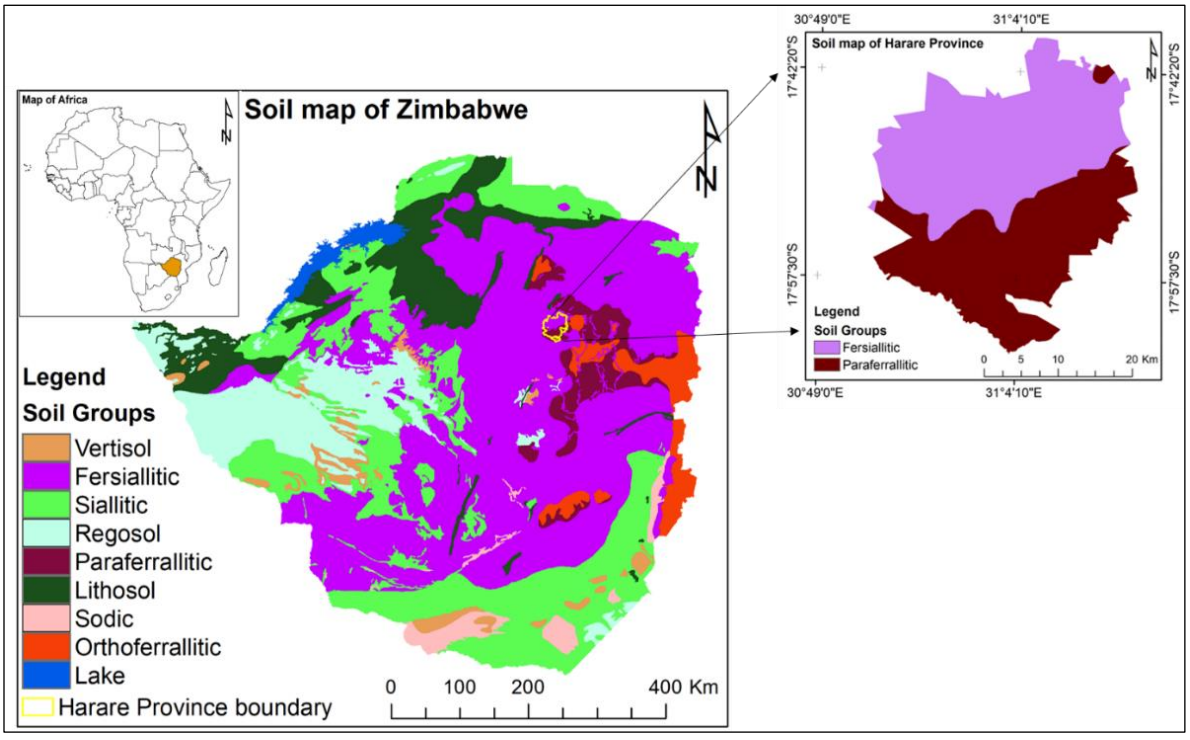

Figure 3. 3 Soil map showing the distribution of the dominating soil types. In plate (**a, Bottom Left**) soil distribution for the entire Zimbabwe and plate (**b, Top right**) soil distribution across the Harare Metropolitan Province. *Source:* (Nyamapfene 1991).

The clayey fersiallitic soils are moderately leached soils that occur in contact zones predominantly to the north or upper parts of the Harare Metropolitan Province and paraferrallitic soils are highly leached soils distributed largely to the south with little proportion of the paraferrallitic soils occurring on the northeast of the Harare Metropolian Province (Figure 3.3). The igneous and metamorphic mafic bedrocks form the parent material for the clay rich fersiallitic soils whilst paraferrallitic soils are predominantly coarse-grained sandy soils comprising proportions of inert clays derived from granites and the gneissic granites (Nyamapfene 1991; Thompson and Purves 1978). Both paraferrallitic and fersiallitic soil families are suitable for agricultural activities due to their mineralogy, however they require management practices according to crop requirements including lime amendments for the paraferrallitic soils (Nyamapfene 1992).

Whitlow (1988) highlights that human activities in Zimbabwe have caused massive loss of natural vegetation and this corroborates with recent studies for the Harare Metropolitan Province (Kamusoko *et al*., 2013; Mushore *et al*., 2017; Wania *et al*., 2014). That is, expansion of built-up area as a result of population and economic activities on the rise attributes to the declining vegetation across the province including the densely vegetated northern suburbs (Mushore *et al*., 2017). For Harare Metropolitan Province, the dominant vegetation consists of shrubs and grass which continuously extend on open areas and the savanna woodlands predominantly constituting of the *Brachsygestia spiciformis* (musasa; igonde) and *Julbernadia globiflora* (munhodo; ishungu) with wide canopies overshadowing grasslands (Whitlow 1988). The spatial distribution or existence of the savanna woodlands in the Harare Metropolitan province follows high rainfall received and the occurrence of sandy soils of the kaolinitic order that has good drainage. Only remnants of the dominant savanna woodland across the province have thrived under harsh anthropogenic and different natural factors such that species diversity reference for the Harare's vegetation has been conserved in protected areas for example in Mukuvisi woodlands, Catholic University of Zimbabwe, Cleveland woodland, Scientific and Industrial Research Development Centre (SIRDC) and the Zimbabwe Parks and Wildlife Management Authority (Mpindu 2018).

3.4 Climate

The climate of Zimbabwe is sub-tropical with four distinct seasons influenced primarily by the Intertropical Convergence Zone (ITCZ) and subtropical anticyclones (Brazier 2015; Manatsa and Mukwada 2012). The collision of warm moist air masses moving from the north and cool

air masses moving from the south contribute to the creation of Zimbabwe's rainfall seasons (Brazier 2015). However, due to Zimbabwe's complexity of climate and physiography the reliance on ITCZ and subtropical anticyclones have greatly influenced the spatial variability and coherence of rainfall across the country. This has been deemed reliable due to its non-randomness approach on different time scales of the year (Manatsa and Mukwada 2012). As a result of distinct rainfall seasons Zimbabwe was divided into 5 agro-ecological zones/natural regions (NRs) based on the areas suitability to rainfed agriculture and the NRs were classified from 1 most suitable to 5 least suitable (Manatsa and Mukwada 2012; Vincent *et al*., 1960). The global climate change major shifts on climate variables temperature and precipitation have been observed to contribute and mimic the unprecedented impacts across the globe. This prompted the revision of agro-ecological zones for the third time in Zimbabwe following second revisions by the Agritex of Zimbabwe in 1984 which omitted the effects of climate change such that the newly revised agro-ecological zones of 2020 gave large reference to the first agro-ecological zones derived by Vincent and Thomas (1960).

A major shift on both rainfall and temperature regimes were observed from 1982 to 2017 against the pre-shift phase between 1951-1981 (Figure 3.4) (Manatsa *et al*., 2020). The cumulative sum technique (CUSUM) applied by Manatsa *et al.* (2020) led to the establishment of the shift year on rainfall patterns (amount and distribution) received in comparison to the pre-shift period between 1951-1981 (Figure 3.4). The revealed shift year on rainfall concurs with significant temperature changes observed from 1982 in relation to prior temperatures recorded between 1951-1981 against the shift between 1982-2017 applying the Regime Shift Detector (RSD) technique (Manatsa *et al*., 2020). Thus far, observed shifts on climate positively contributed to the redefining of Zimbabwe's NRs from the years 1982-2017.

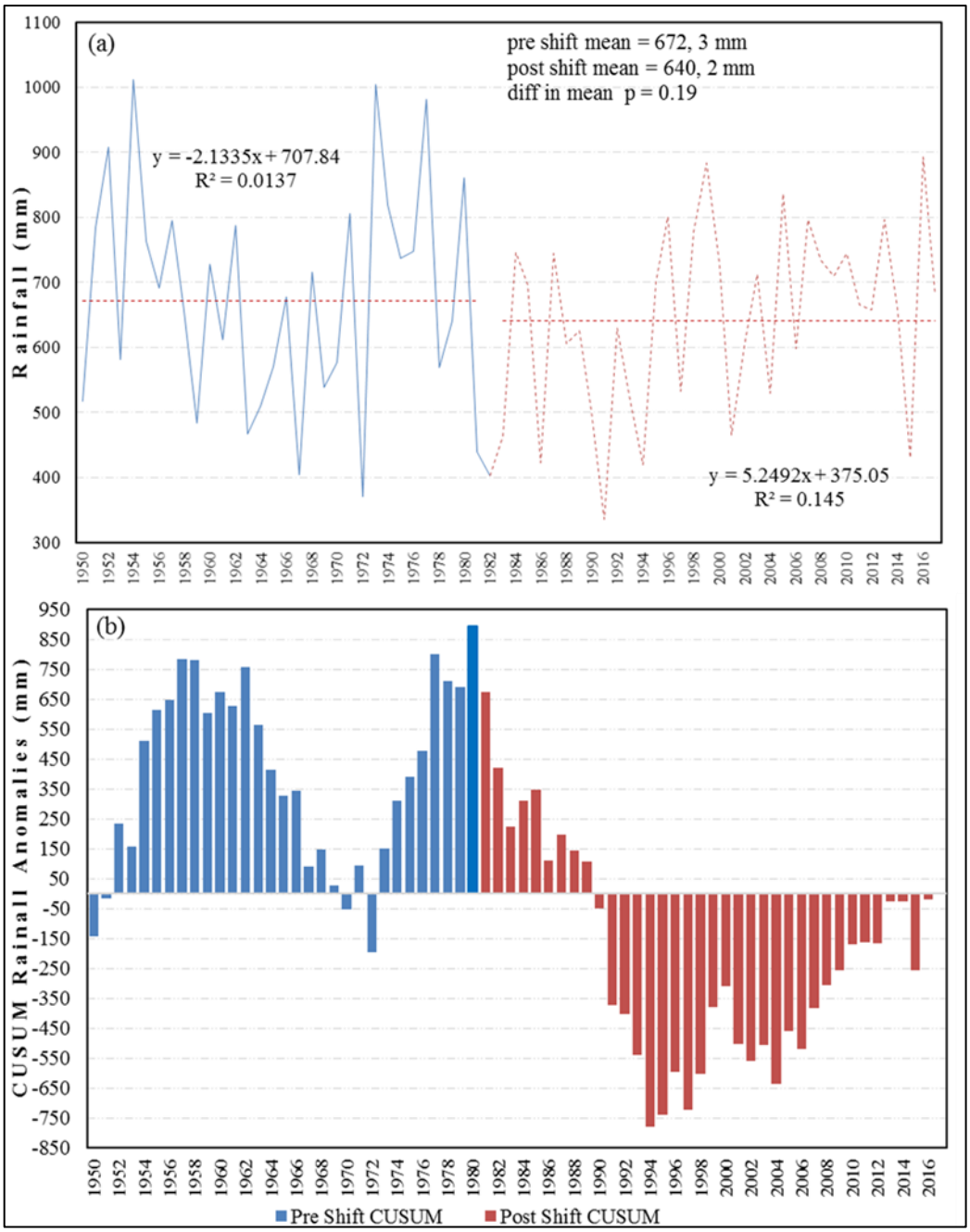

Figure 3. 4 Zimbabwe annual rainfall patterns evaluations from 1950 to 2017 based on the months October to March. (**a**) Total annual rainfall and (**b**) CUSUM based analysis highlighting total observation variations from the average of the same interval against time. *Source:* (Manatsa et al. 2020)

The delineation of new agro-ecological zones (AEZs) reflects the extent and impacts of climate change on national climatology as observed by the increase in aridity on region 5, the increase in consecutive dry days, shrinking of rainfall season with almost 30 days across the country with the exception of the Eastern highlands experiencing rainfall season extension by approximately 15 days (Manatsa *et al.*, 2020). The traditional climate seasons include: a cool–dry season from mid-May to August; a hot–dry season from September to mid-November; a rain–wet season from mid-November to mid-March; and a post rainy season stretching from

mid-March to mid-May (Kamusoko *et al*., 2013; Mushore *et al*., 2017). During the cold–dry season, temperatures range from 7 ˚C to 20 ˚C, while during the hot–dry, season temperatures range from 13 ˚C to 28 ˚C. On average, the Eastern highlands receive above 1500 mm of rainfall annually while dry parts in the south and west of Zimbabwe receive mean annual rainfall less than 500 mm per annum now classified as AEZs Va & Vb formerly NR V the least suitable for rainfed agriculture (Figure 3.5).

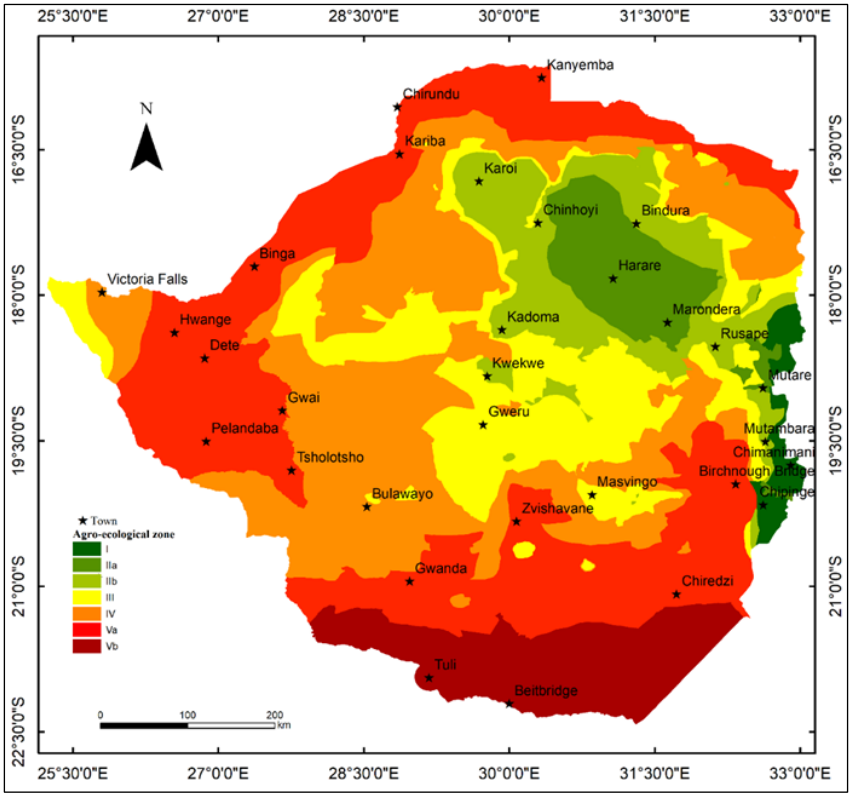

Figure 3. 5 The Agro-Ecological Zones of Zimbabwe. *Source*: (Manatsa *et al.,* 2020)

The Harare Metropolitan Province receives mean annual rainfall between 470 mm to 1350 mm. The observed data recorded at Harare Meteorology Services shows that mean monthly rainfall sharply increased from 32 mm in October to approximately 215 mm in January followed by a steady decline to almost 119 mm in March for the years 1984 to 2018. The post rainfall season and dry periods of the year markedly recorded declining mean monthly rainfall ranging from 30 mm in April to relatively 2 mm between July and September. The long dry period therefore makes soils vulnerable to erosion processes especially from the early rainfall received at the beginning of wet season due to reduced vegetation cover and land preparation processes for urban agricultural practices.

Marondedze, A.K.; Schütt, B. Dynamics of Land Use and Land Cover Changes in Harare, Zimbabwe: A Case Study on the Linkage between Drivers and the Axis of Urban Expansion. Land ***2019***, 8, *155. https://doi.org/10.3390/land8100155.*

CHAPTER 4: MAPPING BUILT-UP AREA AND AXIS OF URBAN EXPANSION USING MULTISPECTRAL REMOTE SENSING AND STATISTICAL MODELLING USING BINARY LOGISTIC REGRESSION

Abstract

With increasing population growth, the Harare Metropolitan Province has experienced accelerated land use and land cover (LULC) changes, influencing the city's growth. This study aims to assess spatiotemporal urban LULC changes, the axis, and patterns of growth as well as drivers influencing urban growth over the past three decades in the Harare Metropolitan Province. The analysis was based on remotely sensed Landsat Thematic Mapper and Operational Land Imager data from 1984–2018, GIS application, and binary logistic regression. Supervised image classification using support vector machines was performed on Landsat 5 TM and Landsat 8 OLI data combined with the soil adjusted vegetation index, enhanced built-up and bareness index and modified difference water index. Statistical modelling was performed using binary logistic regression to identify the influenceof the slope and the distance proximity characters as independent variables on urban growth. The overall mapping accuracy for all time periods was over 85%. Built-up areas extended from 279.5 km^2 (1984) to 445 km^2 (2018) with high-density residential areas growing dramatically from 51.2 km^2 (1984) to 218.4 km^2 (2018). The results suggest that urban growth was influenced mainly by the presence and density of road networks.

Keywords: urban growth; built-up area; Harare Metropolitan Province; binary logistic regression; support vector machines

4.1 Introduction

Temporally and spatially, urbanization is an uneven process supporting residential expansion, including growth in population size of individuals living in urban areas and expansion of physical structures in an urban setup in addition to the previously existing structures (Alaci 2019; Samson 2009). Urbanization is directly changing and affecting the environment, as it is made distinct by the increasing built-up and impervious areas at the expense of wetland areas and agricultural landscapes. Such actions result in the transformation of natural landscapes into agricultural landscapes (Adebowale and Kayode 2015). Consequently, this leads to environmental degradation through deterioration of vegetation and sealing, often resulting in increasing surface runoff, soil erosion, surface water contamination, and exploitation of natural habitats (Müller *et al*., 2013; Owoeye and Popoola 2017; Satterthwaite 2008; Sayemuzzaman and Jha 2014). Muller *et al*. (2013) highlights that urbanization is one of the greatest factors contributing to biodiversity loss due to the expansion of industrial, residential and commercial business areas.

The world's population is projected to increase from 7.0 to 9.3 billion by 2050 (UN 2012). Therefore, during that stipulated period urban areas worldwide are anticipated to absorb large numbers of the growing population. Urbanization is a continuous process, and megacities such as Delhi, India had a total increase in population of 47.02% within a decade between 1991 and 2001 (Mohan *et al*., 2011). For China, the urbanization growth rate tripled

from 17.9% to 57.4% between 1978 and 2016, and it is projected to reach 70% by 2035 (Yu *et al*., 2019). Although countries like Ethiopia are among the least urbanized countries in the world, high rates of in-migration to urban cities have been investigated and projected to reach 42.1% of the total population by 2050 (UN HABITAT 2007). Up-to-date data and information regarding the trends and status of urban ecosystems are required to enable the development of sustainable strategies on improving livelihoods in urban settings. In particular, in sub-Saharan Africa, up-to-date data and information on population are fundamental for developing ways to curb urban demographic transitions (Lohnert 2017). It is estimated that sub-Saharan Africa's urban population will rise by 60–70% by 2050, with most people occupying small cities due to the fact of cultural, socio-economic and political influences (AfDB 2016; Lohnert 2017). Although previous studies have indicated urban growth in terms of population size, studies on landuse and land cover (LULC) changes and the key drivers of such changes remain scarce yet important.

To further understand the relationship between urbanization and environmental alteration, LULC changes need to be assessed and evaluated to determine the extent and the rate at which human activities are contributing to shifts in the environment. The integration of remote sensing data to monitor the state and dynamics of the Earth's surface provides reasonable results in a short space of time (Owoeye and Popoola 2017), compared to on-site surveying techniques (Malaviya *et al*., 2010; Punia and Singh 2012). Moderate resolution Landsat Thematic Mapper images (TM) are a standard tool used for urban mapping and change detection analysis andwere used, for example in Minnesota, USA between 1986 and 2002 for LULC changes (Yuan *et al*., 2005). Landsat images in combination with socio-economic data have been used to determine the effects associated with development and land use shifts. For example, spatial dynamics of LULC changes were analyzed for the Nairobi urban area and showed that the built-up area quadrupled from 1.9% in 1976 to 8.6% of the total area in 2000 (Mundia and Aniya 2005). For Zimbabwe, Hove and Tirimboi (2011) indicated that on a national scale, vast numbers of people migrated to Harare from rural homes soon after independence in 1980. Wania *et al.* (2014) reported on the expansion of built-up areas of Harare using high-resolution SPOT images.

Investigation of LULC change dynamics and classification in heterogeneous landscapes using moderate-resolution satellite imagery potentially has challenges due to the fact of spectral confusion resulting in misleading informationn (Abdullah *et al*., 2019; As-syakur *et al*., 2012). Accurate observation of LULC changes by remote sensing is a vital component of promoting sustainability. Enhancement of land cover class delineation using remote sensing

indices and machine learning algorithms such as random forest (RF) and support vector machines (SVMs) have the relatively desirable characteristic of improving multispectral classification (Abdullah *et al*., 2019; As-syakur *et al*., 2012; Nooni *et al*., 2014). The effectiveness of mapping land-cover types using spectral indices is primarily the result of their ability to characterize relative features of interest over a wide range of the spectrum (Faridatul and Wu 2018). The Harare Metropolitan Province was chosen as a case study because of its vastly reported pressures due to the presence of high population and urbanization rates for this metropolitan area in the northern High Veldt of Southern Africa (Kamusoko *et al*., 2013; Wania *et al*., 2014). Harare Metropolitan Province, being the capital city of Zimbabwe, faces increasing population growth as do other metropolitan cities largely because they are associated with better livelihoods and as centres for economic activities, public services, and amenities (Hegazy and Kaloop 2015; Sinha *et al*., 2016). Among others, Chirisa and Muhomba (2013) revealed that Epworth, a Harare Metropolitan Province district, has approximately 70% of its inhabitants living on unauthorized, non-serviced land and thereby compounding the increased settlement and spread of the metropolitan area. Thus far, monitoring urban growth trends is an important tool for understanding previous trends and present growth patterns and potentially unravelling possible coming developments and their likely impacts (Moghadam and Helbich 2013). Identifying empirical drivers of urban structure change is based on past and current state of LULC changes for the Harare Metropolitan Province. The current study aimed to investigate the axis of change and expansion of the Harare Metropolitan Province. In view of the resource constraints in a developing country, freely available remote sensing data were applied to assess the direction of the urban expansion. Furthermore, the study sought to determine the explanatory drivers of the changes in LULC for the Harare Metropolitan Province.

4.2 Materials and Methods

4.2.1 Study area

The study area lies between 17°49’39.79” south latitude and 31°03’12.13” east longitude and covers three districts of the Harare Metropolitan Province (Figure 4.1) (Kamusoko *et al*., 2013; Mushore *et al*., 2017). Harare is the capital city of Zimbabwe and experiences high urbanization rates from rural–urban shifts, driven by those in search of better livelihoods and employment (Potts 2011; Tibaijuka 2005). The bedrock in Harare Metropolitan Province are granites in the east and southwest and gabbro and dolerite in the north, while phyllite and metagreywacke

dominate the core centre of the Harare Metropolitan Province (Anderson *et al*., 1993; Kamusoko *et al*., 2013; Nyamapfene 1991). The relief is slightly rolling with locally U-shaped incised valleys. Bedrock is widely covered by several decimetre-thick saprolite which is characterized by cyclic surface erosion that exposes bedrock (Lister 1987).

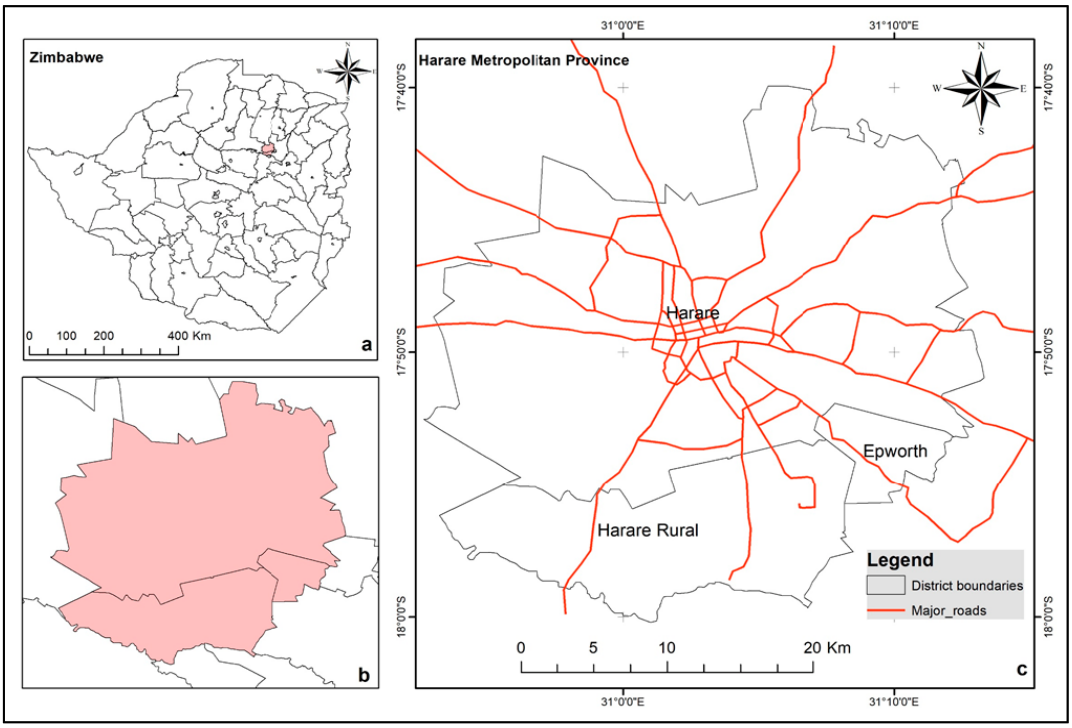

Figure 4. 1 Location of the Harare Metropolitan Province composed of the Harare urban, Harare rural, and Epworth districts. (**a**) Zimbabwe district boundaries highlighting the study area; (**b**) Harare Metropolitan Province study boundaries; (**c**) major roads marked in the Harare Metropolitan Province map indicating the major urbanization axis.

The climate is sub-tropical with four seasons: a cool–dry season from mid-May to August; a hot–dry season from September to mid-November; a rain–wet season from mid-November to mid-March; and a post rainy season stretching from mid-March to mid-May (Kamusoko *et al*., 2013; Mushore *et al*., 2017). During the cold–dry season, temperatures range from 7 ˚C to 20 ˚C, while during the hot–dry, season temperatures range from 13 ˚C to 28 ˚C. On average, the Harare Metropolitan Province receives annually 470 mm to 1350 mm of rainfall, most of it during rainy season (Kamusoko *et al*., 2013). In the Harare Metropolitan Province, the Harare urban district was estimated to have a population of 1,435,784 in 2002 and 1,485,231 in 2012; for the Harare rural district, a population of 23,023 in 2002 and 113,599 in 2012; and for the Epworth district, a total population of 114,047 in 2002 and 167,462 in 2012 (CSO 2004; ZimStats 2012). The total area of the Harare Province, in which the study area was embedded, extends over 940 km^2 (Wania *et al*., 2014).

4.2.2 Data acquisition and pre-processing

Cloud-free Landsat satellite images of 30 m × 30 m resolution were acquired from the United States Global Survey (USGS; www.earthexplorer.usgs.gov). These Landsat satellite images were selected because of their adequacy and availability for LULC classification, as indicated by multiple studies (among others, (Patley *et al*., 2018; Yuan *et al*., 2005)). Landsat 5 Thematic Mapper images were selected for the years 1984, 1990, 2000, 2008 and Landsat 8-OLI image for the year 2018 (Table 4.1).

Table 4.1 The Data used for land use and land cover (LULC) classification and their date of acquisition.

Sensor	Number of Bands	Path/Row	Date of Acquisition
Landsat 5 TM	7	172/072	22 June 1984
Landsat 5 TM	7	172/072	23 June 1990
Landsat 5 TM	7	172/072	30 August 2000
Landsat 5 TM	7	172/072	11 August 2008
Landsat 8 OLI	11	172/072	11 August 2018

All satellite images were acquired for the cool–dry season with completely clear (0%) cloud-free coverage. All satellite images were geometrically corrected using topographic sheets at 1:50,000 and applying 20 ground control points collected using a handheld GPS (Garmin 60Cx) at major road intersections. First-order polynomial transformation was used for the retrieved satellite image scenes and the obtained root mean square errors (RMSEs) were less than half the pixel dimensions. A projected vector map for Harare Province was used to clip the study area from the pre-processed images for classification and modelling. Images provided by the USGS were already corrected for radiometric distortions. Resampling was done using the nearest-neighbourhood technique in order to retain the original pixel values. The QGIS 3.4 software was applied to further correct atmospheric distortions and conversion of digital numbers (DNs) to spectral reflectance through dark object subtraction (Chander *et al*., 2009). Prior conversion of DNs to reflectance urban indices were computed using RStoolbox, a package in R, and then further computation of vegetation indices.

4.2.3 Field data collection and processing

During field observations in December 2018, the LULC class structure (Table 4.2) was determined.Field data were collected, recording randomly 600 land cover sample points using a handheld GPS (Garmin 60Cx). The points were randomly split into two sets: 80% of the data for training and 20% of the data for accuracy assessment and validation (Mushore *et al*., 2017). Polygons (regions of interest (ROIs)) were digitized and used for both LULC classification and accuracy assessment to improve classification and validation range (Chemura and Mutanga 2017).

Table 4.2 Description of the study LULC classes.

ID	LULC Class	Description
1	CBD/Industries	Industries and central business district defined with high fraction of impervious surfaces mainly buildings and little proportion of vegetation
2	LMD residential	Leafy and well established low and medium density suburbs surrounded with high vegetation
3	HD residential	High density residential areas with low vegetation cover or clustered settlements with areas undergoing developments and bare exposed land
4	Irrigated cropland	Cultivated land under irrigation schemes
5	Rainfed cropland	Cultivated land or land with crop residues after harvesting
6	Vegetation	All wooded areas, shrubs and bushes, riverine vegetation and grass covered areas
7	Water	Areas occupied by water, rivers, wetlands, reservoirs and dams

*CBD: central business district *LMD: low to medium density *HD: high density

Statistical testing of spectral separability of the desired classes was verified using the transformed divergence separability index (TD) to ensure classification (Castillejo-González *et al*., 2014). Figure 4.2 documents the approach and flow path used in the study. Topographic maps, expert knowledge and auxiliary data were used to create ground truth areas of interest for Landsat images from 1984, 1990, 2000 and 2008 for classification and accuracy assessment. Field observations and ground control points (GCPs) were obtained for 2018 time slices.

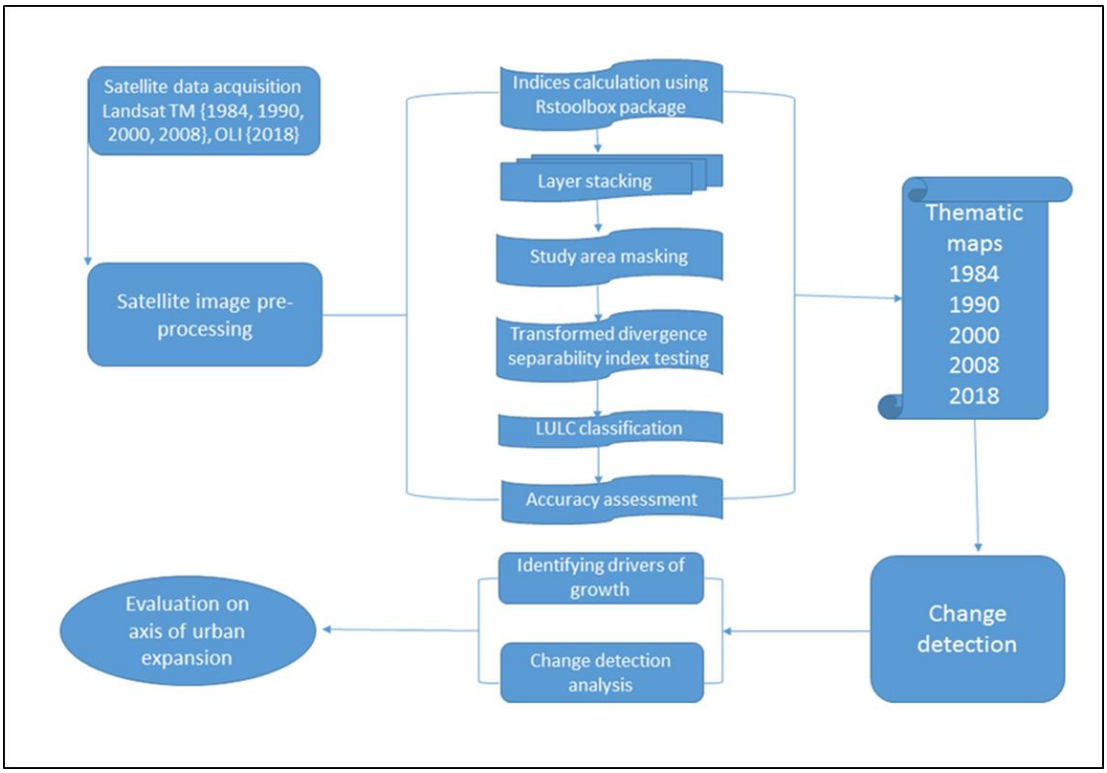

Figure 4. 2 Flow chart showing the determination of drivers and the axis of urban expansion for Harare Metropolitan Province.

4.2.4. Land cover classification

The LULC maps were created for the years 1984, 1990, 2000, 2008 and 2018 using supervised support vector machine (SVM) algorithms on 30 m band stacks for each image scene and an additional three layers applying different indices: enhanced built-up and bareness index (EBBI), modified normalized difference water index (MNDWI) and soil adjusted vegetation index (SAVI) for all stacks. These additional band stacks enhanced the mapping of the major urban LULC cover classes, namely, built-up, open water body and vegetation (Mwakapuja *et al*., 2013; Sinha *et al*., 2016). Support vector machines correspond to machine learning classification methods which have a high ability to minimise misclassification errors by reducing the probability of misclassifying field data collected having an unknown probability distribution (Vapnik 1998). Each image was classified into seven classes that were determined by spectral characterization and field data substantiated training and accuracy assessment.

An accuracy assessment was computed for the Kappa coefficient (Kc), overall accuracy (OA), producer's accuracy (PA) and user's accuracy (UA), applying "ground truth regions of interests" (Chemura and Mutanga 2017; Congalton 1991). Accuracy assessment is a probabilistic approach that computes the association between remotely sensed and referenced data. Post classification change detection matrices were cross tabulated in ENVI using five

interval steps: 1984–1990, 1990 2000, 2000–2008, 2008–2018 and 1984–2018. The post classification change detection method involved pixel-by-pixel change analysis highlighting spatio-temporal LULC changes and distribution.

4.2.5 Computation of spectral indices

Enhancing spectral signals of overbuilt areas, vegetation and water in remotely sensed data was done through computation of multiple spectral bands (Sinha *et al*., 2016). The enhanced built-up and bareness index (EBBI), modified normalized difference water index (MNDWI) (Xu 2006) and soil adjusted vegetation index (SAVI) were selected to improve the extraction of major land-use classes in a heterogeneous urban built-up area. The EBBI allows mapping of built-up and bare areas using a combination of near infrared (NIR), short wave infrared (SWIR) and thermal infrared (TIR) on which these bands were selected according to the contrast reflection and absorption in bare and built-up areas (As-syakur *et al*., 2012) using Equation 4.1.

$$EBBI = \frac{SWIR1-NIR}{10\sqrt{SWIR1+TIRS1}} \quad (4.1)$$

The SAVI requires soil-brightness correction factor L, which varies from 0 for very high vegetation cover to 1 for very low vegetation cover; a 0.5 soil-brightness correction factor L was used because of its moderate (Huete 1988) following Equation 4.2.

$$SAVI = \frac{(NIR+R)}{(NIR+R+L)} x\ (1+L) \quad (4.2)$$

The MNDWI uses SWIR in enhancing open water extraction in a complex heterogeneous setup because of the high reflectance obtained in built-up areas to the spectral band. Henceforth, negative values for built up areas and positive values for water features makes the MNDWI suitable for discriminating built-up areas from water features (Sinha *et al*., 2016; Xu 2006).

$$MNDWI = \frac{GREEN-SWIR}{GREEN+SWIR} \quad (4.3)$$

4.2.6 Binomial logistic regression

A binomial logistic regression was applied to analyse the explanatory drivers of LULC changes. The form variable slope (˚) was used as a topographic factor, while the proximity characters factored in included distance to the main roads, distance to secondary roads, distance to open water bodies, distance to streams and distance from the city centre (Congalton 1991; Mwakapuja *et al*., 2013; Vapnik 1998). For the binomial regression, the growth variables

(dichotomous dependant) applied were raster layers with transformed cells from any LULC to built-up area between 1984 and 2018 (Figure A1). Proximity and topographic characters formed the basis of the independent variables (distance to the main roads, distance to secondary roads, distance to open water bodies, distance to streams and distance from the city centre). Distances were calculated using the Euclidean distance tool in ArcGIS 10.2 to determine the impact of urban expansion relating to the proximity of the selected features encompassing the road network for transportation and watercourses as environmental amenities.

The cell values of the dependant variable (dichotomous raster layer) which had been changed from any other LULC class to an urban built-up area for all time steps (i.e., 1984–1990, 1990–2000, 2000–2008, 2008–2018, 1984–2018) were set to be urban growth (=1), while all cells which did not change to an urban built-up area or had been an urban built-up area previously were set as non-urban growth (=0) using the raster calculator in ArcGIS 10.2. A total of 7000 stratified random sample points were created to extract cell values from the LULC maps of all time slices for regression analysis and available sets of data. A collection of 6139 random sample points was assembled, and the remaining outliers were removed because they were scattered outside of the rasters. Extracted distance proximity parameter values were log-transformed and, during computation, a 30 m value equivalent to cell length was added to all cells in order to counter undefined 0 logarithm for predictors applied in the regression analysis (Anselm *et al*., 2018). The statistical significance of $p < 0.05$ indicated that the relation between predictor and LULC change occurrences were not random, highlighting a statistical relation between the independent proximity variable and an urban built-up area. The evaluation of model performance was calculated using statistical measures of the discriminatory effect of the model, the area under the receiver–operating–characteristic (ROC) curve (AUC) and the percentage of correct predictions (PCPs) (Herron 1999; Pontius Jr and Batchu 2003; Pontius and Schneider 2001).

Data for location characterization was retrieved from various sources. Open water and streams data were digitized from topographic maps (Herron 1999); trunk and secondary roads were extracted from OpenStreetMap data (OSM-Geofabric (Pontius and Schneider 2001)); and the digital elevation model (DEM) of the Shuttle Radar Topography Mission (SRTM) with a 30 m resolution was accessed from United States Geological Survey website (https://earthexplorer.usgs.gov/). Each data set was normalized into ranges from 0–1 using the min–max linear transformation by applying the raster calculator (Map Algebra) in ArcGIS so that all input data used the same range (Pontius Jr and Batchu 2003).

4.3 Results

4.3.1 Area extent and change of LULC

The data revealed an increase in the high-density residential areas and, consequently, a decrease in the area covered by vegetation all over the Harare Metropolitan Province (Figure 4.3, Figure 4.4, Table 4.3). In the year 1984, high-density residential areas covered 51.79 km^2 (5.81%) of the total Harare Metropolitan Province, while, by the year 2018, it had more than quadrupled reaching 218.35 km^2 covering almost a quarter of the Harare Metropolitan Province area. The data also showed a steady increase in central business department (CBD) or industrial areas from 3.7% in 1984 to 7.17% in 2018. In addition, coverage by low- to medium-density suburb areas steadily increased, covering 21.85% of the Harare Metropolitan Province in 1984 to 29.48% in 2018. Apparently, in 1984, vegetation covered almost half of the area (448.67 km^2) of the total Harare Metropolitan Province but decreased by nearly 50% to 223.45 km^2 (25.08%) by the year 2018 (Figure 4.3, Figure 4.4, Table 4.3).

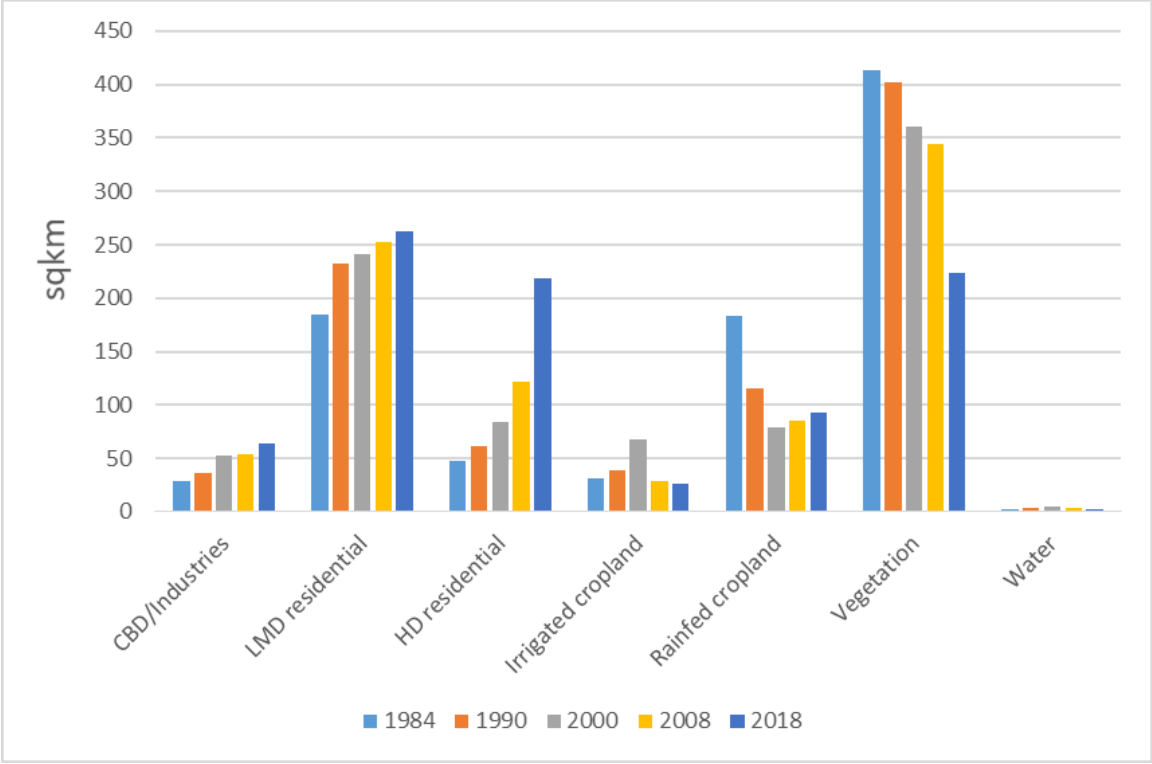

*CBD: central business district *LMD: low to medium density *HD: high density.

Figure 4. 3 Area sizes showing changes in the LULC classes in the Harare Metropolitan Province.

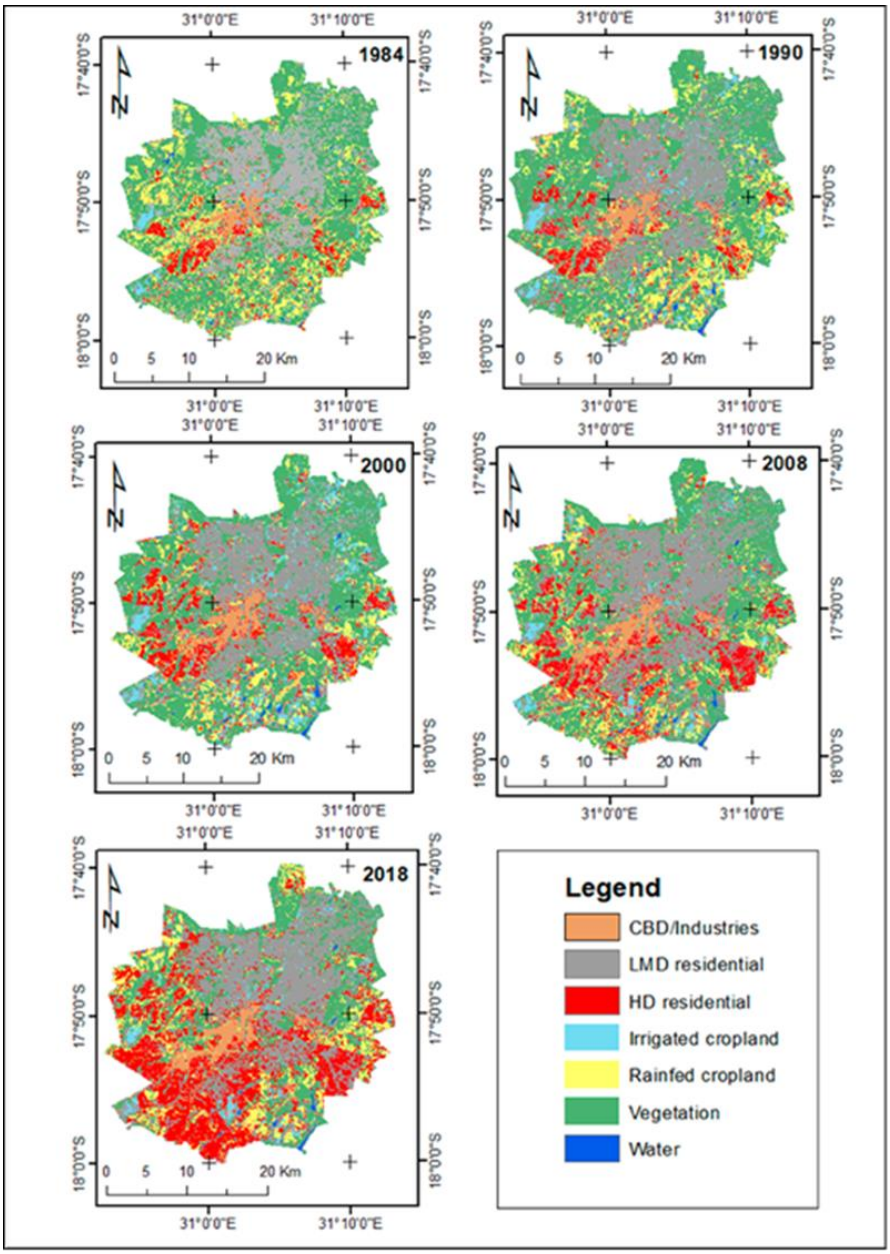

Figure 4. 4 Land use land cover in the Harare Metropolitan Province for the years 1984, 1990, 2000, 2008 and 2018.

The spread of croplands (combined irrigated and rain-fed croplands) decreased from a coverage of 17.89% of the Harare Metropolitan Province in 1984 to 13.40% in 2018. The areas covered by water slightly increased from about 0.40% in 1984 to 0.53% in 2000; however, this coverage declined sharply to 0.31% in 2018. Between 1984 and 1990, high-density residential areas were spreading towards the west and northwest of the city (Figure 4.4). Yet, between 1990 and 2018, a spread of urbanized areas can be seen towards the south, southwest, and southeast of the Harare Metropolitan Province (Figure 4.4). In addition, low- to medium-density suburbs expanded towards the northeast of the Harare Metropolitan Province, increasing from 21.85% in 1984 to almost 30% of the area in 2018 (Figure 4.4; Table 4.3).

Table 4.3 Net change of the LULC by class area extent (km^2) and percentage (%) of the Harare Metropolitan Province.

LULC Class	1984		1990		2000		2008		2018	
	Km^2	%	Km^2	%	km^2	%	Km^2	%	Km^2	%
CBD/Industries	32.95	3.70	36.27	4.07	52.98	5.95	54.27	6.09	63.88	7.17
LMD residential	194.72	21.85	233.02	26.15	241.53	27.11	252.48	28.33	262.74	29.48
HD residential	51.79	5.81	61.13	6.86	84.61	9.49	121.96	13.69	218.35	24.50
Irrigated cropland	18.13	2.04	39.30	4.41	67.77	7.61	28.55	3.20	26.68	2.99
Rainfed cropland	141.26	15.85	115.74	12.99	79.34	8.90	85.42	9.59	93.26	10.47
Vegetation	448.67	50.35	401.88	45.10	360.13	40.41	344.48	38.66	223.45	25.08
Water	3.60	0.40	3.78	0.42	4.76	0.53	3.96	0.44	2.76	0.31

*CBD: central business district *LMD: low to medium density *HD: high density.

4.3.2. LULC classification accuracy

For each time slice 1984, 1990, 2000, 2008 and 2018, each LULC class was compared to the reference data for classification accuracy assessment. The overall accuracy (OA) of the LULC classification varied for the different time slices between 85%–90% (1984: 90.1%, 1990: 85.1%, 2000: 88.9%, 2008: 87.6%, 2018: 89.7%; Table 4.4). The high separability indices produced were due to the enhancing effects from the vegetation and enhanced built-up and bareness indices incorporated and displayed improved mapping accuracy. The transformed divergence separability index (TD) indicates that if values are greater than 1.9, separability among classes will be very high showing that classes are separable, while values smaller than 1.0 are deemed not statistically separable for good classification (Chemura and Mutanga 2017). The highest misclassifications were recorded for the LULC classes, such as high-density residential areas (all time slices), irrigated cropland, and rain-fed cropland (1990), as indicated by the producer´s accuracy (Table 4.4, Table A1, Table A2).

Table 4.4 Land use and land cover classification accuracies in percentages for the study period 1984–2018. The accuracies include Kappa coefficient (Kc), overall accuracy (OA), producer's accuracy (PA) and user's accuracy (UA).

	1984		**1990**		**2000**		**2008**		**2018**	
LULC Class	PA	UA	PA	UA	PA	UA	PA	UA	PA	UA
CBD/Industries	94.7	93.7	99.2	93.7	96.7	90.3	96.4	96.4	96.6	95.3
LMD residential	89.4	90.2	81.9	87.3	87.4	92.4	84.5	75.5	84.1	84.6
HD residential	82.2	85.0	77.7	93.3	83.4	89.9	79.8	83.5	92.9	92.5
Irrigated cropland	87.6	95.1	78.4	91.9	76.2	82.3	93.0	87.4	84.4	83.3
Rainfed cropland	84.1	87.2	67.4	80.5	85.6	79.0	90.9	79.6	86.8	88.7
Vegetation	93.4	90.1	92.9	71.1	90.2	82.4	79.1	91.8	88.9	88.9
Water	89.3	96.9	98.4	100	97.3	99.5	98.9	99.8	99.2	100
OA	90.1		85.1		88.9		87.6		89.7	
Kc	0.87		0.82		0.86		0.85		0.87	

*CBD: central business district *LMD: low to medium density *HD: high density

4.3.3 Binomial logistic regression

The value of the area under the receiver–operating–characteristic (ROC) curve (AUC) shows the discriminatory effect of the model and statistically validates the predictive urban growth drivers' behaviour (Pontius and Schneider 2001). The predictive effect of the AUC ranges from 0.5 to 1, where 0.5 shows a completely random relationship and 1 shows that the model has a perfect discriminatory effect. The true positive rate (TPR) is the proportion of cells which are correctly classified and the false positive rate (FPR) is the proportion of incorrectly classified cells by the real urban growth occurrences (Anselm *et al.*, 2018; Pontius and Schneider 2001). The percentage of correct predictions (PCPs) shows the percentage of correctly predicted points from the total number of available points (Herron 1999; Schubert *et al.*, 2018). The PCPs range from 0 to 1, where values greater than 0.5 (50%) indicate that the model predicts the outcome better than PCP closer to 0 (Herron 1999).

Between 1984 and 1990, the AUC amounted to 0.679 (Figure 4.5) and, according to the regression coefficients, a significant influence from the nearest distance to major and secondary roads was only revealed among all other test predictors. The p-values for the predictors distance to the city centre, distance to the stream, distance to open water, and for variable slope were not significant ($p > 0.05$), suggesting that they had no influence on the growth and spread of the urban built-up area. Between 1990 and 2000, the model reveals that the distance to major and secondary roads and the city centre were significant variables ($p < 0.05$) influencing the urban built-up area expansion with a discriminatory AUC value of 0.669 (Figure 4.5). Between 2000

and 2008, the predictors nearest distance to major and secondary roads, distance to the city centre and distance to open water and slope were significant ($p < 0.05$) in the binomial logistic regression model showing that they had influence on urban built-up area expansion with an overall AUC value of 0.683 (Figure 4.5).

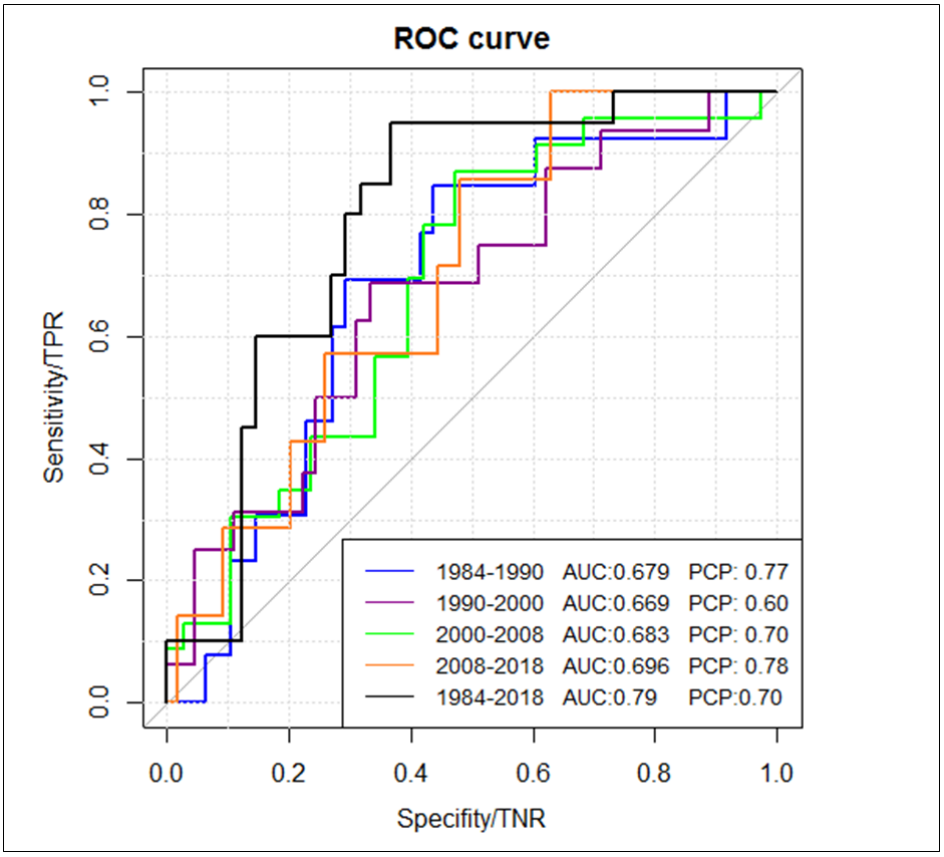

Figure 4. 5 Receiver–operating–characteristic (ROC) curves conveying binomial logistic regression analyses results for Harare Metropolitan Province growth from 1984 to 2018. TPRs: true positive rates; TNRs: true negative rates; AUC: area under the curve; PCPs: percentage of correct predictions.

Distance to the nearest roads, distance to the nearest streams, open water and slope were statistically significant as predictors of the urban built-up area expansion and spread ($p < 0.05$) between 2008 and 2018, with an AUC value of 0.696 (Figure 4.5). The nearest distance to the city centre predictor was not significant ($p > 0.05$). From 1984 to 2018, distance to the nearest major and secondary roads, streams, open water and slope were significant predictors to explain the urban built-up area expansion with an AUC value of 0.79 (Figure 4.5). The influence of the distance to the city centre as a predictor for urban built-up area expansion decreased due to the increasing outward expansion and spread of the Harare Metropolitan Province towards its peripheries.

4.4 Discussion

Urbanization has modified the Harare Metropolitan Province through the expansion of built-up areas at the expense of vegetation, cropland and water bodies (Figures 4.3 and 4.4). Similarly, urbanization processes investigated in Daqahlia, a city in Egypt, depicted that the built-up area expanded from 4.2% of the area under investigation in 1985 to 36.3% in 2010, while areas used as cropland shrank by 30.7% and areas covered by water decreased by 0.45% (Hegazy and Kaloop 2015). An increase of 219.5% in LULC change, mainly attributed to land development at the expense of cropland, fallow land, water, shrub and bare land, was revealed in the Shanghai metropolis between 1997 and 2008 showing the impact of land use change and population growth in urban areas (Zhang *et al*., 2013). Akure city in the southwest of Nigeria experienced a similar loss of areas covered by vegetation and water bodies as the Harare Metropolitan Province due to the fact of built-up area expansion, from 5.1% in 1986 to 53.41% in 2014 for the total area under investigation (Owoeye and Popoola 2017).

In the current study, a SVM classification method was applied because it potentially produces better accuracy in a confusion matrix compared to other neural networks, maximum likelihood and decision trees when mapping LULC (Schubert *et al*., 2018; Zhang *et al*., 2013). However, possible sources of error in the calculations may have emerged from geometric rectification, accuracy in digitizing topographic maps and combining different data sources. The spectral differences and characteristics between Landsat 5 TM and Landsat 8 OLI sensors may have affected the accuracy of the thematic maps (Chemura and Mutanga 2017). Despite these potential discrepancies, the classification and results obtained in the current study have relatively high accuracy considering urban area spectral heterogeneity characteristics and spectral confusion from land cover classes, and the results agree with other published scientific studies carried out at the national and regional level (Hegazy and Kaloop 2015; Kamusoko *et al*., 2013; Owoeye and Popoola 2017; Sinha *et al*., 2016). The use of hyper-spectral data and aggregation of urban built-up areas have been observed to improve and enhance the analysis of remote sensing data in urban areas (Herold *et al*., 2003; Schubert *et al*., 2018). The utilization of additional built-up, water and vegetation remote sensing indices bands on the Landsat imagery scenes provide a substantial improvement in the mapping of an urban area using moderate-resolution imagery (As-syakur *et al*., 2012; Huete 1988; Xu 2006). However, misclassifications and reduction of areas covered by water bodies (water class) might have resulted from the increasing density of water hyacinths along the streams due to the fact of contaminated sewage effluents deposited in the water ecosystem (Herold *et al*., 2004; Kucsicsa and Grigorescu 2018). This is directly linked to the inflow of effluents from industries; sewage

disposal (punctual sources) and urban agriculture (diffuse sources). Consequently, alteration of water bodies as aquatic weeds scattering on the surfaces potentially influences classification (Table 4.4).

The current study looked at the axis of urban development and the drivers posing LULC changes. This study revealed that the distance to the nearest major and secondary roads have a large impact on urban expansion and development. The binary logistic regressions highlight that built-up area development occurred predominantly along the major roads and in dense road network areas (i.e., secondary roads), due to the high connectivity and easy access to transport facilities. Hegazy and Kaloop (2015) reiterate that urban growth follows development along highways or already established cities as a result of population growth and socioeconomic factors. Nevertheless, high-density residential areas are expanding towards the periphery of the south, southeast, southwest and northwest of Harare Metropolitan Province. For comparison, the results of modelling the distance characters in Bucharest were in line with the findings of the current study; major and secondary roads impact positively on urban growth and expansion of built-up areas (Kucsicsa and Grigorescu 2018). For Bucharest, however, independent variables such as distance to lakes and rivers were not significant, while for the Harare Metropolitan Province, these variables have significant influence, as revealed by the binomial regression analysis between 2008 and 2018. Henceforth, the exclusion of the core city of Bucharest from the Bucharest Metropolitan area could have reduced the ability of the model to detect some independent characters. Still the geographic location of the study areas, socioeconomic structure and population sizes are highly different.

The current study reveals that zones of urban area or built-up area expansion were associated with relatively gentle undulating slopes which can be attributed to low housing costs, cheap land acquired through housing schemes and informal urban settlements (Wania et al. 2014). The southwest part of the Harare Metropolitan Province was the main direction of urban spread between 1984 and 1990 (Figure A1). This was associated with the expansion from first old Harare high-density suburbs that were designated during the colonial period such as Highfields, Mufakose and Rugare, among others (Cumming *et al*., 1993). These areas are associated with high-density road networks, low costs and economic residential units compared to the low and medium density residential areas. Between 1990 and 2000, expansion of the Harare Metropolitan Province dominated much in the southwest, west and southeast (Figure 4.4, Figure A1). This expansion can be attributed to urban sprawling and rampant informal settling due to the presence of socio-economic factors in the eastern direction, that is, the Epworth suburbs and Dzivarasekwa extension introduced in 1991 (Araya and Cabral 2010;

Zinyama 1995). Between 2000 and 2008, significant expansion of built-up areas was directed towards the south and northwest direction (Figure 4.4, Figure A1) regardless of "Operation Murambatsvina" (Restore Order), a clean-up campaign that was carried out in June 2005 and left Harare with dismal identifiable illegal, urban built-up structures (Tibaijuka 2005).

The expansion of Harare Metropolitan Province between 2008 and 2018 was dominant in the southern direction, and the city was expanding towards its peripheries (Figure 4.4, Figure A1). The far continued expansion towards the southeast resulted from unplanned urban development because of population pressure (Chirisa and Muhomba 2013). Bureaucracy and rigid and stringent procedures relating to construction plans approval by local authorities posed a hindrance towards sustainable urban growth (Chirisa 2014; Kamete 2007; Toriro 2007). Fast urban built-up area growth was observed on the southeast parts of Harare (Wania *et al.,* 2014) resulting in marginalized urban residents. These marginalized urban residents are residing in poorly serviced areas which are of relatively low cost due to the shunning absence of proper water and sewer reticulation systems. This unplanned development accompanied with poor sanitary conditions resulted in increased chances of severe health issues (Douglas 1983; Turral *et al*., 2011).

The northeast of Harare Metropolitan Province is composed of low-density residential suburbs and is characterized by medium gradient hills covered by high-vegetation density compared to high-density residential suburbs (Figure 4.4) (Anderson *et al*., 1993; Cumming *et al*., 1993). Due to the stratification of Harare, high income earners were pronounced to occupy these vegetation-enriched suburbs (Zinyama 1995). Construction on these landscapes is costly resulting in the variable "slope" as a significant driver for urban-built up area growth since the larger proportion of Harare residents occupied flat to gentle undulating landscapes in the south and other parts of Harare (Figure 4.4). Urban built-up area expansion towards the high-density residential area in the northwest direction follows the establishment of housing schemes such as the University of Zimbabwe's Association of University project and Hatcliffe Consortium development (Chirisa 2014; Tibaijuka 2005). The Hatcliffe Consortium development was a government initiative on Operation "Garikai/Hlalani kuhle" projects meant to provide housing units towards the "Operation Murambatsvina" victims (Tibaijuka 2005). On the other hand, high population density on the northwest suburbs of Harare coincides with increasing urban built-up area expansion (Mushore *et al*., 2017; Wania *et al*., 2014).

The geometry of road network reveals an influence on the spatial distribution and spread of urban built-up area as characterized by the regression models capturing the changes between 1984 and 2018 (Figure 4.5). This indicates a linear pattern on the built-up areas and the road

network systems, contributing to the rapid spreading of informal settlements within the road spheres. Easy access to transportation network systems paves the way for a linear and grid distribution pattern of built-up areas in urban cities such as the Harare Metropolitan Province. The urban population increased faster than anticipated, resulting in accelerated rates of informal settlements and the erratic provision of decent housing by the Zimbabwean Government (Chirisa and Muhomba 2013; Government of Zimbabwe (GoZ) 1991; Toriro 2007). Increased unrestrained built-up area expansion and spread in the south and east of the Harare Metropolitan Province reveals largely urban sprawl (Chirisa and Muhomba 2013; Kamusoko *et al*., 2013). Thus, these increasing rates of informal settlements within the metropolitan area have negatively impacted water resources. Thereby, driving the "distance to the nearest streams and open water" variables as influential characters of the urban built-up area expansion. This has also been attributed to the invasion of the Harare Metropolitan Province's ecosystem with urban construction activities (Chirisa 2014; Kamusoko *et al*., 2013; ZimStats 2012). The outward spreading of built-up areas was not evenly distributed. It concentrated largely in the south and southeast parts of the Harare Metropolitan Province, where fairly flat landscapes occur. This contributes to cheap residential construction costs (Wania *et al*., 2014) compared to the strongly rolling, sloppy landscape in the northeastern suburbs of the Harare Metropolitan Province (Figure 4.4, Figure A1) (Anderson *et al*., 1993).

Without negating population growth rate as a driving force for urban growth, there is a correlation between urban expansion and population growth rate as substantiated by previous Harare Metropolitan Province population statistics (Moghadam and Helbich 2013). The Harare Metropolitan Province population is estimated to have increased from approximately 830,000 in 1982 (Chirisa and Muhomba 2013) to 2,098,199 in 2012 (Moghadam and Helbich 2013). This huge growth of urban population posed large threats to water bodies (open water and streams) thereby making water resources vulnerable. Consequently, urban sprawl and unplanned rampant settling in the Harare Metropolitan Province concurred with the deterioration of water bodies since 2000. Overall, this study indicates that the popularity of water resources as amenities for land estates declined due to urban growth, which has led to the degradation of water resources through various human activities.

4.5 Conclusion

This study investigated the influence of independent variables as urban growth explanatory characters using binary logistic regression. The LULC classification accuracy of the Harare Metropolitan Province was improved through the use of remote sensing indices for spectral

separability considering the heterogeneity of an urban area. There are fundamental changes observed in the urban built-up area expansion and spread over the past three decades as evidenced by the shrinking of vegetation, cropland and water classes. This burdens the environment due to the increased demand for land by processes such as unplanned urban sprawl and informal settlements. However, there is need for a multi-disciplinary approach including land suitability analysis in order to curb the deterioration of these scarce and fragile resources. Models indicate that growth has been driven by the distance to nearest major roads, secondary roads, streams, open water courses and slope. For the phase between 1984 and 2000, binary logistic regressions show that distance to the city centre and distance to the nearest secondary roads and major roads were significant variables for urban built-up area expansion and spread. We observed a decreasing influence of the distance to the city centre as a predictor for urban built-up area expansion with increasing outward urban spread towards its peripheries. The findings revealed that fast urban growth and built-up area expansion were concentrated largely in the low-lying southern parts of the Harare Metropolitan Region and were occupied by high-density suburbs compared to the slow development in the strongly rolling, sloppy landscapes in the northeast of Harare Metropolitan Province with low-density suburbs. Overall, the model indicates that a road network has greater impact on the development of urban built-up area due to the accessibility of a transport network for connectivity and showing potential areas for future development.

Moreover, the research findings provide a guiding approach for town planners and policy makers to respond and pay attention to Harare Metropolitan Province landscapes which are profoundly deteriorating and, furthermore, the need to conserve the remaining amenities to maintain ecosystem balance.

4.6 Acknowledgments

The publication of this article was funded by Freie Universität Berlin. We thank our colleagues from Freie Universität Berlin, who provided valuable insights and expertise that greatly assisted this study. We are grateful to the National Aeronautics and Space Administration (NASA) and the United States Geological Survey (USGS), for providing the high-resolution satellite images and the one Arc-Second Global data from the Shuttle Radar Topography Mission (SRTM) for providing terrain corrected data.

4.7 Link with other chapters

Chapter 4 displayed high urban LULC overall classification accuracy above 80% on moderate resolution Landsat satellite data. This was achieved through: (a) enhancing feature delineation by combining multi-spectral data with specific spectral indices (EBBI, MNDWI and SAVI), (b) testing of separability tendency using the transformed divergence separability index (TD) which indicates if classes are statistically separable for good classification and (c) finally, the generation of LULC classes applying the machine learning Support Vector Machines. The next chapters will apply LULC maps of high accuracy generated in Chapter 4 to further assess the landscape and geomorphology impacts associated with rampant urban expansion and climate change. Further, future predictions of LULC changes and the likely possible responses of the landscape to land use and climate changes will also be based on supervised classification performed in chapter 4 using mapping approaches deemed reliable in Chapter 2.

Marondedze, A.K.; Schütt, B. Assessment of Soil Erosion Using the RUSLE Model for the Epworth District of the Harare Metropolitan Province, Zimbabwe. Sustainability ***2020***, 12, *8531. https://doi.org/10.3390/su12208531.*

CHAPTER 5: MODELLING SPATIAL SOIL EROSION RISK AND POTENTIAL EROSION USING THE EMPIRICAL RUSLE MODEL

Abstract

Urban development without adequate soil erosion control measures is becoming a major environmental concern in developing urban areas across Africa. These environmental disturbances encompass rampart land use and land cover changes (LULC) due to a high population growth rate and increased economic activities. To understand the influence of accelerated LULC changes and urban expansion as major drivers in landscape degradation in the Epworth district of the Harare Metropolitan Province, the RUSLE model was employed. This considers land use, soil, climate and topography as input parameters in the assessment of the extent and impact of these drivers on soil erosion. The Revised Universal Soil Loss Equation (RUSLE) was used to predict the potential erosion between 1984 and 2018 and soil erosion risk for the years 2000 and 2018. The mean rate of the predicted potential soil erosion was 13.2 t ha^{-1} yr^{-1} (1984–2018); areas especially vulnerable to erosion were predicted for foot slope areas with direct tributaries to the major streams and steep sloping zones. The average soil erosion risk was estimated at 1.31 t ha^{-1} yr^{-1} for the year 2000 and 1.12 t ha^{-1} yr^{-1} for 2018. While the overall potential soil loss decreased between 2000 and 2018, the potential soil loss was observed to increase tremendously in residential areas, which doubled in extent between 2000 and 2018. The findings reveal that about 40% of the Epworth district was threatened by unsustainable soil loss resulting from increased soil erosion risk within the built-up areas.

Keywords: land use change; urbanization; LULC; RUSLE.

5.1 Introduction

Urbanization is a continuous process that has boldly accelerated with population increase, expansion and spread of built-up structures in a designated urban area (Alaci 2019). Urbanization in Africa has been growing at alarming rates with an anticipated annual growth rate of approximately 3.9% (African Development Bank 2005). Population growth and increasing economic activities have been linked to aggravate Land Use and Land Cover (LULC) changes (Lambin *et al*., 2001; Khosrokhani and Pradhan 2014; Meshesha *et al*., 2014). As such, urban development inevitably involves construction and sealing activities that alter natural landscapes (McCool *et al*., 1987) resulting in an increase in impervious surfaces, which replace natural vegetation and reduce the capacity for water infiltration.

This in-turn results in surface runoff that substantially threatens soil loss in vulnerable landscapes through erosion processes (Jinren, and Yingkui 2003). While multiple studies on urbanization processes focus on the social and planning aspect and the assessment of the effects of urbanization processes on the (quasi-) natural environment, in the presented study we assess the effects of urbanization on surface processes by water in the strongly urbanizing area of Harare in tropical Africa; as case study we selected the 35 km^2 largest growing informal urban district of the Harare Metropolitan Province, which showed urbanization processes in the sense of surface-sealing of 18 km^2 since the year 2000 (Chirisa and Muhomba 2013; Marondedze and Schütt 2019). Due to the unprecedented growing rates of urban-built up area in Harare

Metropolitan Province (Chirisa 2014; Kamusoko *et al*., 2013; Marondedze and Schütt 2019), there is profound need for mapping potential erosion, and estimating potential soil erosion risk.

Soil erosion by water is a naturally occurring process, which is accelerated by human interference and activities including agriculture, deforestation, urban expansion and potentially climate change (Borrelli *et al*., 2020; Karydas *et al*., 2009; McHugh *et al*., 2002; Ozsahin *et al*., 2018). It is a continuous process that involves the bodily detachment, transport and deposition of particles originating from soils and weathered bedrock (Lahlaoi *et al*., 2015; Lal 2001). This resultant effect of overland flow and surface runoff has degrading effects on soil resources and affects agriculture and infrastructure (Pimentel *et al*., 1995; Rahman *et al*., 2009). The mechanisms involved in soil erosion by water underly a spatio-temporal variability and they are affected by factors such as rainfall, soil characteristics, ground cover and terrain (Moore and Burch 1986). In regions with seasonal rainfall dynamics, vegetation is sparsely distributed during dry season, making surfaces vulnerable to high raindrop energy impacts at the onset of wet season (Moore 1979; Ferreira and Panagopoulos 2014; Shikangalah *et al*., 2017; Chalise *et al*., 2019). Accelerated soil erosion is also reported especially on rainfed agriculture during the pre-monsoon due to high intensity rainfall events occurring concurrently with high wind speeds (Atreya *et al*., 2006; Chalise and Kumar 2020).

The spatial heterogeneity and dynamic mechanisms of soil erosion can be attributed to on-site and off-site effects that trigger landscape degradation (Le Roux and Sumner 2012; Pimentel *et al*., 1995). On-site soil erosion impacts encompass soil sealing and reduced crop productivity (Zhou and Wu 2008). Furthermore, change of soil structure emanating from the loss of topsoil and soil aggregates due to high rainfall erosivity and low infiltration rates severely perturb the sustainability of agricultural systems (Chalise *et al*., 2019; Samanta *et al*., 2016). Off-site damages effect widespread damages such as clogging of canals and drainage systems, siltation of reservoirs and destruction of roads thereby impeding transportation of goods and accessibility to properties (Le Roux and Sumner 2012; Opeyemi *et al*., 2019; Shikangalah *et al*., 2017). Construction activities such as grading and use of heavy machinery on steep and lengthy slope are reported as major sources of sediment loss due to their effect in accentuating erosion potential (USDA. NRCS 2000). Long-term LULC changes negatively impact river systems through the alteration of channel flow, soil deposition processes, soil textural organization and habitat loss (Bruijnzeel 1990; Chalise and Kumar 2020). Henceforth, the need is to assess the spatial distribution and extent of soil erosion in the rapidly transforming Epworth district of the Harare Metropolitan Province.

Globally, almost 84% of land loss results from soil erosion processes (Opeyemi *et al*., 2019). The estimated mean rates of soil erosion across the world range between 12 and 15 t ha^{-1} yr^{-1} (Ashiagbor *et al*., 2013). In Africa, it is estimated that 19% of the total reservoirs are under siltation threat due to soil erosion by water (Ashiagbor *et al*., 2013). About 494 million hectares of land in Africa are subjected to different types of degradation with degradation influenced by water estimated at 227 million ha (FAO and ITPS 2015). A countrywide annual soil loss of $1.5 * 10^9$ t was predicted for Ethiopia, with cultivated lands recording the highest soil loss rate at 42 t ha^{-1} yr^{-1} (Hurni 1988). Soil erosion rates in Ethiopia's cultivated lands and highlands have been highly influenced by increasing demographic pressure, climate change, terrain and depletion of vegetative cover (Food and Agriculture Organization 1986; Legesse *et al*., 2004). Only a few studies focus on an assessment of soil erosion risk in urbanized areas. For Kinshasa/DR Kongo, approximately 4.3% of the total urban area was predicted under high-risk of soil erosion with over 15 t ha^{-1} yr^{-1} annual average loss (Kabantu *et al*., 2018). A study on Kuala Lumpar/Malaysia Metropolitan city shows that approximately 38.1% of the city area was above the soil loss tolerable rates (> 1 t ha^{-1} yr^{-1}) due to high soil erodibility and steep slopes in some parts of the city (Khosrokhani and Pradhan 2014). At all, urban flooding falls among other problems associated with water induced urban soil erosion. This further aggravates risks on downstream water quality from overflowing sewers and street solids transported in concentrated urban runoff (Nhapi 2009).

A wide range of empirical, conceptual and physical models have been developed to estimate soil loss risks and these models vary in complexity, data requirements, processes considered and calibration (Merritt *et al*., 2003; Ranzi *et al*., 2012). These models include, among others, the statistical model of the Universal Soil Loss Equation (Wischmeier and Smith, 1978) and its derivatives the Revised Universal Soil Loss Equation (Renard *et al*., 1997), the Soil and Water Assessment Tool (Arnold *et al*., 1998) or the Water Erosion Prediction Project (Laflen *et al*., 1991). In general, model selection is particularly dependent on the availability of data, attributes of a working area and intended use (Ranzi et al. 2012; Renard et al. 1997). However, (Shikangalah *et al*., 2017) point out that the complexity of urban land use makes standard soil erosion recording and sampling techniques difficult to apply.

The suitability of satellite remote sensing and Geographic Information Systems (GIS) applications to extract, delineate and manipulate land characteristics, and their integration with the Revised Universal Soil Loss Equation (RUSLE), makes them fundamental tools for spatial soil erosion estimation (Wang *et al*., 2003; Lu *et al*., 2004; Li *et al*., 2011; Chalise *et al*., 2018). The RUSLE model is widely used and has been validated over decades, in addition to the fact

that its limitations have been well documented (Renard *et al*., 1997; Shamshad *et al*., 2008). Various studies on the prediction and assessment of soil erosion rates using RUSLE have been reported for Africa, with much attention to highlands and river watersheds (Igbokwe *et al*., 2008; Okereke *et al*., 2012; Woldemariam *et al*., 2018). However, there is paucity in research on mapping potential erosion and soil erosion risk modelling in urban built-up areas (Kabantu *et al*., 2018; Opeyemi *et al*., 2019; Shikangalah *et al*., 2017). The advances in urban development and soil erosion management have shown that land managers and policy makers consider the spatial distribution of soil erosion risk more than actual soil loss values (Khosrokhani and Pradhan 2014).

The objectives of this paper are: (a) to model the spatial distribution of the soil erosion risk and potential erosion for Epworth district over different time slices: 2000 and 2018 in order to assess the dynamics of soil erosion over time in heterogenous urban landscapes; (b) to assess the influence of rampart land use and land cover changes on soil erosion risk in the Epworth district through the analysis of temporal soil erosion estimations between 2000 and 2018. The temporal investigation makes use of the RUSLE model for estimating quantitative and spatial data on potential erosion and soil erosion risk in the Epworth district of the Harare Metropolitan province (Aiello *et al*., 2015) in order to enhance and support soil conservation planning (Renard *et al*., 1997). The study implements field observations, direct erosion feature registration and quantification towards establishing comparison and validation tools for Epworth district soil erosion models (Cerri *et al*., 2001). Overall, our study results aim to provide scientific advice towards the sustainability of urban growth.

5.2 Materials and Methods

5.2.1 Study area

Harare Metropolitan Province is the capital city of Zimbabwe (Figure 5.1), located between 17°40'-18°00' S and 30°55'-31°15' E. Harare Metropolitan Province is situated in the headwater areas of the Mukuvisi, Marimba and Manyame rivers, which supply Lake Chivero, a reservoir that supplies Harare with water (Nhapi 2009). The Harare Metropolitan Province is composed of four districts: Harare urban, Harare rural, Chitungwiza and Epworth. Epworth district is located about 12 km southeast of the central business district (Figure 5.1). Epworth district has been purposively selected as a study site because it is the largest informal settlement across urban districts in Zimbabwe (Chirisa and Muhomba 2013). Epworth counted

approximately 500 families in 1950 (Butcher 1986) while in 2012 the district had an estimated total population of 167,462 (ZimStats 2012).

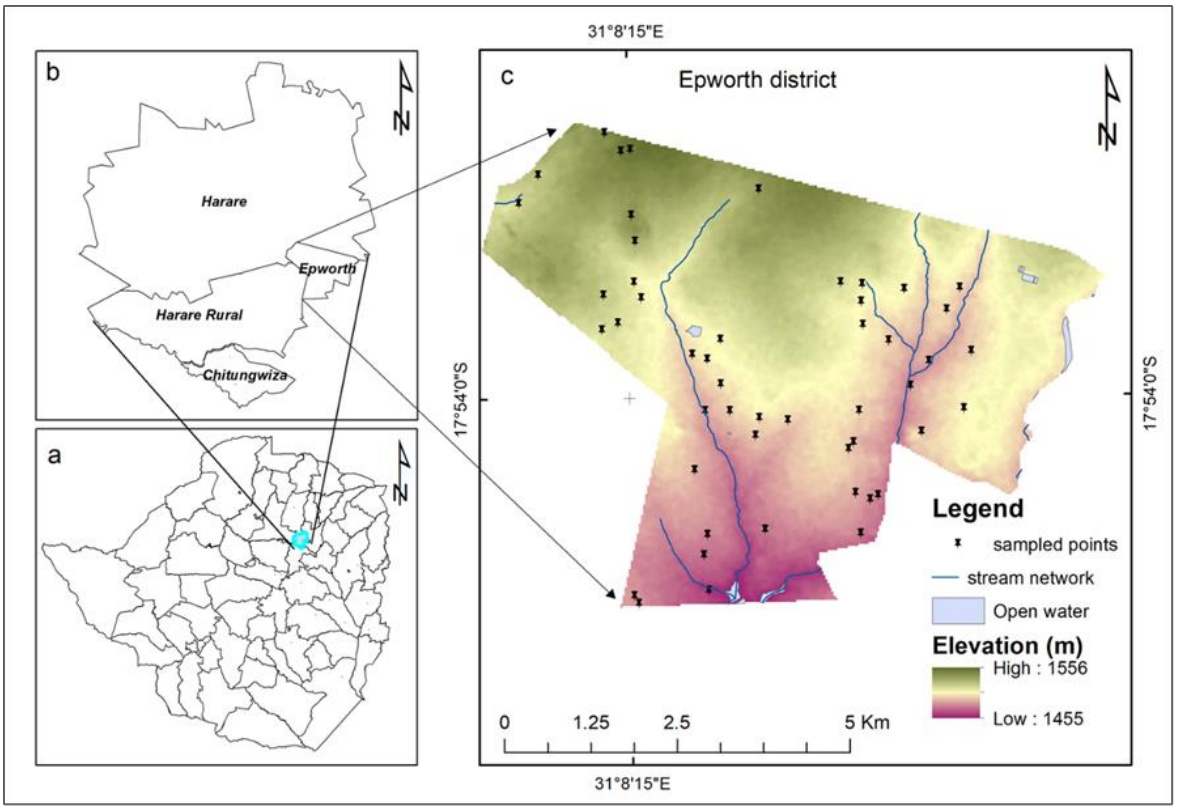

Figure 5. 1 Location of the Harare Metropolitan Province composed of the Harare urban, Harare rural, Epworth and Chitungwiza districts. (**a**) Zimbabwe district boundaries depicting the Harare Metropolitan Province; (**b**) districts of Harare Metropolitan Province; (**c**) Epworth district showing areas of recorded current soil erosion damages.

Settlement activities such as urban agriculture, construction, illegal sand mining, brick molding and effluent discharge from industries pose water quality threats to the Lake Chivero drainage basin (Chirisa and Muhomba 2013; Hove and Tirimboi 2011). Epworth district is largely dominated by high-density residential areas. These are characterized by overcrowdings and concentrated housing residential structures due to densification; only little vegetation occurs across the settlements (Chirisa and Muhomba 2013).

The general topography of Epworth district is characterized by undulating and slightly rolling terrain in the upland areas, being part of the southern Africa Highveld. Elevations range from 1455 m to 1556 m a.s.l. For Epworth district, clayey Fersiallistic soils (moderately leached soils of the kaolinitic order) occur in contact zones and Paraferrallitic soils (comprises of highly leached soils) are widely distributed across the entire district (Nyamapfene 1991; Thompson and Purves 1978). The sub-tropical climate of Harare Metropolitan Province is dominated by four distinct seasons: the cool-dry season (mid-May to August), hot-dry season (September to

mid-November), rain-wet season (mid-November to mid-March) and the post rainy season (mid-March to mid-May) (Kamusoko *et al*., 2013). Harare Metropolitan Province receives 470–1350 mm of precipitation annually; rainfall predominantly occurs during the four months of rainy season. Average temperatures range from 7 °C to 20 °C during dry periods and from 13 °C to 28 °C in hot-dry periods (Kamusoko *et al*., 2013).

5.2.2 Soil erosion modelling

Parameter estimation for Soil erosion risk assessment using RUSLE

The RUSLE model is simple and the mostly used computerized version of the Universal Soil Loss Equation (USLE), a statistical model developed to estimate the annual soil loss per unit area based on erosion factors (Renard *et al*., 1997; Zhou *et al*., 2008). The RUSLE model has been widely implemented for the prediction of average annual soil losses caused by sheet and rill erosion and to display the spatial distribution of potential erosion risk (Cerri *et al*., 2001; Zhou *et al*., 2008; Prasannakumar *et al*., 2012; Al-Abadi *et al*., 2016; Karamage *et al*., 2017; Shikangalah *et al*., 2017; Tundu *et al*., 2018). The application of the RUSLE model for soil erosion risk considers the rainfall erosivity factor (R), soil erodibility factor (K), slope length and steepness factor (LS), land cover and management factor (C) and the support practice factor (P) (Renard *et al*., 1997). In the current study, the RUSLE model was adapted for mapping potential erosion using C and P factors as identity elements (C and P = 1) and for the spatial distribution of soil erosion risk.

According to (Renard *et al*., 1997), the Revised Universal Soil Loss Equation (RUSLE) states that:

$$A = K\ x\ R\ x\ LS\ x\ C\ x\ P \tag{5.1}$$

where: *A* is the annual average of soil erosion rate factor (t ha^{-1} yr^{-1}); R is the rainfall erosivity factor (MJ mm ha^{-1} h^{-1} yr^{-1}); *K* is the soil erodibility factor (t h MJ^{-1} mm^{-1}); *LS* is the dimensionless slope length and steepness factor; *C* is the dimensionless crop management factor (ranging between 0 and 1) and *P* is the dimensionless conservation support practice factor (ranging between 0 and 1). The calculation of the potential erosion is based on the same formula while adjusting factors C and P to one (Khosrokhani and Pradhan, 2014; Karamage *et al*., 2017).

Spatial analyses in the study were performed using ArcGIS 10.2 software to assess the dynamics of soil erosion over time in the heterogenous urban landscapes for the years 2000, 2018 and the overall, 1984-2018 long-term rainfall data were used for rainfall erosivity factor computation (Figure 5.2). The LS factor RUSLE geospatial input factor was computed using a

hydrology module (LS-factor field base) in SAGA GIS (Panagos et al. 2015a). The acquired geospatial input parameters for the RUSLE model (Table 5.1) were used to produce thematic maps for the estimation of potential erosion and soil erosion risk generated within every cell grid (Farhan and Nawaiseh 2015; Mati *et al*., 2000; Millward and Mersey 1999). For data harmonization, we resampled all data sources to determine 30 m x 30 m grid cell size using nearest neighborhood technique so as to retain original pixel value before carrying out grid cell calculations. This was performed to enhance data compatibility from varying data sources used for modelling (Ai *et al*., 2013).

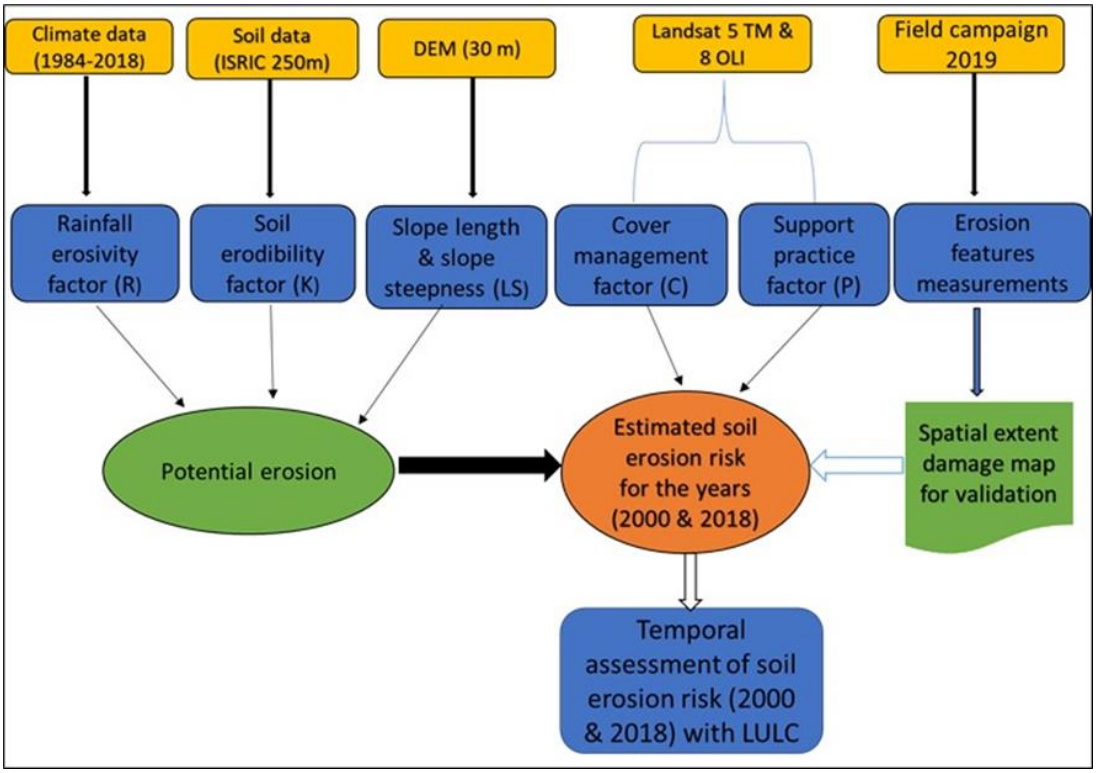

Figure 5. 2 Flowchart for modelling potential erosion and soil erosion risk in Epworth district. LULC: Land Use and Land Cover, ISRIC: International Soil Reference Information Centre.

Table 5.1 Principal data used for soil erosion modelling showing the resolution and the source.

Data type	Resolution	Source
K Factor	250 m	Global Soil map and attributes in raster (TIF format) (International Soil Reference and Information Centre (ISRIC) World Soil Information) 2019) "SoilGrids"
R Factor	-	Average monthly rainfall data from the Zimbabwe Department of Meteorological Services (Harare) database.
LS Factor	30 m	Digital Elevation Model (DEM) (USGS (United States Geologic Service) 2018)
C Factor	30 m	Obtained by assigning weighted C factor values to the LULC maps adopted from Marondedze and Schütt, 2019
P Factor	30 m	The value of 1 was assigned to all-over the study area.

Rainfall erosivity factor (R)

Rainfall erosivity factor (R) describes the ability of rainfall to trigger soil erosion (Stocking and Elwell 1976; Lal 1990; Farhan and Nawaiseh 2015). The RUSLE model makes use of this erosivity factor (R [MJ mm ha^{-1} h^{-1} yr^{-1}]) in integrating the effects of raindrop impact, rainfall duration and resulting runoff rates, which are coupled with the amount and the energy within each recorded rainfall pattern (Farhan and Nawaiseh 2015; Renard *et al*., 1997). Rainfall erosivity was calculated using mean annual rainfall data collected from three gauging stations in Harare Metropolitan Province (Harare Belvedere, Harare airport and Harare Kutsaga; Table 5.2) following Equation 5.2 (Merritt *et al*., 2003; Tundu *et al*., 2018):

$$R = 38.5 + 0.35\ x\ M \qquad (5.2)$$

where R = Rainfall erosivity factor, M = Mean annual rainfall.

Table 5.2 Location of gauging stations and mean annual precipitation for the study periods.

Rain stations	Coordinates	Mean annual precipitation (mm)		
		1984–2000	2000–2018	1984–2018
Belvedere	17° 50' S, 31° 01' E	880.2	851.1	865.7
Airport	17° 55' S, 31° 06' E	834.3	774.2	804.3
Kutsaga	17° 55' S, 31° 08' E	804.6	792.8	798.7

To analyze possibly changing rainfall erosivity since 1984, annual rainfall averages were calculated for the time steps: 1984–2000, 2000–2018 and overarching, 1984–2018. The mean annual precipitation data were interpolated over entire district by applying the inverse distance weighting (IDW) interpolation technique and converted to rainfall erosivity by applying Equation (5.2).

Soil erodibility factor (k)

The responsive effect of a particular soil in a given location to the erosive power of rainfall and runoff impacts is referred to as the soil erodibility factor (K) (Lal 2001; Alexakis *et al*., 2013). Soil erodibility is regarded as a function of the soil texture, organic matter content, soil structure and the degree of permeability (Yang and Zhang 2011; Ranzi *et al*., 2012). Soils being highly susceptible to erosion have soil erodibility values close to 1, whereas corresponding values close to 0 indicate a resistive nature of the soil (Farhan *et al*., 2013; Woldemariam *et al*., 2018). In the current study, information on soil structure and profile permeability was not available. Therefore, the K factor was estimated using the ISRIC (International Soil Reference Information Centre)-World Soil Information data (Hengl *et al*., 2017), following the equation by (Sharpley and Williams, 1990).

Topographic factor (LS)

The LS factor summarizes the effects of topography on soil erosion and combines the influence of slope length and slope angle on soil loss; while the S-factor measures the effect of slope steepness, the L-factor defines the impact of slope length. The slope length L is defined as the distance between the upslope starting point of a slope segment to the downslope point where deposition begins (Ashiagbor *et al*., 2013; Panagos *et al*., 2015). Increasing slope length and steepness per unit area results in increased runoff and flow velocity and consequently in increased soil loss exposure (Wischmeier and Smith, 1978; Desmet and Govers, 1996; Alexakis *et al*., 2013). The Shuttle Radar Topography Mission (SRTM) digital elevation model (DEM) with a spatial resolution of 30 m was used for the LS factor computation applying SAGA software 2.3/Hydrology module (Desmet and Govers 1996; Panagos *et al*., 2015a). For data pre-processing, fill sink algorithm was employed using the spill elevation method for filling sinks on the DEM (Wang and Liu 2006). Multiple flow direction tool (MFD) incorporated in the Hydrology module was applied to the DEM to assign flow directions and flow accumulation (Freeman 1991; Tarboton 1997).

Land cover and management factor (C)

The Land cover and management factor C's pivotal role is to capture differences in soil loss in vegetated areas by dissipating raindrop impact on the soil surface compared to bare areas (Renard *et al*., 1997; Lee 2004; Kheir *et al*., 2008). The C factor decreases from 1 to 0 depending on vegetation cover and cropping management systems implemented to mitigate soil erosion (Desmet and Govers 1996; Ranzi *et al*., 2012). In order to determine the C factor, land use maps

generated from the supervised classification of satellite images were adapted for use (Marondedze and Schütt 2019). The C factor values for each land use are a result of weighted average of the soil loss ratio deduced from a reference plot (bare) with a C factor of 1 (Panagos *et al*., 2015; Renard *et al*., 1997). Henceforth, the C factor values of each land use type were evaluated from literature (Singh and Phadke 2006; Leh *et al*., 2013; Khosrokhani and Pradhan 2014; Asiedu 2018); weighting of the data was performed following field observations and the biophysical characteristics per sampling plot (canopy cover, prior land uses, and surface cover) (Renard *et al*., 1997; Panagos *et al*., 2014). The weighted C factor evaluation considered plant growth, height and the extent of canopy cover in-situ (Alena *et al*., 2013; Panagos *et al*., 2014), in relation to bare and sealed area. Further, previous urban farming practices and residues of the plant material influence were majorly factored in during surface cover subfactor assessment per sampling plot. For croplands the C factor was estimated by averaging the values of predominant crops within the study area's croplands (Ochoa-Cueva *et al*., 2015). The availability of remote sensing data, especially the supervised classification maps, appropriately aided the evaluation of spatial variability of the C factor (Panagos *et al*., 2014). Overall, the weighted C factors were estimated as a result of multiplying the scaled percentages of the evaluated C subfactors (Table 5.3), reviewed RUSLE C factors according to the literature (Singh and Phadke 2006; Leh *et al*., 2013; Asiedu 2018) and the ratio of sealed area proportion (Marondedze and Schütt 2019) in relation to the reference plot (bare).

Table 5.3 C factor values and relative proportion of LULC classes for 1984, 2000 and 2018.

Land use class	Weighted C factor value	Land area (%)		
		1984	2000	2018
CBD/ Industrial areas	0.017	0.1	0.4	0.5
LMD (Less concentrated)	0.066	2.8	15.5	31.5
HD (Concentrated)	0.083	16.6	38	52.6
Irrigated cropland	0.166	1	7	0.4
Rainfed cropland	0.239	17.9	17	9.1
Green spaces	0.03	61.5	22	5.9
Water	0	0.1	0.1	0.04

*CBD: Central Business District *LMD: Low-Medium Density *HD: High Density

Support practice factor (P)

The Support practice factor P expresses the effects of surface management practices that are applied to reduce soil loss through erosion processes (Opeyemi *et al*., 2019; Renard *et al*., 1997). These practices include among others terracing, strip cropping and contour ploughing (Renard *et al*., 1997). The P factor value ranges between 0 and 1, where 0 shows the highest

effectiveness of the conservation practice and 1 indicates that there are no support practices or measures implemented (Renard *et al*., 1997; Adornado *et al*., 2009). In this study, a P factor of 1 has been all-over applied due to the area wide absence of support or management practices.

5.2.3 Mapping and surveying soil erosion dynamics

The complexity of the setup of urban built-up areas and the distribution of the different land use require soil erosion field survey mapping to receive reference data (Shikangalah *et al*., 2017). In this regard, a simple snap-shot sampling procedure was implemented during the field survey in December 2019 to estimate the spatial extent of eroded areas on plots 40 m x 80 m in size (Shikangalah *et al*., 2017). In total, 49 sites were randomly surveyed, covering varying land use. Mapping of spatial soil erosion assessment was geocoded using a hand-held GPS (Garmin 60Cx); parallel on-site soil erosion features were measured, considering the erosion features (inter-rills and rills) individually calculating their area and volumes (Cerri *et al*., 2001; Bewket and Sterk 2003). Rills were defined as linear erosion channels not more than 0.5 m deep and with a cross-sectional area < 929 cm^2 to make them distinct from ephemeral gullies and deep incised gully features (Imeson and Kwaad 1980; Poesen *et al*., 2003).

Overall, total percentages of disturbed surface area data were registered for the sample plots in the Epworth district to estimate the spatial extent of perturbed regions of the district. The spatial extent of eroded areas was estimated as percentage per plot (Shikangalah *et al*., 2017) and classified into five severity classes. Mapping results are displayed in a positional diagram map.

5.3 Results

5.3.1 Factors controlling soil erosion

The rainfall erosivity factor map for Harare's Epworth district depicts very small variations over the study periods between 1984 and 2018 (Figure 5.3). The annual area wide R factor averaged 329 MJ mm ha^{-1} h^{-1} yr^{-1} between 1984 and 2000 (std = 0.55, n=16), 315 MJ mm ha^{-1} h^{-1} yr^{-1} between 2000 and 2018 (std = 0.27, n=18) (Figure A2). As for both observation periods, the R factor did not vary significantly ($\alpha > 0.05$), the area wide averaged R factor for the time period 1984–2018 with 322 MJ mm ha^{-1} h^{-1} yr^{-1} (std = 0.38, n=34) was applied (Figure 5.3).

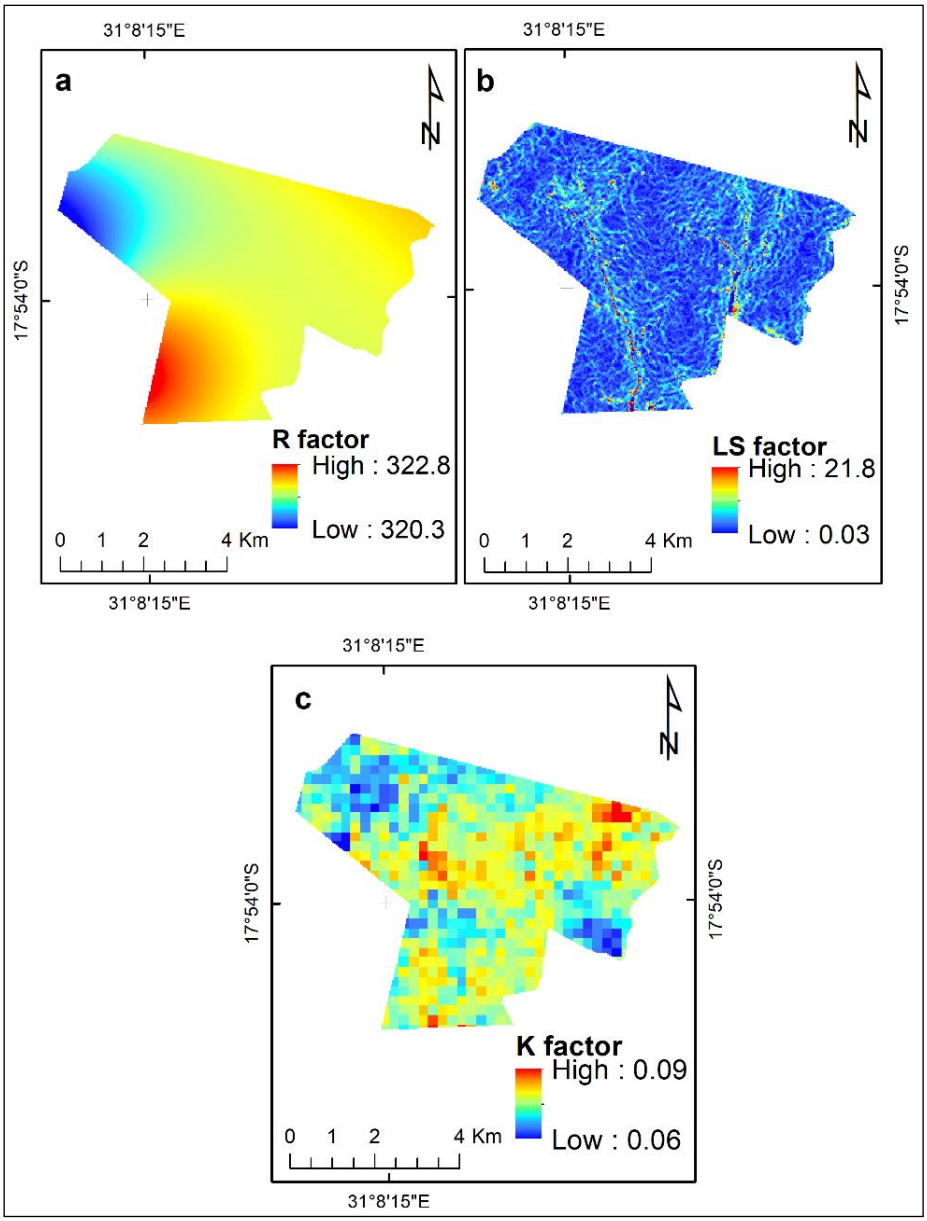

Figure 5. 3 Input factor maps for modelling potential soil erosion for the Epworth district. (a) shows the overall rainfall erosivity factor between 1984 and 2018; (b) topographic factor (LS) and (c) soil erodibility factor (K).

Soils in the Epworth district upland's areas are dominated by sandy to clayey loams and sandy loam along the alluvial plains; also, at sloping positions sandy loam soils frequently appear. Correspondingly, K factor values vary in the Epworth district between 0.06 and 0.09 t h MJ^{-1} mm^{-1} and are highest along the slopes flanking the valleys while they are lowest in the plateau area. Relief in the Epworth district is due to its location at the northern extension of the Highveld slightly rolling. Slopes at the plateau vary between 0.74° and 2.0°, while along the valley flanks they increase in steepness up to 4.6°. Correspondingly, the values of the topographic factor (LS) are highest along the valley flanks, increasing from the headwater areas moving downstream of

the Epworth district (Figure 5.3). Overall, the topographic factor values range from 0 in the plateau areas to 21.74 in steep areas.

The land cover management factor weighted values are based on field observations and satellite images on LULC analysis (Table 5.1, Table 5.4, Figure 5.4). Data for the LULC changes from 1984-2000 and 2000-2018 were adapted from (Marondedze and Schütt 2019).

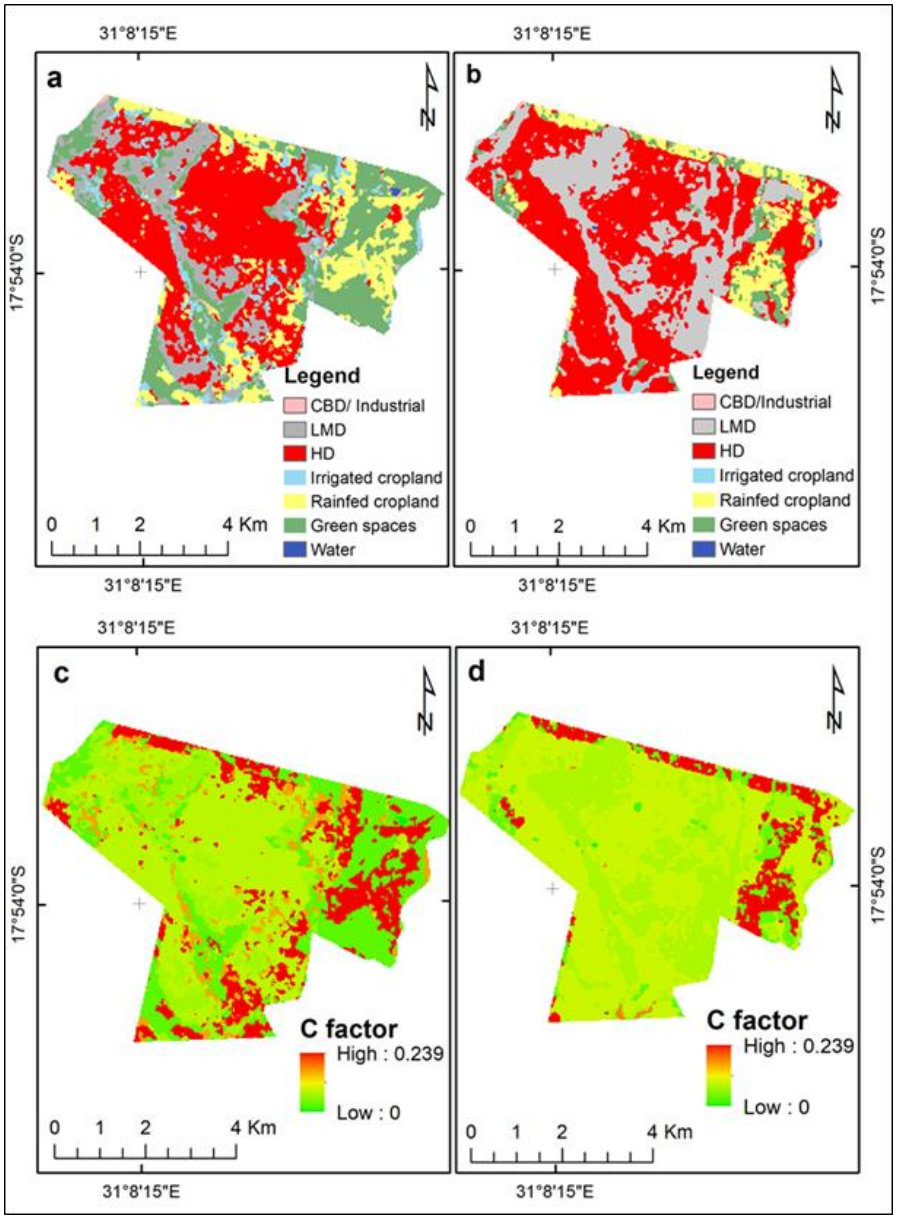

Figure 5. 4 LULC maps for the Epworth district over the years (a) 2000; (b) 2018 and crop management factor maps for the years (c) 2000; (d) 2018.

Table 5.4 Description of study area LULC classes.

ID	Land Use and Land Cover class	Description
1	CBD/Industries	Industries and central business district defined with high fraction of impervious surfaces mainly buildings and little proportion of vegetation
2	LMD residential (less concentrated)	Leafy and well established low and medium density suburbs surrounded with high vegetation
3	HD residential (concentrated)	High density residential areas with low vegetation cover or clustered settlements with areas undergoing developments and bare exposed land
4	Irrigated cropland	Cultivated land under irrigation schemes
5	Rainfed cropland	Cultivated land or land with crop residues after harvesting
6	Green spaces	All wooded areas, shrubs and bushes, riverine vegetation and grass covered areas
7	Water	Areas occupied by water, rivers, wetlands, reservoirs and dams

*CBD: Central Business District *LMD: Low-Medium Density *HD: High Density

5.3.2 Potential erosion risk analysis

The potential erosion risk map was derived from the application of the "natural" RUSLE factors for soil characters, rainfall erosivity and topography (K, R and LS) for the Epworth district. Resulting data are classified into five potential erosion risk classes showing how erosion varies in the Epworth district (Figure A3). The potential erosion risk map indicates the vulnerability of the landscape independent from vegetation cover and crop management. The findings reveal that very high to extreme erosion risk areas occur in areas of steep slopes (Figure A3); the only spatially slight variations of R and K factors cause a strong control of potential erosion risk by topographic factors' LS. Due to the general orientation of the drainage network to the south and downstream with increasing inclination of the slopes along the valley flanks, the areas with high erosion risk expand from the north to south. Very high to extreme erosion risk areas are also observed in the eastern parts of the Epworth district resulting from locally occurring steep slopes towards the middle course of the Jacha river and tributaries. In contrast, low to moderate potential erosion risk areas occur in the plateau areas of the Highveld. Extreme potential erosion risk zones occur in the immediate vicinity of streams and at steep slopes. The area wide average potential erosion risk rate in the Epworth district was 13.2 t ha^{-1} yr^{-1} since 1984, referring to the precipitation data 1984–2018 (Figure A3, Table 5.5).

Table 5.5 Potential erosion risk classes with erosion rate and area covered proportion.

Soil erosion risk	Soil loss ($t\ ha^{-1}\ yr^{-1}$)	1984–2018	
		Area (km^2)	Area (%)
Low	0 - 1	0.5	1.4
Moderate	1 - 2	2.3	6.6
High	2 - 5	0.4	1.1
Very high	5 - 10	11.3	32.3
Extreme	>10	20.5	58.6

5.3.3 Soil erosion risk

The estimated soil erosion risk maps were generated for 2000 and 2018. The estimated soil erosion risk averaged 1.31 $t\ ha^{-1}\ yr^{-1}$ in 2000 and 1.12 $t\ ha^{-1}\ yr^{-1}$ in 2018; with highest total soil loss rate for the Epworth district amounting to 92.79 $t\ ha^{-1}\ yr^{-1}$ in 2000. The spatial patterns of the estimated soil erosion risk indicate areas with high soil erosion loss predominantly along the river courses (Figure 5.5). Correspondingly, areas of high soil erosion risk can also be found in the southwestern and southeastern parts of the Epworth district with highest soil erosion risk close to the river courses.

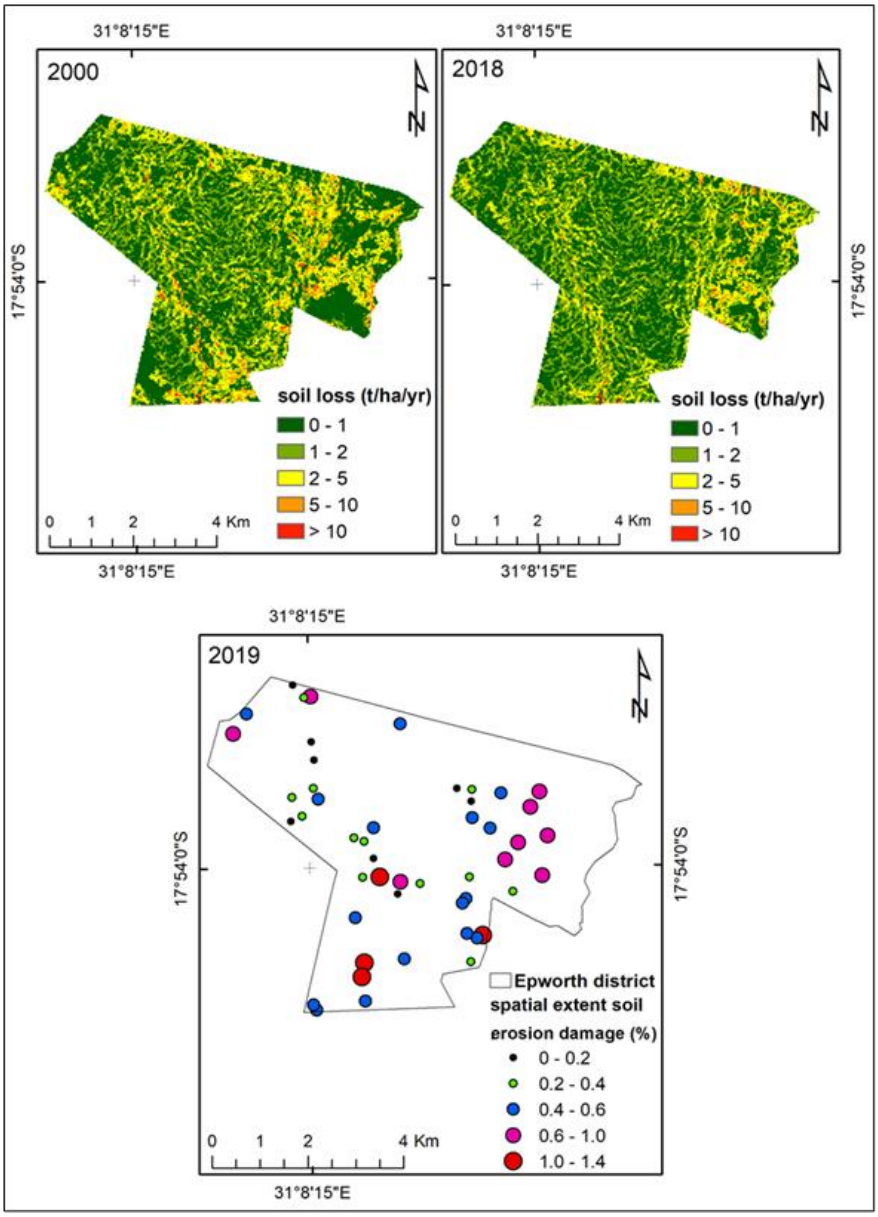

Figure 5. 5 Spatial distribution of soil erosion risk. (**a**) 2000; (**b**) 2018 and (**c**) shows the spatial extent soil erosion damage in percentages based on field mapping in December 2019 for selected plots (plot size measured 40 m x 80 m; in total 49 sites were randomly surveyed, covering varying land use).

The soil erosion damage map shows plot-wise surface area damages in the Epworth district calculated from the soil erosion feature dimensions, expressed in percentages of the total surface area for each plot (Figure 5.5). According to this soil erosion damage map, the southeastern and southwestern plots of the Epworth district experience higher soil erosion compared to the other areas investigated. The spatial extent of the soil eroded area ranges from 0% to 1.4% for the surveyed plots in the Epworth district. The magnitude of soil erosion observed during field mapping in 2019 indicated that slope, high proportion of sealed and impervious surfaces attributed to increased soil erosion damages in the Epworth district (Figure 5.6).

Figure 5. 6 The extent of soil erosion observed in Epworth district. The extent of soil erosion observed in Epworth district. (**a**) paved roadside erosion feature; (**b**) erosion occurring in an unpaved road.

The estimated soil erosion risk for the year 2000 highlights that 56.3% of the Epworth district was exposed to low soil erosion risk and 25.9% to moderate soil erosion risk, while 15% of the Epworth district was exposed to high, and 2.8% to very high and extreme soil erosion (Figure 5.5, Table 5.6). For 2018 modelling of soil erosion risk displays a slight decline of risk of exposure with 59.5% of the area being exposed to low soil erosion risk and 29.3% to moderate soil erosion risk; the spatial extent of areas exposed to high soil erosion risk declined to 10% and areas exposed to very high to extreme soil erosion risk covered 1.2% of the Epworth district (Table 5.6).

Table 5.6 Estimated soil erosion risk in Epworth district for 2000 and 2018.

Soil loss ($t\ ha^{-1}\ yr^{-1}$)	Soil erosion risk	2000		2018	
		Area (km^2)	Area (%)	Area (km^2)	Area (%)
0–1	Low	19.6	56.3	20.7	59.5
1–2	Moderate	9.0	25.9	10.2	29.3
2–5	High	5.2	15.0	3.5	10.0
5–10	Very high	0.9	2.5	0.4	1.1
>10	Extreme	0.1	0.3	0.04	0.1

5.3.4 Magnitude of soil erosion in Epworth district

A spatial extent of about 765 m^2 was eroded with an average area of 31 m^2 affected by soil erosion as calculated from the 49 randomly selected sample plots in Epworth district during the field survey in 2019 (Table 5.7). The soil erosion damage measured approximately 0.5% of the total area mapped (15.7 ha). The occurrence of soil erosion features varied in the surveyed plots corresponding to vegetation cover, slope characteristics and human activities.

Table 5.7 The extent of soil erosion in Epworth district summarized for 2019 field survey.

	Spatial Eroded Area (m^2)
Number of mapped sites	49
Total extent of erosion	765
Mean	31
Standard Deviation	10.5
Standard Mean Error	1.5

Model validation was done using the empirical RUSLE model data in comparison with on-site field measurements. The results showed good RUSLE model performance as there was satisfactory moderate positive correlation between field measurements and model results for sample areas ($r = 0.76$ and $R^2 = 0.581$, $p < 0.05$) (Figure 5.7). This provides confidence in the application of the model for sustainable land use planning and decision-making processes.

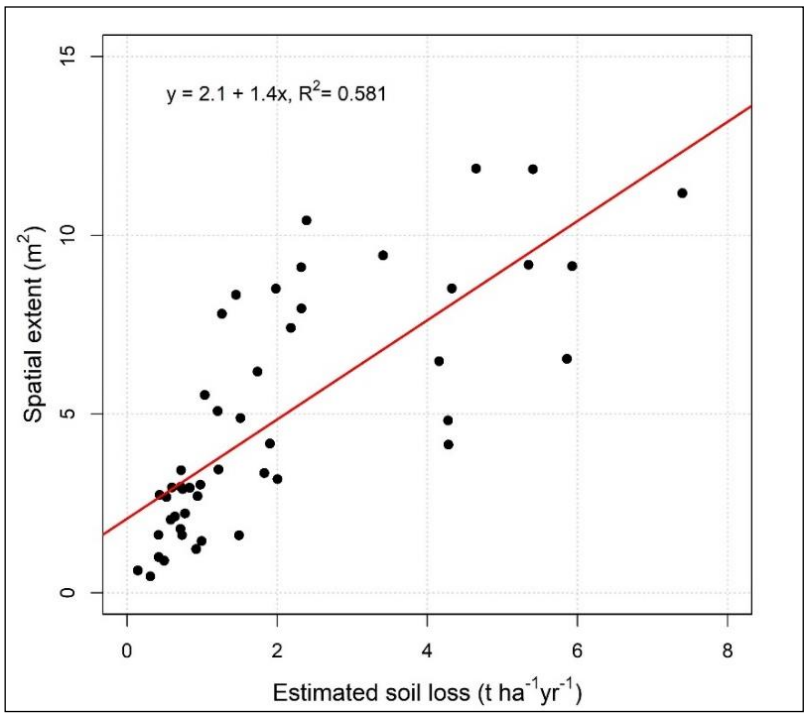

Figure 5. 7 Evaluation of soil erosion modelling and field measurements.

5.3.5 Land use and soil loss analysis

The results show that about 50,408 tons of soil were estimated to be lost under 2000 LULC conditions, while an estimated total soil loss of 42,934 tons was calculated for 2018 (Table 5.8). For the industrial areas of Epworth district, approximately 40 tons of soil loss were estimated for 2000, while an increase of up to 47 tons of soil loss was estimated for the same land use type for 2018. For 2000, for the land use type "less concentrated residential area" (15.5% of the Epworth district in 2000) 6218 tons of soil loss were estimated while, for the land use type "concentrated residential areas" (38% of the Epworth district in 2000) about 14,018 tons total soil loss were estimated. An increase in soil erosion risk for less concentrated and concentrated residential areas were estimated to amount 12,203 tons for the "less concentrated residential areas "(31.5% of the Epworth district in 2018) and 19,858 tons for the "concentrated residential areas" (52.6% of the Epworth district in 2018). A decline in the estimated soil loss was observed for land use types either of agricultural use or covered by green spaces (undifferentiated) between 2000 and 2018, decreasing proportional to the reduction of the areas of these land use types (Table 5.8).

Table 5.8 Estimated soil loss for the different LULC classes in Epworth district based on the assessment of soil erosion risk and LULC analysis for the years 2000 and 2018.

LULC class.	2000			2018		
	Soil loss (tons)	Area(km²)	Percentage (%)	Soil loss (tons)	Area(km²)	Percentage (%)
CBD/Industrial area	40	0.12	0.4	47	0.19	0.5
LMD (less concentrated)	6218	5.41	15.5	12,203	10.96	31.5
HD (concentrated)	14,018	13.17	38	19,858	18.32	52.6
Irrigated cropland	6970	2.45	7	733	0.13	0.38
Rainfed cropland	19,228	5.85	17	9239	3.16	9.1
Green spaces	3934	7.78	22	854	2.06	5.9
Water	0	0.05	0.1	0	0.01	0.04
Total	50,408	34.83	100	42,934	34.83	100

*CBD: Central Business District *LMD: Low-Medium Density *HD: High Density

5.4 Discussion

For the tropics, studies reported average soil loss rates of 5 t ha^{-1} yr^{-1} (Bamutaze 2015; Lufafa *et al*., 2003), while (Morgan 2009) highlights that a soil loss limit of 11 t ha^{-1} yr^{-1} may be accepted as reasonable mean annual loss due to soil erosion. However, (Hudson 1981) argues that for sensitive and fragile land areas average soil loss tolerance of 2 t ha^{-1} yr^{-1} could be recommended. In contrast, considering the slow rate of soil formation and spatio-temporal effects of soil loss on water quality and productivity, tolerance limits for soil erosion loss are set for the tropics at 1 t ha^{-1} yr^{-1} (Khosrokhani and Pradhan, 2014; Karamage *et al.*, 2017; Abdulkareem *et al.*, 2019). The occurrence of soil loss exceeding 1 t ha^{-1} yr^{-1} was considered as the critical rate for the Epworth district due to the low rate of soil formation as typical for the tropics (Khosrokhani and Pradhan 2014). This agrees with the recommendation of (Abdulkareem *et al*., 2019) that the rate of soil loss through soil erosion should be relatively balanced with the soil formation rate to minimize excessive environmental damage. As such, average soil loss rates exceeding the suggested 1 t ha^{-1} yr^{-1} are classified as unsustainable to continue supporting land use (Verheijen *et al*., 2009; Jones *et al*., 2013).

The empirical RUSLE model implemented in this study was applied to predict potential erosion risk and soil erosion risk for the Epworth district of the Harare Metropolitan Province (Figures A3 and Figure 5.5). The calculation of the potential erosion risk is based on the assumption that there is no land use and no land management as well as no support practice; potential erosion is understood as the erosion processes only controlled by physical factors. Consequently, potential erosion risk depicts areas vulnerable to erosion even without considering land use (Karamage *et al.*, 2017). For the Epworth district the potential erosion risk was averaged at 13.2 t ha^{-1} yr^{-1} between 1984 and 2018, significantly exceeding the soil loss tolerance limit of 1 t ha^{-1} yr^{-1} for the tropics (Khosrokhani and Pradhan 2014; Abdulkareem *et al*., 2019).

Estimated soil losses due to soil erosion risk averages amounted to 1.31 t ha^{-1} yr^{-1} and 1.12 t ha^{-1} yr^{-1} in the years 2000 and 2018, respectively. Correspondingly, the revealed soil loss due to soil erosion risk for Epworth district was slightly above the recommended tolerable limits of 1 t ha^{-1} yr^{-1} (Khosrokhani and Pradhan, 2014; Karamage *et al.*, 2017; Abdulkareem *et al.*, 2019). Considering the proposed range of tolerable maximum annual soil loss in tropical regions, it can be deduced that the mean estimated soil loss during all study periods slightly causes irreversible soil erosion. The occurrence of high potential erosion risk compared to low soil erosion risk is due to the assumption that for the calculation of potential erosion risk, the factors land cover and management (C) and support practice (P) are not considered, and consequently,

these factors are mathematically handled as identity elements in order to assess the impact of RUSLE "natural factors" on the study area. In the application of the RUSLE this corresponds to dealing with C and P factors as bare ground (Khosrokhani and Pradhan 2014). Such conditions earmark the impact of soil erosion on cleared land area and also reveal the significance of vegetation cover in dissipating raindrop energy impact on the bare ground. Nevertheless, such scenarios merely occur in urban areas as a result of built-up densification and spread of impervious surfaces unless croplands and disturbed green spaces exist at larger scale.

The decrease of soil loss due soil erosion risk for the Epworth district calculated for the period 2000–2018 probably resulted from the expansion of built-up areas at the expense of green spaces and cropland areas and thus with sealing the underground impeding surface exposure to erosion (De Meyer *et al*., 2011; Meshesha *et al*., 2014). However, soil disturbance has been triggered by human activities in the district due to high population pressure and demand for shelter (Cantón *et al*., 2011; Shuster *et al*., 2005). This contributes to increased soil loss within the urban built-up areas compared to the previous years (Table 5.8). The replacement of green spaces with impervious surfaces causes a reduction in surface area for water infiltration (Dams et al. 2013; Phil-Eze 2010), causing increased overland flow either by sheet flow or by concentrated surface runoff. This substantially threatens soil loss through erosion where the overland flow reaches areas where soils are exposed to the surface making them highly vulnerable landscapes with mostly bare grounds (Jinren, and Yingkui 2003; Meshesha *et al*., 2014).

Construction activities create artificial slopes and reduce vegetation canopy cover exposing soil surfaces to raindrop impact thereby exacerbating rates of soil detachment and transportation during rainstorm events (Opeyemi *et al*., 2019). Beyond, construction activities repeated earth movements affect the stability of the soil structure and increase soil erodibility (Lal 1990; Jim 1993) and soil compaction resulting in the reduction of infiltration capacity and increase surface runoff generation (Jim 1993; Dams *et al*., 2013). Therefore, continued LULC changes dominated by the expansion of built-up areas largely perpetuate soil loss within the built-up areas (De Meyer *et al*., 2011). To ensure that soil erosion risk thresholds remain sustainable, land suitability analysis should be considered to enhance land use allocation and proper land servicing require to be implemented by responsible authorities in order to meet competing demands for land. The findings of this study highlight that zones with high potential erosion risk and soil erosion risk correspond to zones of strong relief and high slope lengths (high LS factors).

The weighted C factor values derived based on the biophysical properties observed and measured in the field (Wischmeier and Smith, 1978; Panagos *et al*., 2015). The approach integrated LULC maps derived from satellite images. However, there are limitations on the use of LULC data resulting from misclassifications, heterogeneity and spatial distribution of vegetation densities across the entire district. The resulting approach anticipates that the same LULC class poses the same land cover and management factor C value (Lu *et al*., 2004; Ma *et al*., 2003; Panagos *et al*., 2014; Vrieling 2006). However, uncertainties and limitations influencing the results could have also emanated from omitting other biophysical characteristics during estimations of the C factor including surface roughness and below-ground biomass (Wischmeier and Smith, 1978; Panagos *et al.*, 2015; Teng *et al.*, 2018).

An analysis of the relationship between LULC and estimated soil erosion risk was performed by overlaying LULC and soil erosion risk maps for the time slices 2000 and 2018 (Table 5.8). This relationship has been observed as a useful tool monitoring patterns of LULC change against soil erosion risk (Abdulkareem *et al*., 2019; Khosrokhani and Pradhan 2014); the analysis reveal spatial patterns and changes for each LULC class majorly as influenced by human activities in relation to soil erosion risk. Soil erosion risk was extremely high in rain fed croplands in the year 2000, highlighting their vulnerability to water induced erosion. This might have been propelled by leaving little to no crop residues as soil cover on the fields, exposing bare soil to rainfall at the onset of rainy season (Ferreira and Panagopoulos 2014; Giang *et al*., 2017; Chalise *et al*., 2019). In addition, pre-season land preparation exposes fine tilled land to raindrop impact, exacerbating soil loss due to reduced surface and ground cover in dissipating and scattering raindrop energy (Smith *et al*., 1987), while concurrently ploughing increases surface roughness and pore volume, both fostering infiltration (Nyamangara *et al*., 2014; Jakab *et al*., 2017).

The estimated soil loss in areas covered by green spaces initially was predicted to be high considering the vegetation's ability to intercept raindrop impacts (Panagos *et al*., 2015a). However, it has to be clearly differentiated what character the vegetation cover has and whether the area is disturbed or undisturbed by human impact. Especially areas with sparse disturbed green spaces are exposed to erosion processes by the first rains coming after a dry period due to the hydrophobic character of dried out soils while parallel the soil stabilization by roots is insufficient (Ferreira and Panagopoulos 2014; Shikangalah *et al*., 2017); footpaths spreading across areas increase soil sealing along the paths and thus foster generation of concentrated runoff (Chalise *et al*., 2019; Jakab *et al*., 2017). Other local human activities including harvesting of firewood for domestic use, burning of bricks during their processing and fencing

of gardens have negative impacts on vegetation cover. The more intense land use gets, especially transferring fallow land covered by sparse green spaces into built-up areas, the higher the soil erosion risk in this area, which is highly affected by the increasing areas characterized by sealed and impervious surfaces (McCool *et al.*, 1989). Soil erosion risk investigations on the Epworth district show that, despite the decreasing of the overall estimated soil loss from 50,408 tons to 42,934 tons between 2000 and 2018, the expansion of urban built-up areas at the expense of croplands and green spaces has locally increased soil loss risk.

The expansion and spread of residential areas have been linked with increases in soil erosion risk within areas of intense human activities (Table 5.8). The relationship between LULC and soil erosion risk analysis reveals that in concentrated residential areas in 2000 about 14,018 tons of estimated soil loss occurred, while about 19,858 tons of estimated soil loss occurred in 2018. The estimated increase of soil loss in concentrated residential areas corresponds to the massive growth of built-up areas and the coinciding increase of impervious surfaces (Gumindoga *et al*., 2014). The observed changes in built-up areas are significantly attributed to population growth in the Epworth district. The population was estimated to have increased from approximately 114,067 in 1992 to about 167,462 in 2012 (ZimStats 2012). The resulting reduced infiltration rates contributing to high rates of surface runoff (Braud et al. 2013), result in soil damage down the slope and parallel to roads (Dams *et al*., 2013). The increase in estimated soil loss in the residential areas of the Epworth district are comparable with those in Kinshasa/DRC, where it is observed that highest soil erosion risk rates spatially correlate with steep slopes along river flanks and increasing density of informal settlements (Kabantu *et al*., 2018). Estimated soil loss in less concentrated residential areas increased from 6218 tons in 2000 to approximately 12,203 tons in 2018. This corresponds to a doubling in size of the land use class “less concentrated residential areas” in the Epworth district from 15.5% in 2000 to 31.5% in 2018 (Table 5.8). The increase in soil loss for less concentrated residential areas may have resulted from the registered decrease in green spaces (Table 5.8). This is possibly attributed to high population pressure and demand for shelter, hence propelling landowners to informally construct shacks on their backyards to curtail housing demand. These activities inevitably occur at the expense of green spaces and ground cover resulting from clearing of land for construction (Lee and Pradhan 2006; McCool *et al*., 1987).

Steep areas have high potential erosion risk as well as estimated soil erosion risk, especially on the flanks of the streams (Evans 2002; Kamuju 2016). This corresponds to the high loading of slope steepness in the RUSLE model (Assouline and Ben-Hur 2006; Koirala *et al*., 2019). The combination of slope inclination with slope length contributes to the cumulative effect of

increasing surface flow with increasing the drainage basin resulting in increased soil erosion risk (Kabantu *et al*., 2018; Opeyemi *et al*., 2019). For the Epworth district, wall around homesteads and industrial areas most likely acted as physical barriers for surface runoff, reducing slope length and affecting flow velocity and flow direction of surface runoff.

The spatial pattern of current soil erosion damage as documented in a diagram map is based of field survey in December 2019 (Figures 5.5 and 5.6). The field measurements data serve as a validation tool for the estimated soil erosion risk modelling for the Epworth district. The plot-based field measurements recorded reflect the extent of erosion prevalent within the mapped area. The RUSLE model is presumed to predict the amount of soil moved on the field (Alewell *et al*., 2015; Trirnble and Crosson 2000); henceforth, the spatial damage data from the field measurements represented the proportions of soil moved. These mapped sites of the spatial extent damage map spatially concur with soil loss estimated using the RUSLE model. This, however, improves the model evaluation despite the lack of sheet erosion assessment. Even though, (Auerswald *et al*., 2006; Lazzari *et al*., 2015) reiterated that empirical modelling requires long-term field measurements and the analysis of sedimentation rates for validation purposes. The utilization of point-like plot-based data from field surveys for validation improves the evaluation of the model outputs and its understanding (Cerri *et al*., 2001; Montgomery 2007; Seutloali *et al*., 2017). Validation of soil erosion risk modelling by comparison with outcomes of current damage mapping was further coupled with an analysis of the relationship between LULC and estimated soil erosion risk (Prasannakumar *et al*., 2012; Abdulkareem *et al*., 2019).

A total area of 765 m^2 was subjected to soil erosion in 2019 recorded for the 49 randomly selected sampling plots covering an area of 15.7 ha in the Epworth district. The randomized locations of the plot measurements indicate that eroded areas occurred in high frequency in the southwestern and southeastern parts of the Epworth district. Evidently, the spatial extent soil erosion damage in the diagram map indicates altogether low percentages of disturbance with a range of 0%–1.4% damaged area in the surveyed plots. However, during the field survey, the observed damage resulting from soil erosion (Figure 5.6) appears to be greater in extent and magnitude than the depicted damage illustrated on the soil erosion damage map (Figure 5.5). In comparison to the maps displaying the soil erosion risk based on the application of the RUSLE model, the spatial extent of soil erosion damage has been observed to spatially concur majorly in the southwestern and southeastern parts of the district where LS factor is presumably high. Areas of high surface damage could be identified in the southeast of the district and were predominantly observed in croplands and areas undergoing construction.

The field survey positively contributes to the study through the identification and registration of areas vulnerable to soil erosion (Figure 5.5), which therefore lessens the burden of the resource strained land managers and local boards in developing conservation strategies direct on hotspots rather than concentrating on the entire district (McDowell and Srinivasan 2009; Meshesha *et al*., 2014). Areas of high soil erosion risk which occur in zones with high topographic (LS) factors can be confirmed by strong surface damages (Figure 5.5). Nevertheless, the exclusion of sheet erosion recording and quantification during conducting damage mapping reduces the usability of the soil erosion damage map for the validation of the soil erosion risk mapping applying the RUSLE model (van Dijk *et al*., 2005); this is because sheet erosion has a major contribution to erosion damage and is included in the RUSLE model (Asiedu 2018; Tundu *et al*., 2018; Koirala *et al*., 2019). However, the conclusions were drawn on the basis of field observations due to the heterogeneity of the urban set-up and the widespread nature of impervious surfaces.

The modelling findings reveal that topographic characteristics (LS factor) significantly influence potential erosion and soil erosion risk in the Epworth district, which concurs with the findings by (Shikangalah *et al*., 2017) that model-based distribution patterns of soil erosion risk in the area of Windhoek, Namibia were mainly defined basing on the spatial structure of slope. The high soil erosion risk observed on sloppy areas in Epworth district corresponds to areas with convex to straight profile curvature and to the occurrence of ridges (Hill and Schütt 2000; Pickup and Chewings 1988). Furthermore, along the channel flanks modelled soil erosion risk was in general high, predominantly controlled by relief (Evans 2002). Due to the southward drainage of the stream network in Epworth district and thus, southward increasing incision of the streams, increased soil erosion risk along the river flanks can be predominantly observed and also on the southeast areas (Figure 5.5). In contrast, the analysis of the effects of LULC change on soil erosion pointed out that increasing distribution of built-up areas as a result of high population pressure and demand for shelter substantially propels soil erosion risk within residential areas.

5.5 Conclusion

Soil erosion is a global environmental concern impacting negatively on agricultural productivity, accessibility to properties and also posing flooding risk in urban areas. The empirical RUSLE model was implemented to assess vulnerable areas and the computation of soil erosion risk through the integration of GIS and remote sensing techniques. The quantitative assessment of average annual soil loss for the Epworth district using the RUSLE model

considers climate, soil, land use and topographic datasets as input parameters. Areas with high soil erosion risk were found to spatially correlate with topographic characteristics, especially slope length and slope steepness. The unrestricted LULC changes resulting from rampart informal settlements growth have accentuated soil erosion risk in the Epworth district. The analysis of LULC and estimated soil erosion risk improves the understanding of the spatial distribution patterns of soil loss for the different land uses in the years 2000 and 2018. The predicted soil erosion loss in the Epworth district amounted to 50,408 tons in 2000 while, 42,934 tons were estimated for 2018. Thus, the findings reveal that estimated soil erosion risk in total decreased over the study period (2000–2018). This is attributed to the reduction of croplands and areas covered by green spaces at the expense of built-up areas. Soil loss massively increased in the residential areas from 20,236 tons in 2000 to 32,061 tons 2018, regardless of the concentration of built-up areas (concentrated and less concentrated residential areas); in total the area covered by residential areas almost doubled between 2000 and 2018. Increasing impervious surfaces, sealed areas and avoidance of paved areas during high traffic flow have been observed as contributing factors towards increased generation of surface runoff and hereby affected soil erosion risk in the growing residential areas of the Epworth district.

The soil erosion damage map generated from the field measurements served as a validation tool for the study as it revealed areas vulnerable to soil erosion within the Epworth district that concur with the results of the application of soil erosion risk models. The area affected by soil erosion in the surveyed plots showed damages of 0%–1.4% in the spatial extent of the mapped plot area. Therefore, field mapping data have been observed as necessary in ascertaining and improving an understanding of quantitative soil erosion modelling. Model validation demonstrated that the RUSLE model performance was good due to positive correlation between field measurements and model results basing on sample areas ($r = 0.76$, $R^2 = 0.58$, $p < 0.05$). It can be concluded that the spread of urban built-up areas without implementation of sound conservation practices, such as proper land suitability analysis and the construction of runoff drainage canals, will increase soil erosion damage by water. Although, the research has predicted potential erosion risk and soil erosion risk, it is important to outline that there are uncertainties with the modelled data provided by the RUSLE model arising from the lack of site-specific parameterization. Limited studies on water-induced soil erosion for urban areas within the region reduce options for data comparison. However, the computed soil erosion risk maps may assist environmental managers and land and policymakers on planning mitigatory measures for the study area.

5.6 Acknowledgments

The publication of this article was funded by Freie Universität Berlin. We thank our colleagues from Freie Universität Berlin, who provided valuable insights and expertise that greatly assisted this study. We are grateful to the National Aeronautics and Space Administration (NASA) and the United States Geological Survey (USGS), for providing the high-resolution satellite images and the one Arc-Second Global data from the Shuttle Radar Topography Mission (SRTM) for providing terrain corrected data.

5.7 Link with other chapters

Chapter 5 mapped the spatial distribution of soil erosion risk and estimated soil loss rates for the years 2000 and 2018 for Epworth district of the Harare Metropolitan Province applying the empirical RUSLE model. The work on this chapter embraced the machine learning SVMs supervised classification maps for the estimation of soil loss and risk assessment over two time periods to evaluate the spatial extent due to land use changes and climate variability. The study also mapped potential soil erosion risk making crop cover management and support practices independent elements in order to assess the impact of vegetation and land management on the landscape. However, the study only mapped past and current soil erosion risk allowing the introduction of Chapter 6, which demonstrated the likely future impacts of urbanization and climate change on the urban environment.

Marondedze, A. K.; Schütt, B. Predicting the Impact of Future Land Use and Climate Change on Potential Soil Erosion Risk in an Urban District of the Harare Metropolitan Province, Zimbabwe. Remote Sens. **2021**, *13(21), 4360. https://doi.org/10.3390/rs13214360*

CHAPTER 6: PREDICTING IMPACTS OF FUTURE LAND USE LAND COVER AND CLIMATE CHANGE ON URBAN LANDSCAPE

Abstract

Monitoring urban area expansion through multispectral remotely sensed data and other geomatics techniques is fundamental for sustainable urban planning. Forecasting of future land use and land cover (LULC) change for the years 2034 and 2050 was performed using the Cellular Automata Markov model for the current fast-growing Epworth district of the Harare Metropolitan Province, Zimbabwe. The stochastic CA–Markov modelling procedure validation yielded kappa statistics above 80%, ascertaining good agreement. The spatial distribution of the LULC classes CBD/Industrial area, water and irrigated croplands as projected for 2034 and 2050 show slight notable changes. For projected scenarios in 2034 and 2050, low–medium-density residential areas are predicted to increase from 11.1 km^2 to 12.3 km^2 between 2018 and 2050. Similarly, high-density residential areas are predicted to increase from 18.6 km^2 to 22.4 km^2 between 2018 and 2050. Assessment of the effects of future climate change on potential soil erosion risk for Epworth district were undertaken by applying the representative concentration pathways (RCP4.5 and RCP8.5) climate scenarios, and model ensemble averages from multiple general circulation models (GCMs) were used to derive the rainfall erosivity factor for the RUSLE model. Average soil loss rates for both climate scenarios, RCP4.5 and RCP8.5, were predicted to be high in 2034 due to the large spatial area extent of croplands and disturbed green spaces exposed to soil erosion processes, therefore increasing potential soil erosion risk, with RCP4.5 having more impact than RCP8.5 due to a higher applied rainfall erosivity. For 2050, the predicted wide area average soil loss rates declined for both climate scenarios RCP4.5 and RCP8.5, following the predicted decline in rainfall erosivity and vulnerable areas that are erodible. Overall, high potential soil erosion risk was predicted along the flanks of the drainage network for both RCP4.5 and RCP8.5 climate scenarios in 2050.

Keywords: land use and land cover (LULC); Cellular Automata Markov model; representative concentration pathways; climate scenarios

6.1 Introduction

Soil erosion by water has become a global threat undermining environmental sustainability (Borrelli *et al*., 2020). This is attributed to various controlling factors related to Land Use and Land Cover (LULC) changes influenced by population growth, rising economic activities, unsustainable agricultural practices and climate change (Mondal *et al*., 2015; Karydas *et al*., 2009). LULC change has been reviewed as one of the main driving forces of global environmental change, making it an important factor to assess at different spatio-temporal levels (Islam *et al*., 2018; Lambin 1997). The LULC changes at both local and global levels are dynamic processes (Mondal *et al*., 2015) and their drivers correspond to complex systems with dependent characteristics and interactions having a wide array of implications for the future ecological balance and environmental sustainability. Urbanization, as one among the major drivers of LULC change, depends on population growth, migration and desires to change the current state of the Earth. These actions could be for the betterment of livelihoods and in turn could be detrimental to the environment and humankind (Brueckner and Helsley 2011; Jat *et*

al., 2017). The resulting ramifications include the modification of the landscape due to the sprawling of unplanned urban built-up areas, development of urban heat islands and over-exploitation of natural resources as direct impacts, and collateral land degradation, climate change, soil erosion and siltation (Hegazy and Kaloop 2015; Jat *et al.*, 2017; Mushore *et al*., 2017).

The United Nation's World Urbanization Prospects reveal that the global urban population increased from about 30% in 1950 to approximately 54% in 2014, with almost 2.5 billion urban dwellers expected by 2050 (UN 2014). For India, approximately 50% of the population have been projected to be living in cities by 2050 as a result of rural–urban migration due to increased economic activities in the urban areas, which have become a strong pulling factor (UN 2012). Rapid urbanization in Africa has been reported due to population growth and it has been projected to almost triple by 2030 (UN 2012). However, according to information from the World Economic Forum, in 2020 56.2% of the global population already lived in cities (World Economic Forum 2020), with highly variable rates between regions, ranging from 81.2% urban dwellers in Latin America and the Caribbean to 43.5% in Africa (UN. Population Division 2020). Breaking these data down to Zimbabwe, about a quarter of the country's population lives in urban areas. Focusing on the case study of Epworth district, being part of the Harare Metropolitan Province, approximately 47% of the population increase was registered between 1992 and 2012 (ZimStats 2012), with a triplication of built-up areas from about 19.5% in 1984 to 61.3% in 2018 (Marondedze and Schütt 2019). Such trends in urban population growth directly impact the ecosystem of the urbanizing area, including the peri-urban area. This earmarks a gap which requires monitoring of the impacts driven by rampant LULC changes through urban expansion on the ecosystem as a basis to implement a proper spatial policy to enable effective decision-making processes (Aburas *et al*., 2016; Myers 2011). This implies a rich understanding of the trends of urban expansion and development, and it requires the integration of spatially differentiated data, applying geomatics to quantify and predict future spatial distributions (Pontius 2000; Sudhira *et al*., 2004). By the case study of the Epworth district in the Harare Metropolitan Province, it will be demonstrated that future land use models provide a valuable basis for foresight spatial planning to ensure environmental sustainability.

The LULC changes occurring at unprecedented levels threaten multiple ecological processes such as surface runoff, soil erosion, siltation and agricultural non-point source pollution, resulting in landscape degradation, habitat loss and inaccessibility to properties (Chalise *et al*., 2019; Shikangalah *et al*., 2017). Focusing on sub-Saharan metropolitan areas, the example of the Harare Metropolitan Province documents a rapid transformation of urban

agricultural land and shrub lands to built-up areas and other sealed settlement areas over the past decades (Kamusoko *et al*., 2013; Mushore *et al*., 2017). For example, Epworth district, as part of the Harare Metropolitan Province, has witnessed an increase in built-up areas linked with high soil erosion risk due to increased impervious surfaces and construction activities which facilitate surface runoff (Marondedze and Schütt 2020). This results in accelerated soil loss in sensitive areas mostly within active built-up areas. The radical LULC changes in this area also include the loss of water bodies due to siltation resulting from sand mining and brick moulding along the river banks; encroachment of wetlands by construction activities; and grading of unpaved roads which later facilitate accelerated surface runoff due to compaction (USDA. NRCS 2000).

Furthermore, climate change is reiterated to be heavily associated with locally increasing rainfall intensity, frequency and extent, resulting in increasing rainfall erosivity (Pruski and Nearing 2002). The Fifth Assessment Report (AR5) of the IPCC (Intergovernmental Panel on Climate Change) highlights that global mean precipitation and surface temperatures have significantly changed with reference to observed changes between 1850 and 1900, and these changes are likely to continue to be experienced in the 21st century (IPCC 2014). Several studies point out that accelerated soil erosion by water due to climate change accentuates processes that alter soil physiochemical and biological properties (Gupta and Kumar 2017; Li and Fang 2016; Segura *et al*., 2014). This entails the need to curb soil erosion through minimizing the removal of vegetation cover, improving surface roughness to facilitate infiltration capacity and reducing rainfall-runoff processes (Simonneaux *et al*., 2015). Climate change also inevitably triggers a shift in land use, forcing the adoption of new management practices and planting new crops in order to mitigate detrimental impacts (Feng *et al*., 2010; Routschek *et al*., 2014).

The sketched interrelations between LULC change and climate change and its possible environmental impacts emphasize the need to investigate future potential impacts of LULC change and climate change on potential soil erosion risks caused by water. For the coming decades, for wider areas, the increasing intensity of the hydrological cycle is projected by multiple global circulation models (GCMs), pronouncing more intense rainfall events that directly influence rainfall erosivity (IPCC 2014). We want to investigate these interrelations using the example of Epworth district, a fast-growing urban area of the Harare Metropolitan Province. Soil erosion by water has been repeatedly investigated in different regions of Zimbabwe, focusing on either catchments or arable areas (Makwara and Gamira 2012; Tundu *et al*., 2018; Whitlow 1988). There is limited knowledge regarding estimated future soil loss

rates and potential soil erosion risk in Zimbabwe as impacted by future climate change and land use changes, knowledge indispensable for future policy decision-making processes. The current study examines the potential future effects of land use change as well as of climate change on soil erosion risk. Overall, climate change scenarios as provided by the IPCC (2014) and forecasts of LULC change were applied for the assessment of future potential soil erosion risk for the years 2034 and 2050.

6.1.1 Modelling land use changes in urban areas

Multiple studies on future soil erosion focus mainly on the dynamics of climate variables such as temperature and rainfall (Mullan *et al*., 2012; Routschek *et al*., 2014), while land use changes are rarely considered regardless of the high awareness of processes such as population growth, immigration and urbanization occurring at alarming rates. There is a wide range of spatial models able to simulate and predict land use changes based on the application of remote sensing techniques (Herold *et al*., 2003; Tang *et al*., 2007). The spatial transition model and statistical description model are the two major models widely used for the assessment and monitoring of land use changes (Herold *et al*., 2003; Hegazy and Kaloop 2015; Tang and Di 2019). Furthermore, the Markov chain model is widely applied to simulate urban growth due to its capability of quantifying land use changes, their trends and their dimensions (Ahmed and Ahmed 2012; Halmy *et al*., 2015; Hashem and Balakrishnan 2015; Kamusoko *et al*., 2013; Mushore *et al*., 2017; Sang *et al*., 2011). Markov chain models correspond to stochastic processes (Balzter 2000) that summarize changes by developing a transition probability matrix of land use change, indicating that the probability of a system being in one state at a given time can be determined if the state at an earlier period is known (Ahmed and Ahmed 2012; Yang *et al*., 2014). The Cellular Automata (CA) are simple and flexible dynamic spatial systems able to integrate complex urban systems in order to simulate future urban growth patterns (Clarke *et al*., 1997; Fitawok *et al*., 2020; White and Engelen 1993). The CA are based on the supposition that land use change for any given location (grid cell) can be explained by its present state and the transformations in its neighbouring cells (Koomen and Beurden 2011). Therefore, the inability of the Markov chain model to simulate spatial changes over time is superseded by integrating it into the CA to enhance the spatial predictive accuracy of the urban land use dynamics (Aburas *et al*., 2017; Alsharif and Pradhan 2014; Fitawok *et al*., 2020; Sibanda and Ahmed 2020; Wang *et al*., 2019).

Previous studies have adopted simulation models that apply GIS and remote sensing techniques for land use change modelling and monitoring of dynamic urban growth patterns

(Aburas *et al*., 2017; Ahmed and Ahmed 2012; Clarke *et al*., 1997). In the case of Harare Metropolitan Province, due to the dynamic nature of urban growth, some parts of its districts were simulated using the CA–Markov model in order to predict the impact of urban land use change on future microclimate (Mushore *et al*., 2017), while Sibanda and Ahmed (2020) predicted the future LULC and their impacts on wetland areas in the Shashe sub-catchment of Zimbabwe. According to Mushore et al. (2017), accelerated urban growth without the conservation of green spaces and adherence to mitigation policies contribute to locally increasing microclimate temperatures, causing thermal discomfort in urban areas. The CA–Markov model was also applied to project future LULC scenarios for Arasbaran biosphere reserve in Iran (Parsa *et al*., 2016). Future LULC distribution patterns were also simulated with high accuracy using the CA–Markov model for Jordan's Irbid governorate, with built-up areas predicted to increase from about 19.5% to approximately 64.6% between 2015 and 2050 (Khawaldah *et al*., 2020). Due to the plausible outcomes, recommendations indicate that the CA–Markov model is an effective tool in monitoring and assessing future land use patterns for policy and decision-making processes (Ahmed and Ahmed 2012; Alsharif and Pradhan 2014; Sibanda and Ahmed 2020; Wang *et al*., 2019).

6.1.2 Climate change emission scenarios

The establishment of the Representative Concentration Pathways (RCPs) as future climate change mitigation scenarios followed a response call on the effectiveness of climate policy inclusion in future climate change modelling and research (IPCC 2014; Moss *et al*., 2010; van Vuuren *et al*., 2011). The RCPs illustrate how the future climate may evolve, considering a range of variables which encompass socio-economic changes, technological advancement, energy, greenhouse gas emissions and land use changes (IPCC 2014). Most precipitation projections from GCMs have been widely used on land surface processes for the assessment of climate change impacts and adaptation (Borrelli *et al*., 2020; Panagos *et al*., 2017; Vrieling 2006). However, uncertainties in GCMs primarily exist on biases of raw outputs, resulting in either over or underestimation of climate variables due to erroneous assumptions in the model's development (Nasrollahi *et al*., 2015; Räisänen 2007). As such, many studies have embarked on the use of multi-modelling techniques to minimize the uncertainty of future predictions in order to obtain plausible future projections (Ahmadalipour *et al*., 2017; Chemura *et al*., 2021; Demirel and Moradkhani 2016; Murphy *et al*., 2004; Najafi and Moradkhani 2016).

The climate change emission scenarios approximate radiative forcing levels of greenhouse gas concentrations, aerosols, and tropospheric ozone precursors by 2100 (van

Vuuren *et al*., 2011). The RCP8.5 scenario is characterized by increasing levels of greenhouse gas concentrations (Riahi *et al*., 2007). Further, the RCP8.5 is a highly energy-intensive scenario attributed to high population growth and a lower rate of technology development; this is a scenario with little to no climate policy, making it possible to represent all future climatic possibilities (IPCC 2014; van Vuuren *et al*., 2011). For the RCP4.5 scenario, historical emissions and land cover information are integrated in order to follow a cost-effective pathway through stabilization of anthropogenic components to reach the target radiative forcing (Moss *et al*., 2010; Thomson *et al*., 2011). The RCP4.5 considers technological advances such as combining bioenergy production with CO_2 capture and geologic storage to enhance more energy production with negative carbon emissions (Luckow *et al*., 2010; Thomson *et al*., 2011).

6.2 Materials and Methods

6.2.1 Study area

The Harare Metropolitan Province is the capital city of Zimbabwe, with Epworth district 17°40'–18°00' S, 30°55'–31°15' E located approximately 12 km southeast of the Central Business District (CBD) (Figure 6.1). Epworth district is a high-density residential suburb of Harare Metropolitan Province and the smallest in terms of area-wide coverage among the four districts which comprise the Harare Metropolitan Province, occupying an estimated area of 35 km^2; the area is characterized by the densification of built-up structures and overcrowdings (Chirisa and Muhomba 2013) and an above-average increase in informal urban development in comparison to other urban districts in Zimbabwe (Potts 2011; Tibaijuka 2005). There has been rampant population growth and mushrooming urban built-up structures due to rural–urban migration which dates back to the pre-and post-independence phase (1980) in search of better livelihoods, employment and a hive of economic activities in the capital city (Butcher 1986; Tibaijuka 2005; ZimStats 2012). Since then, Epworth district has grown from about 500 families recorded in 1950, to a total population of approximately 114,047 in 2002, to a total population of 167,462 in 2012 (Butcher 1986; CSO 2004; ZimStats 2012).

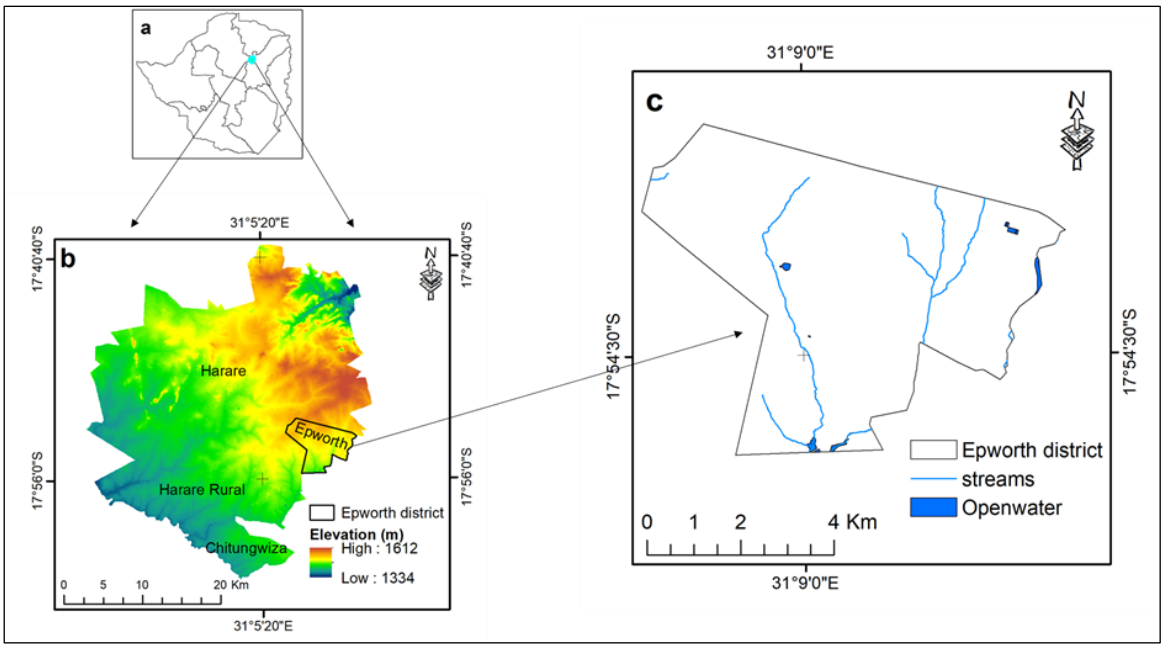

Figure 6. 1 Study site—Epworth district of the Harare Metropolitan Province. (**a**) Zimbabwe provincial boundaries including the Harare Metropolitan Province. (**b**) Elevation and district boundaries of the Harare Metropolitan Province. (**c**) Epworth district with hydrological network, retrieved from OSM data (OSM-Geofabric).

The Harare Metropolitan area is located on the Highveld at an elevation between 1455 m and 1556 m a.s.l., with a general topography characterized by undulating to slightly rolling terrain in the plateau areas. Annual precipitation in Harare Metropolitan Province varies between 470 mm and 1350 mm, falling mainly during the four months of the rainy season between mid-November to mid-March. Daily temperature ranges between 13 °C and 28 °C during the hot-dry season (September to mid-November) and low temperature averages between 7 °C and 20 °C are experienced during the cool-dry season (mid-May to August) (Kamusoko *et al*., 2013). Dominating soil types in Epworth district are the widely spread Paraferrallitic soils (coarse grained) covering the high-altitude areas and clayey Fersiallistic soils developed predominantly from dolerite in the central plateau (Nyamapfene 1991). Both soil types are largely influenced by nutrient loss through moderately to strongly occurring leaching processes (Nyamapfene 1991; Thompson and Purves 1978).

6.2.2 Urban land use change modelling using CA–Markov

The CA–Markov analysis was adopted to predict land use future scenarios. The CA–Markov model is embedded into the IDRISI software (Clarks Lab), an image processing software useful for improved digital image display and spatial analysis (Eastman 2009). The Markov chain analysis describes the probability of LULC changes from one state to another at given times t_1 and t_2 by developing a transition probability (Araya and Cabral 2010; Eastman 2000; Koomen

and Beurden 2011). The Markov chain model simulates land use changes and generates a transition probability matrix, which indicates the probability of each LULC to change from one state to another, and this is obtained by cross tabulation of the earlier and later LULC maps. The proportional changes become the transition probability, indicating that each land use class will change to other categories using Equation (2). The conditional suitability maps are produced and display the probability that each land use category might be found at each pixel, with values standardized between 0 and 255 (Hashem and Balakrishnan 2015; Kumar *et al*., 2014; Mushore *et al*., 2017; Subedi *et al*., 2013; Ye and Bai 2008). The transition probability of converting the current state of a system to another state in the next time step is determined using the mathematical expression Equation (6.1) (Guan *et al*., 2008; Kumar *et al*., 2014):

$$P = (P_{ij}) = \begin{vmatrix} P_{11} & P_{12} \cdots & P_{1n} \\ P_{21} & P_{22} \cdots & P_{2n} \\ \cdots & \cdots & \cdots \\ P_{n1} & P_{n2} & P_{nm} \end{vmatrix} \quad (6.1)$$

where P*ij* is the probability from state *i* to state *j* and P_n is the state probability of any time. Equation (1) must satisfy the following conditions:

$$\sum_{j=1}^{n} P_{ij} = 1 \quad (i, j = 1, 2,3\ldots\ldots\ldots, n) \quad (6.2)$$

$$0 \leq P_{ij} \leq 1 \ (i, j = 1, 2,3\ldots\ldots\ldots, n) \quad (6.3)$$

These steps are performed to obtain the Markov chain model's primary matrix and the matrix of the transition probability (P_{ij}). The Markov prediction model is expressed as:

$$P_{(n)} = P_{(n-1)} \quad P_{ij} = P_{(0)} P_{ij}^{n} \quad (6.4)$$

where P_n refers to the state probability of any time and $P_{(0)}$ stands for the primary matrix. High transitions have probabilities near 1, while low transitions attract probabilities near 0 (Hamad *et al*., 2018; Kumar *et al*., 2014).

The Markov chain probabilities of change represent all multi-directional LULC changes between land use classes (Ye and Bai 2008). The Markov chains were selected as a result of their simplicity, robustness and capability in mapping LULC transitions in complex urban areas (Mushore *et al*., 2017; Subedi *et al*., 2013). Despite forecasting transition probabilities per land use category and their growth trends, the major limitation of the Markov chain model is its inability to simulate the spatial distribution of each land use category's occurrence (Eastman 2000; Hashem and Balakrishnan 2015; Ye and Bai 2008). Due to the heterogeneity of urban

systems and structures, historical information is essential for a better understanding and interpretation of simulated future spatial trends (Sudhira *et al*., 2004). The subsequent limitations of the Markov chains can be addressed by combining their outputs with other models that have open structures, including the Cellular Automata (CA), Multi-Layer Perceptron (MLP) and the Stochastic Choice (Eastman 2009; Hamad *et al*., 2018). In the present study, we integrated the CA into the Markov chain approach to address the spatiality limitations of the Markov chain model and the probable spatial transitions occurring in the study area over the given time (Ahmed and Ahmed 2012; Fitawok *et al*., 2020; Parsa *et al*., 2016; Subedi *et al*., 2013).

The CA have high spatial resolution and computational efficiency, enabling the prediction of future urban growth trends based on the supposition that the state of each cell at the present time depends on the previous state of cells within the neighbourhood (Clarke *et al*., 1997; Santé *et al*., 2010; White and Engelen 1993). Thus, the CA models are based on four major attributes, which include the cell, the state, the neighbourhood, and the transition rule (Fitawok *et al*., 2020; Jafari *et al*., 2016). The cell element of the CA signifies spatial shapes and sizes on the ground, while real characteristics of the area (land use) at a discrete time, represented as grid cells, show the state (Fitawok *et al*., 2020; Jafari *et al*., 2016; White and Engelen 1993). The neighbourhood cells are the immediate adjacent cells that form the kernel, and the transition rules theoretically code for the transformation from one cell state to another state resulting from the changes in neighbouring cells at a discrete time and state (Fitawok *et al*., 2020; Tang and Di 2019). Despite being a powerful and simple tool in modelling urban growth patterns, the CA models have a limited capability for quantifying aspects, and the simulation processes do not include urban growth driving forces (Aburas *et al*., 2017; Alsharif and Pradhan 2014).

The CA–Markov modules embedded in the IDRISI GIS software were used to simulate LULC distribution patterns for the year 2018 and to predict future LULC for the years 2034 and 2050. Primarily, the simulation phase of the 2018 LULC scenarios applied the Markov chain to generate a transition probability matrix, and transition suitability images between 1990 and 2008 using the LULC maps of the same period were generated using support vector machines (SVMs) by Marondedze and Schütt (2019). A proportional error of 15% was set during the modelling of the transition probability matrix (Eastman 2009). The Markov chain analysis outputs from 1990 and 2008 formed the basis of input parameters for the probable simulation of LULC spatial characteristics and their occurrence in the CA for the prediction of LULC patterns for 2018 (Figure 6.2). The contiguity filter specified the spatial characteristics

applied by the CA modelling approach (Ahmed and Ahmed 2012; Eastman 2009). For this study, a contiguity filter of 5*5 pixels was applied to define the kernel due to higher spatial characterization when applied to determine the occurrence or position of the simulated LULC category compared to 3*3 or 7*7 (Mondal *et al*., 2020, 2012).

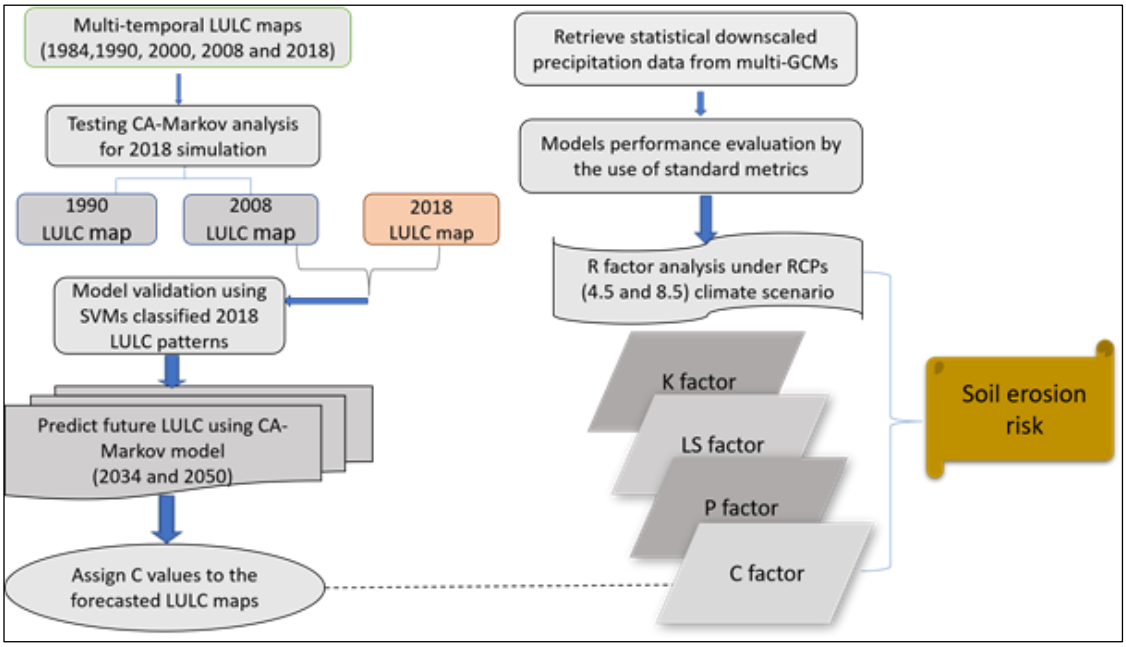

Figure 6. 2 Conceptual framework for the prediction of future LULC and soil erosion risk for Epworth district. LULC: land use and land cover. RCPs: representative concentration pathways, GCMs: global circulation models.

The spatiality characteristics in the CA approach were developed in a spatially explicit weighting that enabled the transformation of single and random grid cells in areas closer to the existing and widely spread land use (Parsa *et al*., 2016; Zubair 2006). This is further simplified by assuming that a pixel that is near one specific land cover class is more likely to be transformed to that category than pixels farther apart (Araya and Cabral 2010). This assumption was used to initially test the predictive capability of the CA–Markov model set of the LULC distribution patterns for 2018. The cross validation of the 2018 simulated LULC patterns was performed applying the LULC patterns as provided by a support vector machines (SVMs) supervised classification map (Marondedze and Schütt 2019). Finally, the CA–Markov techniques were applied between the LULC patterns of 2000 and 2018 for the prediction of future LULC distribution patterns for 2034, whilst the LULC distribution patterns of 1984 and 2018 were applied for the future prediction of 2050 LULC patterns. A 5*5 contiguity filter was applied for the prediction of future LULC patterns for the years 2034 and 2050.

6.2.3 CA–Markov chain validation

The simulated LULC distribution patterns for 2018 were compared with the SVMs classified map for the same year to test the level of agreement. A two-phase validation approach was performed, which includes visual inspection and quantitative evaluation (Mushore *et al*., 2017; Sayemuzzaman and Jha 2014). Visual inspection allowed close comparison and the agreement assessment between the simulated 2018 LULC map and the SVMs supervised classification LULC map. The kappa index of agreement (KIA) was used to assess the prediction accuracy for the 2018 actual map and the simulated LULC maps (Ahmed *et al*., 2013; Parsa *et al*., 2016; Sayemuzzaman and Jha 2014). In general, kappa is referred to as a member of a family of indices with the properties (a) kappa = 1, when the level of agreement is perfect, and (b) kappa = 0, when the observed agreement is equal to the expected proportion due to chance (Pontius 2000). Considering the model validity and performance in predicting LULC patterns for 2018, the LULC patterns for 2000–2018 and 1984–2018 were used in the prediction of 2034 and 2050 LULC spatial trends in the CA–Markov model. This introduces kappa indices to assess the performance and agreement of the model: the traditional kappa, which measures a simulation's ability to attain perfect classification, that is, the closer to 1 the values are, the higher the level of agreement ($K_{standard}$); the improved general kappa statistic, which is described as kappa for no ability (K_{no}); followed by the sophisticated kappa statistics ($K_{quantity}$ and $K_{location}$) used for distinguishing placement accuracies in both the quantity and location (Ahmed *et al*., 2013; Parsa *et al*., 2016). The K_{no} denotes the proportion classified correctly relative to the expected proportion classified correctly by a simulation without the ability to accurately specify quantity or location (Ahmed *et al*., 2013; Pontius 2000).

6.2.4 Predicting future soil erosion risk

The empirical RUSLE model was used to predict the spatially differentiated risk of long-term average annual soil loss. The selection of the empirical RUSLE model to assess future potential soil erosion risk considered the availability of data, robustness, complexity of the landscape and calibration (Merritt *et al*., 2003; Ranzi *et al*., 2012). The RUSLE model is widely used and a powerful tool to quantitatively assess spatial interactions of land use, topographic characteristics, climate, and soil characters in order to predict the spatial distribution of soil erosion (Renard *et al.*, 1997; Feng *et al.*, 2010; Prasannakumar *et al.*, 2012; Karamage *et al.*, 2017; Tundu *et al*., 2018). The wide use of the empirical RUSLE model is based on its simplicity and easy accessibility of data compared to complex physical models (Borrelli *et al*.,

2020; Smith 1999). Unlike other physical and process-based soil erosion models, the stochastic RUSLE model does not address soil deposition but mainly displays areas of sheet and rill erosion processes (Smith 1999), allowing land managers to direct limited resources for landscape management (Meshesha *et al*., 2014). The estimation of spatial soil erosion risk by the RUSLE model makes use of the factors soil erodibility (K), rainfall erosivity (R), slope length and steepness (LS), land cover and management (C) and the support practices (P) (Renard *et al*., 1997). The RUSLE model calculates the risk of long-term average annual soil loss rates by multiplying the different factors following Equation 6.5:

$$A = K * R * C * LS * P \quad (6.5)$$

where A: annual average soil loss (t ha^{-1} yr^{-1}), R: rainfall erosivity factor (MJ mm ha^{-1} h^{-1} yr^{-1}), K: soil erodibility factor (t ha h ha^{-1} MJ^{-1} mm^{-1}), C: cover-management factor (dimensionless), LS: slope length and slope steepness factor (dimensionless) and P: support practices factor (dimensionless).

The RUSLE factors harmonized at 30 × 30 m spatial resolution for the compatibility of data from different sources (Ai *et al*., 2013) are multiplied to predict the soil erosion risk for the district using raster calculator in ArcGIS® 10.2. The computation of the RUSLE model integrates remote sensing and GIS techniques to analyse factors and geostatistics for the graphical interpretation (Ferreira *et al*., 2016; Renard *et al*., 1997).

Soil erodibility factor (K). The soil erodibility factor (K) represents the susceptibility of the soil to detachment due to rainfall erosivity (R) (Renard *et al*., 1997). The soil erodibility factor varies corresponding to soil properties such as soil texture, type and size of aggregates, shear strength, soil structure, infiltration capacity, bulk density, soil depth, organic matter and other chemical constituents (Wischmeier and Smith, 1978; Renard *et al*., 1997). Based on the RUSLE model, the estimated K-factor values range between 0 and 1, indicating the degree of soils' susceptibility to erosion (Renard *et al*., 1997). Thus, soils being highly susceptible to erosion have soil erodibility values near 1, whereas the corresponding values close to 0 designate the resistive ability of a particular soil to erosion processes (Woldemariam *et al*., 2018). For this research, available data for the computation of the K factor were retrieved from ISRIC (International Soil Reference Information Centre), available at 250 m spatial resolution (Hengl *et al*., 2017). The estimation of the K factor was performed using the equation by Sharpley and Williams (1990), which excludes soil structure and profile permeability due to the unavailability of experimental based information.

Slope length and slope steepness factor (LS). The RUSLE model considers the effects of topography on soil erosion, including slope length (L) and slope steepness (S). The Shuttle Radar Topography Mission (SRTM) digital elevation model (DEM) with a spatial resolution of 30 × 30 m (https://earthexplorer.usgs.gov/SRTM1Arc; accessed on 19 September 2020) was used for the computation of the LS factor using the Hydrology module (field-based), embedded in SAGA 2.3 software (Desmet and Govers 1996; Panagos *et al*., 2015a).

Land cover and management factor (C) and support practice factor (P). The land cover and management factor of the RUSLE model represents the effects of vegetation cover on soil erosion rates (Renard *et al*., 1997). The C factor ranges from 0 for high-density vegetation to 1 for barren land; bare land is frequently used as the reference land use for C factor calibration (Kefi *et al*., 2011; Panagos *et al*., 2015b). The vegetation cover plays a vital role in dissipating raindrop energy before reaching the surface, thereby reducing the harsh effects posed by raindrop impact on the soil surface (Ferreira *et al*., 2016; Kefi *et al*., 2011). The C factor values in Table 6.1 result from the weighted field-based observations, and additional biophysical characterizations were adopted (Marondedze and Schütt 2020). The support practice factor (P) was assigned to be 1, corresponding to the lack of support practice all over the study area (Marondedze and Schütt 2020).

Table 6.1 The weighted C factor values.

Land Use Class	Weighted C Factors
CBD/industrial areas	0.017
LMD (less concentrated residential area)	0.066
HD (concentrated residential area)	0.083
Irrigated cropland	0.166
Rainfed cropland	0.239
Green spaces	0.03
Water	0

Rainfall erosivity factor (R) estimation: The R factor describes the soil loss potential triggered by rainfall (Stocking and Elwell, 1976; Wischmeier and Smith, 1978; Renard *et al.*, 1997). As such, the analysis of the spatial distribution of rainfall erosivity was computed following the empirical relations developed by El-Swaify *et al*., (1987) Equation 6.6, as cited (Tundu *et al*., 2018; Merritt *et al*., 2004),

$$R = 38.5 + 0.35\ x\ M \quad (6.6)$$

where R = rainfall erosivity factor (MJ mm ha^{-1} h^{-1} yr^{-1}), and M = mean annual rainfall.

The further analysis highlights the likely potential effects of climate change on the R factor. The representative concentration pathway (RCP) 4.5 and 8.5 climate scenarios projected by multiple general circulation models (GCMs) were selected for the assessment of future climate change, primarily variations in precipitation magnitudes on soil erosion risk (downloaded from https://earthobservatory.nasa.gov/images/86027/; accessed on 02 October 2020). These climate change scenarios constitute a set of greenhouse gas concentration and emission pathways to facilitate decision and policy makers in the crafting of sustainable climate policies due to their plausibility (Thomson *et al*., 2011; van Vuuren *et al*., 2011). To predict future rainfall erosivity, future RCP 4.5 and 8.5 climate scenarios proposed by the Intergovernmental Panel on Climate Change (IPCC 2014) were applied (Table 6.2). Annual rainfall, as required for Equation 6.6, was the sum of mean monthly rainfall data retrieved from the NASA Exchange Global Daily Downscaled Projections (NEX-GDDP), as listed in Table 6.2, which was statistically downscaled to a 0.25° by 0.25° spatial resolution (Ahmadalipour *et al*., 2017; Thrasher *et al*., 2012). The NEX-GDDP general circulation models grid point data locations do not match with the Harare Meteorological gauging points, as the spatial coverage of station data is not uniform; to cope with the varying spatial resolutions, annual averages were interpolated using the inverse distance-weighted methods (Mondal *et al*., 2015).

Table 6.2 Global circulation models (GCMs) used for data retrieval.

Global Circulation Model	Source	Original Resolution
		(Lat × Lon) °
ACCESS1-0	Commonwealth Scientific and Industrial Research Organization/Bureau of Meteorology, Australia	1.875 × 1.25
BNU-ESM	College of Global Change and Earth System Science, Beijing Normal University, China	2.8 × 2.8
CanESM2	Canadian Centre for Climate Modeling and Analysis, Canada	2.8 × 2.8
CCSM4	National Centre for Atmospheric Research, United States	1.25 × 0.94
CNRM-BGC	National Centre for Meteorological Research, France	1.4 × 1.4
GFDL-ESM2G	NOAA/Geophysical Fluid Dynamics Laboratory, United States	2.5 × 2.0
GFDL-ESM2M	NOAA/Geophysical Fluid Dynamics Laboratory, United States	2.5 × 2.0
IPSL-CM5A-MR	L'Institut Pierre-Simon Laplace, France	2.5 × 1.25
MIROC-ESM	Japan Agency for Marine-Earth Science and Technology, Atmosphere and Ocean Research Institute (The University of Tokyo), and National Institute for Environmental Studies	2.8 × 2.8
MIROC-ESM-CHEM	Japan Agency for Marine-Earth Science and Technology, Atmosphere and Ocean Research Institute (The University of Tokyo), and National Institute for Environmental Studies	2.8 × 2.8
MIROC5	Atmosphere and Ocean Research Institute (The University of Tokyo), National Institute for Environmental Studies, and Japan Agency for Marine-Earth Science and Technology, Japan	1.4 × 1.4
MPI-ESM-LR	Max Planck Institute for Meteorology, Germany	1.9 × 1.9
MPI-ESM-MR	Max Planck Institute for Meteorology, Germany	1.9 × 1.9
MRI-CGCM3	Meteorological Research Institute, Japan	1.1 × 1.1
NorESMI-M	Norwegian Climate Center, Norway	2.5 × 1.9

General circulation models' performance was assessed, comparing their average annual rainfall data as provided per grid cell between 1980 and 2005 with the observed data from Harare gauging stations. This evaluation was processed by applying the interpolated GCMs average rainfall data from six available grid points within the Harare Metropolitan Province in parallel with observed average precipitation from the Harare Meteorological stations (Table 6.3) using the standard statistical metrics (Sardari *et al*., 2019). The evaluation of the GCMs performance was assessed using the standard metrics to outweigh GCMs that are not representative: the coefficient of determination (R^2), relative root mean square error (rRMSE) (%), correlation coefficient (r), and index of agreement (d) (Bsaibes *et al*., 2009; Chen *et al*., 2011; Chemura *et al*., 2021). With values ranging between 0 and 1, the lower the values of the rRMSE, the better the model's performance, while the higher the value for R^2, the better the goodness of fit of the model (Bsaibes *et al*., 2009; Chen *et al*., 2011, 2013). For the index of agreement (d), the closer values are to 1, the better they document the increasing goodness of the fit of the model,

ascertaining that there is good agreement between the simulated and observed annual precipitation (Araya *et al*., 2015; Chemura *et al*., 2021; Willmott 1982).

Table 6.3 Location of Harare Metropolitan Province gauging stations.

Rain Stations	Coordinates	Altitude (m.a.s.l)	Mean Annual Precipitation (mm)
			1980–2005
Kutsaga	17° 55′ S, 31° 08′ E	1488	825.3
Belvedere	17° 50′ S, 31° 01′ E	1474	862.6
Airport	17° 55′ S, 31° 06′ E	1502	798.2

Separate runs of the GCMs ensemble averages from 2019 to 2034 and 2035 to 2050 were used for the assessment of climate variability and its impact on future soil erosion risk under RCP4.5 and RCP8.5 climate scenarios. Estimations of future climate change scenarios from single GCMs relay limited information required for the direct calculation of the R factor (Nearing 2001; Zhang 2007). Therefore, the application of multi-GCM ensemble averages decreases individual model errors and provides more robust predictions for future climate change (Räisänen 2007; Sperna Weiland *et al*., 2012; Vrochidou *et al*., 2013; Demirel and Moradkhani 2016; Chemura *et al*., 2021). Accordingly, empirical relations were used between monthly and annual precipitation in order to analyse GCM outputs relative to R factor changes (Nearing 2001). Thus, long-term model ensemble averages were analysed for trends in rainfall erosivity factor (R) using suitable empirical relations (Ferro *et al*., 1999; Renard *et al*., 1997; Zhang 2007).

6.3 Results

6.3.1 Land use land cover changes

The LULC maps (1990–2008, 2000–2018 and 1984–2018) generated by supervised classification applying SVMs (Marondedze and Schütt 2019) were used to simulate LULC distribution patterns for 2018; simultaneously, they were used as the reference for the simulation accuracy and to forecast future land use for 2034 and 2050 (Figure 6.3). The adopted supervised classification maps of the years 1984–2018 (Marondedze and Schütt 2019) show seven distinct classes (Table 6.4). The overall classification of each LULC map for 1984, 1990, 2000, 2008 and 2018 was estimated to be 90.1, 85.1, 88.9, 87.6 and 89.7%, respectively. The overall Kappa coefficient values produced were 0.87, 0.82, 0.86, 0.85 and 0.87 (Marondedze and Schütt 2019). The data reveal that spatial LULC patterns will significantly change during the forecasted periods, indicating that the expansion of the built-up areas will be at the expense

of green spaces and croplands (Figure 6.3). The built-up areas will continue to grow towards the peripheries and into the southward direction of the Epworth district (Figure 6.3).

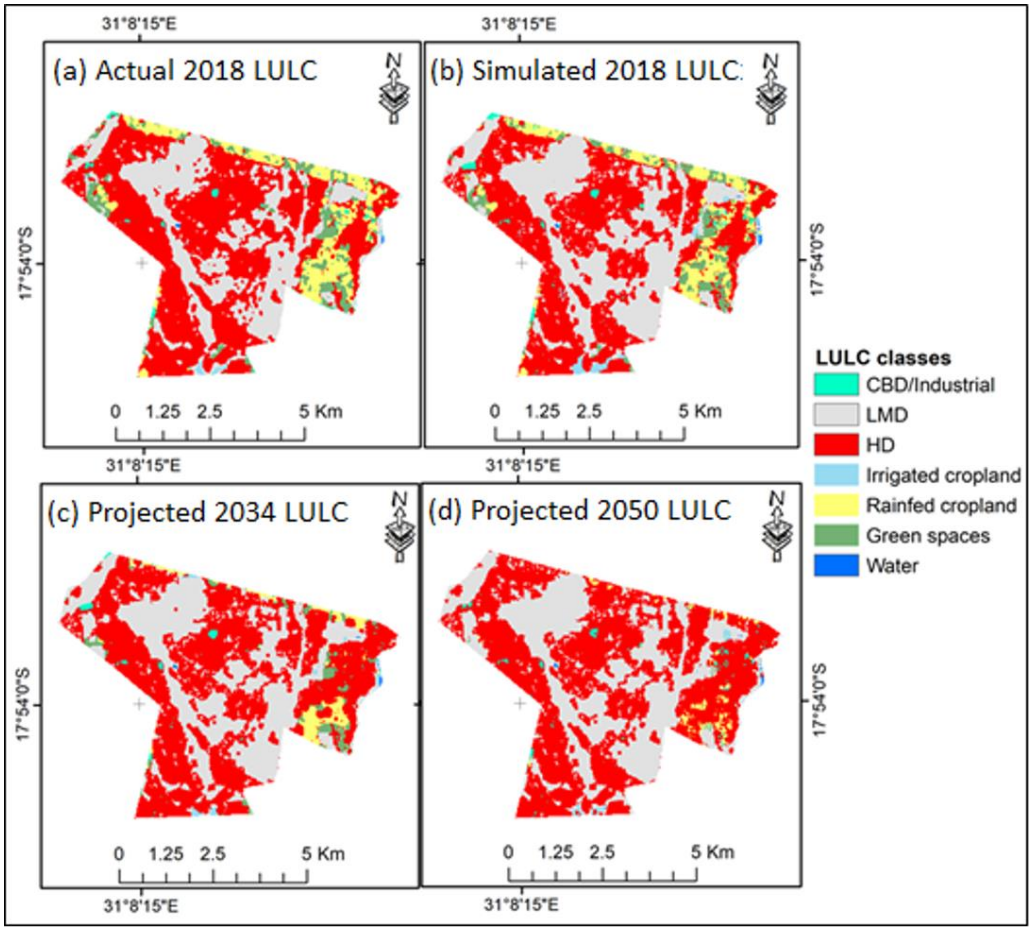

Figure 6. 3 LULC maps for Epworth district. (**a**) actual 2018 supervised classification (Marondedze and Schütt 2019), (**b**) simulated 2018, (**c**) projected 2034 and (**d**) projected 2050. CBD: central business department, LMD: low–medium density, HD: high density.

Table 6.4 Description of LULC classes for the study.

LULC Class	Description
CBD/industries	Industries and central business district defined with high fraction of impervious surfaces, mainly buildings, and a low proportion of vegetation
LMD residential	Leafy and well-established low- and medium-density suburbs surrounded by high vegetation
HD residential	High-density residential areas with low vegetation cover or clustered settlements with areas undergoing developments and bare exposed land
Irrigated cropland	Cultivated land under irrigation schemes
Rainfed cropland	Cultivated land or land with crop residues after harvesting
Vegetation	All wooded areas, shrubs and bushes, riverine vegetation and grass-covered areas
Water	Areas occupied by water, rivers, wetlands, reservoirs and dams

Comparison of LULC areas for 2018, resulting from the supervised classification applying SVMs, with 2018 simulated LULC classes shows that the LULC classes CBD/industrial, croplands, green spaces and water (Figure 6.3a and b) fit reasonably when comparing each class category, while slight differences between mapped and simulated distribution patterns occur for low–medium density and high-density residential areas (Figure 6.4). To summarize, for the period 2018 to 2050, the LULC class of CBD/industrial areas are estimated to remain stable, with an area expansion of +/−0.5–0.6% (Table 6.5). The spatial distribution of the LULC classes CBD/industrial area, water and irrigated croplands as projected for 2034 and 2050 widely correspond to those as mapped for 2018 (Figure 6.4). For both projected scenarios 2034 and 2050, the low–medium residential areas are predicted to increase slightly from 11.1 km^2 to approximately 11.9 km^2 between 2018 and 2034 and up to 12.3 km^2 in scenario 2050. Similarly, high-density residential areas are predicted to increase from 18.6 km^2 to 20.3 km^2 between 2018 and 2034, and to reach 22.4 km^2 in 2050 (Figure 6.4).

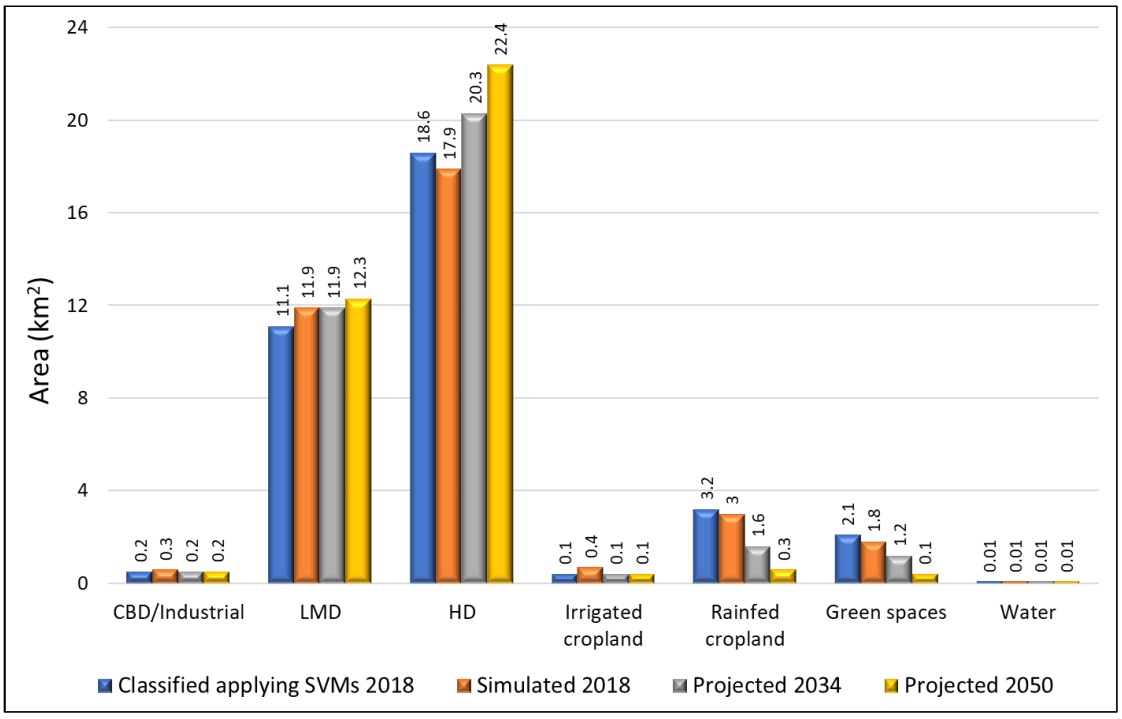

Figure 6. 4 The spatial area extent of different LULC classes for Epworth district. CBD: central business department, LMD: low–medium density, HD: high density.

Low–medium-density residential areas (LMD) are predicted to increase in coverage from 31.5% to 34.8% between 2018 and 2050, while high-density (HD) residential areas are predicted to increase in coverage from 52.6% to 63.3% between 2018 and 2050 (Table 6.5). During the period 2018–2050, the spatial distribution of croplands is predicted to decrease

from 9.5% to 1.1% of the total Epworth district area, while green spaces will shrink from 5.8% to 0.1%, largely due to the spatial expansion of built-up areas.

Table 6.5 Relative proportions of LULC classes by area extent (km^2) and percentage (%) for the adapted 2018 and the projected 2034 and 2050.

LULC Class	2018		2034		2050	
	Km²	%	Km²	%	Km²	%
CBD/industrial	0.2	0.5	0.2	0.6	0.2	0.6
LMD residential	11.1	31.5	11.9	33.7	12.3	34.8
HD residential	18.6	52.6	20.3	57.3	22.4	63.3
Irrigated cropland	0.1	0.4	0.1	0.2	0.1	0.1
Rainfed cropland	3.2	9.1	1.6	4.6	0.3	1.0
Green spaces	2.1	5.8	1.2	3.5	0.1	0.1
Water	0.01	0.04	0.01	0.03	0.01	0.03

*CBD: central business department *LMD: low–medium density *HD: high density

The summary of the probability matrix for major LULC conversions that occurred in Epworth district between 1990 and 2008 is documented in Table 6.6. The probability of change for CBD/industrial areas to remain CBD/industrial areas between 1990 and 2008 was 96.5%, displaying that built-up areas widely remained stable and will remain stable (Table 6.6). In contrast, irrigated croplands had a probability of change of 19.1%, that is, to remain irrigated cropland between 1990 and 2008, while the probability of change of irrigated cropland to rainfed cropland was 7.3% and to high-density residential areas was 47.2%. For green spaces, the probability to remain as green spaces between 1990 and 2008 was as low as 18.3%, while the probability of the change of green spaces to low–medium-density residential areas was 18.5%, to high-density residential areas was 40.8% and to croplands was 13.9% (Table 6.6).

Table 6.6 Markov chain transition probability matrix from LULC maps between 1990 and 2008.

Changing from:	Probability of changing to other land use class by 2008:							Total
1990	CBD/Industrial	LMD	HD	Irrigated cropland	Rainfed cropland	Green spaces	Water	
CBD/Industrial	0.9650	0.0183	0.0129	0.0033	0.0000	0.0005	0.0000	1.000
LMD residential	0.0062	0.9716	0.0150	0.0051	0.0000	0.0005	0.0016	1.000
HD residential	0.0071	0.0138	0.9712	0.0027	0.0052	0.0000	0.0000	1.000
Irrigated cropland	0.0708	0.1630	0.4721	0.1910	0.0725	0.0273	0.0033	1.000
Rainfed cropland	0.0416	0.2110	0.4357	0.0574	0.2041	0.0502	0.0000	1.000
Green spaces	0.0850	0.1848	0.4080	0.0412	0.0976	0.1834	0.0000	1.000
Water	0.0295	0.0838	0.0521	0.1121	0.0000	0.0213	0.7012	1.000

*CBD: central business department *LMD: low–medium density *HD: high density

The Markov chain transition probability matrix computed LULC maps between 2000 and 2018 for the prediction of 2034 future LULC distribution patterns (Table 6.7), which indicates that in 2018 the built-up area classes have a probability of more than 95% to remain as built-up areas in the future, documenting a stable distribution at least until 2034. For the irrigated croplands, a probability of 10.1% is indicated to remain as irrigated croplands until 2034, while at the same time 24.1% of the irrigated croplands have a probability to be converted into low–medium-density residential areas, and even 40.4% of the irrigated croplands underly a probability to be converted into high-density residential areas until 2034. For rainfed cropland, a probability of 33% is indicated to remain as rainfed cropland until 2034, while there is a 42.8% probability that rainfed cropland will be converted into high-density residential areas. There is a probability of 14.1% that rainfed cropland will be converted into low–medium-density residential areas by 2034, while at the same time there is an 8.3% probability that the rainfed croplands will be converted into green spaces. Similarly, green spaces have a probability of 24.7% to remain as green spaces until 2034, while for the same period, green spaces have a 30.6% probability to be converted into high-density residential areas, and a 16.1% probability to be converted into low–medium-density residential areas.

Table 6.7 Markov chain transition probability matrix from LULC maps between 2000 and 2018.

Changing From:	**Probability of Changing to Another Land use Class by 2018:**							**Total**
2000	**CBD/Industrial**	**LMD**	**HD**	**Irrigated Cropland**	**Rainfed Cropland**	**Green Spaces**	**Water**	
CBD/industrial	0.9523	0.0109	0.0186	0.0081	0.0043	0.0058	0.0000	1.000
LMD residential	0.0000	0.9507	0.0212	0.0164	0.0000	0.0102	0.0015	1.000
HD residential	0.0064	0.0185	0.9694	0.0000	0.0057	0.0000	0.0041	1.000
Irrigated cropland	0.0500	0.2405	0.4036	0.1011	0.1310	0.0697	0.0033	1.000
Rainfed cropland	0.0000	0.1405	0.4282	0.0183	0.3297	0.0833	0.0000	1.000
Green spaces	0.0370	0.1606	0.3062	0.0641	0.1852	0.2469	0.0000	1.000
Water	0.0026	0.1332	0.1071	0.1290	0.0000	0.0000	0.6281	1.000

*CBD: central business department *LMD: low–medium density *HD: high density

Based on the period 1984–2018, the transition probability matrix for the prediction of 2050 LULC distribution patterns was calculated (Table 6.8). The results indicate that built-up areas have probabilities higher than 90% to remain as built-up areas until 2050. In contrast, irrigated croplands have only a probability of 15% to remain as irrigated croplands until 2050, while they simultaneously have a probability of 41% to be transformed into high-density residential areas and a 21.4% probability to be transformed into low–medium-density residential areas. The rainfed croplands have a probability of 22.3% to remain as rainfed cropland until 2050; simultaneously, a 5.1% probability occurs that rainfed cropland will be transformed into

irrigated croplands, a 5.3% probability occurs that rainfed cropland will be transformed into green spaces and a 42.5% probability occurs that rainfed cropland will be transformed into high-density residential areas.

Table 6.8 Markov chain transition probability matrix from LULC maps between 1984 and 2018.

Changing From: Probability of Changing to Another Land use Class by 2018:								Total
1984	**CBD/Industrial**	**LMD**	**HD**	**Irrigated Cropland**	**Rainfed Cropland**	**Green Spaces**	**Water**	
CBD/industrial	0.9240	0.0308	0.0404	0.0000	0.0017	0.0031	0.0000	1.000
LMD residential	0.0000	0.9467	0.0251	0.0162	0.0000	0.0103	0.0017	1.000
HD residential	0.0064	0.0191	0.9621	0.0041	0.0060	0.0000	0.0023	1.000
Irrigated cropland	0.0612	0.2140	0.4104	0.1501	0.1268	0.0363	0.0012	1.000
Rainfed cropland	0.0640	0.1813	0.4251	0.0534	0.2229	0.0513	0.0002	1.000
Green spaces	0.0454	0.2102	0.4305	0.0313	0.0904	0.1922	0.0000	1.000
Water	0.0142	0.0965	0.1013	0.1199	0.0500	0.0000	0.6181	1.000

*CBD: central business department *LMD: low–medium density *HD: high density

6.3.2 Validation of CA–Markov model

A two-stage model validation approach was performed, including the visual inspection and quantitative assessment. The visual inspection shows that there is close agreement between the 2018 LULC distribution patterns derived from the support vector machines supervised classification (actual) and the 2018 LULC patterns simulated using the CA–Markov model (Figure 6.3). The computed kappa statistics recorded a kappa for a no ability K_{no} of 0.8893, a kappa for quantity accuracy $K_{locationStrata}$ of 0.8943, a traditional kappa $K_{standard}$ of 0.9044 and a kappa for location accuracy $K_{location}$ of 0.925. To summarize, the kappa index of agreement values indicates that there is good agreement between the actual and simulated 2018 LULC maps. Therefore, the model can be applied with a high confidence in its reliability to forecast LULC maps for 2034 and 2050 (Table 6.9).

Table 6.9 Kappa indices computed between the actual and simulated 2018 LULC maps.

K Indices	2018
K_{no}	0.8893
$K_{location}$	0.9251
$K_{standard}$	0.9044
$K_{locationStrata}$	0.8943

6.3.3 Future climate data analysis

The predicted meteorological data, as provided by the global circulation model ensemble, show slightly diverging data in terms of precipitation regimes by the different climate scenarios for

the observation period 2019–2050. Comparing annual rainfall predictions as provided by the RCP8.5 climate scenario and RCP4.5 climate scenario (Figure 6.5) indicates similar trends with varying magnitude. In climate scenario RCP4.5, the predicted annual rainfall oscillates with an overall decrease until 2050; the maximum predicted annual precipitation reaches around 950 mm in the years 2022, 2025, 2029 and 2031 and then decreases, reaching 855 mm in 2041 and around 785 mm in 2045 and 2050 (Figure 6.5). Underlying the same overall decline in precipitation, the minimum annual precipitation as predicted by climate scenario RCP4.5 varies between 814 mm in 2027 and 770–780 mm in 2034 and 2046. In climate scenario RCP8.5, the predicted annual rainfall also oscillates but does not show a distinct decrease during the forecasted period until 2050, as shown by the outcomes of RCP8.5. Maximum predicted annual precipitation varies between 800 and 900 mm and minimum predicted annual precipitation varies between 705 and 740 mm. The years of maximum predicted annual precipitation in RCP4.5 and RCP8.5 widely concur, but offsets can also be repeatedly observed (Figure 6.5).

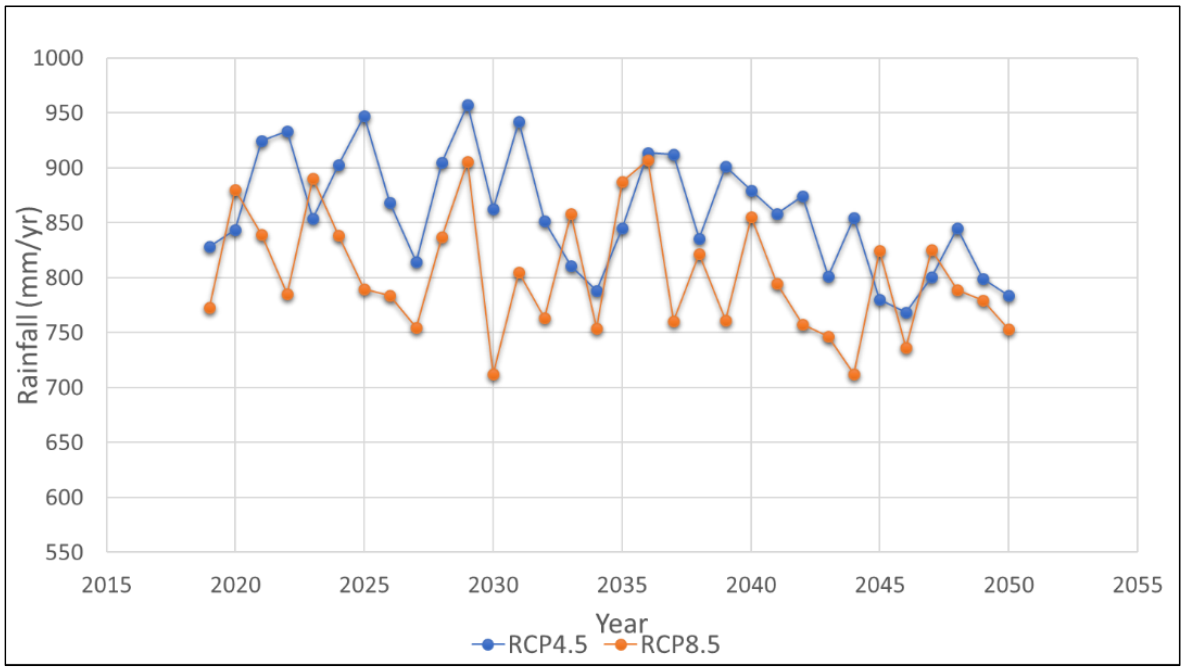

Figure 6. 5 Annual rainfall variations for Epworth district, 2019–2050, based on GCM ensemble climate scenarios RCP4.5 and RCP8.5.

6.3.4 Model performance evaluation

The performance evaluation carried out for each of the 15 statistically downscaled global circulation models' outcomes with in situ historical observations from the Harare gauging stations varied, as displayed in Table 6.10. The global circulation model performance evaluations show that fourteen GCMs (ACCESS1-0, BNU-ESM, CanESM2, CNRM-BGC, GFDL-ESM2G, GFDL-ESM2M, MIROC-ESM, MIROC5, MPI-ESM-LR, MPI-ESM-MR and

NorESM1-M, CCSM4, IPSL-CM5A-LR, MIROC-ESM-CHEM) have sufficient performance when evaluated against observations ($d > 0.7$, $r > 0.7$ and $R^2 > 0.5$). The least successful performance in terms of accuracy when evaluating historical observations and global circulation models' average precipitation data was observed for MRI-CGCM3 ($R^2 < 0.5$), but the results show that the model has a strong positive correlation ($r > 0.7$) with a high index of agreement ($d > 0.7$), and an rRMSE below 20% (Table 6.10). As such, there is confidence to apply the GCM data for future soil erosion risk estimation for Epworth district (Table 6.10).

Table 6.10 The GCMs' performance evaluation against the observed precipitation dataset from 1980 to 2005.

GCM	RRMSE (%)	d	r	R^2
ACCESS1-0	15.64	0.84	0.77	0.60
BNU-ESM	16.36	0.79	0.78	0.62
CanESM2	16.49	0.80	0.78	0.61
CCSM4	18.70	0.75	0.71	0.51
CNRM-BGC	16.34	0.85	0.78	0.61
GFDL-ESM2G	17.65	0.82	0.79	0.61
GFDL-ESM2M	17.73	0.80	0.79	0.62
IPSL-CM5A-LR	17.43	0.77	0.71	0.51
MIROC-ESM	18.69	0.78	0.78	0.61
MIROC-ESM-CHEM	17.82	0.77	0.71	0.55
MIROC5	15.38	0.80	0.79	0.64
MPI-ESM-LR	16.55	0.80	0.77	0.60
MPI-ESM-MR	16.43	0.81	0.78	0.61
MRI-CGCM3	18.10	0.75	0.69	0.47
NorESMI-M	14.45	0.87	0.79	0.63

6.3.5. RUSLE model factor maps

To be able to later assess the impact of future climate change on the future long-term potential soil erosion risk for Epworth district, the analysis of future predicted precipitation was split into two-time intervals, 2019–2034 and 2035–2050. Applying the RCP4.5 climate scenario between 2019 and 2034, annual rainfall averages 886 mm, and for the time interval 2035–2050, annual rainfall averages 839 mm; applying the RCP8.5 climate scenario between 2019 and 2034, annual rainfall averages 827 mm, and for the time interval 2035–2050 annual rainfall averages 799 mm. For the time period 2019–2034, rainfall erosivity factor (R) values, as derived from RCP4.5 model ensemble, are on average between 333 and 338 MJ mm ha^{-1} h^{-1} yr^{-1} and significantly exceed the values of the R factor based on the RCP8.5 model ensemble of 318–324 MJ mm ha^{-1} h^{-1} yr^{-1} (Figure 6.6). For the period 2035–2050, the R factor calculated on the basis of the RCP4.5 climate scenario varies between 321 and 328 MJ mm ha^{-1} h^{-1} yr^{-1}, again exceeding the R factor derived from the RCP8.5 model ensemble, which varies between 313

and 318 MJ mm ha^{-1} h^{-1} yr^{-1}. The variation in the R factor values dictates the temporal variation in annual rainfall for different climate scenarios. High R factor values were recorded from the RCP4.5 model ensemble averages for both future periods considered, the highest R factor being predicted for the period 2019–2034.

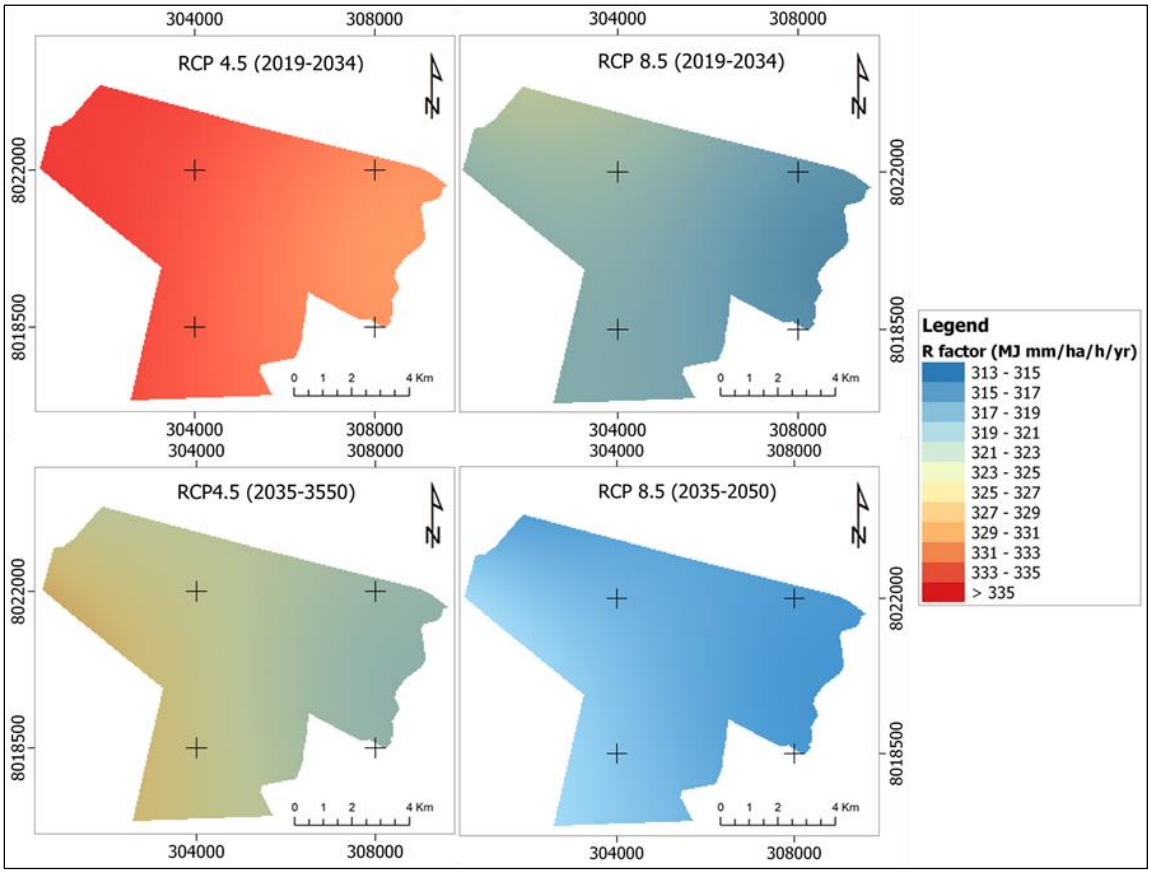

Figure 6. 6 The rainfall erosivity factors (R) for Epworth district. (**Top right**) 2019–2034 (RCP4.5); (**Top left**) 2019–2034 (RCP8.5); (**Bottom right**) 2035–2050 (RCP4.5); and (**Bottom left**) 2035–2050 (RCP8.5).

The soil texture in Epworth district corresponds largely to sand, sandy loam and clayey loam; only along the alluvial plains do predominantly sandy loams occur. Correspondingly, soil erodibility factor values (K) range between 0.06 and 0.09 (Figure 6.7b). The topography of Epworth district is undulating to gently rolling, with steep sloping areas along the river banks and at the intersections of tributary channels into the major receiving streams. Related topographic factor values (LS) range from 0 in the plateau areas up to approximately 22 on the steep sloping areas (Figure 6.7a). The width of the weighted land cover and management factor values (C) range between 0 and 0.239, with different distribution patterns in 2034 and 2050 (Figure 6.7c and d). Major differences in land cover and management relate to shifts in land use over time, as predicted by the CA–Markov model (Figure 6.3). Due to the lack of support practices in the study area, the support practice factor values (P) are set as 1.

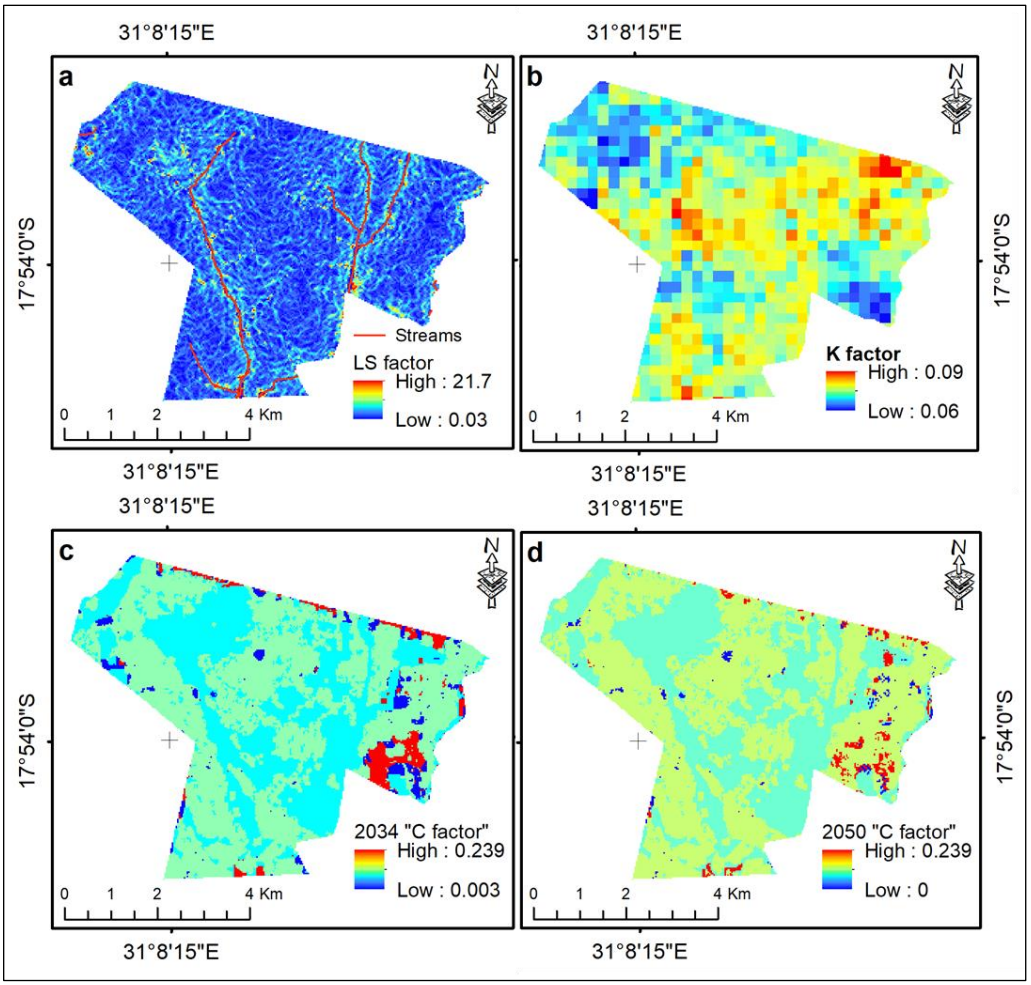

Figure 6. 7 The RUSLE input factors for modelling potential soil erosion risk for Epworth district. (**a**) Topographic factor (LS); (**b**) soil erodibility factor (K); (**c**) the crop cover and management factor (C) for 2034; (**d**) the crop cover and management factor (C) for 2050.

6.3.6 Potential soil erosion risk

Potential soil erosion risk mapping was performed independently for the years 2034 and 2050 as selected time slices, considering the two climate scenarios RCP4.5 and RCP8.5. The predicted average soil erosion risk, applying precipitation data as provided by RCP4.5 for the period 2019–2034, totals 1.2 t ha^{-1} yr^{-1} for 2034 and 1.1 t ha^{-1} yr^{-1} for the period 2035–2050. Applying the R factor based on the annual precipitation data, as provided by climate scenario RCP8.5, the predicted average potential soil erosion risk amounts to 1.1 t ha^{-1} yr^{-1} in 2034 and 1.0 t ha^{-1} yr^{-1} in 2050. The estimated soil loss rate for the climate scenario RCP4.5 in 2034 varies between 0 and 69.3 t ha^{-1} yr^{-1} and 0 and 48.9 t ha^{-1} yr^{-1} in 2050. Applying the R factor based on the annual precipitation data, as provided by climate scenario RCP8.5, soil loss rates ranged between 0 and 62.4 t ha^{-1} yr^{-1} in 2034 and 0 and 42.3 t ha^{-1} yr^{-1} in 2050. Future potential soil erosion risk predictions for climate scenarios RCP4.5 and RCP8.5 were significantly different ($p < 0.05$) for each time interval, 2034 and 2050, highlighting that the presented

changes can be attributed to various predicted factors, including land use and rainfall erosivity changes.

High potential soil erosion risk areas are predicted for the south-eastern periphery of Epworth district and along the tributaries, as well moving downwards in the south direction along the stream, as depicted in Figure 6.8. The predicted spatial patterns of potential soil erosion risk applying annual precipitation data, as provided by the RCP4.5 and RCP8.5 climate scenarios for the time slices 2034 and 2050, reveal in all cases high potential soil erosion risk along the flanks of the major rivers and along the flanks of steep tributaries (Figure 6.8). The displayed potential soil erosion risk maps in Figure 6.8 reveal that the predicted decrease in the R factor in the long term, corresponding to decrease in annual rainfall averages, reduces soil erosion processes, which simultaneously is on the rise in some localized parts of the district, and this is purportedly triggered by land use changes. Environmental characters, predominantly topography and soil properties (Figure 6.7), control the overall vulnerability of the area to soil erosion, finally displayed as potential soil erosion risk, including rainfall and land use.

The area-wide potential soil erosion risk predicted for the year 2034, applying R factors derived from the RCP4.5 climate scenario, indicates that 62.0% of the Epworth district will be exposed to low potential soil erosion risk and 27.9% to moderate potential soil erosion risk, while 8.1% will be exposed to high potential soil erosion risk and 2.0% to very high and extreme potential soil erosion risk (Table 6.11). The predicted results evidently show that there is an extensive distribution of areas of low potential soil erosion risk across the district, while high potential soil erosion risk is predicted predominantly along the channel networks. Applying R factors from the same climate scenario, RCP4.5, for the year 2050, approximately 74.3% of the entire district will be exposed to low potential soil erosion risk, 14.7% will be exposed to moderate potential soil erosion risk, 5.6% will be exposed to high potential soil erosion risk and 5.4% to very high and extreme potential soil erosion risk. The area-wide proportion of low potential soil erosion risk extended extensively across the entire district in 2050, attributed to the decline in the average rainfall erosivity in climate scenario RCP4.5. Applying R factors based on the RCP8.5 climate scenario in the year 2034, about 66.7% of the Epworth district is predicted to be exposed to low potential soil erosion risk, 24.6% to moderate potential soil erosion risk, 7.4% to high potential soil erosion risk and 1.3% to very high and extreme potential soil erosion risk (Table 6.11). Furthermore, for the year 2050, based on RCP8.5 climate scenario, the predicted area of Epworth district exposed to low potential soil erosion risk will be 77.7%, 14.1% will be exposed to moderate potential soil erosion risk, 4.6% to high potential soil erosion risk and 3.6% of the entire district will be exposed to very high and extreme

potential soil erosion risk (Table 6.11). Applying climate scenario RCP8.5, similar to the application of climate scenario RCP4.5, high-intensity potential soil erosion is predicted predominantly along channel networks and predominates in the southern area of Epworth district (Figure 6.8).

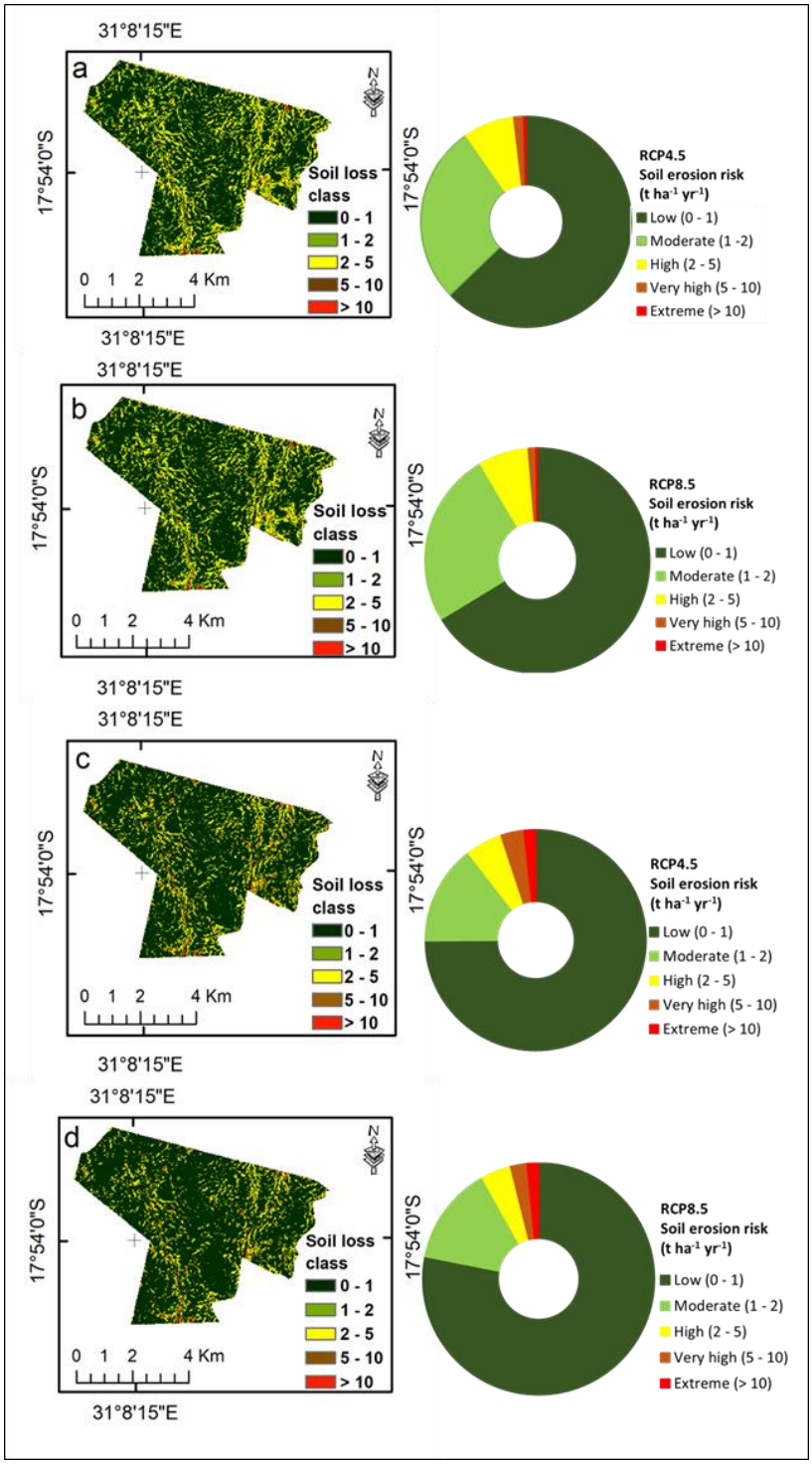

Figure 6. 8 Predicted spatio-temporal potential soil erosion risk for Epworth district. (**a**) Potential soil erosion risk for 2034 applying R factors based on RCP4.5; (**b**) potential soil erosion risk for 2034 applying R factors based on RCP8.5; (**c**) potential soil erosion risk for 2050 applying R factors based on RCP4.5; and (**d**) potential soil erosion risk for 2050 applying R factors based on RCP8.5.

Table 6.11 Predicted proportion of the spatial area of Epworth district exposed to potential soil erosion risk.

Soil Loss (t ha^{-1} yr^{-1})	Soil erosion Risk	Area (%) in 2018	Area (%) in 2034		Area (%) in 2050	
			RCP4.5	RCP8.5	RCP4.5	RCP8.5
0–1	Low	59.5	62.0	66.7	74.3	77.7
1–2	Moderate	29.3	27.9	24.6	14.7	14.1
2–5	High	10.0	8.1	7.4	5.6	4.6
5–10	Very high	1.1	1.6	1.1	3.5	2.3
>10	Extreme	0.1	0.4	0.2	1.9	1.3

The average area-wide potential soil erosion risk in Epworth district predicted for the time slices 2034 and 2050 shows extended areas exposed to low potential soil erosion rates between 0 and 1 t ha^{-1} yr^{-1}, considering annual precipitation as provided by the RCP8.5 climate scenario. In contrast, the average area-wide potential soil erosion risk predicted for the time slices 2034 and 2050, considering annual precipitation as provided by RCP4.5 climate scenario, distinctively exposes a smaller area to low soil loss rates between 0 and 1 t ha^{-1} yr^{-1} compared to the respective predictions applying climate scenario RCP8.5. In relation to the study on the present-day soil erosion risk in Epworth district (Marondedze and Schütt 2020), the current area exposed to low soil erosion risk amounts to 59.5%; thus, it is predicted to distinctly increase in the future (Table 6.11). In contrast, currently 10% of the Epworth district is exposed to high soil erosion risk and up to 1.2% is exposed to very high and extreme soil erosion risk (Table 6.11). Correspondingly, it is expected that in the future, the areas in Epworth district exposed to high potential soil erosion risk with soil loss rates between 2 and 5 t ha^{-1} yr^{-1} will markedly decrease, and most likely will even halve by 2050.

Furthermore, areas exposed to very high to extreme potential soil erosion risk with soil loss rates of more than 5 t ha^{-1} yr^{-1} will massively increase under future changes in land use and climate, while in 2034, under the RCP8.5 climate scenario, areas exposed to very high potential soil erosion risk will be widely stable compared to 2018 area coverage. By 2050, the spread of this category will double and might even triple when applying R-factors from the RCP4.5 climate scenario (Table 6.11). This development is even more distinctive when focusing on areas exposed to extreme potential soil erosion risk compared to the present-day situation until 2034, where areas exposed to extreme potential soil erosion risk will steadily increase by doubling the area extent when applying R-factors resulting from the RCP8.5 climate scenario, and up to 4 times the area extent when applying R-factors resulting from the RCP4.5 climate scenario. In 2050, areas exposed to extreme potential soil erosion risk will have increased by more than tenfold, independent of whether applying R-factors resulting from the

RCP8.5 or RCP4.5 climate scenario. However, the total area exposed to extreme potential soil erosion risk remains small and predominantly will occur along the river banks (Table 6.11).

6.4 Discussion

The predicted CA–Markov model results reveal an increase in the spatio-temporal pattern of built-up area, with built-up area expected to cover over 95% in 2050 from an approximated total of 84.5% in 2018 (Figure 6.3, Table 6.5). The forecasted results indicate that green spaces and croplands will continue to decline at the expense of built-up area (Table 6.5). Thus, the transition probability matrices for different periods reveal the probability of each class (n) in the LULC maps changing in the next distinct period (t_{n+1}) in respect of the surrounding cells (Kamusoko *et al*., 2013; Subedi *et al*., 2013). These predictions of built-up area growth at the expense of green spaces and croplands in the Harare Metropolitan Province concur with the conversion rates predicted by Mushore *et al*. (2017) using CA–Markov model analysis. The same analysis agrees with the predicted urban growth and the development of Irbid's governorate of Jordan, with projected built-up area growth amounting to almost 65% in total area from an estimated 14.5% between 2015 and 2050, at the expense of vegetation and farmlands (Khawaldah *et al*., 2020). Therefore, such developments indicate the core principle of the CA models, which stipulates that the present state of development is a continuation of historical changes induced by the neighbourhood interactions (Ahmed and Ahmed 2012; Koomen and Beurden 2011; Subedi *et al*., 2013). This predicted expansion pattern is a result of the neighbourhood effect, which exhibits that the converted land use is next or close to the existing dominant land use, and predominantly built-up area exists for this scenario (Fitawok *et al*., 2020; Koomen and Beurden 2011; Tang and Di 2019).

The predicted loss of green spaces and croplands may result in the detrimental loss of urban agricultural land and areas of aesthetic value to the ecosystem, which provide environmental protection. With the escalating socioeconomic woes and poverty in the city (Chirisa and Muhomba 2013), the loss of urban agricultural land to urban development will leave many poorly resourced Epworth residents with detrimental food insecurities, threatening their livelihoods since many survive on market gardening and other urban farming activities (Tawodzera 2011; UNDP 1996). The loss of green spaces also results in the reduction in vegetation cover and biomass which dissipates rainfall, reducing its direct impacts on the soil surface and facilitating percolation (Ferreira *et al*., 2016). Further, with the current economic meltdown and population growth, the surge of urban built-up area predicted by the CA–Markov model can be justified; the Epworth district will be no exception in terms of absorbing more

inhabitants from other spheres of the Harare Metropolitan Province. This push could be exacerbated by unaffordable rental charges and cost of living in other affluent suburbs of the Harare Metropolitan Province, resulting in further densification and overcrowding in Epworth district. However, due to excessive demand for shelter and anticipated population growth, the conversion of croplands and green spaces to a built-up area will intensify impervious surfaces across the district (Marondedze and Schütt 2019; Wania *et al*., 2014).

The GCM ensembles were used to quantify the hydrological impacts of climate change under different climate scenarios, RCP4.5 and RCP8.5, to obtain reliable projections (Hagemann *et al*., 2009; Murphy *et al*., 2004; Räisänen 2007; Sperna Weiland *et al*., 2012). Based on statistical metrics, the evaluation of the performance showed that fourteen GCMs (Table 6.10) have sufficient performance when evaluated with observations from Harare Metropolitan gauging stations ($d > 0.7$, $r > 0.7$ and $R^2 > 0.5$), with the exception of MRI-CGCM3, observed to have the lowest determination coefficient of 0.47. This may suggest that the general circulation model could have other specific years that were not properly simulated (Chemura *et al*., 2021); however, the analysis shows that most GCMs displayed good simulation. Above all, the GCMs have an rRMSE below 20%, which is reasonably acceptable (Arumugam *et al*., 2020; Chen *et al*., 2011, 2013). Further, coarse grid resolutions from GCMs make it difficult to match, with few in situ observations which are not uniformly distributed attributed to increases in spatial variation and uncertainty to clearly define local precipitation characteristics, therefore increasing the simulation bias (Hudson and Jones 2002; Pinto *et al*., 2016; Shongwe and Oldenborgh 2011).

For the RUSLE model, potential soil erosion risk maps were produced using the geostatistical ArcGIS package (raster calculator) to multiply the RUSLE factor maps (Figures 6.6 and 6.7). The predicted potential soil erosion risk averaged at 1.2 t ha^{-1} yr^{-1} in 2034 and 1.1 t ha^{-1} yr^{-1} in 2050 for the RCP4.5 climate scenario, while 1.1 t ha^{-1} yr^{-1} and 1.0 t ha^{-1} yr^{-1} were the predicted averages for 2034 and 2050 for the RCP8.5 climate scenario. Meanwhile, studies on the influence of land use change or the impact of soil erosion risk on crop productivity indicated that a tolerable soil loss rate at 1 t ha^{-1} yr^{-1} was sustainable for the tropics (Kouli *et al*., 2009; Khosrokhani and Pradhan, 2014; Karamage *et al.*, 2017; Abdulkareem *et al.*, 2019). Based on the slow rate of soil formation across the tropics, including Europe and America (<1 t ha^{-1} yr^{-1}) (Jones *et al.*, 2003; Verheijen *et al.*, 2009; Karamage *et al.*, 2017; Abdulkareem *et al.*, 2019), the sustainable soil loss tolerance at 1 t ha^{-1} yr^{-1} was considered across the entire Epworth district. The resulting arguments around the proposed 10 t ha^{-1} yr^{-1} as the estimated soil erosion tolerance threshold for tropical ecosystems showed that it was highly

overestimated, considering threats to the landscape and impacts on crop productivity likely to occur at such a high risk threshold (Morgan 2005). Furthermore, other studies indicated that average soil loss rates of 5 t ha^{-1} yr^{-1} may be sustainable soil loss rates in the tropics (Bamutaze 2015; Lufafa *et al*., 2003). Nevertheless, an estimated 1 t ha^{-1} yr^{-1} soil loss threshold subsisted for the current study and the predicted area-wide averages were unsustainable in that they slightly surpassed the recommended soil loss threshold, except for the RCP8.5 climate scenario in 2050. However, the slight notable deviation from the 1 t ha^{-1} yr^{-1} sustainable threshold can be justified as the averages fall within the applicable tolerable range of c.a 1.4 t ha^{-1} yr^{-1} proposed for some parts of the tropics, including America and Europe (Verheijen *et al*., 2009). Thus, the estimated soil loss tolerance threshold was used to describe a sustainable soil loss rate (Alewell *et al*., 2015).

The integrated average annual precipitation between 2019 and 2034, based on the climate scenario RCP4.5 results, shows high average annual soil loss rates ranging between 0 and 69.3 t ha^{-1} yr^{-1} and 0 and 62.4 t ha^{-1} yr^{-1} for the RCP8.5 climate scenario in 2034. In contrast, applying average annual precipitation between 2035 and 2050, the R factor-based values show a decline in soil loss rates for the year 2050 in both climate scenarios ranging between 0 and 48.9 t ha^{-1} yr^{-1} for RCP4.5 and 0 and 42.3 t ha^{-1} yr^{-1} for RCP8.5. However, these results show a continuous declining trend of soil loss rates when compared with the baseline period that applied the R factor based on the average annual precipitation data derived from in situ observations between 1984 and 2000 for Epworth district, estimating high soil erosion risk with average annual soil loss rates between 0 and 92.8 t ha^{-1} yr^{-1} in 2000 (Marondedze and Schütt 2020). In summary, the soil loss rates for both the RCP4.5 and RCP8.5 climate scenarios are observed to be decreasing in spatial coverage over the years 2034 and 2050. Regardless of the high rainfall erosivity predicted between 2019 and 2034 in comparison with soil loss rates estimated for the year 2000 (Marondedze and Schütt 2020), it is revealed that land use changes, including the shrinking of croplands and disturbed shrublands, predominantly reduce the soil loss impact due to increases in impervious surfaces across the Epworth district.

The increasing potential soil erosion risk predicted for Epworth district along the channel networks has been attributed to the steep slopes along the streams in combination with massive impervious surfaces, resulting in the accumulation of overland flow (Braud *et al*., 2013). Correspondingly, high topographic factor values appear on valley flanks (Figure 6.7), exposing surfaces to severe runoff and flooding resulting from the increased slope inclination and reduced infiltration capacity (Dams *et al*., 2013; Le Roux and Sumner 2012). Displayed

soil loss rates exceeding 1 t ha^{-1} yr^{-1} for Epworth district will be considered unsustainable (Verheijen *et al.*, 2009; Karamage *et al.*, 2017), and therefore, the need for sound policy implementation to avoid detrimental environmental damage. Such estimates, as indicated in Table 6.11, reveal that a larger proportion of the study area will be exposed to tolerable soil loss rates (Khosrokhani and Pradhan, 2014; Karamage *et al.*, 2017; Abdulkareem *et al.*, 2019). Nevertheless, there is a predicted increase in soil erosion risk in vulnerable areas, mainly downslope and low-lying areas along the flanks of the channel networks (Braud *et al*., 2013; Marondedze and Schütt 2020; Opeyemi *et al*., 2019).

The study results predict that soil loss rates vary with precipitation and land use changes for all the climate scenarios. The results suggest that the soil erosion response with regard to climate change could be complex, as it varies with time and on a climate scenario basis (Pruski and Nearing 2002). Consequently, the proportion of area exposed to high potential soil erosion risk with average soil loss rates between 2 and 5 t ha^{-1} yr^{-1} will markedly decline and most likely will even halve by 2050, as opposed to the doubling and triplicating proportional areas exposed to very high and extreme potential soil erosion risk for both climate scenarios in 2050. This is linked with the increasing vulnerability to smaller proportional area occupied by sparse green spaces and bare areas along channel networks. Such increasing trends in potential soil erosion risks are primarily accelerated by concentrated overland flow resulting from reduced infiltration processes across the Epworth district (Dams *et al*., 2013; Meshesha *et al*., 2014; Phil-Eze 2010). This vulnerability and response to rainfall impact and runoff processes with regard to reduced spatial area exposed to direct soil displacement in 2050 underpins the effects of land use changes and sloping topography along the channel network (Renschler *et al*., 1999; Sardari *et al*., 2019).

The decreasing rainfall erosivity for both scenarios over time concurs with the future analysis that incorporated regional climate models (RCMs) by Hudson and Jones (2002), in which they highlighted the likelihood of increasing consecutive dry days in southern Africa; however, with some increases in other parts of the region (Shongwe *et al*., 2009). Additionally, interannual high rainfall intensity impact is relatively expressed as this would be masked in annual rainfall averages due to low rain-day frequency (Shongwe *et al*., 2009). The contraction of the rainfall season was projected following the observed late onset and early rainfall cessation in sub-Saharan Africa, mostly in central Mozambique, large parts of Botswana and the northern and southern parts of Zimbabwe (Shongwe *et al*., 2009). Such responses to climate change tally with the predicted decline in overall soil erosion risk in 2050, which, however, still require more robust regional analysis on precipitation uncertainties to global climate change (Hudson and

Jones 2002; IPCC 2007; Shongwe *et al*., 2009). Nevertheless, the use of model ensemble averages could have limited the impact of other predicted extreme rainfall events (Murphy *et al*., 2004; Räisänen 2007; Sperna Weiland *et al*., 2012). Such changes and manipulations of rainfall intensities could negatively impact the final soil erosion prediction outcome (Boardman 2006; Turnbull *et al*., 2013). Furthermore, the use of coarse grid resolutions and numerical methods reduces models' data independency, and therefore increases the bias and uncertainty range of the outcomes (Räisänen 2007; Sperna Weiland *et al*., 2012; Vrochidou *et al*., 2013). The empirical RUSLE model is also limited only to the predictive capacity of sheet, inter-rill and rill soil erosion processes spanning over long periods, as it is not an event-based model, which also does not consider gullying erosion processes (Borrelli *et al*., 2020; Merritt *et al*., 2003; Phinzi and Ngetar 2019; Renard *et al*., 1997; Shamshad *et al*., 2008). Other data-driven processes integrated in the empirical RUSLE technique increase the uncertainty of future soil erosion risk due to varying data sources applied without rigorous quantification of their uncertainties and propagation (Borrelli *et al*., 2020; Falk *et al*., 2010).

Overall, high potential soil erosion risk displayed within the vicinity of Jacha river and tributaries extending from the north and southeast parts of the district draining southwards continue to increase, as predicted by the RUSLE model widely in 2050. This is attributed to the increasing sealed surface area and the sloping topography contributing to increased overland flow and surface runoff (Cantón *et al*., 2011; Dams *et al*., 2013). Taking into account human activities, previous studies reiterated that sand poaching activities along riverbanks are associated with heavy trucks ferrying sand to construction sites, contributing to high soil compaction on unpaved roads (Braud *et al*., 2013; Marondedze and Schütt 2020; USDA. NRCS 2000), reducing the infiltration capacity, and hence increasing surface runoff processes. For Epworth district, activities such as sand poaching and extraction along the riverbanks will be inevitable due to the predicted built-up area expansion and due to the fact, that for many locals, informal activities provide employment for the sustenance of their livelihoods. Therefore, there is a need to implement sound policies and sustainable environmental management approaches in order to curb environmental damage and the future extinction of water bodies and their ecosystem services. Uncertainties exist in this study about policy amendments regarding the functionality of the Local Boards and Authorities in regulating developmental plans. This, in turn, will affect LULC changes in the Epworth district of the Harare Metropolitan Province. However, this was held constant in the prediction of future LULC distribution patterns for Epworth district.

6.5 Conclusions

The study uses LULC distribution patterns between 1990 and 2008 to apply a Markov chain model, which allows the development of a transition probability matrix and suitability maps, and later defines the complex dynamic spatial patterns of urban area by the flexible Cellular Automatons. The validation of the simulated 2018 LULC distribution patterns and the actual 2018 LULC map displayed strong spatial agreement, both quantitatively and through visual inspection. The strong agreement and consistency of the LULC spatial patterns from the cross validation displayed the reliability and usability of the CA–Markov model to predict 2034 and 2050 future LULC distribution patterns for Epworth district. The predicted findings show a continuous increase in urban built-up area over the years 2034 and 2050 at the expense of croplands and perturbed green spaces, predominantly with the expansion of high-density residential areas towards Epworth district peripheries.

Further, future potential soil erosion risk was predicted for the years 2034 and 2050 using the RUSLE model, which integrated R factors based on the average annual precipitation between 2019 and 2034 and 2035 and 2050, as provided by climate scenarios RCP4.5 and RCP8.5. The goodness of fit measures highlighted that the general circulation models (GCMs) are useful for the assessment of future soil erosion risk, following the evaluation of GCMs performance with gauged observations, which showed a good performance, ascertaining their feasibility. As such, ensemble average outcomes from multiple GCMs under both the RCP4.5 and RCP8.5 climate scenarios were incorporated in the regional statistical relations equation to derive the rainfall erosivity factor for use in the RUSLE model.

Future trends in climate variability reveal that the projected high rainfall for the RCP4.5 climate scenario between 2019 and 2050 compared to the RCP8.5 climate scenario will contribute to high-localized soil erosion risk in vulnerable areas, including perturbed green spaces, agricultural land and stream banks. High soil loss rates were predicted in 2034 for both climate scenarios RCP4.5 and RCP8.5, in comparison with low soil loss rates in 2050 for both climate scenarios, and this is largely attributable to the predicted dynamic land use changes resulting in the reduction in surface area exposed to soil erosion processes over time. The predicted results also indicate that average annual soil loss rates will approximately halve in 2050 from an estimated 0–93 t ha^{-1} yr^{-1} in 2000, independent of whether the RCP4.5 or RCP8.5 climate scenario is applied. Nevertheless, for 2050, increasing soil erosion risks have been predicted along the flanks of the drainage networks.

Overall, this study highlights the application of the CA–Markov model in combination with the RUSLE model to derive useful simulations for predicting future LULC and soil erosion

risk. In addition, based on the stipulated IPCC policy recommendations from the Fifth Assessment Report (AR5), governments and policy makers need to implement sound climate policies in order to curtail and curb environmental degradation and landscape fragmentation at the local scale.

6.6 Acknowledgments

The publication of this article was funded by Freie Universität Berlin. We thank our colleagues from Freie Universität Berlin for their valuable insights that greatly assisted this research work. We are grateful to the United States Geological Survey (USGS) for providing Landsat images and the terrain-corrected Shuttle Radar Topography Mission (SRTM) DEM. We extend our gratitude to the Department of Meteorology in Harare, Zimbabwe for providing rainfall data and NASA Earth Exchange Global Daily Downscaled Projections (NEX-GDDP) for providing statistically downscaled global climate models.

CHAPTER 7: MODELLING SPATIAL LANDSCAPE RESPONSES TO URBANIZATION AND CLIMATE CHANGE BY APPLYING REMOTE SENSING DATA- A SYNTHESIS

7.1 Introduction

Urbanization as a process involving the expansion of built-up areas due to increases in population and economic activities has both negative and positive impacts on the landscape and provision of ecosystem services. In the case of Harare Metropolitan Province, industrial areas have been located close to the central business district (CBD) and their growth entails the need for human resources. This becomes a bait for labour driving the need for shelter to house the growing population that is providing work force for developing and improving the economic status of the city. Unrestrained and unplanned urban growth negatively impacts urban landscapes. That is, development of informal structures haphazardly in an urban setting drives the erection of structures on fragile ecosystems, for instance on wetlands, hindering their ecosystem functions to supply and purify water and act as a habitat. Unrestrained creation of build-up areas in urban environments facilitates the unprecedented LULC changes and modification of the urban landscapes. Associated impacts include the development of an urban microclimate including urban heat islands, which causes outdoor thermal discomfort (Mushore *et al*., 2017). Also, widespread traffic and impervious surfaces facilitate concentrated runoff and increase trails of soil erosion on bare land areas and downslope sediment deposition. However, this varies with soil physical properties, vegetation cover, topographic steepness and other topographical landscape characteristics (Ashiagbor *et al*., 2013; Kabantu *et al*., 2018). The increase in surface sealing (impermeable) also contributes to reduced water infiltration capacity thereby minimizing ground water recharge and consequently, annihilating water supply to aquifers.

In addition, population movements facilitate compaction along footpaths, roadsides parallel to paved roads and unpaved roads. This results from soaring traffic flows and triggers increases in soil erosion due to induced surface runoff and overland flow. Accelerated LULC changes due to increase in population dynamics are also associated with flash floods in urban areas. These flash floods result from the blockage of water channels and culverts by deposited sediments from upslope limiting the smooth flow of water on the installed drainage channels. Monitoring of urban growth through built-up areas mapping is important to reduce and mitigate environmental impacts. This enables urban planning through ideal policy formulation and implementation in order to safeguard the environment and raise awareness to the population.

However, there is little information or data paucity in Southern Africa, specifically in Zimbabwe, on urban landscape responses to rampant urban development and expansion. In the past, much focus has been given to rural landscapes and forest areas on soil erosion risk and soil loss (Makwara and Gamira 2012; Shikangalah *et al*., 2017; Tundu *et al*., 2018; Whitlow 1988).

The objective assessment of urban landscape responses to urbanization process by applying remote sensing data provides significant ways of spatiotemporal monitoring relevant for managing the environment. This curbs environmental degradation and extinction of biodiversity. However, there are challenges and limitations in the application of remote sensing techniques in urban built-up areas mapping, assessing and quantifying the extent of landscape damage and the prediction of future impacts. These challenges include the delineation of haphazard small housing units of different roofing materials using moderate resolution images due to spectral confusion (As-syakur *et al*., 2012; Kadhim *et al*., 2016). Further, spectral perplexity emanating from bare surfaces and rooftops limits classification accuracy, therefore, affecting modelling estimations of soil loss on the landscape. Secondly, the fact that the empirical soil erosion models applied are limited to address rill and inter-rill erosion processes negating gully erosion extents, pose a gap in addressing major threats to landscape as driven by urbanization process within active built-up areas and in secluded urban land areas. Thirdly, due to the mushrooming of urban settlements with minimum restraints as a consequence of political connotations and soaring population in cities the implementation of gazetted policies tends to be breached. All these aspects make it difficult to understand constant parameters for use in the prediction of future urban growth and expansion. However, the need to understand the current and future impacts of urbanization and climate change processes on urban landscapes is fundamental for the formulation and implementation of policies to enhance human-environment interactions and curb environmental degradation.

Therefore, this chapter provides a synopsis of the following objectives:

1. Determine the explanatory drivers influencing LULC change and to assess the axis of expansion of the Harare Metropolitan province using multispectral remotely sensed data between 1984 and 2018.
2. Assess and estimate spatial soil erosion risk and soil loss for Epworth district of the Harare Metropolitan province between 2000 and 2018 applying the RUSLE model.

3. Predict future LULC distribution patterns for the years 2034 and 2050, and to assess climate change impacts on soil erosion risk for Epworth district for the same periods applying the RUSLE model incorporating the predicted precipitation data outcomes from multiple GCMs.

7.2 Mapping built-up areas using multispectral remote sensing data and statistical modelling using binary logistic regression – Executive summary of Paper 1

Mapping of urban built-up areas using remote sensing techniques present challenges due to their heterogeneity and the complexity brought by spectral confusion (Jat et al. 2017; Sakieh et al. 2015). This is due to the varying reflectance of different rooftops produced from different materials and other land uses including bare areas, concrete and asphalt layered surfaces. However, developing LULC maps is important to monitor urban growth through quantification of the rate at which land use changes are occurring. In addition, urban monitoring assists urban planning managers and legislators in urban policy development to ensure sustainable urban development. The objective of this study is to assess independent variables influencing urban expansion and the axis of growth applying freely accessible Landsat 5 TM and 8 OLI data applying the machine learning support vector machines (SVMs) in developing LULC maps coupled with spectral indices to improve feature delineation. The overall outcome is that it is possible to improve feature delineation on moderate resolution Landsat imagery using spectral indices calculated for selected features in a complex heterogenous built-up area. Effectively, this has been observed by applying machine learning algorithms that performed supervised classification using training samples that underwent statistical testing for their separability using the transformed divergence separability Index (TDSI) (Chemura and Mutanga 2017). This improved the ability to achieve reliable classification accuracy for urban built-up areas to evaluate explanatory variables influencing urban growth applying the binary logistic regression. The current study confirmes the importance of the robust non-parametric support vector machines (SVMs) supervised classification aided by the separability testing of LULC classes which sheds light on the independency of each LULC attribute (Chemura and Mutanga 2017). The success of developing LULC maps with high overall accuracy (> 85%) is postulated to the application of spectral indices and SVMs for a complex urban-built up area. The generated LULC maps of high accuracy and the computed area statistics resulting from the robust machine learning aided classification and spectral indices improved the provision of urban growth rates and trends using change detection analysis. Further, the LULC maps were resampled to provide dichotomous raster layers applied to assess independent variables influencing axis of urban

expansion applying the binomial logistic regression modelling techniques. Due to the limited availability of independent variables for the analysis, topographic characteristics were considered such as slope variable and the proximity characteristics include distance to (1) the main roads, (2) secondary roads, (3) open water bodies, (4) streams and (5) the city centre. There is need to interrogate factors such as population distribution, gross domestic product (GDP) and other socio-economic related parameters to further understand urban growth drivers, their interrelations and associated impacts to the landscape.

7.3 Modelling spatial soil erosion risk and potential erosion using the empirical RUSLE model – Executive summary of Paper 2

Monitoring urban growth and development using remotely sensed data and geoinformatics technology is fundamental to attain sustainable cities and communities as enshrined in the United Nations SDGs (11) for 2030 and for the provision of clean water and sanitation (SDG 6). As such, landscape responses to urbanization processes such as potential erosion and soil erosion were assessed for the years 2000 and 2018 for Epworth district of the Harare Metropolitan Province. Estimation of spatial extent of soil loss rates and potential areas at high soil erosion risk were performed applying the empirical RUSLE model. The RUSLE model is statistical based and considers various factors: soil erodibility (K), rainfall erosivity (R), slope length and steepness (LS), crop cover management (C) and support practices (P). The RUSLE model integrates long-term mean annual rainfall thereby making it rigorous, however, impossible to assess spatial distribution of soil loss or potential erosion risk based on events.

The outcome of this study was that absolute soil loss rates were declining between 2000 and 2018, with observed increases of localized soil erosion risk in active built-up areas and along the drainage channels. The study reveals that increasing sealed area due to high traffic volumes and impervious surfaces contributed to concentrated runoff causing steady increase on spatial soil erosion risks primarily along drainage networks and parallel to paved roads. Further, fluctuations and changes of soil erosion risk within active build-up areas resulted from artificial slope propagated by construction activities, overcrowding and intense LULC changes exposing surfaces to raindrop impacts and surface runoff.

Weighted C factors were generated from literature-based data, field observations and biophysical characteristics evaluation of plant growth, height, canopy cover in relation to bare and sealed area in each sampling plot of 40 m x 80 m (Alena *et al*., 2013; Panagos *et al*., 2014; Renard *et al*., 1997). The study at hand also validates the generated RUSLE model estimates of spatial soil erosion risk distribution for 2018 applying the statistical metrics (Pearson's

correlation and the coefficient of determination) to evaluate RUSLE model performance in relation to the field-based soil damage maps. Validation of the RUSLE model showed satisfactory model performance when weighted against the field-based soil damage for 2018 ($p < 0.05$, $r = 0.76$, $r^2 = 0.581$); establishing the applicability of the RUSLE model in providing reasonably reliable potential soil loss and soil erosion risk estimates (Alewell *et al*., 2015; Montgomery 2007; Trirnble and Crosson 2000).

The inability to assess gully erosion processes and sediment deposition when applying the RUSLE model limit the deterministic approach and the overall assessment of soil erosion extent in urban districts. However, the application of the RUSLE model facilitates the direct assignment of resources on areas potentially vulnerable to strong soil erosion processes. Assessment of rainfall-runoff and deposition processes on urban built-up landscape would be fundamental to mitigate the development of flash floods resulting from the blockage of water canals and culverts, siltation of the scarce water bodies which unequivocally leads to the destruction of properties, roads and utilities in urban areas. Overall, the generated soil erosion risk maps for 2000 and 2018 were used in the subsequent study for comparative analysis of the current and future predictions of soil erosion risk for Epworth district of the Harare Metropolitan Province.

7.4 Predicting impacts of future LULC and climate change on urban landscape – Executive summary of Paper 3

Forecasting future LULC change distribution patterns for Epworth district of the Harare Metropolitan Province was successfully performed applying LULC maps of high accuracy for the years 1984, 1990, 2000, 2008 and 2018 adapted from (Marondedze and Schütt 2019). The LULC maps were generated by applying the machine learning SVMs, a supervised classification technique on enhanced moderate resolution Landsat images for improved feature delineation by calculating specific spectral indices. The CA-Markov model was used to forecast 2034 and 2050 LULC distribution patterns for Epworth district assuming the current urban development policies were constant. The validation of the simulated 2018 LULC against the actual 2018 LULC map generated using SVMs showed strong agreement of both “quantified and observed” data adding confidence for the application of CA-Markov models for future LULC predictions. This is because the Markov chain analysis generates transition probability matrices indicating the LULC changes from one state to another on discrete times coupled with the CA, which adds the spatial characteristics based on the neighbouring attributes as defined by the kernel. The predicted CA-Markov model results revealed an increase in the spatio-

temporal pattern of built-up areas, with built-up areas expected to cover over 90% of Epworth district in 2050 from an approximated total of 84.5% in 2018. This increase in the built-up areas is at the expense of green spaces and croplands which were predicted to decline. The predicted developments indicate that the present state of development is a continuation of historical changes induced by the neighbourhood interactions (Ahmed and Ahmed 2012).

In addition to predicting future LULC distribution patterns for 2034 and 2050, the likely landscape responses to climate change based on the representative concentration pathways (RCP4.5 and 8.5) climate scenarios were computed. Applying models' ensemble mean precipitation outcomes from 15 statistically downscaled GCMs (Chapter 6) as climate variables into the spatial soil erosion modelling underscores the determination of assessing the influence of climate change on the urbanizing landscape. The RUSLE model approach was integrated to predict estimates of future soil erosion risk and soil loss in 2034 and 2050. This integrated the predicted future LULC distribution patterns for Epworth district to assign C factor values and also applying the rainfall erosivity factor (R) derived from RCP4.5 and RCP8.5 climate scenarios. The study results reveal that precipitation would decline between 2019 and 2050. The predicted low estimates of soil loss for the years 2034 and 2050 under RCP8.5 climate scenario is attributed to the applied low rainfall erosivity factors combined with reduced erodible surfaces due to land use changes. The applied RCP4.5 climate scenario also reveals declining rainfall erosivity due to steady decreases on overall annual mean precipitation, which is however higher compared to RCP8.5 climate scenario. Declining rainfall outcomes displayed from several GCMs for the study at hand corroborate with the projected outcomes for other parts of Zimbabwe and surrounding countries mainly central Mozambique and Botswana (Shongwe *et al*., 2009). The assessment of future landscape responses to climate change and urban development shows that soil loss rates vary with precipitation and land use changes for all the climate scenarios. These results suggest that soil erosion response with regards to climate change could be complex as it varies spatially and on climate scenario basis. For Epworth district, the RUSLE model predicted high soil erosion risk within the vicinity of the hydrological channels extending from the northern and southeastern parts of the district. Soil erosion risk increases were also predicted downslope in 2050 under both RCP4.5 and RCP8.5 climate scenarios. This is attributed to the increasing sealed surface area and sloping topography contributing to increased overland flow and concentrated surface runoff (Cantón *et al*., 2011; Dams *et al*., 2013).

It is important to mention that coarse resolution precipitation data outcomes from multiple GCMs could have increased bias and uncertainty on the overall spatial soil erosion

risk estimates with regards to area wide coverage of Epworth district which is relatively small. Further, the inability of the RUSLE model estimations to account for event-based soil loss rates and the masking of interannual high intensity precipitation into long-term mean annual rainfall reduce the direct expression of rainfall influence and impact on landscapes (Borrelli *et al*., 2017; Renard *et al*., 1997). Overall, the study at hand provides the basis for application of remote sensing in predicting future urban LULC distribution patterns and soil erosion risk assessments. This is significant for drafting sustainable urban planning policies and land management practices to curb further environmental damage and raising environmental awareness to the communities to mitigate future landscape fragmentation.

7.5 Implications of urban development on the environment

The application of remote sensing data in assessing current and future trends of urban growth is significant for sustainable urban planning to safeguard a healthy environment. As such, the adoption of these approaches and techniques for monitoring urban growth and impacts associated with the environment are indispensable. This is through the provision of estimates that are necessary to alert land managers, authorities and communities of the detrimental effects and threats posed to the environment and socio-economic state by human activities. The impacts on the landscape turns out to affect livelihoods for instance rampant LULC changes through expansion of built-up areas encroaching fragile ecosystems such as wetlands reduce market gardening activities and obliterate wetland ecosystem functions and services in the environment. The application of remote sensing data in predicting future LULC changes and associated climate change scenarios shed light on the likely possible impacts induced by accelerated urbanization on the environment that will directly or indirectly affect the well-being of communities. The continued increase in built-up areas at the expense of croplands, wetlands and green spaces will highly attract the emergency of flash floods following blockage of water canals with eroded sediments from exposed bare land and compacted surfaces (Dams *et al.*, 2013).

Identification of main variables influencing urban growth and direction of expansion such as major and secondary roads is not only ideal for understanding urban growth dynamics but creates a gap for further research on land suitability analysis vis-à-vis environmental sustainability. The application of moderate resolution satellite remote sensing data and supervised machine learning algorithms displayed reasonable results suitable for the assessment of urban growth parameters and impacts of urban expansion on the environment. As such, it is possible to adopt high-resolution satellite images at a cost to improve estimates of landscape

responses to urban development and the development of near-real time urban growth statistics and trends as a monitoring tool and practice. That is, the monitoring of urban growth trends and assessment of landscape responses using multispectral remote sensing data has furnished Epworth district with estimates of the current and the likely future environmental impacts displaying that the processes are timely, cost-effective, spatially explicit and reproducible. Field assessments on the spatial extent of soil erosion damage revealed opportunities for the development and applicability of validation techniques for the empirical soil erosion models based on spatial extent soil erosion damage measurements and analysis. Ascertaining or validation procedures facilitate the understanding of empirical methods including the deterministic RUSLE model, which, however, has shortcomings such as the exclusion of gully and sheet erosion and the precise inter-rill soil erosion phenomena measurements. Soil erosion phenomena measurements could potentially provide the current state of soil erosion risk and estimates of soil loss in comparison with the ascertaining of study results based on reviewed estimates from other studies of the same climatic conditions.

7.6 Conclusions

The aim of this study at hand was to investigate independent variables influencing LULC changes by applying the binary logistic regression, a statistical modelling approach. Secondly, the study assesses landscape responses to LULC and climate change processes through the modelling of current and future spatial soil erosion risk using the empirical RUSLE model on multispectral remote sensing data. Based on the findings, the following conclusions are drawn:

1. Moderate resolution Landsat 5 TM and 8 OLI data enhanced with spectral indices provide detailed information of the urban growth trend on heterogenous urban built-up areas through the application of machine learning support vector machines a supervised classification technique and change detection analysis. The modelling of independent variables influencing urban growth and axis of expansion using binary logistic regression revealed the potential of statistical modelling to identify independent variables influencing urban growth. This was successful regardless of the limited independent variables applied for the study due to data unavailability and omission of variables that auto correlates with growth and expansion of urban districts such as population density. The potential benefit of multispectral moderate resolution satellite images is their cost effectiveness, accessibility, ability to be enhanced by spectral indices, and the availability of historical/archived datasets for trend analysis. The

utilization of moderate resolution datasets is more valuable than the cost of environmental degradation without sound monitoring and future planning. Overall, rampant build-up area increases were observed at the expense of green spaces and croplands. Subsequently, major and secondary roads dominated as independent variables influencing the axis of urban expansion regardless of haphazard development in the southern and eastern parts of the Harare Metropolitan Province.

2. Remote sensing data can be reliably used to estimate and map spatial soil erosion risk and soil loss rates on urban landscapes. The use of empirical RUSLE model to estimate soil erosion risk, soil loss rates and potential erosion on urban built landscape helps to inform land managers, local authorities and the society on areas threatened by soil erosion that require attention in order to direct resources on specific areas estimated to have high soil erosion risk.

3. The CA-Markov model can be used for predicting future LULC changes for urban areas. In addition, the empirical RUSLE model can also be reliably used to estimate future soil erosion risk on the predicted urban areas, while incorporating the predicted rainfall erosivity factors driven from multiple GCMs in order to predict future climate change impacts on urban landscapes applying climate scenarios (RCP4.5 and 8.5).

4. To enable sustainable urbanization, there is need for the integration of smart urban design policy on the government framework which embraces technology, innovation, educating societies and legislators on the extent to which their activities impact the environment. Further, fluctuations and shifting of rainfall patterns due to climate change were predicted and this requires holistic approaches from household to global level towards the mitigation of emissions and adapting to the prevailing conditions. As such, this heeds a call for policy and decision makers to align national climate policies and action plans with the Paris Agreement as agreed upon at the COP 26 global climate summit.

7.7 Outlook for future research

Findings of the current research are conclusive within the scope of the study area; however, the study creates opportunities for further research and for array of disciplines. The following recommendations based on this study are laid out for future research:

1. The techniques and results from this study are based on statistical and empirical models giving much emphasis on spectral features that are used to produce thematic maps. Further, future predictions performed predominantly relied on features derived from spectral characterization with little mechanistic understanding of the identified relationships. As such, more research is required on exploring urban growth drivers and parameters.

2. The research focused on soil erosion modelling using empirical models. Therefore, it is important to understand how physical and conceptual models can perform on urban systems and to understand soil erosion processes through mechanical soil erosion demonstration on plots using treatments and controls to further validate the RUSLE model. The inclusion of gully formation, sheet erosion and deposition processes and extent of their impacts to urban environments should be considered on further research work to enable sustainable urban development with substantiated scientific information.

3. Assuming that urban growth patterns predicted between 2034 and 2050 persists under current and assumed conditions, it entails dramatic conversion rates of green spaces and urban agricultural land at the expense of built-up areas. This conclusive prediction could be positive however, there is need to research on social and technical possibilities of developing the modelling procedures for better understanding of the causal mechanism.

4. The study utilized moderate resolution Landsat 5 TM and 8 OLI remote sensing data for the classification of LULC maps and showed promising results. However, there is need to investigate using high-resolution satellite data such as GeoEye, WorldView and IKONOS in the spatial modelling of urban built-up areas for accurate monitoring of urban growth processes and effective sustainable future planning.

5. Future climate change impacts investigated for Epworth district on the landscape responses resemble minimum spatial variability that is due to the differences on spatial resolution of precipitation data against the areal extent of the study area. Consequently, it is important to understand the likely possible spatial soil erosion risks over large spatial areal extent of an urban setting and the inclusion of all climate scenarios including RCP2.6, 4.5, 6.0 and 8.5. Further, spatio-temporal potential erosion runs on regional scale applying RCPs climate scenarios is deemed necessary to enable future landscape sustainability.

Overall, the findings in this cumulative doctoral thesis contribute to the understanding of the interrelationships between humans and their environment. The urban landscape responses to LULC and climate change have been explored applying remote sensing data and geoinformatics techniques. This was combined with field snapshot surveys to geo-reference and measure soil erosion phenomena to ascertain empirical methods and derive crop cover management factors. That is, the remote sensing offers great capabilities to accurately and timely monitor urban growth trends and their associated impacts on the landscape to enable environmental sustainability through the provision of scientific based information.

Bibliography

Abbas, A. W., N. Minallh, N. Ahmad, S. A. R. Abid, and M. A. A. Khan, 2016: Si Ndh University research Journal (science series). *Sindh Univ Res Jour Sci Ser*, **48**, 315–318.

Abdulkareem, J. H., B. Pradhan, W. N. A. Sulaiman, and N. R. Jamil, 2019: Prediction of spatial soil loss impacted by long-term land-use/land-cover change in a tropical watershed. *Geosci. Front.*, **10**, 389–403, https://doi.org/10.1016/j.gsf.2017.10.010.

Abdullah, A. Y. M., A. Masrur, M. S. G. Adnan, Md. A. A. Baky, Q. K. Hassan, and A. Dewan, 2019: Spatio-temporal Patterns of Land Use/Land Cover Change in the Heterogeneous Coastal Region of Bangladesh between 1990 and 2017. *Remote Sens.*, **11**, 790, https://doi.org/10.3390/rs11070790.

Aburas, M. M., Y. M. Ho, M. F. Ramli, and Z. H. Ash'aari, 2016: The simulation and prediction of spatio-temporal urban growth trends using cellular automata models: A review. *Int. J. Appl. Earth Obs. Geoinformation*, **52**, 380–389, https://doi.org/10.1016/j.jag.2016.07.007.

Aburas, M. M., Y. M. Ho, M. F. Ramli, and Z. H. Ash'aari, 2017: Improving the capability of an integrated CA-Markov model to simulate spatio-temporal urban growth trends using an Analytical Hierarchy Process and Frequency Ratio. *Int. J. Appl. Earth Obs. Geoinformation*, **59**, 65–78, https://doi.org/10.1016/j.jag.2017.03.006.

Adebowale, B. I., and S. E. Kayode, 2015: Geospatial Assessment of Urban Expansion and Land Surface Temperature in Akure, Nigeria. In Proceedings of the ICUC9—9th International Conference on Urban Climate Jointly with 12th Symposium on the Urban Environment, Toulouse, France. 6.

Adelabu, S., O. Mutanga, and E. Adam, 2015: Testing the reliability and stability of the internal accuracy assessment of random forest for classifying tree defoliation levels using different validation methods. *Geocarto Int.*, **30**, 810–821, https://doi.org/10.1080/10106049.2014.997303.

Adornado, H. A., M. Yoshida, and H. A. Apolinares, 2009: Erosion Vulnerability Assessment in REINA, Quezon Province, Philippines with Raster-based Tool Built within GIS Environment. *Agric. Inf. Res.*, **18**, https://doi.org/10.3173/air.18.24.

AfDB, 2016: African Development Bank Organisation for Economic Co-operation and Development (AfDB). United Nations Development Programme: Part II Sustainable cities and structural transformation.

African Development Bank, 2005: Gender, Poverty and Environmental Indicators on African Countries: African Development Bank volume vi.

Ahmadalipour, A., H. Moradkhani, and M. Svoboda, 2017: Centennial drought outlook over the CONUS using NASA-NEX downscaled climate ensemble: Drought Projection using NASA-NEX ensemble over the CONUS. *Int. J. Climatol.*, **37**, 2477–2491, https://doi.org/10.1002/joc.4859.

Ahmed, B., and R. Ahmed, 2012: Modeling Urban Land Cover Growth Dynamics Using Multi-Temporal Satellite Images: A Case Study of Dhaka, Bangladesh. *ISPRS Int. J. Geo-Inf.*, **1**, 3–31, https://doi.org/10.3390/ijgi1010003.

Ahmed, B., R. Ahmed, and X. Zhu, 2013: Evaluation of Model Validation Techniques in Land Cover Dynamics. *ISPRS Int. J. Geo-Inf.*, **2**, 577–597, https://doi.org/10.3390/ijgi2030577.

Ai, L., N. F. Fang, B. Zhang, and Z. H. Shi, 2013: Broad area mapping of monthly soil erosion risk using fuzzy decision tree approach: integration of multi-source data within GIS. *Int. J. Geogr. Inf. Sci.*, **27**, 1251–1267, https://doi.org/10.1080/13658816.2012.752095.

Aiello, A., M. Adamo, and F. Canora, 2015: Remote sensing and GIS to assess soil erosion with RUSLE3D and USPED at river basin scale in southern Italy. *CATENA*, **131**, 174–185, https://doi.org/10.1016/j.catena.2015.04.003.

Akhter, S. T., and M. H. Noon, 2016: Modeling Spillover Effects of Leapfrog Development and Urban Sprawl upon Institutional Delinquencies: A Case for Pakistan. *Procedia - Soc. Behav. Sci.*, **216**, 279–294, https://doi.org/10.1016/j.sbspro.2015.12.039.

Al-Abadi, A. M. A., H. B. Ghalib, and W. S. Al-Qurnawi, 2016: Estimation of soil erosion in Northern Kirkuk governorate, Iraq using RUSLE, Remote Sensing and GIS. *Carpathian J. Earth Environ. Sci.*, **11**, 153–166.

Alaci, D. S. A., 2019: Regulating urbanisation in Sub-Saharan Africa through cluster settlements: 16.

Al-Bilbisi, H., 2019: Spatial Monitoring of Urban Expansion Using Satellite Remote Sensing Images: A Case Study of Amman City, Jordan. *Sustainability*, **11**, 2260, https://doi.org/10.3390/su11082260.

Alena, J., and T. Miloslav Janeček and Martin, 2013: Field Determination of the Specific Input Characteristics to Calculate the Value of C Factor of Time-variable Crops for the Revised Universal Soil Loss Equation (RUSLE). *Soil Water Res.*, **1**, 10–15, https://doi.org/10.17221/6500-SWR.

Alewell, C., M. Egli, and K. Meusburger, 2015: An attempt to estimate tolerable soil erosion rates by matching soil formation with denudation in Alpine grasslands. *J. Soils Sediments*, **15**, 1383–1399, https://doi.org/10.1007/s11368-014-0920-6.

Alewell, C., P. Borrelli, K. Meusburger, and P. Panagos, 2019: Using the USLE: Chances, challenges and limitations of soil erosion modelling. *Int. Soil Water Conserv. Res.*, **7**, 203–225, https://doi.org/10.1016/j.iswcr.2019.05.004.

Alexakis, D. D., D. G. Hadjimitsis, and A. Agapiou, 2013: Integrated use of remote sensing, GIS and precipitation data for the assessment of soil erosion rate in the catchment area of "Yialias" in Cyprus. *Atmospheric Res.*, **131**, 108–124, https://doi.org/10.1016/j.atmosres.2013.02.013.

Al-Hameedi, W. M. M., J. Chen, C. Faichia, B. Al-Shaibah, B. Nath, A.-A. Kafy, G. Hu, and A. Al-Aizari, 2021: Remote Sensing-Based Urban Sprawl Modeling Using Multilayer Perceptron Neural Network Markov Chain in Baghdad, Iraq. *Remote Sens.*, **13**, 4034, https://doi.org/10.3390/rs13204034.

Alsharif, A. A. A., and B. Pradhan, 2014: Urban Sprawl Analysis of Tripoli Metropolitan City (Libya) Using Remote Sensing Data and Multivariate Logistic Regression Model. *J. Indian Soc. Remote Sens.*, **42**, 149–163, https://doi.org/10.1007/s12524-013-0299-7.

Anderson, I. P., P. J. Brinn, M. Moyo, and B. Nyamwanza, 1993: *Physical resource inventory of the Communal Lands of Zimbabwe-An overview (NRI Bulletin 60)*. Natural Resources Institute: Chatham Maritime, Kent, UK,.

Anselm, N., G. Brokamp, and B. Schütt, 2018: Assessment of Land Cover Change in Peri-Urban High Andean Environments South of Bogotá, Colombia. *Land*, **7**, 75, https://doi.org/10.3390/land7020075.

Araya, A., G. Hoogenboom, E. Luedeling, K. M. Hadgu, I. Kisekka, and L. G. Martorano, 2015: Assessment of maize growth and yield using crop models under present and future climate in southwestern Ethiopia. *Agric. For. Meteorol.*, **214–215**, 252–265, https://doi.org/10.1016/j.agrformet.2015.08.259.

Araya, Y. H., and P. Cabral, 2010: Analysis and Modeling of Urban Land Cover Change in Setúbal and Sesimbra, Portugal. *Remote Sens.*, **2**, 1549–1563, https://doi.org/10.3390/rs2061549.

Arnold, J. G., R. Srinivasan, R. S. Muttiah, and J. R. Williams, 1998: Large Area Hydrologic Modeling and Assessment Part I: Model Development. *J. Am. Water Resour. Assoc.*, **34**, 73–89, https://doi.org/10.1111/j.1752-1688.1998.tb05961.x.

Arnoldus, H. M. J., 1977: *Methodology used to determine the maximum potential average annual soil loss due to sheet and rill erosion in Morocco. Assessing Soil Degradation.* FAO Soils Bulletin (FAO), 39–51 pp.

Arnoldus, H. M. J., 1980: *An approximation of the rainfall factor in the USLE. In: M. DeBoodt and D. Gabriels (Editors), Assessment of Erosion.* John Wiley & Sons, 127–132 pp.

Arumugam, P., A. Chemura, B. Schauberger, and C. Gornott, 2020: Near Real-Time Biophysical Rice (Oryza sativa L.) Yield Estimation to Support Crop Insurance Implementation in India. *Agronomy*, **10**, 1674, https://doi.org/10.3390/agronomy10111674.

Ashiagbor, G., E. K. Forkuo, P. Laari, and R. Aabeyir, 2013: Modeling soil erosion using RUSLE and GIS tools. *Int. J. Remote Sens.*, **2**, 12.

Asiedu, J. B., 2018: Assessing the Threat of Erosion to Nature-Based Interventions for Stormwater Management and Flood Control in the Greater Accra Metropolitan Area, Ghana. *J. Ecol. Eng.*, **19**, 1–13, https://doi.org/10.12911/22998993/79418.

Assouline, S., and M. Ben-Hur, 2006: Effects of rainfall intensity and slope gradient on the dynamics of interrill erosion during soil surface sealing. *CATENA*, **66**, 211–220, https://doi.org/10.1016/j.catena.2006.02.005.

As-syakur, Abd. R., I. W. S. Adnyana, I. W. Arthana, and I. W. Nuarsa, 2012: Enhanced Built-Up and Bareness Index (EBBI) for Mapping Built-Up and Bare Land in an Urban Area. *Remote Sens.*, **4**, 2957–2970, https://doi.org/10.3390/rs4102957.

Atreya, K., S. Sharma, R. M. Bajracharya, and N. P. Rajbhandari, 2006: Applications of reduced tillage in hills of central Nepal. *Soil Tillage Res.*, **88**, 16–29, https://doi.org/10.1016/j.still.2005.04.003.

Auerswald, K., M. Kainz, and P. Fiener, 2006: Soil erosion potential of organic versus conventional farming evaluated by USLE modelling of cropping statistics for agricultural districts in Bavaria. *Soil Use Manag.*, **19**, 305–311, https://doi.org/10.1111/j.1475-2743.2003.tb00320.x.

Awad, M., and R. Khanna, 2015: Support Vector Machines for Classification. *Efficient Learning Machines*, Apress, 39–66.

Ball, G. H., and D. G. Hall, 1965: ISODATA, a Novel Method of Data Analysis and Pattern Classification. Stanford Research Institute, Menlo Park.

Balzter, H., 2000: Markov chain models for vegetation dynamics. *Ecol. Model.*, **126**, 139–154, https://doi.org/10.1016/S0304-3800(00)00262-3.

Bamutaze, Y., 2015: Revisiting socio-ecological resilience and sustainability in the coupled mountain landscapes in Eastern Africa. *Curr. Opin. Environ. Sustain.*, **14**, 257–265, https://doi.org/10.1016/j.cosust.2015.06.010.

Bannari, A., D. Morin, F. Bonn, and A. R. Huete, 1995: A review of vegetation indices. *Remote Sens. Rev.*, **13**, 95–120, https://doi.org/10.1080/02757259509532298.

Beck, M. B., 1987: Water quality modeling: A review of the analysis of uncertainty. *Water Resour. Res.*, **23**, 1393–1442, https://doi.org/10.1029/WR023i008p01393.

Belal, A. A., and F. S. Moghanm, 2011: Detecting urban growth using remote sensing and GIS techniques in Al Gharbiya governorate, Egypt. *Egypt. J. Remote Sens. Space Sci.*, **14**, 73–79, https://doi.org/10.1016/j.ejrs.2011.09.001.

Benavidez, R., B. Jackson, D. Maxwell, and K. Norton, 2018: A review of the (Revised) Universal Soil Loss Equation ((R)USLE): with a view to increasing its global applicability and improving soil loss estimates. *Hydrol. Earth Syst. Sci.*, **22**, 6059–6086, https://doi.org/10.5194/hess-22-6059-2018.

Berry, M. W., A. Mohamed, and B. W. Yap, eds., 2020: *Supervised and Unsupervised Learning for Data Science*. Springer International Publishing,.

Bewket, W., and G. Sterk, 2003: Assessment of soil erosion in cultivated fields using a survey methodology for rills in the Chemoga watershed, Ethiopia. *Agric. Ecosyst. Environ.*, **97**, 81–93, https://doi.org/10.1016/S0167-8809(03)00127-0.

Bhatta, B., 2010: *Analysis of urban growth and sprawl from remote sensing data.* Springer New York,.

Black, D., and V. Henderson, 1999: A Theory of Urban Growth. *J. Polit. Econ.*, **107**, 252–284, https://doi.org/10.1086/250060.

Boardman, J., 2006: Soil erosion science: Reflections on the limitations of current approaches. *CATENA*, **68**, 73–86, https://doi.org/10.1016/j.catena.2006.03.007.

Borrelli, P., D. A., R. F, Larissa, E, Lugato, C, Ballabio, K, Meusburger, S, Meusburger, B, Schütt, V, Ferro, V, Bagarello, K. V, Oost, L, Montanarella., and P, Panagos, 2017: An assessment of the global impact of 21st century land use change on soil erosion. *Nat. Commun.*, **8**, 2013, https://doi.org/10.1038/s41467-017-02142-7.

Borrelli, P., Robinson, P, Panagos, E, Lugato, J. E, Yang, C, Alewell, D, Wuepper, L, Montanarella, and C, Ballabio, 2020: Land use and climate change impacts on global soil erosion by water (2015-2070). *Proc. Natl. Acad. Sci.*, **117**, 21994–22001, https://doi.org/10.1073/pnas.2001403117.

Braud, I., P. Breil, F. Thollet, M. Lagouy, F. Branger, C. Jacqueminet, S. Kermadi, and K. Michel, 2013: Evidence of the impact of urbanization on the hydrological regime of a medium-sized periurban catchment in France. *J. Hydrol.*, **485**, 5–23, https://doi.org/10.1016/j.jhydrol.2012.04.049.

Brazier, A., 2015: *Climate Change in Zimbabwe: Facts for Planners and Decision Makers*. Konrad-Adenauer-Stiftung, 2–11 pp.

Brueckner, J. K., and R. W. Helsley, 2011: Sprawl and blight. *J. Urban Econ.*, **69**, 205–213, https://doi.org/10.1016/j.jue.2010.09.003.

Bruijnzeel, L., A., 1990: *Hydrology of moist tropical forests and effects of conversion: a state of knowledge review*. Free University: Amsterdam, The Netherlands,.

Brundtland, G. H., M. Khalid, S. Agnelli, B. Chidzero, L. M. Fadika, M. M. D. Botero, V. Hauff, and M. Shijun, 1987: United Nations World Commission on Environment and Development.

Bsaibes, A., D. Courault, F. Baret, M. Weiss, A. Olioso, F. Jacob, O. Hagolle, O. Marloie, N. Bertrand, V. Desfond, and F. Kzemipour, 2009: Albedo and LAI estimates from FORMOSAT-2 data for crop monitoring. *Remote Sens. Environ.*, **113**, 716–729, https://doi.org/10.1016/j.rse.2008.11.014.

Burges, C. J. C., 1998: A Tutorial on Support Vector Machines for PatternRecognition. *Data Min. Knowl. Discov.*, **2**, 121–167, https://doi.org/10.1023/A:1009715923555.

Butcher, C., 1986: Low income housing in Zimbabwe: A case study of the Epworth squatter upgrading programme.

Cammeraat, E. L. H., 2004: Scale dependent thresholds in hydrological and erosion response of a semi-arid catchment in southeast Spain. *Agric. Ecosyst. Environ.*, **104**, 317–332, https://doi.org/10.1016/j.agee.2004.01.032.

Cantón, Y., A. Solé-Benet, J. de Vente, C. Boix-Fayos, A. Calvo-Cases, C. Asensio, and J. Puigdefábregas, 2011: A review of runoff generation and soil erosion across scales in semiarid south-eastern Spain. *J. Arid Environ.*, **75**, 1254–1261, https://doi.org/10.1016/j.jaridenv.2011.03.004.

Castels, M., 1978: *"Is there an urban sociology?" Reprinted in C. Pickvance, ed., Urban Sociology: Critical Essays.* 33–59 pp.

Castillejo-González, I. L., J. M. Pena-Barragán, M. Jurado-Expósito, F. J. Mesas-Carrascosa, and F. López-Granados, 2014: Evaluation of pixel-and object-based approaches for mapping wild oat (Avena sterilis) weed patches in wheat fields using QuickBird imagery for site-specific management. *Eur. J. Agron.*, **59**, 57–66.

Cerri, C. E. P., J. A. M. Demattě, M. V. R. Ballester, L. A. Martinelli, R. L. Victoria, and E. Roose, 2001: GIS erosion risk assessment of the Piracicaba river basin, southeastern Brazil. *Mapp. Sci. Remote Sens.*, **38**, 157–171, https://doi.org/10.1080/07493878.2001.10642173.

Chalise, D., and L. Kumar, 2020: Land use change affects water erosion in the Nepal Himalayas. *PLOS ONE*, **15**, e0231692, https://doi.org/10.1371/journal.pone.0231692.

Chalise, D., L. Kumar, C. P. Shriwastav, and S. Lamichhane, 2018: Spatial assessment of soil erosion in a hilly watershed of Western Nepal. *Environ. Earth Sci.*, **77**, 685, https://doi.org/10.1007/s12665-018-7842-3.

Chalise, D., L, Kumar, and P. Kristiansen, 2019: Land Degradation by Soil Erosion in Nepal: A Review. *Soil Syst.*, **3**, 12, https://doi.org/10.3390/soilsystems3010012.

Chander, G., B. L. Markham, and D. L. Helder, 2009: Summary of current radiometric calibration coefficients for Landsat MSS, TM, ETM+, and EO-1 ALI sensors. *Remote Sens. Environ.*, **113**, 893–903.

Chemura, A., and O. Mutanga, 2017: Developing detailed age-specific thematic maps for coffee (*Coffea arabica* L.) in heterogeneous agricultural landscapes using random forests applied on Landsat 8 multispectral sensor. *Geocarto Int.*, **32**, 759–776, https://doi.org/10.1080/10106049.2016.1178812.

Chemura, A., A. W. Yalew, and C. Gornott, 2021: Quantifying Agroforestry Yield Buffering Potential Under Climate Change in the Smallholder Maize Farming Systems of Ethiopia. *Front. Agron.*, **3**, 609536, https://doi.org/10.3389/fagro.2021.609536.

Chen, C.-N., S. S. Tfwala, and C.-H. Tsai, 2020: Climate Change Impacts on Soil Erosion and Sediment Yield in a Watershed. *Water*, **12**, 2247, https://doi.org/10.3390/w12082247.

Chen, J.-L., H.-B. Liu, W. Wu, and D.-T. Xie, 2011: Estimation of monthly solar radiation from measured temperatures using support vector machines – A case study. *Renew. Energy*, **36**, 413–420, https://doi.org/10.1016/j.renene.2010.06.024.

Chen, J.-L., G.-S. Li, and S.-J. Wu, 2013: Assessing the potential of support vector machine for estimating daily solar radiation using sunshine duration. *Energy Convers. Manag.*, **75**, 311–318, https://doi.org/10.1016/j.enconman.2013.06.034.

Chen, X.-L., H.-M. Zhao, P.-X. Li, and Z.-Y. Yin, 2006: Remote sensing image-based analysis of the relationship between urban heat island and land use/cover changes. *Remote Sens. Environ.*, **104**, 133–146, https://doi.org/10.1016/j.rse.2005.11.016.

Chirisa, I., 2014: Building and urban planning in Zimbabwe with special reference to Harare: Putting needs, costs and sustainability in focus. *Consilience*, 1–26.

Chirisa, I. E. W., and K. Muhomba, 2013: Constraints to managing urban and housing land in the context of poverty: a case of Epworth settlement in Zimbabwe. *Local Environ.*, **18**, 950–964, https://doi.org/10.1080/13549839.2012.748727.

Clarke, K. C., S. Hoppen, and L. Gaydos, 1997: A self-modifying cellular automaton model of historical urbanization in the San Francisco Bay area. *Environ. Plan. B Plan. Des.*, **24**, 247–261.

Congalton, R. G., 1991: A review of assessing the accuracy of classifications of remotely sensed data. *Remote Sens. Environ.*, **37**, 35–46.

CSO, 2004: Census 2002 Population Census: Provincial Profile Harare. CSO (Central Statistical Office): Harare, Zimbabwe.

Cumming, S. D., D. S. Tevera, and L. M. Zinyama, 1993: *Harare: The Growth and Problems of the City*. University of Zimbabwe Publications,.

D. K. McCool, G. R. Foster, C. K. Mutchler, and L. D. Meyer, 1989: Revised Slope Length Factor for the Universal Soil Loss Equation. *Trans. ASAE*, **32**, 1571–1576, https://doi.org/10.13031/2013.31192.

Dams, J., J. Dujardin, R. Reggers, I. Bashir, F. Canters, and O. Batelaan, 2013: Mapping impervious surface change from remote sensing for hydrological modeling. *J. Hydrol.*, **485**, 84–95, https://doi.org/10.1016/j.jhydrol.2012.09.045.

De Meyer, A., J. Poesen, M. Isabirye, J. Deckers, and D. Raes, 2011: Soil erosion rates in tropical villages: A case study from Lake Victoria Basin, Uganda. *CATENA*, **84**, 89–98, https://doi.org/10.1016/j.catena.2010.10.001.

Demirel, M. C., and H. Moradkhani, 2016: Assessing the impact of CMIP5 climate multi-modeling on estimating the precipitation seasonality and timing. *Clim. Change*, **135**, 357–372, https://doi.org/10.1007/s10584-015-1559-z.

Desmet, P. J. J., and A. Govers, 1996: A GIS procedure for automatically calculating the USLE LS factor on topographically complex landscape units. *J. Soil Water Conserv.*, **51**, 427–433.

Dibaba, W. T., T. A. Demissie, and K. Miegel, 2020: Watershed Hydrological Response to Combined Land Use/Land Cover and Climate Change in Highland Ethiopia: Finchaa Catchment. *Water*, **12**, 1801, https://doi.org/10.3390/w12061801.

van Dijk, P. M., A. V. Auzet, and M. Lemmel, 2005: Rapid assessment of field erosion and sediment transport pathways in cultivated catchments after heavy rainfall events. *Earth Surf. Process. Landf.*, **30**, 169–182, https://doi.org/10.1002/esp.1182.

Dougherty, J., R. Kohavi, and M. Sahami, 1995: Supervised and unsupervised discretization of continuous features. In Machine Learning Proceedings.

Douglas, I., 1983: The urban environment. *Edw. Anorld Publ. Ltd Lond. UK*,.

Dubeau, P., D. King, D. Unbushe, and L.-M. Rebelo, 2017: Mapping the Dabus Wetlands, Ethiopia, Using Random Forest Classification of Landsat, PALSAR and Topographic Data. *Remote Sens.*, **9**, 1056, https://doi.org/10.3390/rs9101056.

Dunn, J. C., 1973: A Fuzzy Relative of the ISODATA Process and Its Use in Detecting Compact Well-Separated Clusters. *J. Cybern.*, **3**, 32–57, https://doi.org/10.1080/01969727308546046.

Durigon, V. L., D. F. Carvalho, M. A. H. Antunes, P. T. S. Oliveira, and M. M. Fernandes, 2014: NDVI time series for monitoring RUSLE cover management factor in a tropical watershed. *Int. J. Remote Sens.*, **35**, 441–453, https://doi.org/10.1080/01431161.2013.871081.

Eastman, J. R., 2000: IDRISI 32 Guide to GIS and Image Processing. Clark University, Worcester, MA, USA, Volume 1, pp.109-142.

Eastman, J. R., 2009: IDRISI Taiga Guide to GIS and Image Processing. Clark University, Worcester, MA, USA.

El-Swaify, S. A., C. L. Gramier, and A. Lo, 1987: Recent advances in soil conservation in steepland in humid tropics.

Evans, R., 2002: An alternative way to assess water erosion of cultivated land – field-based measurements: and analysis of some results. *Appl. Geogr.*, **22**, 187–207, https://doi.org/10.1016/S0143-6228(02)00004-8.

Falk, M., R. J. Denham, and K. L. Mengersen, 2010: Estimating un-certainty in the revised universal soil loss equation via Bayesian melding. *J Agric Biol Env. Sta*, **15**, 20–37.

FAO and ITPS, 2015: Status of the World's Soil Resources (SWSR) – Main Report.

Farhan, Y., and S. Nawaiseh, 2015: Spatial assessment of soil erosion risk using RUSLE and GIS techniques. *Environ. Earth Sci.*, **74**, 4649–4669, https://doi.org/10.1007/s12665-015-4430-7.

Farhan, Y., D. Zregat, and I. Farhan, 2013: Spatial Estimation of Soil Erosion Risk Using RUSLE Approach, RS, and GIS Techniques: A Case Study of Kufranja Watershed, Northern Jordan. *J. Water Resour. Prot.*, **05**, 1247–1261, https://doi.org/10.4236/jwarp.2013.512134.

Faridatul, M. I., and B. Wu, 2018: Automatic Classification of Major Urban Land Covers Based on Novel Spectral Indices. *ISPRS Int. J. Geo-Inf.*, **7**, 453, https://doi.org/10.3390/ijgi7120453.

Favis-Mortlock, D. T., and A. J. T. Guerra, 1999: The implications of general circulation model estimates of rainfall for future erosion: a case study from Brazil. *CATENA*, **37**, 329–354, https://doi.org/10.1016/S0341-8162(99)00025-9.

Feng, X., Y. Wang, L. Chen, B. Fu, and G. Bai, 2010: Modeling soil erosion and its response to land-use change in hilly catchments of the Chinese Loess Plateau. *Geomorphology*, **118**, 239–248, https://doi.org/10.1016/j.geomorph.2010.01.004.

Ferreira, V., and T. Panagopoulos, 2014: Seasonality of Soil Erosion Under Mediterranean Conditions at the Alqueva Dam Watershed. *Environ. Manage.*, **54**, 67–83, https://doi.org/10.1007/s00267-014-0281-3.

Ferreira, V., A. Samora-Arvela, and T. Panagopoulos, 2016: Soil erosion vulnerability under scenarios of climate land-use changes after the development of a large reservoir in a semi-arid area. *J. Environ. Plan. Manag.*, **59**, 1238–1256, https://doi.org/10.1080/09640568.2015.1066667.

Ferro, V., P. Porto, and B. Yu, 1999: A comparative study of rainfall erosivity estimation for southern Italy and southeastern Australia. *Hydrol. Sci. J.*, **44**, 3–24.

Fitawok, M. B., B. Derudder, A. S. Minale, S. Van Passel, E. Adgo, and J. Nyssen, 2020: Modeling the Impact of Urbanization on Land-Use Change in Bahir Dar City, Ethiopia: An Integrated Cellular Automata–Markov Chain Approach. *Land*, **9**, 115, https://doi.org/10.3390/land9040115.

Flangan, D. C., and M. A. Nearing, 1995: NSERL Report No. 10. *USDA Water Erosion Prediction Project: Hill Slope Profile and Watershed Model Documentation;*, Vol. 47 of, USDA-ARS National Soil Erosion Research Laboratory: West Lafayette, 907–1194.

Food and Agriculture Organization, (FAO), 1986: Ethiopian Highlands Reclamation Study: Ethiopia. *FAO Rome Italy*, 354.

Foody, G. M., and A. Mathur, 2004: A relative evaluation of multiclass image classification by support vector machines. *IEEE Trans. Geosci. Remote Sens.*, **42**, 1335–1343.

Foody, G. M., and A. Mathur, 2006: The use of small training sets containing mixed pixels for accurate hard image classification: Training on mixed spectral responses for classification by a SVM. *Remote Sens. Environ.*, **103**, 179–189, https://doi.org/10.1016/j.rse.2006.04.001.

Forgy, E. W., 1965: Cluster Analysis of Multivariate Data: Efficiency versus Interpretability of Classifications. *Biometrics*, **21**, 768–769.

Fournier, F., 1972: Soil Conservation Nature and Environment Series. Council of Europe, p. 320.

Freeman, T. G., 1991: Calculating catchment area with divergent flow based on a regular grid. *Comput. Geosci.*, **17**, 413–422, https://doi.org/10.1016/0098-3004(91)90048-I.

Ghani, S. E., and R. Kanbur, 2013: *Urbanization and (in) Formalization*. World Bank: Washington, DC,.

Giang, P., L. Giang, and K. Toshiki, 2017: Spatial and Temporal Responses of Soil Erosion to Climate Change Impacts in a Transnational Watershed in Southeast Asia. *Climate*, **5**, 22, https://doi.org/10.3390/cli5010022.

Girmay, G., A. Moges, and A. Muluneh, 2021: Assessment of Current and Future Climate Change Impact on Soil Loss Rate of Agewmariam Watershed, Northern Ethiopia. *Air Soil Water Res.*, **14**, 117862212199584, https://doi.org/10.1177/1178622121995847.

Government of Zimbabwe (GoZ), 1991: Report on development of human settlements in Zimbabwe.

Green, K., D. kempka, and L. Lackey, 1994: Using Remote Sensing to Detect and Monitor Land-Cover and Land-Use Change. *Photogramm. Eng. Remote Sens.*, **60**, 7.

Guan, D., W. Gao, K. Watari, and H. Fukahori, 2008: Land use change of Kitakyushu based on landscape ecology and Markov model. *J. Geogr. Sci.*, **18**, 455–468, https://doi.org/10.1007/s11442-008-0455-0.

Gumindoga, W., T. Rientjes, M. Shekede, D. Rwasoka, I. Nhapi, and A. Haile, 2014: Hydrological Impacts of Urbanization of Two Catchments in Harare, Zimbabwe. *Remote Sens.*, **6**, 12544–12574, https://doi.org/10.3390/rs61212544.

Gupta, S., and S. Kumar, 2017: Simulating climate change impact on soil erosion using RUSLE model − A case study in a watershed of mid-Himalayan landscape. *J. Earth Syst. Sci.*, **126**, 43, https://doi.org/10.1007/s12040-017-0823-1.

Haan, C. T., B. J. Barfield, and J. C. Hayes, 1994: *Design hydrology abd sedimentology for small catchments*. Academic Press, 588 pp.

Hagemann, S., H. Göttel, D. Jacob, P. Lorenz, and E. Roeckner, 2009: Improved regional scale processes reflected in projected hydrological changes over large European catchments. *Clim. Dyn.*, **32**, 767–781, https://doi.org/10.1007/s00382-008-0403-9.

Halmy, M. W. A., P. E. Gessler, J. A. Hicke, and B. B. Salem, 2015: Land use/land cover change detection and prediction in the north-western coastal desert of Egypt using Markov-CA. *Appl. Geogr.*, **63**, 101–112, https://doi.org/10.1016/j.apgeog.2015.06.015.

Hamad, R., H. Balzter, and K. Kolo, 2018: Predicting Land Use/Land Cover Changes Using a CA-Markov Model under Two Different Scenarios. *Sustainability*, **10**, 3421, https://doi.org/10.3390/su10103421.

Harris, C. D., and E. L. Ullman, 1945: *The nature of cities.* Annals of the American academy of political and social science., 7–17 pp.

Harvey, D., 1973: *Social Justice and the City*. Baltimore, MD: Johns Hopkins Press.

Hashem, N., and P. Balakrishnan, 2015: Change analysis of land use/land cover and modelling urban growth in Greater Doha, Qatar. *Ann. GIS*, **21**, 233–247, https://doi.org/10.1080/19475683.2014.992369.

Hegazy, I. R., and M. R. Kaloop, 2015: Monitoring urban growth and land use change detection with GIS and remote sensing techniques in Daqahlia governorate Egypt. *Int. J. Sustain. Built Environ.*, **4**, 117–124, https://doi.org/10.1016/j.ijsbe.2015.02.005.

Hengl, T., and Coauthors, 2017: SoilGrids250m: Global gridded soil information based on machine learning. *PLOS ONE*, **12**, e0169748, https://doi.org/10.1371/journal.pone.0169748.

Herold, M., N. C. Goldstein, and K. C. Clarke, 2003: The spatiotemporal form of urban growth: measurement, analysis and modeling. *Remote Sens. Environ.*, **86**, 286–302, https://doi.org/10.1016/S0034-4257(03)00075-0.

Herold, M., D. A. Roberts, M. E. Gardner, and P. E. Dennison, 2004: Spectrometry for urban area remote sensing—Development and analysis of a spectral library from 350 to 2400 nm. *Remote Sens. Environ.*, **91**, 304–319, https://doi.org/10.1016/j.rse.2004.02.013.

Herron, M. C., 1999: Postestimation Uncertainty in Limited Dependent Variable Models. *Polit. Anal.*, **8**, 83–98, https://doi.org/10.1093/oxfordjournals.pan.a029806.

Hill, J., and B. Schütt, 2000: Mapping Complex Patterns of Erosion and Stability in Dry Mediterranean Ecosystems. *Remote Sens. Environ.*, **74**, 557–569, https://doi.org/10.1016/S0034-4257(00)00146-2.

Hogarth, W. L., C. W. Rose, J. Y. Parlange, G. C. Sander, and G. Carey, 2004: Soil erosion due to rainfall impact with no inflow: a numerical solution with spatial and temporal effects of sediment settling velocity characteristics. *J. Hydrol.*, **294**, 229–240, https://doi.org/10.1016/j.jhydrol.2004.02.014.

Hove, M., and A. Tirimboi, 2011: Assessment of Harare Water Service Delivery. *Afr. J. Sustain. Dev.*, 61–84.

Hoyt, H., 1939: *The structure and growth of residential neighborhoods in American cities.* Federal Housing Adminstration, Washington D.C,.

Hu, X., and Q. Weng, 2013: *Extraction of impervious surfaces from hyperspectral imagery: Linear versus nonlinear methods*. Remote Sensing of Natural Resources,.

Huang, C., L. S. Davis, and J. R. G. Townshend, 2002: An assessment of support vector machines for land cover classification. *Int. J. Remote Sens.*, **23**, 725–749, https://doi.org/10.1080/01431160110040323.

Hudson, D. A., and R. G. Jones, 2002: Regional Climate Model Simulations of Present-Day and Future Climates of Southern Africa. *Tech Rep Hadley Cent. Tech. Note 39 Hadley Cent. Clim. Predict. Res. Met Off.*, 42.

Hudson, N. W., 1981: *Soil Conservation,*. 2nd ed. Batsford, London.

Huete, A. R., 1988: A soil-adjusted vegetation index (SAVI). *Remote Sens. Environ.*, **25**, 295–309.

Hugo, G., 2016: *New Forms of Urbanization: Beyond the Urban-Rural Dichotomy;* Routledge: Abingdon-on-Thames,.

Hurni, H., 1988: Degradation and Conservation of the Resources in the Ethiopian Highlands. *Mt. Res. Dev.*, **8**, 123, https://doi.org/10.2307/3673438.

Igbokwe, J. I., J. O. Akinyede, B. Dang, T. Alaga, M. N. Ono, V. C. Nnodu, and L. O. Anike, 2008: Mapping and monitoring of the impact of gully erosion in Southeastern Nigeria with satellite remote sensing and Geographic Information System. *Int. Arch. Photogramm. Remote Sens. Spat. Inf. Sci.*, **37**, 8.

Im, J., and J. R. Jensen, 2008: Hyperspectral Remote Sensing of Vegetation: Hyperspectral remote sensing of vegetation. *Geogr. Compass*, **2**, 1943–1961, https://doi.org/10.1111/j.1749-8198.2008.00182.x.

Imeson, A. C., and F. J. P. M. Kwaad, 1980: Gully types and gully prediction. *KNAG Geogr. Tijdschr. XIV 5*, 430–441.

International Soil Reference and Information Centre (ISRIC) World Soil Information), 2019:

IPCC, (Intergovernmental Panel on Climate Change), 2007: Climate change: The physical science basis, contribution of working group I to the fourth assessment report of the intergovernmental panel on climate change.

IPCC, (Intergovernmental Panel on Climate Change), 2014: Climate Change 2014: Impacts, Adaptation, and Vulnerability. Contribution of Working Group II to the Fifth Assessment Report of the Intergovernmental Panel on Climate Change.

Islam, K., M. Jashimuddin, B. Nath, and T. K. Nath, 2018: Land use classification and change detection by using multi-temporal remotely sensed imagery: The case of Chunati wildlife sanctuary, Bangladesh. *Egypt. J. Remote Sens. Space Sci.*, **21**, 37–47, https://doi.org/10.1016/j.ejrs.2016.12.005.

Jafari, M., H. Majedi, S. Monavari, A. Alesheikh, and M. Kheirkhah Zarkesh, 2016: Dynamic Simulation of Urban Expansion Based on Cellular Automata and Logistic Regression Model: Case Study of the Hyrcanian Region of Iran. *Sustainability*, **8**, 810, https://doi.org/10.3390/su8080810.

Jain, A. K., 2010: Data clustering: 50 years beyond K-means. *Pattern Recognit. Lett.*, **31**, 651–666, https://doi.org/10.1016/j.patrec.2009.09.011.

Jakab, G., B. Madarász, J. Szabó, A. Tóth, D. Zacháry, Z. Szalai, Á. Kertész, and J. Dyson, 2017: Infiltration and Soil Loss Changes during the Growing Season under Ploughing and Conservation Tillage. *Sustainability*, **9**, 1726, https://doi.org/10.3390/su9101726.

Jat, M. K., M. Choudhary, and A. Saxena, 2017: Application of geo-spatial techniques and cellular automata for modelling urban growth of a heterogeneous urban fringe. *Egypt. J. Remote Sens. Space Sci.*, **20**, 223–241, https://doi.org/10.1016/j.ejrs.2017.02.002.

Jetten, V., G. Govers, and R. Hessel, 2003: Erosion models: quality of spatial predictions. *Hydrol. Process.*, **17**, 887–900.

Jim, C. Y., 1993: Soil Compaction as a Constraint to Tree Growth in Tropical & Subtropical Urban Habitats. *Environ. Conserv.*, **20**, 35–49, https://doi.org/10.1017/S0376892900037206.

Jinren, R. N., and K. L. Yingkui, 2003: Approach to soil erosion assessment in terms of land-use structure changes. *J. Soil Water Conserv.*, **58**, 158–169.

Jones, R. J., and Coauthors, 2013: Nature and extent of soil erosion in Europe. Reports of the Technical Working Groups Established under the Thematic Strategy for Soil Protection.

Jones, R. J. A., and Coauthors, 2003: Interim Report version 3.31, 28 October 2003. **3**, 28.

Kabantu, M. T., R. M. Tshimanga, J. M. O. Kileshye, W. Gumindoga, and J. T. Beya, 2018: A GIS-based estimation of soil erosion parameters for soil loss potential and erosion hazard in the city of Kinshasa, the Democratic Republic of Congo. *Proc IAHS*, **378**, 51–57.

Kadhim, N., M. Mourshed, and M. Bray, 2016: Advances in remote sensing applications for urban sustainability. *Euro-Mediterr. J. Environ. Integr.*, **1**, 7, https://doi.org/10.1007/s41207-016-0007-4.

Kamete, A. Y., 2007: Cold-hearted, negligent and spineless? Planning, planners and the (r) ejection of "filth" in urban Zimbabwe. *Int. Plan. Stud.*, **12**, 153–171.

Kamuju, N., 2016: Spatial Identification and Classification of Soil Erosion Prone Zones Using Remote Sensing & Gis Integrated 'Rusle' Model and 'Sateec Gis System.' *Int. J. Eng. Sci. Res. Technol.*, https://doi.org/10.5281/ZENODO.163095.

Kamusoko, C., J. Gamba, and H. Murakami, 2013: Monitoring Urban Spatial Growth in Harare Metropolitan Province, Zimbabwe. *Adv. Remote Sens.*, **02**, 322–331, https://doi.org/10.4236/ars.2013.24035.

Karamage, F., C. Zhang, T. Liu, A. Maganda, and A. Isabwe, 2017: Soil Erosion Risk Assessment in Uganda. *Forests*, **8**, 52, https://doi.org/10.3390/f8020052.

Karydas, C. G., T. Sekuloska, and G. N. Silleos, 2009: Quantification and site-specification of the support practice factor when mapping soil erosion risk associated with olive plantations in the Mediterranean island of Crete. *Environ. Monit. Assess.*, **149**, 19–28, https://doi.org/10.1007/s10661-008-0179-8.

Kefi, M., K. Yoshino, Y. Setiawan, K. Zayani, and M. Boufaroua, 2011: Assessment of the effects of vegetation on soil erosion risk by water: a case of study of the Batta watershed in Tunisia. *Environ. Earth Sci.*, **64**, 707–719, https://doi.org/10.1007/s12665-010-0891-x.

Khawaldah, H. A., I. Farhan, and N. M. Alzboun, 2020: Simulation and prediction of land use and land cover change using GIS, remote sensing and CA-Markov model. *Glob. J. Environ. Sci. Manag.*, **6**, https://doi.org/10.22034/gjesm.2020.02.07.

Kheir, R. B., C. Abdallah, and M. Khawlie, 2008: Assessing soil erosion in Mediterranean karst landscapes of Lebanon using remote sensing and GIS. *Eng. Geol.*, **99**, 239–254, https://doi.org/10.1016/j.enggeo.2007.11.012.

Khosrokhani, M., and B. Pradhan, 2014: Spatio-temporal assessment of soil erosion at Kuala Lumpur metropolitan city using remote sensing data and GIS. *Geomat. Nat. Hazards Risk*, **5**, 252–270, https://doi.org/10.1080/19475705.2013.794164.

Knorn, J., A. Rabe, V. C. Radeloff, T. Kuemmerle, J. Kozak, and P. Hostert, 2009: Land cover mapping of large areas using chain classification of neighboring Landsat satellite images. *Remote Sens. Environ.*, **113**, 957–964, https://doi.org/10.1016/j.rse.2009.01.010.

Koirala, P., S. Thakuri, S. Joshi, and R. Chauhan, 2019: Estimation of Soil Erosion in Nepal Using a RUSLE Modeling and Geospatial Tool. *Geosciences*, **9**, 147, https://doi.org/10.3390/geosciences9040147.

Koomen, E., and B. J. Beurden, eds., 2011: *Land-Use Modelling in Planning Practice*. Springer Netherlands,.

Kouli, M., P. Soupios, and F. Vallianatos, 2009: Soil erosion prediction using the Revised Universal Soil Loss Equation (RUSLE) in a GIS framework, Chania, Northwestern Crete, Greece. *Environ. Geol.*, **57**, 483–497, https://doi.org/10.1007/s00254-008-1318-9.

Kucsicsa, G., and I. Grigorescu, 2018: Urban Growth in the Bucharest Metropolitan Area: Spatial and Temporal Assessment Using Logistic Regression. *J. Urban Plan. Dev.*, **144**, 05017013, https://doi.org/10.1061/(ASCE)UP.1943-5444.0000415.

Kulkarni, G., A. Muley, N. Deshmukh, and P. Bhalchandra, 2020: Land Use Land Cover Change Detection Through GIS and Unsupervised Learning Technique. *Information and Communication Technology for Sustainable Development*, M. Tuba, S. Akashe, and A. Joshi, Eds., Vol. 933 of *Advances in Intelligent Systems and Computing*, Springer Singapore, 239–247.

Kumar, S., N. Radhakrishnan, and S. Mathew, 2014: Land use change modelling using a Markov model and remote sensing. *Geomat. Nat. Hazards Risk*, **5**, 145–156, https://doi.org/10.1080/19475705.2013.795502.

Laflen, J. M., L. J. Lane, and G. R. Foster, 1991: WEPP: A new generation of erosion prediction technology. *J. Soil Water Conserv. 46*, 34–38.

Lahlaoi, H., H. Rhinane, A. Hilali, S. Lahssini, and L. Khalile, 2015: Potential Erosion Risk Calculation Using Remote Sensing and GIS in Oued El Maleh Watershed, Morocco. *J. Geogr. Inf. Syst.*, **07**, 128–139, https://doi.org/10.4236/jgis.2015.72012.

Lal, R., 1985: Soil erosion and sediment transport research in tropical Africa. *Hydrol. Sci. J.*, **30**, 239–256, https://doi.org/10.1080/02626668509490987.

Lal, R., 1990: Soil Erosion in the Tropics: Principles and Management. New York: McGraw-Hill, 23.

Lal, R., 1994: *Soil Erosion Research Method*. 2nd ed. Soil and Water Conservation Society: Ankeny.

Lal, R., 2001: Soil degradation by erosion. *Land Degrad. Dev.*, **12**, 519–539.

Lambin, E. F., 1997: Modelling and monitoring land-cover change processes in tropical regions. *Prog. Phys. Geogr. Earth Environ.*, **21**, 375–393, https://doi.org/10.1177/030913339702100303.

Lambin, E. F., B. L. Turner, H. J. Geist, S. B. Agbola, J. W. Bruce, O. T. Coomes, R. Dirzo, G. Fischer, C. Folke, P. S. George, K. Homewood, J. Imbernon, R. Leemans, X. Li, E. F. Moran, M. Mortimore, P. S. Ramakrishnan, J. F. Richards, H. Skånes, W. Steffen, G. D. Stone, U. Svedin, T. A. Veldkamp, C. Vogel, J. Xu, 2001: The causes of land-use and land-cover change: moving beyond the myths. *Glob. Environ. Change*, **11**, 261–269, https://doi.org/10.1016/S0959-3780(01)00007-3.

Lary, D. J., 2010: Artificial Intelligence in Geoscience and Remote Sensing. *Geoscience and Remote Sensing New Achievements*, P. Imperatore and D. Riccio, Eds., InTech.

Lazzari, M., D. Gioia, M. Piccarreta, M. Danese, and A. Lanorte, 2015: Sediment yield and erosion rate estimation in the mountain catchments of the Camastra artificial reservoir (Southern Italy): A comparison between different empirical methods. *CATENA*, **127**, 323–339, https://doi.org/10.1016/j.catena.2014.11.021.

Le Roux, J. J., and P. D. Sumner, 2012: Factors controlling gully development: Comparing continuous and discontinuous gullies. *Land Degrad. Dev.*, **23**, 440–449, https://doi.org/10.1002/ldr.1083.

Lee, S., 2004: Soil erosion assessment and its verification using the universal soil loss equation and geographic information system: A case study at Boun, Korea. *Environ. Geol.*, **45**, 457–465.

Lee, S., and B. Pradhan, 2006: Probabilistic landslide hazards and risk mapping on Penang Island, Malaysia. *J. Earth Syst. Sci.*, **115**, 661–672, https://doi.org/10.1007/s12040-006-0004-0.

Legesse, D., C. Vallet-Coulomb, and F. Gasse, 2004: Analysis of the hydrological response of a tropical terminal lake, Lake Abiyata (Main Ethiopian Rift Valley) to changes in climate and human activities. *Hydrol. Process.*, **18**, 487–504, https://doi.org/10.1002/hyp.1334.

Leh, M., S. Bajwa, and I. Chaubey, 2013: Impact of land use change on erosion risk: An integrated Remote Sensing, Geographic Information System and modelling methodology: Impact of land use change on erosion risk. *Land Degrad. Dev.*, 409–421, https://doi.org/10.1002/ldr.1137.

Li, X. S., B. F. Wu, H. Wang, and J. Zhang, 2011: Regional soil erosion risk assessment in Hai Basin. *J. Remote Sens.*, **15**, 372–387.

Li, Z., and H. Fang, 2016: Impacts of climate change on water erosion: A review. *Earth-Sci. Rev.*, **163**, 94–117, https://doi.org/10.1016/j.earscirev.2016.10.004.

Ligonja, P. J., and R. P. Shrestha, 2015: Soil Erosion Assessment in Kondoa Eroded Area in Tanzania Using Universal Soil Loss Equation, Geographic Information Systems and Socioeconomic Approach: Soil Erosion Assessment in Kondoa Eroded Area in Tanzania. *Land Degrad. Dev.*, **26**, 367–379, https://doi.org/10.1002/ldr.2215.

Lister, L. A., 1987: The Erosion Surfaces of Zimbabwe. *Zimb. Geol. Surv.*, **no. 90**, 177.

Liu, K., G. Tang, L. Jiang, A.-X. Zhu, J. Yang, and X. Song, 2015: Regional-scale calculation of the LS factor using parallel processing. *Comput. Geosci.*, **78**, 110–122, https://doi.org/10.1016/j.cageo.2015.02.001.

Lo, A., S. A. El-Swaify, E. W. Dangler, and L. Shinshiro, 1985: *Effectiveness of El30 as an erosivity index in Hawaii. In: S.A. E1-Swaify, W.C. Moldenhauer and A. Lo (Editors), Soil Erosion and Conservation.* Soil Conservation Society of America, Ankeny, 384 392. pp.

Lohnert, B., 2017: *Migration and the rural-urban transition in Sub-Saharan Africa*. Seminar für ländliche Entwicklung (SLE), 70 pp.

Long, W., and S. Srihar, 2004: Land cover classification of SSC image: unsupervised and supervised classification using ERDAS imagine. *IEEE International Geoscience and Remote Sensing Symposium, 2004. IGARSS '04. Proceedings. 2004*, Vol. 4 of, Anchorage, AK, USA, IEEE, 2707–2712.

Lu, D., G. Li, G. S. Valladares, and M. Batistella, 2004a: Mapping soil erosion risk in Rondônia, Brazilian Amazonia: using RUSLE, remote sensing and GIS. *Land Degrad. Dev.*, **15**, 499–512, https://doi.org/10.1002/ldr.634.

Lu, D., P. Mausel, E. Brondizio, and E. F. Moran, 2004b: "Change Detection Techniques." *Int. J. Remote Sens.*, **25**, 2365-401.

Luckow, P., M. A. Wise, J. J. Dooley, and S. H. Kim, 2010: Large-scale utilization of biomass energy and carbon dioxide capture and storage in the transport and electricity sectors under stringent CO2 concentration limit scenarios. *Int. J. Greenh. Gas Control*, **4**, 865–877, https://doi.org/10.1016/j.ijggc.2010.06.002.

Lufafa, A., M. M. Tenywa, M. Isabirye, M. J. G. Majaliwa, and P. L. Woomer, 2003: Prediction of soil erosion in a Lake Victoria basin catchment using a GIS-based Universal Soil Loss model. *Agric. Syst.*, **76**, 883–894, https://doi.org/10.1016/S0308-521X(02)00012-4.

Ma, J. W., Y. Xue, C. F. Ma, and Z. G. Wang, 2003: A data fusion approach for soil erosion monitoring in the Upper Yangtze River Basin of China based on Universal Soil Loss Equation (USLE) model. *Int. J. Remote Sens.*, **24**, 4777–4789, https://doi.org/10.1080/0143116021000056028.

Makinde, E. O., and E. I. Oyebanji, 2018: The Application of Remote Sensing and GIS Technology to Erosion Risk Mapping. *Proceedings*, **2**, 1398, https://doi.org/10.3390/proceedings2221398.

Makwara, E. C., and D. Gamira, 2012: About to Lose all the Soil in Zaka's Ward 5, Zimbabwe: Rewards of Unsustainable Land Use. *Eur. J. Sustain. Dev.*, **1**, 457, https://doi.org/10.14207/ejsd.2012.v1n3p457.

Malaviya, S., M. Munsi, G. Oinam, and P. K. Joshi, 2010: Landscape approach for quantifying land use land cover change (1972–2006) and habitat diversity in a mining area in Central India (Bokaro, Jharkhand). *Environ. Monit. Assess.*, **170**, 215–229.

Manatsa, D., and G. Mukwada, 2012: Rainfall Mechanisms for the Dominant Rainfall Mode over Zimbabwe Relative to ENSO and/or IODZM. *Sci. World J.*, **2012**, 1–15, https://doi.org/10.1100/2012/926310.

Manatsa, D., T. D, Mushore, I. Gwitira, M. Wuta, A. Chemura, M. Shekede, R. Mungandani, L.C. Sakala, L. H. Ali, G. I, MasukwedzaY, J. M. Mupuro, and N. M. Muzira, 2020: Revision of Zimbabwe's Agro-Ecological Zones.

Marondedze, A. K., and B. Schütt, 2019: Dynamics of Land Use and Land Cover Changes in Harare, Zimbabwe: A Case Study on the Linkage between Drivers and the Axis of Urban Expansion. *Land*, **8**, 155, https://doi.org/10.3390/land8100155.

Marondedze, A. K., and B. Schütt, 2020: Assessment of Soil Erosion Using the RUSLE Model for the Epworth District of the Harare Metropolitan Province, Zimbabwe. *Sustainability*, **12**, 8531, https://doi.org/10.3390/su12208531.

Massey, D., 1991: *Flexible sexism.* 1st ed. Environment and Planning D: Society and Space, 31–57 pp.

MathWorks, 2016: Applying supervised learning. Machine Learning with MATLAB.

Mati, B. M., R. P. Morgan, F. N. Gichuki, J. N. Quinton, T. R. Brewer, and H. P. Liniger, 2000: Assessment of erosion hazard with the USLE and GIS: A case study of the Upper Ewaso Ng'iro North basin of Kenya. *Int. J. Appl. Earth Obs. Geoinformation*, **2**, 78–86, https://doi.org/10.1016/S0303-2434(00)85002-3.

Mazvimavi, D., H. Williams, H. Makurira, and S. Kusangaya, 2005: Assessment of Surface Water Resources of Zimbabwe and Guidelines for Planning: Manyame Catchment Harare.

McCool, D. K., L. C. Brown, G. R. Foster, C. K. Mutchler, and L. D. Meyer, 1987: Revised Slope Steepness Factor for the Universal Soil Loss Equation. *Trans. ASAE*, **30**, 1387–1396, https://doi.org/10.13031/2013.30576.

McDonagh, J., 1997: Theories of Urban Land Use and their Application to the Christchurch Property Market. *Prop. Land Econ. Inst. N. Z. Newsl.*, 20.

McDowell, L., 1983: Towards an understanding of the gender division of urban space. *Environ. Plan. D*, 59–72.

McDowell, R. W., and M. S. Srinivasan, 2009: Identifying critical source areas for water quality: 2. Validating the approach for phosphorus and sediment losses in grazed headwater catchments. *J. Hydrol.*, **379**, 68–80, https://doi.org/10.1016/j.jhydrol.2009.09.045.

McHugh, M., T. Harrod, and R. Morgan, 2002: The extent of soil erosion in upland England and Wales. *Earth Surf. Process. Landf.*, **27**, 99–107, https://doi.org/10.1002/esp.308.

Melesse, A., Q. Weng, P. Thenkabail, and G. Senay, 2007: Remote Sensing Sensors and Applications in Environmental Resources Mapping and Modelling. *Sensors*, **7**, 3209–3241, https://doi.org/10.3390/s7123209.

Melgani, F., and L. Bruzzone, 2004: Classification of hyperspectral remote sensing images with support vector machines. *IEEE Trans. Geosci. Remote Sens.*, **42**, 1778–1790, https://doi.org/10.1109/TGRS.2004.831865.

Merritt, W. S., R. A. Letcher, and A. J. Jakeman, 2003: A review of erosion and sediment transport models. *Environ. Model. Softw.*, **18**, 761–799, https://doi.org/10.1016/S1364-8152(03)00078-1.

Merritt, W. S., B. F. W. Croke, A. J. Jakeman, R. A. Letcher, and P. Perez, 2004: A Biophysical Toolbox for assessment and management of land and water resources in rural catchments in Northern Thailand. *Ecol. Model.*, **171**, 279–300, https://doi.org/10.1016/j.ecolmodel.2003.08.010.

Meshesha, D. T., A. Tsunekawa, M. Tsubo, S. A. Ali, and N. Haregeweyn, 2014: Land-use change and its socio-environmental impact in Eastern Ethiopia's highland. *Reg. Environ. Change*, **14**, 757–768, https://doi.org/10.1007/s10113-013-0535-2.

Mhangara, P., V. Kakembo, and K. J. Lim, 2012: Soil erosion risk assessment of the Keiskamma catchment, South Africa using GIS and remote sensing. *Environ. Earth Sci.*, **65**, 2087–2102, https://doi.org/10.1007/s12665-011-1190-x.

Millward, A. A., and J. E. Mersey, 1999: Adapting the RUSLE to model soil erosion potential in a mountainous tropical watershed. *CATENA*, **38**, 109–129, https://doi.org/10.1016/S0341-8162(99)00067-3.

Mohan, M., S. K. Pathan, K. Narendrareddy, A. Kandya, and S. Pandey, 2011: Dynamics of Urbanization and Its Impact on Land-Use/Land-Cover: A Case Study of Megacity Delhi. *J. Environ. Prot.*, **02**, 1274–1283, https://doi.org/10.4236/jep.2011.29147.

Mondal, A., D. Khare, S. Kundu, P. K. Meena, P. K. Mishra, and R. Shukla, 2015: Impact of Climate Change on Future Soil Erosion in Different Slope, Land Use, and Soil-Type Conditions in a Part of the Narmada River Basin, India. *J. Hydrol. Eng.*, **20**, https://doi.org/10.1061/(ASCE)HE.1943-5584.0001065.

Mondal, M. S., N. Sharma, M. Kappas, and P. K. Garg, 2012: Modeling of spatio-temporal dynamics of LULC–a review and assessment. *J Geom*, **6**, 29–39.

Mondal, M. S., N. Sharma, M. Kappas, and P. K. Garg, 2020: Cellular Automata (CA) Contiguity Filters Impacts on CA Markov Modeling of Land Use Land Cover Change Predictions Results. *Int. Arch. Photogramm. Remote Sens. Spat. Inf. Sci.*, **XLIII-B3-2020**, 1585–1591, https://doi.org/10.5194/isprs-archives-XLIII-B3-2020-1585-2020.

Montgomery, D. R., 2007: Soil erosion and agricultural sustainability. *Proc. Natl. Acad. Sci.*, **104**, 13268–13272, https://doi.org/10.1073/pnas.0611508104.

Moore, I. D., and G. J. Burch, 1986: Physical Basis of the Length-slope Factor in the Universal Soil Loss Equation. *Soil Sci. Soc. Am. J.*, **50**, 1294–1298, https://doi.org/10.2136/sssaj1986.03615995005000050042x.

Moore, T. R., 1979: Rainfall Erosivity in East Africa. *Geogr. Ann. Ser. Phys. Geogr.*, **61**, 147–156, https://doi.org/10.1080/04353676.1979.11879987.

Morgan, R. P. C., 2005: *Soil Erosion and Conservation*. 3rd ed. Blackwell Publishing Ltd.

Morgan, R. P. C., 2009: *Soil Erosion and Conservation*. John Wiley & Sons, 315 pp.

Moss, R. H., and Coauthors, 2010: The next generation of scenarios for climate change research and assessment. *Nature*, **463**, 747–756, https://doi.org/10.1038/nature08823.

Mou, L., P. Ghamisi, and X. X. Zhu, 2018: Unsupervised Spectral–Spatial Feature Learning via Deep Residual Conv–Deconv Network for Hyperspectral Image Classification. *IEEE Trans. Geosci. Remote Sens.*, **56**, 391–406, https://doi.org/10.1109/TGRS.2017.2748160.

Moura-Bueno, J. M., R. S. D. Dalmolin, A. ten Caten, L. F. C. Ruiz, P. V. Ramos, and A. C. Dotto, 2016: Assessment of Digital Elevation Model for Digital Soil Mapping in a Watershed with

Gently Undulating Topography. *Rev. Bras. Ciênc. Solo*, **40**, https://doi.org/10.1590/18069657rbcs20150022.

Mpindu, T., 2018: Changes in built-up and vegetation structure and composition of indigenous patches in Harare, Zimbabwe (Doctoral dissertation).

Mukherjee, S., 1987: Land use maps for conservation of ecosystems. *Geogr Rev Ind*, **3**, 23–28.

Mukherjee, S., W. Bebermeier, and B. Schütt, 2018: An Overview of the Impacts of Land Use Land Cover Changes (1980–2014) on Urban Water Security of Kolkata. *Land*, **7**, 91, https://doi.org/10.3390/land7030091.

Mullan, D., D. Favis-Mortlock, and R. Fealy, 2012: Addressing key limitations associated with modelling soil erosion under the impacts of future climate change. *Agric. For. Meteorol.*, **156**, 18–30, https://doi.org/10.1016/j.agrformet.2011.12.004.

Müller, N., M. Ignatieva, C. H. Nilon, P. Werner, and W. C. Zipperer, 2013: Patterns and trends in urban biodiversity and landscape design. T. Elmqvist et al., Eds.

Mundia, C. N., and M. Aniya, 2005: Analysis of land use/cover changes and urban expansion of Nairobi city using remote sensing and GIS. *Int. J. Remote Sens.*, **26**, 2831–2849, https://doi.org/10.1080/01431160500117865.

Murphy, J. M., D. M. H. Sexton, D. N. Barnett, G. S. Jones, M. J. Webb, M. Collins, and D. A. Stainforth, 2004: Quantification of modelling uncertainties in a large ensemble of climate change simulations. *Nature*, **430**, 768–772, https://doi.org/10.1038/nature02771.

Musemwa, M., 2010: From 'Sunshine City' to a Landscape of Disaster: The Politics of Water, Sanitation and Disease in Harare, Zimbabwe, 1980–2009. *J. Dev. Soc.*, **26**, 165–206, https://doi.org/10.1177/0169796X1002600202.

Mushore, T. D., J. Odindi, T. Dube, and O. Mutanga, 2017: Prediction of future urban surface temperatures using medium resolution satellite data in Harare metropolitan city, Zimbabwe. *Build. Environ.*, **122**, 397–410, https://doi.org/10.1016/j.buildenv.2017.06.033.

Mwakapuja, F., E. Liwa, and J. Kashaigili, 2013: Usage of Indices for Extraction of Built-up Areas and Vegetation Features from Landsat TM Image: A Case of Dar Es Salaam and Kisarawe Peri-Urban Areas, Tanzania. *Int. J. Agric. For.*, **3**, 273–283.

Myers, G., 2011: *African Cities: Alternative Visions of Urban Theory and Practice*. Zed Books Ltd.,.

Najafi, M. R., and H. Moradkhani, 2016: Ensemble Combination of Seasonal Streamflow Forecasts. *J. Hydrol. Eng.*, **21**, 04015043, https://doi.org/10.1061/(ASCE)HE.1943-5584.0001250.

Nasrollahi, N., A. AghaKouchak, L. Cheng, L. Damberg, T. J. Phillips, C. Miao, K. Hsu, and S. Sorooshian, 2015: How well do CMIP5 climate simulations replicate historical trends and patterns of meteorological droughts? *Water Resour. Res.*, **51**, 2847–2864, https://doi.org/10.1002/2014WR016318.

Nearing, M. A., 1997: A Single, Continuous Function for Slope Steepness Influence on Soil Loss. *Soil Sci. Soc. Am. J.*, **61**, 917–919, https://doi.org/10.2136/sssaj1997.03615995006100030029x.

Nearing, M. A., 2001: Potential changes in rainfall erosivity in the U.S with climate change during the 21st century. *J. Soil Water Conserv.*, **56 (3)**, 229–232.

Nearing, M. A., V. Jetten, C. Baffaut, O. Cerdan, A. Couturier, M. Hernandez, Y. Le Bissonnais, M. H. Nichols, J. P. Nunes, C. S. Renschler, V. Souchère, and K. van Oost, 2005: Modeling response of soil erosion and runoff to changes in precipitation and cover. *CATENA*, **61**, 131–154, https://doi.org/10.1016/j.catena.2005.03.007.

Nemmour, H., and Y. Chibani, 2006: Multiple support vector machines for land cover change detection: An application for mapping urban extensions. *ISPRS J. Photogramm. Remote Sens.*, **61**, 125–133, https://doi.org/10.1016/j.isprsjprs.2006.09.004.

Nhapi, I., 2009: The water situation in Harare, Zimbabwe: a policy and management problem. *Water Policy*, **11**, 221–235, https://doi.org/10.2166/wp.2009.018.

Nooni, I. K., A. A. Duker, I. Van Duren, L. Addae-Wireko, and E. M. Osei Jnr, 2014: Support vector machine to map oil palm in a heterogeneous environment. *Int. J. Remote Sens.*, **35**, 4778–4794, https://doi.org/10.1080/01431161.2014.930201.

Nyakatawa, E. Z., K. C. Reddy, and J. L. Lemunyon, 2001: Predicting soil erosion in conservation tillage cotton production systems using the revised universal soil loss equation (RUSLE). *Soil Tillage Res.*, **57**, 213–224, https://doi.org/10.1016/S0167-1987(00)00178-1.

Nyamangara, J., A. Marondedze, E. N. Masvaya, T. Mawodza, R. Nyawasha, R. Tirivavi, P. Nyamugafata, and M. Wuta, 2014: Influence of basin-based conservation agriculture on selected soil quality parameters under smallholder farming in Zimbabwe. *Soil Use Manag.*, **30**, 550–559, https://doi.org/10.1111/sum.12149.

Nyamapfene, K., 1991: *Soils of Zimbabwe*. Nehanda Publishers (Pvt) Ltd.

Nyamapfene, K., 1992: A Geographical Overview of the Soils of Zimbabwe and Their Agricultural Potential.

Ochoa-Cueva, P., A. Fries, P. Montesinos, J. A. Rodríguez-Díaz, and J. Boll, 2015: Spatial Estimation of Soil Erosion Risk by Land-Cover Change in the Andes of Southern Ecuador: Soil Erosion Risk by Land-Cover Change in Southern Ecuador. *Land Degrad. Dev.*, **26**, 565–573, https://doi.org/10.1002/ldr.2219.

Okereke, C. N., N. N. Onu, C. Z. Akaolisa, D. O. Ikoro, S. I. Ibeneme, B. Ubechu, E. S. Chinemelu, and L. O. Amadikwa, 2012: Mapping gully erosion using remote sensing technique: a case study of Okigwe area, southeastern Nigeria. *Int. J. Eng. Res. Appl. IJERA*, **2**, 1955–1967.

Opeyemi, O. A., F. H. Abidemi, and O. K. Victor, 2019: Assessing the Impact of Soil Erosion on Residential Areas of Efon-Alaaye Ekiti, Ekiti-State, Nigeria. **5**, 9.

Owoeye, J. O., and O. O. Popoola, 2017: Predicting urban sprawl and land use changes in Akure region using markov chains modeling. *J. Geogr. Reg. Plan.*, **10**, 197–207, https://doi.org/10.5897/JGRP2016.0578.

Owusu, G., 2012: A GIS-Based Estimation of Soil Loss in the Densu Basin in Ghana. *West Afr. J. Appl. Ecol.*, **20**, 12.

Ozsahin, E., U. Duru, and I. Eroglu, 2018: Land Use and Land Cover Changes (LULCC), a Key to Understand Soil Erosion Intensities in the Maritsa Basin. *Water*, **10**, 335, https://doi.org/10.3390/w10030335.

Pal, M., and P. M. Mather, 2005: Support vector machines for classification in remote sensing. *Int. J. Remote Sens.*, **26**, 1007–1011, https://doi.org/10.1080/01431160512331314083.

Panagos, P., C. Karydas, P. Borrelli, C. Ballabio, and K. Meusburger, 2014: Advances in soil erosion modelling through remote sensing data availability at European scale. D.G. Hadjimitsis, K. Themistocleous, S. Michaelides, and G. Papadavid, Eds., In Proceedings of the Second International Conference on Remote sensing and Geoinformation of the Environment, Paphos, Cyprus, 12 August 2014; Hadjimitsis, D.G., Themistocleous, K., Michaelides, S., Papadavid, G., Eds, Paphos, Cyprus, International Society for Optics and Photonics, 92290I.

Panagos, P., P. Borrelli, and K. Meusburger, 2015a: A New European Slope Length and Steepness Factor (LS-Factor) for Modeling Soil Erosion by Water. *Geosciences*, **5**, 117–126, https://doi.org/10.3390/geosciences5020117.

Panagos, P., P. Borrelli, J. Poesen, C. Ballabio, E. Lugato, K. Meusburger, L. Montanarella, and C. Alewell, 2015b: The new assessment of soil loss by water erosion in Europe. *Environ. Sci. Policy*, **54**, 438–447, https://doi.org/10.1016/j.envsci.2015.08.012.

Panagos, P., C. Ballabio, K. Meusburger, J. Spinoni, C. Alewell, and P. Borrelli, 2017: Towards estimates of future rainfall erosivity in Europe based on REDES and WorldClim datasets. *J. Hydrol.*, **548**, 251–262, https://doi.org/10.1016/j.jhydrol.2017.03.006.

Pappas, E. A., D. R. Smith, C. Huang, W. D. Shuster, and J. V. Bonta, 2008: Impervious surface impacts to runoff and sediment discharge under laboratory rainfall simulation. *CATENA*, **72**, 146–152, https://doi.org/10.1016/j.catena.2007.05.001.

Park, R. E., and E. W. Burgess, 1967: *The city*. 2 Eds. University of Chicago Press,.

Parsa, A. V., A. Yavari, and A. Nejadi, 2016: Spatio-temporal analysis of land use/land cover pattern changes in Arasbaran Biosphere Reserve: Iran. *Model. Earth Syst. Environ.*, **2**, 1–13, https://doi.org/10.1007/s40808-016-0227-2.

Patino, J. E., and J. C. Duque, 2013: A review of regional science applications of satellite remote sensing in urban settings. *Comput. Environ. Urban Syst.*, **37**, 1–17, https://doi.org/10.1016/j.compenvurbsys.2012.06.003.

Patley, M., Rishabh Tripathi, and Patel Lokesh, 2018: Urbanization and Change Detection of Land Use Land Cover of the Holy City Ujjain. https://doi.org/10.13140/rg.2.2.21651.37920.

Pax-Lenney, M., and C. E. Woodcock, 1997: "Monitoring Agricultural Lands in Egypt with Multitemporal Landsat TM Imagery: How Many Images Are Needed?" *Remote Sens. Environ.*, **59**, 522–529.

Phil-Eze, P. O., 2010: Variability of soil properties related to vegetation cover in a tropical rainforest landscape. *J. Geogr. Reg. Plan.*, **3**, 174–188.

Phinzi, K., and N. S. Ngetar, 2019: The assessment of water-borne erosion at catchment level using GIS-based RUSLE and remote sensing: A review. *Int. Soil Water Conserv. Res.*, **7**, 27–46, https://doi.org/10.1016/j.iswcr.2018.12.002.

Pickup, G., and V. H. Chewings, 1988: Forecasting patterns of soil erosion in arid lands from Landsat MSS data. *Int. J. Remote Sens.*, **9**, 69–84, https://doi.org/10.1080/01431168808954837.

Pimentel, D., C. Harvey, P. Resosudarmo, K. Sinclair, D. Kurz, S. Crist, L. Shpritz, L. Fitton, R. Saffouri, and R. Blair, 1995: Environmental and Economic Costs of Soil Erosion and Conservation Benefits. *Science*, **267**, 1117–1123, https://doi.org/10.1126/science.267.5201.1117.

Pinto, I., C. Lennard, M. Tadross, B. Hewitson, A. Dosio, G. Nikulin, H.-J. Panitz, and M. E. Shongwe, 2016: Evaluation and projections of extreme precipitation over southern Africa from two CORDEX models. *Clim. Change*, **135**, 655–668, https://doi.org/10.1007/s10584-015-1573-1.

Poesen, J., J. Nachtergaele, G. Verstraeten, and C. Valentin, 2003: Gully erosion and environmental change: importance and research needs. *CATENA*, **50**, 91–133, https://doi.org/10.1016/S0341-8162(02)00143-1.

Pontius Jr, R. G., and K. Batchu, 2003: Using the relative operating characteristic to quantify certainty in prediction of location of land cover change in India. *Trans. GIS*, **7**, 467–484.

Pontius, R. G., 2000: Quantification error versus location error in comparison of categorical maps. *Photogramm Eng Remote Sens*, **66,** 1011-1016.

Pontius, R. G., and L. C. Schneider, 2001: Land-cover change model validation by an ROC method for the Ipswich watershed, Massachusetts, USA. *Agric. Ecosyst. Environ.*, **85**, 239–248, https://doi.org/10.1016/S0167-8809(01)00187-6.

Posthumus, H., L. K. Deeks, R. J. Rickson, and J. N. Quinton, 2015: Costs and benefits of erosion control measures in the UK. *Soil Use Manag.*, **31**, 16–33, https://doi.org/10.1111/sum.12057.

Potts, D., 2011: "We Have A Tiger By The Tail": Continuities and Discontinuities in Zimbabwean City Planning and Politics. *Crit. Afr. Stud.*, **4**, 15–46.

Prasannakumar, V., H. Vijith, S. Abinod, and N. Geetha, 2012: Estimation of soil erosion risk within a small mountainous sub-watershed in Kerala, India, using Revised Universal Soil Loss Equation (RUSLE) and geo-information technology. *Geosci. Front.*, **3**, 209–215, https://doi.org/10.1016/j.gsf.2011.11.003.

Pruski, F. F., and M. A. Nearing, 2002: Climate-induced changes in erosion during the 21st century for eight U.S. locations: Climate-induced changes in erosion. *Water Resour. Res.*, **38**, 34-1-34–11, https://doi.org/10.1029/2001WR000493.

Punia, M., and L. Singh, 2012: Entropy Approach for Assessment of Urban Growth: A Case Study of Jaipur, India. *J. Indian Soc. Remote Sens.*, **40**, 231–244, https://doi.org/10.1007/s12524-011-0141-z.

Rahaman, M., B. Thakur, A. Kalra, and S. Ahmad, 2019: Modeling of GRACE-Derived Groundwater Information in the Colorado River Basin. *Hydrology*, **6**, 19, https://doi.org/10.3390/hydrology6010019.

Rahman, Md. R., Z. H. Shi, and C. Chongfa, 2009: Soil erosion hazard evaluation—An integrated use of remote sensing, GIS and statistical approaches with biophysical parameters towards management strategies. *Ecol. Model.*, **220**, 1724–1734, https://doi.org/10.1016/j.ecolmodel.2009.04.004.

Räisänen, J., 2007: How reliable are climate models? *Tellus Dyn. Meteorol. Oceanogr.*, **59**, 2–29, https://doi.org/10.1111/j.1600-0870.2006.00211.x.

Ranzi, R., T. H. Le, and M. C. Rulli, 2012: A RUSLE approach to model suspended sediment load in the Lo river (Vietnam): Effects of reservoirs and land use changes. *J. Hydrol.*, **422–423**, 17–29, https://doi.org/10.1016/j.jhydrol.2011.12.009.

Renard, K. G., and J. R. Freimund, 1994: Using monthly precipitation data to estimate the R-factor in the revised USLE. *J. Hydrol.*, **157**, 287–306, https://doi.org/10.1016/0022-1694(94)90110-4.

Renard, K. G., G. R. Foster, G. A. Weesies, D. K. McCool, and D. C. Yoder, 1997: Predicting soil erosion by water: a guide to conservation planning with the Revised Universal Soil Loss Equation (RUSLE).

Renschler, C. S., C. Mannaerts, and B. Diekkrüger, 1999: Evaluating spatial and temporal variability in soil erosion risk—rainfall erosivity and soil loss ratios in Andalusia, Spain. *CATENA*, **34**, 209–225, https://doi.org/10.1016/S0341-8162(98)00117-9.

Riahi, K., A. Grübler, and N. Nakicenovic, 2007: Scenarios of long-term socio-economic and environmental development under climate stabilization. *Technol. Forecast. Soc. Change*, **74**, 887–935, https://doi.org/10.1016/j.techfore.2006.05.026.

Routschek, A., J. Schmidt, and F. Kreienkamp, 2014: Impact of climate change on soil erosion — A high-resolution projection on catchment scale until 2100 in Saxony/Germany. *CATENA*, **121**, 99–109, https://doi.org/10.1016/j.catena.2014.04.019.

Rwasoka, D. T., W. Gumindoga, and J. Gwenzi, 2011: Estimation of actual evapotranspiration using the Surface Energy Balance System (SEBS) algorithm in the Upper Manyame catchment in Zimbabwe. *Phys. Chem. Earth Parts ABC*, **36**, 736–746, https://doi.org/10.1016/j.pce.2011.07.035.

Sakieh, Y., A. Salmanmahiny, J. Jafarnezhad, A. Mehri, H. Kamyab, and S. Galdavi, 2015: Evaluating the strategy of decentralized urban land-use planning in a developing region. *Land Use Policy*, **48**, 534–551, https://doi.org/10.1016/j.landusepol.2015.07.004.

Salisbury, R., G. Bácsmegi, and P. Sümegi, 2013: Preliminary environmental historical results to reconstruct prehistoric human-environmental interactions in Eastern Hungary. *Open Geosci.*, **5**, https://doi.org/10.2478/s13533-012-0133-8.

Samanta, S., C. Koloa, D. K. Pal, and B. Palsamanta, 2016: Estimation of potential soil erosion rate using RUSLE and E30 model. *Model. Earth Syst. Environ.*, **2**, 149, https://doi.org/10.1007/s40808-016-0206-7.

Samson, K., 2009: Squatter settlement and the issue of regulation: A case of Dire Dawa. *Ethiop. Local Gov. Dev. J.*, **3**, 55–66.

Sang, L., C. Zhang, J. Yang, D. Zhu, and W. Yun, 2011: Simulation of land use spatial pattern of towns and villages based on CA–Markov model. *Math. Comput. Model.*, **54**, 938–943, https://doi.org/10.1016/j.mcm.2010.11.019.

Santé, I., A. M. García, D. Miranda, and R. Crecente, 2010: Cellular automata models for the simulation of real-world urban processes: A review and analysis. *Landsc. Urban Plan.*, **96**, 108–122, https://doi.org/10.1016/j.landurbplan.2010.03.001.

Sardari, M. R. A., O. Bazrafshan, T. Panagopoulos, and E. R. Sardooi, 2019: Modeling the Impact of Climate Change and Land Use Change Scenarios on Soil Erosion at the Minab Dam Watershed. *Sustainability*, **11**, 21, https://doi.org/doi:10.3390/su11123353.

Satterthwaite, D., 2008: Climate change and urbanization: Effects and implications for urban governance. *In Proceedings of the United Nations Expert Group meeting on population distribution, urbanization, internal migration and development*, DESA New York, 21–23.

Sayemuzzaman, M., and M. K. Jha, 2014: Modeling of Future Land Cover Land Use Change in North Carolina Using Markov Chain and Cellular Automata Model. *Am. J. Eng. Appl. Sci.*, **7**, 295–306, https://doi.org/10.3844/ajeassp.2014.295.306.

Schubert, H., A. Caballero Calvo, M. Rauchecker, O. Rojas-Zamora, G. Brokamp, and B. Schütt, 2018: Assessment of Land Cover Changes in the Hinterland of Barranquilla (Colombia) Using Landsat Imagery and Logistic Regression. *Land*, **7**, 152, https://doi.org/10.3390/land7040152.

Scott, A. J., and M. Storper, 2014: "The Nature of Cities: The Limits and Scope of Urban Theory." *Int. J. Urban Reg. Res.*, https://doi.org/10. 1111/1468-2427.12134.

SDI, 2009: Epworth Profiling Report 2019: Our stories as told from within. Capetwon, South Africa.

Segura, C., G. Sun, S. McNulty, and Y. Zhang, 2014: Potential impacts of climate change on soil erosion vulnerability across the conterminous United States. *J. Soil Water Conserv.*, **69**, 171–181, https://doi.org/10.2489/jswc.69.2.171.

Seutloali, K. E., T. Dube, and O. Mutanga, 2017: Assessing and mapping the severity of soil erosion using the 30-m Landsat multispectral satellite data in the former South African homelands of Transkei. *Phys. Chem. Earth Parts ABC*, **100**, 296–304, https://doi.org/10.1016/j.pce.2016.10.001.

Shafizadeh Moghadam, H., and M. Helbich, 2013: Spatiotemporal urbanization processes in the megacity of Mumbai, India: A Markov chains-cellular automata urban growth model. *Appl. Geogr.*, **40**, 140–149, https://doi.org/10.1016/j.apgeog.2013.01.009.

Shalaby, A., and R. Tateishi, 2007: Remote sensing and GIS for mapping and monitoring land cover and land-use changes in the Northwestern coastal zone of Egypt. *Appl. Geogr.*, **27**, 28–41, https://doi.org/10.1016/j.apgeog.2006.09.004.

Shamshad, A., M. N. Azhari, M. H. Isa, W. M. A. W. Hussin, and B. P. Parida, 2008: Development of an appropriate procedure for estimation of RUSLE EI30 index and preparation of erosivity maps for Pulau Penang in Peninsular Malaysia. *CATENA*, **72**, 423–432, https://doi.org/10.1016/j.catena.2007.08.002.

Sharpley, A. N, and J. R. Williams, 1990: *EPIC - Erosion/Productivity Imappct Calculator: 1. Model Documentation.* p. 235 pp pp.

Shikangalah, R., E. Paton, F. Jetlsch, and N. Blaum, 2017: Quantification of areal extent of soil erosion in dryland urban areas: an example from Windhoek, Namibia. *Cities and the Environment (CATE)*, **10**, 22.

Shongwe, M. E., and G. J. V. Oldenborgh, 2011: Projected Changes in Mean and Extreme Precipitation in Africa under Global Warming. Part II: East Africa. *J. Clim.*, **24**, 16, https://doi.org/10.1175/2010JCLI2883.1.

Shongwe, M. E., G. J. van Oldenborgh, B. J. J. M. van den Hurk, B. de Boer, C. A. S. Coelho, and M. K. van Aalst, 2009: Projected Changes in Mean and Extreme Precipitation in Africa under Global Warming. Part I: Southern Africa. *J. Clim.*, **22**, 3819–3837, https://doi.org/10.1175/2009JCLI2317.1.

Shuster, W. D., J. Bonta, H. Thurston, E. Warnemuende, and D. R. Smith, 2005: Impacts of impervious surface on watershed hydrology: A review. *Urban Water J.*, **2**, 263–275, https://doi.org/10.1080/15730620500386529.

Sibanda, S., and F. Ahmed, 2020: Modelling historic and future land use/land cover changes and their impact on wetland area in Shashe sub-catchment, Zimbabwe. *Model. Earth Syst. Environ.*, https://doi.org/10.1007/s40808-020-00963-y.

Simonneaux, V., A. Cheggour, C. Deschamps, F. Mouillot, O. Cerdan, and Y. Le Bissonnais, 2015: Land use and climate change effects on soil erosion in a semi-arid mountainous watershed (High Atlas, Morocco). *J. Arid Environ.*, **122**, 64–75, https://doi.org/10.1016/j.jaridenv.2015.06.002.

Singh, A., 1989: Review Article Digital change detection techniques using remotely-sensed data. *Int. J. Remote Sens.*, **10**, 989–1003, https://doi.org/10.1080/01431168908903939.

Singh, R., and V. S. Phadke, 2006: Assessing soil loss by water erosion in Jamni River Basin, Bundelkhand region, India, adopting universal soil loss equation using GIS. *Curr. Sci. Assoc.*, **90**, 1431–1435.

Sinha, P., and L. Kumar, 2013: Binary images in seasonal land-cover change identification: a comparative study in parts of New South Wales, Australia. *Int. J. Remote Sens.*, **34**, 2162–2186, https://doi.org/10.1080/01431161.2012.742214.

Sinha, P., N. K. Verma, and E. Ayele, 2016: Urban Built-up Area Extraction and Change Detection of Adama Municipal Area using Time-Series Landsat Images. *Int. J. Adv. Remote Sens. GIS*, **5**, 1886–1895, https://doi.org/10.23953/cloud.ijarsg.67.

Smith, H. J., 1999: Application of Empirical Soil Loss Models in southern Africa: a review. *South Afr. J. Plant Soil*, **16**, 158–163, https://doi.org/10.1080/02571862.1999.10635003.

Smith, M. S., W. W. Frye, and J. J. Varco, 1987: Legume Winter Cover Crops. *Advances in Soil Science*, B.A. Stewart, Ed., Vol. 7 of *Advances in Soil Science*, Springer New York, 95–139.

Smithen, A. A., and R. E. Schulze, 1982: The spatial distribution in Southern Africa of rainfall erosivity for use in the universal soil loss equation. *Water Afr*, **8**, 74–78.

Song, Y., 2005: A review of soil erodibility in water and wind erosion research. *J. Geogr. Sci.*, **15**, 167, https://doi.org/10.1360/gs050205.

Sperna Weiland, F. C., L. P. H. van Beek, A. H. Weerts, and M. F. P. Bierkens, 2012: Extracting information from an ensemble of GCMs to reliably assess future global runoff change. *J. Hydrol.*, **412–413**, 66–75, https://doi.org/10.1016/j.jhydrol.2011.03.047.

Stefanidis, S., and D. Stathis, 2018: Effect of Climate Change on Soil Erosion in a Mountainous Mediterranean Catchment (Central Pindus, Greece). *Water*, **10**, 1469, https://doi.org/10.3390/w10101469.

Stocking, M. A., and H. A. Elwell, 1976: Rainfall Erosivity over Rhodesia. *Trans. Inst. Br. Geogr.*, **1**, 231, https://doi.org/10.2307/621986.

Strand, G. H., W. Dramstad, and G. Engan, 2002: The effect of field experience on the accuracy of identifying land cover types in aerial photographs. *Int. J. Appl. Earth Obs. Geoinformation*, **4**, 137–146, https://doi.org/10.1016/S0303-2434(02)00011-9.

Subedi, P., K. Subedi, and B. Thapa, 2013: Application of a Hybrid Cellular Automaton – Markov (CA-Markov) Model in Land-Use Change Prediction: A Case Study of Saddle Creek Drainage Basin, Florida. *Appl. Ecol. Environ. Sci.*, **1**, 126–132, https://doi.org/10.12691/aees-1-6-5.

Sudhira, H. S., T. V. Ramachandra, and K. S. Jagadish, 2004: Urban sprawl: metrics, dynamics and modelling using GIS. *Int. J. Appl. Earth Obs. Geoinformation*, **5**, 29–39, https://doi.org/10.1016/j.jag.2003.08.002.

Tang, J., and L. Di, 2019: Past and Future Trajectories of Farmland Loss Due to Rapid Urbanization Using Landsat Imagery and the Markov-CA Model: A Case Study of Delhi, India. *Remote Sens.*, **11**, 180, https://doi.org/10.3390/rs11020180.

Tang, J., L. Wang, and Z. Yao, 2007: Spatio-temporal urban landscape change analysis using the Markov chain model and a modified genetic algorithm. *Int. J. Remote Sens.*, **28**, 3255–3271, https://doi.org/10.1080/01431160600962749.

Tarboton, D. G., 1997: A new method for the determination of flow directions and upslope areas in grid digital elevation models. *Water Resour. Res.*, **33**, 309–319, https://doi.org/10.1029/96WR03137.

Tawodzera, G., 2011: Vulnerability in crisis: urban household food insecurity in Epworth, Harare, Zimbabwe. *Food Secur.*, **3**, 503–520, https://doi.org/DOI 10.1007/s12571-011-0152-1.

Teng, H., Z. Liang, S. Chen, Y. Liu, R. A. Viscarra Rossel, A. Chappell, W. Yu, and Z. Shi, 2018: Current and future assessments of soil erosion by water on the Tibetan Plateau based on RUSLE and CMIP5 climate models. *Sci. Total Environ.*, **635**, 673–686, https://doi.org/10.1016/j.scitotenv.2018.04.146.

Thompson, J. G., and W. D. Purves, 1978: *A guide to the soils of Rhodesia. Technical handbook No. 3*. Rhodesia Agriculural Journal.

Thomson, A. M., K. V. Calvin, S. J. Smith, G. P. Kyle, A. Volke, P. Patel, S. Delgado-Arias, B. Bond-Lamberty, M. Wise, L. E. Clarke, and J. A. Edmonds, 2011: RCP4.5: a pathway for stabilization of radiative forcing by 2100. *Clim. Change*, 18.

Thrasher, B., E. P. Maurer, C. McKellar, and P. B. Duffy, 2012: Technical Note: Bias correcting climate model simulated daily temperature extremes with quantile mapping. *Hydrol. Earth Syst. Sci.*, **16**, 3309–3314, https://doi.org/10.5194/hess-16-3309-2012.

von Thünen, J. H., 1910: *Der Isolerte Staat in Beziehung auf Landwirtschaft und Nationalökomie.* 2 Eds. Verlag von Gustav Fischer, Jena.

Tibaijuka, A. K., 2005: Report of the Fact-Finding Mission to Zimbabwe to Assess the Scope and Impact of Operation Murambatsvina. United Nations: New York, NY, USA.

Tibugari, H., G. Mafere, S. Dube, M. Chakavarika, R. Mandumbu, J. P. Musara, T. Gumbo, A. Banda, N. Mathema, T. Goche, B. M. Zvigumbu, N. Mpofu, and T. Zang, 2020: Worrying cadmium and lead levels in a commonly cultivated vegetable irrigated with river water in Zimbabwe. *Cogent Biol.*, **6**, 1802814, https://doi.org/10.1080/23312025.2020.1802814.

Toriro, P., 2007: Town planning in Zimbabwe: History challenges and the urban renewal operation Murambatsvina and operation Garikayi. *OSSREA Harare Zimb.*,.

Toutin, T., and L. Gray, 2000: State-of-the-art of elevation extraction from satellite SAR data. *ISPRS J. Photogramm. Remote Sens.*, **55**, 13–33, https://doi.org/10.1016/S0924-2716(99)00039-8.

Trirnble, S. W., and P. Crosson, 2000: U.S. Soil Erosion Rates- Myth and Reality. *Science*, **289**, 248–250.

Tundu, C., M. J. Tumbare, and J.-M. Kileshye Onema, 2018: Sedimentation and Its Impacts/Effects on River System and Reservoir Water Quality: case Study of Mazowe Catchment, Zimbabwe. *Proc. Int. Assoc. Hydrol. Sci.*, **377**, 57–66, https://doi.org/10.5194/piahs-377-57-2018.

Turnbull, L., A. J. Parsons, J. Wainwright, and J. P. Anderson, 2013: Runoff responses to long-term rainfall variability in a shrub-dominated catchment. *J. Arid Environ.*, **91**, 88–94, https://doi.org/10.1016/j.jaridenv.2012.12.002.

Turral, H., J. Burke, and J. M. Faurès, 2011: Climate change, water and food security. *Water Rep. FAO Rome Italy*,.

UN, 2012: World Urbanization Prospects: The 2011 Revision United Nations. New York: Population Division of the Department of Economic and Social Affairs. ESA/P/WP/224.

UN, 2014: World Urbanization Prospects: The 2014 Revision, Highlights. United Nations: New York, NY, USA. Available at: http://esa.un.org/unpd/wup/).

UN HABITAT, 2007: State of the World Cities 2010/2011: Bridging the Urban Divide. United Nations Human Settlements Programme, Nairobi, Kenya.

UN. Population Division, 2020: Then & Now: Urban Population Worldwide. United Nations: New York, NY, USA. Available at: https://www.statista.com/chart/23349/share-of-urban-population-by-continent/.

UNDP, 1996: Urban Agriculture: Foods, Jobs and Sustainable Cities. Publication for Habitat II, Volume One. New York, USA, United Nations Development Programme.

USDA. NRCS, 2000: Soil Quality – Urban Technical Note No. 1: Erosion and Sedimentation on Construction Sites. Soil Quality Institute: Washington, DC, USA. Available at: https://www.nrcs.usda.gov/Internet/FSE_DOCUMENTS/nrcs142p2_053285.

USGS (United States Geologic Service), 2018: Shuttle Radar Topography Mission (SRTM) 1 Arc-Second Global Data. Available at: https://earthexplorer.usgs.gov/SRTM1Arc (Accessed: 19 September 2018).

Van der Knijff, J. M., R. J. A. Jones, and L. Montanarella, 1999: Soil erosion risk assessment in Italy. European Soil Bureau, Joint Research Centre of the European Commission.

Vapnik, V., 1998: The Nature of Statistical Learning Theory. John Wiley & Sons. *Inc N. Y.*,.

Vapnik, V. N., 1999: An overview of statistical learning theory. *IEEE Trans. Neural Netw.*, **10**, 988–999, https://doi.org/10.1109/72.788640.

Venkateswaran, K., N. Kasthuri, K. Balakrishnan, and K. Prakash, 2013: Performance Analysis of K-Means Clustering For Remotely Sensed Images. *Int. J. Comput. Appl.*, **84**, 23–27, https://doi.org/10.5120/14628-2981.

de Vente, J., and J. Poesen, 2005: Predicting soil erosion and sediment yield at the basin scale: Scale issues and semi-quantitative models. *Earth-Sci. Rev.*, **71**, 95–125, https://doi.org/10.1016/j.earscirev.2005.02.002.

Verheijen, F. G. A., R. J. A. Jones, R. J. Rickson, and C. J. Smith, 2009: Tolerable versus actual soil erosion rates in Europe. *Earth-Sci. Rev.*, **94**, 23–38, https://doi.org/10.1016/j.earscirev.2009.02.003.

Vincent, V., R. G. Thomas, and R. R. Staples, 1960: *An agricultural survey of Southern Rhodesia. Part 1. Agro-ecological survey.* An Agricultural Survey of Southern Rhodesia. Part 1. Agro-Ecological Survey.,.

Vrieling, A., 2006: Satellite remote sensing for water erosion assessment: A review. *CATENA*, **65**, 2–18, https://doi.org/10.1016/j.catena.2005.10.005.

Vrochidou, A.-E. K., M. G. Grillakis, and I. K. Tsanis, 2013: Drought Assessment Based on Multi-Model Precipitation Projections for the Island of Crete. *J. Earth Sci. Clim. Change*, **04**, https://doi.org/10.4172/2157-7617.1000158.

van Vuuren, D. P., and Coauthors, 2011: RCP2.6: exploring the possibility to keep global mean temperature increase below 2°C. *Clim. Change*, **109**, 95–116, https://doi.org/10.1007/s10584-011-0152-3.

Wang, C., S. Lei, A. J. Elmore, D. Jia, and S. Mu, 2019: Integrating Temporal Evolution with Cellular Automata for Simulating Land Cover Change. *Remote Sens.*, **11**, 301, https://doi.org/10.3390/rs11030301.

Wang, D., and B. Cheng, 2010: An Unsupervised Classification Method of Remote Sensing Images Based on Ant Colony Optimization Algorithm. *Advanced Data Mining and Applications*, L. Cao, Y. Feng, and J. Zhong, Eds., Vol. 6440 of *Lecture Notes in Computer Science*, Springer Berlin Heidelberg, 294–301.

Wang, G., G. Gertner, S. Fang, and A. B. Anderson, 2003: Mapping Multiple Variables for Predicting Soil Loss by Geostatistical Methods with TM Images and a Slope Map. *Photogramm. Eng. Remote Sens.*, **69**, 889–898, https://doi.org/10.14358/PERS.69.8.889.

Wang, L., and H. Liu, 2006: An efficient method for identifying and filling surface depressions in digital elevation models for hydrologic analysis and modelling. *Int. J. Geogr. Inf. Sci.*, **20**, 193–213, https://doi.org/10.1080/13658810500433453.

Wang, L., J. Qian, W.-Y. Qi, S.-S. Li, and J.-L. Chen, 2018: Changes in soil erosion and sediment transport based on the RUSLE model in Zhifanggou watershed, China. *Proc. Int. Assoc. Hydrol. Sci.*, **377**, 9–18, https://doi.org/10.5194/piahs-377-9-2018.

Wania, A., T. Kemper, D. Tiede, and P. Zeil, 2014: Mapping recent built-up area changes in the city of Harare with high resolution satellite imagery. *Appl. Geogr.*, **46**, 35–44, https://doi.org/10.1016/j.apgeog.2013.10.005.

Weeks, J. R., A. Hill, D. Stow, A. Getis, and D. Fugate, 2007: Can we spot a neighborhood from the air? Defining neighborhood structure in Accra, Ghana. *GeoJournal*, **69**, 9–22, https://doi.org/10.1007/s10708-007-9098-4.

Weng, Q., 2001: Modeling Urban Growth Effects on Surface Runoff with the Integration of Remote Sensing and GIS. *Environ. Manage.*, **28**, 737–748, https://doi.org/10.1007/s002670010258.

Weng, Q., 2012: Remote sensing of impervious surfaces in the urban areas: Requirements, methods, and trends. *Remote Sens. Environ.*, **117**, 34–49, https://doi.org/10.1016/j.rse.2011.02.030.

White, R., and G. Engelen, 1993: Cellular Automata and Fractal Urban Form: A Cellular Modelling Approach to the Evolution of Urban Land-Use Patterns. *Environ. Plan. Econ. Space*, **25**, 1175–1199, https://doi.org/10.1068/a251175.

Whitlow, R., 1988: Soil erosion and conservation policy in Zimbabwe. *Land Use Policy*, **5**, 419–433, https://doi.org/10.1016/0264-8377(88)90076-2.

Willmott, C. J., 1982: Some comments on the evaluation of model perfomance. *Am. Meteorol. Soc.*, **63**, https://doi.org/10.1175/1520-0477(1982)063%3C1309:SCOTEO%3E2.0.CO;2.

Wischmeier, W. H., and D. D. Smith, 1978: *Predicting Rainfall Erosion Losses: A Guide to Conservation Planning*. Department of Agriculture, Science and Education Administration, 72 pp.

Woldemariam, G., A. Iguala, S. Tekalign, and R. Reddy, 2018: Spatial Modeling of Soil Erosion Risk and Its Implication for Conservation Planning: The Case of the Gobele Watershed, East Hararghe Zone, Ethiopia. *Land*, **7**, 25, https://doi.org/10.3390/land7010025.

World Economic Forum, 2020: Global-continent-urban-population-urbanisation-percent. Available at: https://www.weforum.org/agenda/2020/11/global-continent-urban-population-urbanisation-percent/.

Xu, C., M. Liu, C. Zhang, S. An, W. Yu, and J. M. Chen, 2007: The spatiotemporal dynamics of rapid urban growth in the Nanjing metropolitan region of China. *Landsc. Ecol.*, **22**, 925–937, https://doi.org/10.1007/s10980-007-9079-5.

Xu, H., 2006: Modification of normalised difference water index (NDWI) to enhance open water features in remotely sensed imagery. *Int. J. Remote Sens.*, **27**, 3025–3033, https://doi.org/10.1080/01431160600589179.

Xu, H., 2007: Extraction of Urban Built-up Land Features from Landsat Imagery Using a Thematic oriented Index Combination Technique. *Photogramm. Eng. Remote Sens.*, **73**, 1381–1391, https://doi.org/10.14358/PERS.73.12.1381.

Xu, H., 2008: A new index for delineating built-up land features in satellite imagery. *Int. J. Remote Sens.*, **29**, 4269–4276, https://doi.org/10.1080/01431160802039957.

Xu, H., X. Wang, and G. Xiao, 2000: A remote sensing and GIS integrated study on urbanization with its impact on arable lands: Fuqing City, Fujian Province, China. *LAND Degrad.*, 15.

Yang, J. L., and G. L. Zhang, 2011: Water infiltration in urban soils and its effects on the quantity and quality of runoff. *J. Soils Sediments*, **11**, 751–761, https://doi.org/10.1007/s11368-011-0356-1.

Yang, L., G. Xian, J. M. Klaver, and B. Deal, 2003: Urban Land-Cover Change Detection through Sub-Pixel Imperviousness Mapping Using Remotely Sensed Data. *Photogramm. Eng. Remote Sens.*, **69**, 1003–1010, https://doi.org/10.14358/PERS.69.9.1003.

Yang, X., X.-Q. Zheng, and R. Chen, 2014: A land use change model: Integrating landscape pattern indexes and Markov-CA. *Ecol. Model.*, **283**, 1–7, https://doi.org/10.1016/j.ecolmodel.2014.03.011.

Ye, B., and Z. Bai, 2008: Simulating Land Use/Cover Changes of Nenjiang County Based on CA-Markov Model. *Computer and Computing Technologies In Agriculture, Volume I*, D. Li, Ed., Vol. 258 of *The International Federation for Information Processing*, Springer US, 321–329.

Yu, D., L. Yanxu, and F. Bojie, 2019: Urban growth simulation guided by ecological constraints in Beijing city: Methods and implications for spatial planning. *J. Environ. Manage.*, **243**, 402–410, https://doi.org/10.1016/j.jenvman.2019.04.087.

Yuan, F., K. E. Sawaya, B. C. Loeffelholz, and M. E. Bauer, 2005: Land cover classification and change analysis of the Twin Cities (Minnesota) Metropolitan Area by multitemporal Landsat remote sensing. *Remote Sens. Environ.*, **98**, 317–328.

Zakerinejad, R., and M. Maerker, 2015: An integrated assessment of soil erosion dynamics with special emphasis on gully erosion in the Mazayjan basin, southwestern Iran. *Nat. Hazards*, **79**, 25–50, https://doi.org/10.1007/s11069-015-1700-3.

Zhai, H., C. Lv, W. Liu, C. Yang, D. Fan, Z. Wang, and Q. Guan, 2021: Understanding Spatio-Temporal Patterns of Land Use/Land Cover Change under Urbanization in Wuhan, China, 2000–2019. *Remote Sens.*, **13**, 3331, https://doi.org/10.3390/rs13163331.

Zhang, H., Z. Qi, X. Ye, Y. Cai, W. Ma, and M. Chen, 2013: Analysis of land use/land cover change, population shift, and their effects on spatiotemporal patterns of urban heat islands in metropolitan Shanghai, China. *Appl. Geogr.*, **44**, 121–133, https://doi.org/10.1016/j.apgeog.2013.07.021.

Zhang, X.-C., 2007: A comparison of explicit and implicit spatial downscaling of GCM output for soil erosion and crop production assessments. *Clim. Change*, **84**, 337–363, https://doi.org/10.1007/s10584-007-9256-1.

Zhang, Y., M. Hernandez, E. Anson, M. A. Nearing, H. Wei, J. J. Stone, and P. Heilman, 2012: Modeling climate change effects on runoff and soil erosion in southeastern Arizona rangelands and implications for mitigation with conservation practices. *J. Soil Water Conserv.*, **67**, 390–405, https://doi.org/10.2489/jswc.67.5.390.

Zhang, Z., and G. He, 2006: A study on urban growth, vegetation space variation and thermal environmental changes of Beijing city based on TM imagery data. *Proc. 2nd WSEAS Int. Conf. Remote Sens. Tenerife Canary Isl. Spain Dec.*, 16–18.

Zhang, Z., R. Xiao, A. Shortridge, and J. Wu, 2014: Spatial Point Pattern Analysis of Human Settlements and Geographical Associations in Eastern Coastal China — A Case Study. *Int. J. Environ. Res. Public. Health*, **11**, 2818–2833, https://doi.org/10.3390/ijerph110302818.

Zhou, P., O. Luukkanen, T. Tokola, and J. Nieminen, 2008: Effect of vegetation cover on soil erosion in a mountainous watershed. *CATENA*, **75**, 319–325, https://doi.org/10.1016/j.catena.2008.07.010.

Zhou, W., and B. Wu, 2008: Assessment of soil erosion and sediment delivery ratio using remote sensing and GIS: a case study of upstream Chaobaihe River catchment, north China. *Int. J. Sediment Res.*, **23**, 167–173, https://doi.org/10.1016/S1001-6279(08)60016-5.

ZimStats, 2012: (Zimbabwe National Statistics Agency) Census 2012: Preliminary Report.

Zinyama, Lovemore., 1995: *The evolution of spatial structure in greater Harare. In: L.M. Zinyama, D.S. Tevera & D. Cumming, eds. Harare: the growth and problems of the city*. University of Zimbabwe Publications, 7–31 pp.

Zubair, A., 2006: Change detection in land use and land cover using remote sensing data and Gis (a case study of Ilorin and its environs in Kwara State).

Appendix

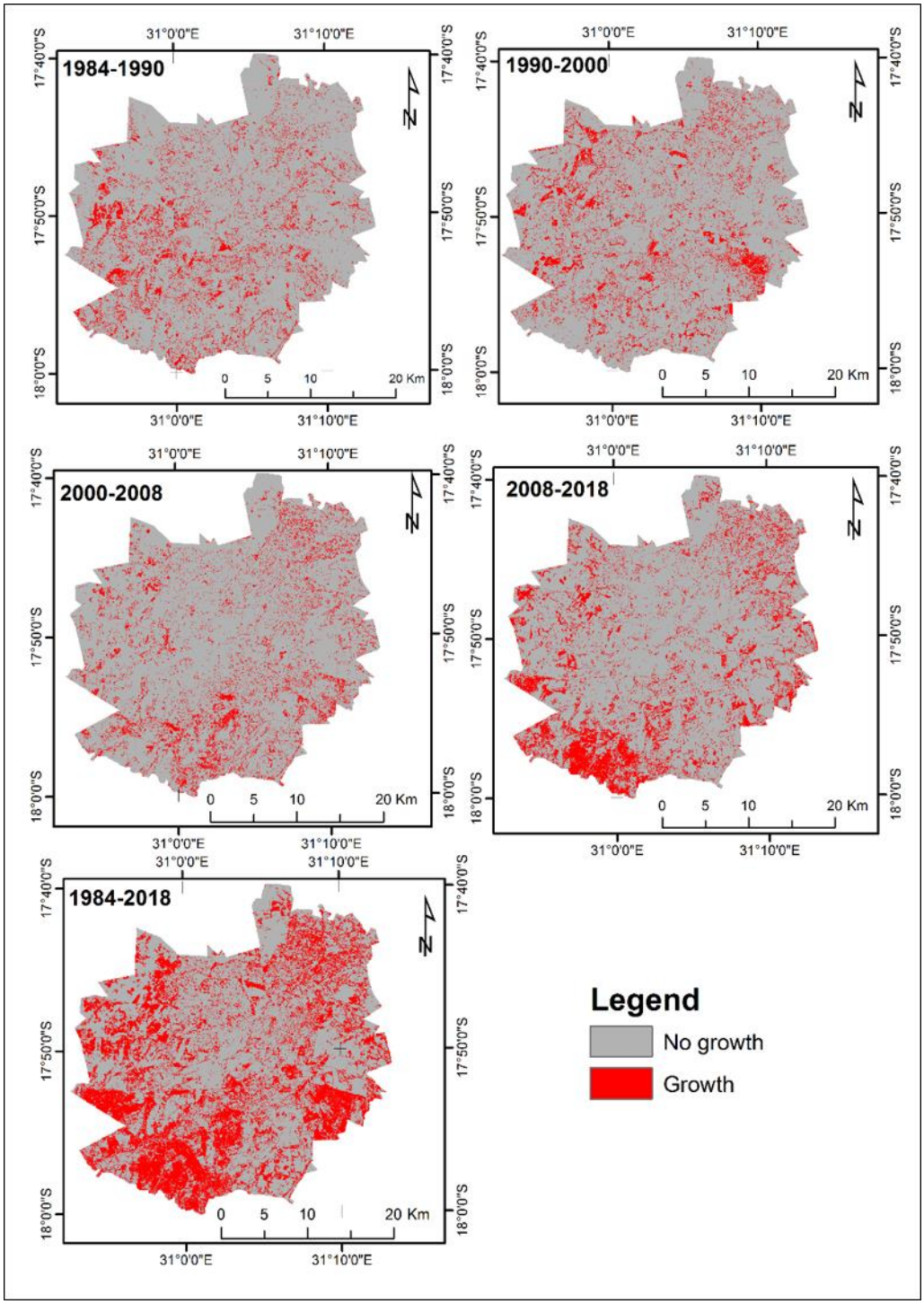

Figure A1. Raster layers for dependant variables for all time slices derived from change detection: 1984-1990; 1990-2000; 2000-2008; 2008-2018 and 1984-2018 with urban built-up area growth (=1) and non-built-up area (=0).

Table A1. Confusion matrix and associated classification accuracies produced from Landsat 5 TM (1984, 1990, 2000 and 2008). These include kappa coefficient (Kc), overall accuracy (OA), producer's accuracy (PA) and user's accuracy (UA).

1984 Landsat 5 TM						Reference Class				
	Class	CBD/Industries	LMD	HD	Irrigated cropland	Rainfed cropland	Vegetation	Water	Total	PA
Classified	CBD/Industries	4012	182	81	0	3	2	2	4282	94.7
	LMD	92	9353	164	213	8	495	47	10372	89.4
	HD	98	105	2005	0	135	17	0	2360	82.2
	Irrigated cropland	0	108	2	2602	1	22	0	2735	87.6
	Rainfed cropland	19	37	165	7	5996	655	0	6879	84.1
	Vegetation	10	665	23	148	987	16765	11	18609	93.4
	Water	7	9	0	0	0	0	500	516	89.3
	Total	4238	10459	2440	2970	7130	17956	560	45753	
	UA	93.7	90.2	85.0	95.1	87.2	90.1	96.9		
	OA	90.1				Kc	0.87			
1990 Landsat 5 TM						Reference Class				
	Class	CBD/Industries	LMD	HD	Irrigated cropland	Rainfed cropland	Vegetation	Water	Total	PA
Classified	CBD/Industries	1827	62	61	0	0	0	0	1950	99.2
	LMD	1	2335	127	137	0	64	10	2674	81.9
	HD	10	55	979	4	1	0	0	1049	77.7
	Irrigated cropland	0	45	40	1030	6	0	0	1121	78.4
	Rainfed cropland	2	56	45	29	964	102	0	1198	67.4
	Vegetation	2	299	8	114	459	2172	0	3054	92.6
	Water	0	0	0	0	0	0	601	601	98.4
	Total	1842	2852	1260	1314	1430	2338	611	11647	
	UA	93.7	87.3	93.3	91.9	80.5	71.1	100		
	OA	85.1				Kc	0.82			

Table A1. *Cont.*

2000 Landsat 5 TM						Reference Class				
	Class	CBD/Industries	LMD	HD	Irrigated cropland	Rainfed cropland	Vegetation	Water	Total	PA
Classified	CBD/Industries	1946	113	85	1	8	3	0	2156	96.7
	LMD	10	3225	30	47	8	157	14	3491	87.4
	HD	50	34	1053	35	0	0	0	1172	83.4
	Irrigated cropland	0	70	53	596	0	5	0	724	76.2
	Rainfed cropland	5	24	38	93	602	0	0	762	85.6
	Vegetation	1	220	3	10	85	1520	6	1845	90.2
	Water	0	3	0	0	1	1	728	732	97.3
	Total	2012	3689	1262	782	703	1686	748		
	UA	90.3	92.4	89.9	82.3	79.0	82.4	99.5		
	OA	88.9				Kc	0.86			
2008 Landsat 5 TM						Reference Class				
	Class	CBD/Industries	LMD	HD	Irrigated cropland	Rainfed cropland	Vegetation	Water	Total	PA
Classified	CBD/Industries	2217	21	61	0	0	0	0	2299	96.4
	LMD	15	1629	116	37	0	355	6	2158	84.5
	HD	37	76	746	12	15	8	0	894	79.8
	Irrigated cropland	0	87	2	647	0	4	0	740	93.0
	Rainfed cropland	6	11	3	0	666	151	0	837	90.9
	Vegetation	11	105	7	0	52	1961	1	2137	79.1
	Water	1	0	0	0	0	0	606	607	98.9
	Total	2287	1929	935	695	733	2479	613	9672	
	UA	96.4	75.5	83.5	87.4	79.6	91.8	99.8		
	OA	87.6				Kc	0.85			

*CBD: central business department *LMD: low–medium density *HD: high density

Table A2. Confusion matrix and associated classification accuracies produced from Landsat 8 OLI (2018). The accuracies include kappa (Kc), overall accuracy (OA), producer's accuracy (PA) and user's accuracy (UA).

2018 Landsat 8 OLI		Reference Class								
Classified	Class	CBD/Industries	LMD	HD	Irrigated cropland	Rainfed cropland	Vegetation	Water	Total	PA
	CBD/Industries	2492	63	60	0	1	0	0	2616	96.6
	LMD	23	2721	59	124	64	219	5	3215	84.1
	HD	43	86	1778	10	3	3	0	1923	92.9
	Irrigated cropland	1	134	3	806	0	24	0	968	84.4
	Rainfed cropland	18	7	11	15	1352	122	0	1525	86.8
	Vegetation	4	223	3	0	137	2942	0	3309	88.9
	Water	0	0	0	0	0	0	601	601	99.2
	Total	2581	3234	1914	955	1557	3310	606	14157	
	UA	95.3	84.6	92.5	83.3	88.7	88.9	100		
	OA	89.7				Kc	0.87			

*CBD: central business department *LMD: low–medium density *HD: high density

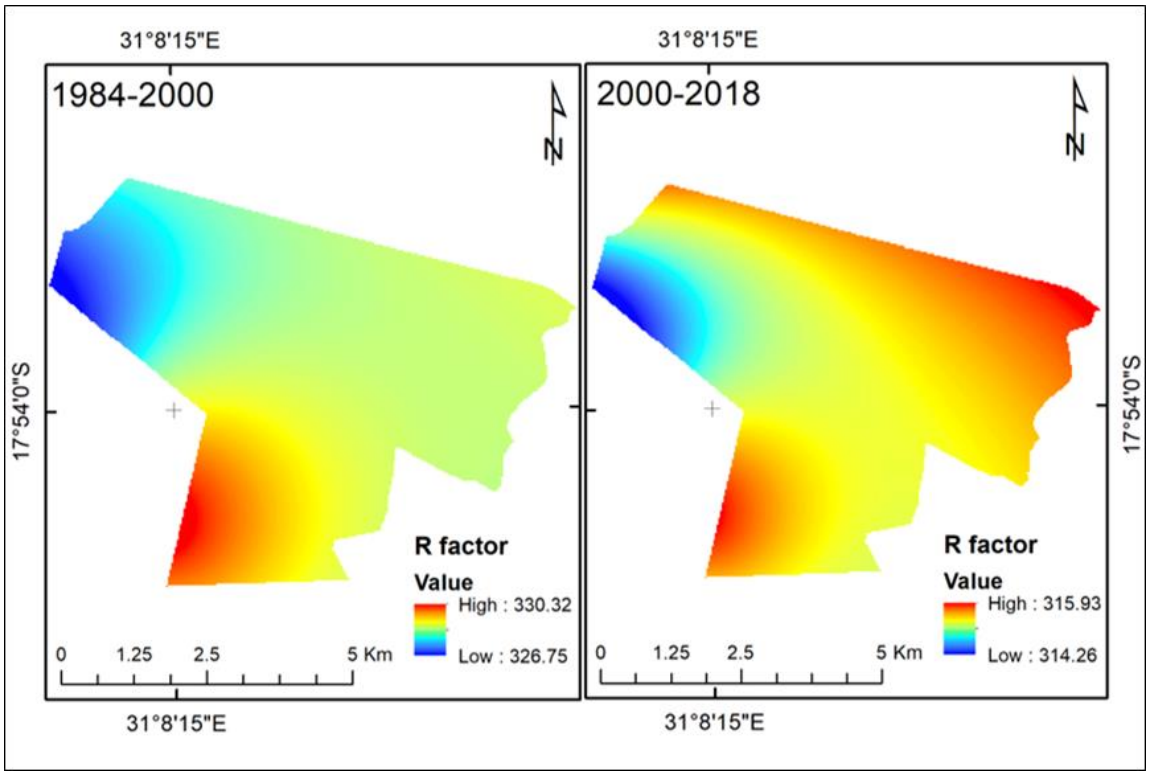

Figure A2. The rainfall erosivity factor map for Harare's Epworth district over the study periods 1984-2000 and 2000-2018.

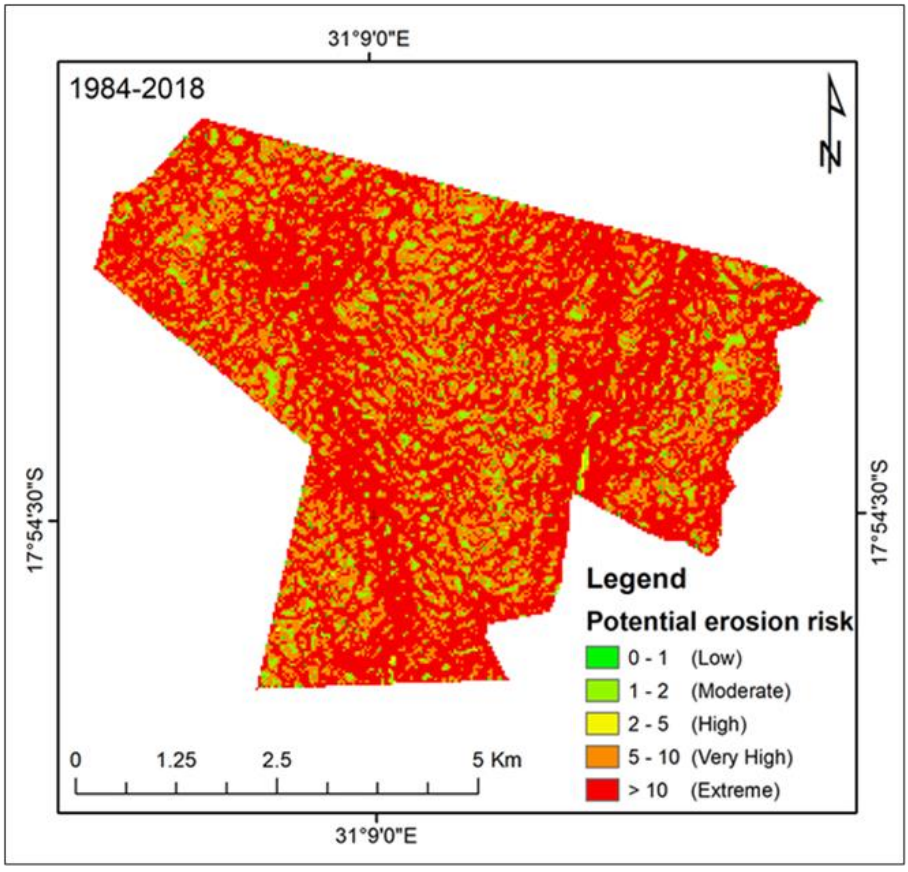

Figure A3. Potential erosion risk map for Epworth district generated for 2018 applying rainfall erosivity between 1984 and 2018.

Der Lebenslauf ist in der Onlineversion aus Datenschutzgründen nicht enthalten.

Der Lebenslauf ist in der Onlineversion aus Datenschutzgründen nicht enthalten.

Affidavit / Eidesstattliche Erklärung

Hiermit erkläre ich, dass ich die Dissertation "*The geography of contemporary urbanization and its effects on landscape sustainability in Harare Metropolitan Province*" selbstständig angefertigt und keine anderen als die von mir angegebenen Quellen und Hilfsmittel verwendet habe.

Ich erkläre weiterhin, dass die Dissertation bisher nicht in dieser oder in anderer Form in einem anderen Prüfungsverfahren vorgelegen hat.

Berlin, den
17.08.2022
…….

Andrew Kudzanayi Marondedze
…….